Upcycling CO_2 to Cyclic Carbonates Using Aluminosilicates, Transition Metal Complexes, and Their Zeolite Encapsulated Analogues

THESIS

Submitted in partial fulfillment of the requirements for the Degree of

DOCTOR OF PHILOSOPHY

by

AISHWARYA RAMESH

ID No. 2017PHXF0028P

Under the Supervision of

Prof. SAUMI RAY

Birla Institute of Technology and Science Pilani,
Pilani Campus, Rajasthan-333031, India

April 2024

Dedicated to
My Beloved Parents
And
My Sweet Sister

BIRLA INSTITUTE OF TECHNOLOGY AND SCIENCE

PILANI (RAJASTHAN)

CERTIFICATE

This is to certify that the thesis entitled **"Upcycling CO_2 to Cyclic Carbonates Using Aluminosilicates, Transition Metal Complexes, and Their Zeolite Encapsulated Analogues**" submitted by **Ms. Aishwarya Ramesh** ID No **2017PHXF0028P** for the award of Ph.D. Degree of the Institute embodies the original work done by her under my supervision.

Signature in full of the Supervisor

Name in capital block letters: **Prof. SAUMI RAY**

Designation: Professor

BITS Pilani, Pilani Campus

Date:

Table of Contents

	Particulars	Page No.
Certificate		
Acknowledgments		viii
Abstract		xiii
List of Tables		xv
List of Figures		xix
List of Schemes		xxv
List of Abbreviations & Symbols		xxvi
Chapter 1: Introduction		
1.1	**Introduction**	3
1.1.1	**Carbon Dioxide as a synthon**	6
1.1.1.1	Stability of CO_2	7
1.1.1.2	Reactions with CO_2	7
1.1.2	**Mechanisms of cyclic carbonate synthesis**	8
1.1.2.1	Epoxide activation	9
1.1.2.2	CO_2 activation	11
1.1.2.3	Dual activation	11
1.1.3	**Homogeneous Schiff base complexes as catalysts for cyclic carbonate synthesis**	12
1.1.3.1	Versatile nature and activity of Schiff base transition metal complexes	13
1.1.3.2	Schiff base transition metal complexes as catalysts for upcycling CO_2	13

Table of Contents

	Particulars	Page No.
1.1.3.3	Schiff base metal complexes of zinc and cobalt as catalysts for the synthesis of cyclic carbonates	16
1.1.4	**Heterogeneous aluminosilicates as catalysts for cyclic carbonate synthesis**	**28**
1.1.4.1	What are aluminosilicates?	29
1.1.4.2	Structure and nature of aluminosilicates	29
1.1.4.3	Aluminosilicates as catalysts for cyclic carbonate synthesis	33
1.1.5	**Metal complexes encaged in zeolite as heterogeneous catalysts for cyclic carbonate synthesis**	**39**
1.1.5.1	Heterogenization of transition metal complexes and methods of encapsulation	39
1.1.5.2	Importance and effects of encapsulation on the structure and property of the guest metal complexes	43
1.1.5.3	Applications of zeolite encapsulated complexes as catalysts	46
1.2	**Gaps in the literature and scope of the present thesis**	**48**
1.3	**References**	**50**

Chapter 2: Materials and Methods

2.1	**Introduction**	**63**
2.2	**Materials**	**63**
2.3	**Experimental Methods**	**65**
2.3.1	Synthesis of Al-MCM-41	65

Table of Contents

	Particulars	Page No.
2.3.2	Synthesis of Schiff-base ligands	65
2.3.3	Synthesis of metal (Co, Zn) Schiff-base complexes	66
2.3.4	Synthesis of metal [M(II)] exchanged zeolite-Y	67
2.3.5	Synthesis of encapsulated M(II)-Schiff base complexes in zeolite-Y	67
2.3.6	Synthesis of cyclic carbonate from epoxide using different aluminosilicates as catalysts at high pressure	68
2.3.7	Synthesis of cyclic carbonate from epoxide using cobalt(II) free state and encapsulated catalysts at high pressure	68
2.3.8	Synthesis of cyclic carbonate from epoxide using zinc(II) Schiff base complexes	68
2.3.9	Synthesis of cyclic carbonate from epoxide using zinc(II) encapsulated complexes	69
2.4	**Characterization techniques**	70
2.4.1	UV-visible/Diffuse Reflectance Spectroscopy (DRS)	70
2.4.2	Fourier Transform Infrared spectroscopy (FT-IR)	70
2.4.3	Brunauer-Emmett-Teller (BET) surface analysis	71
2.4.4	X-ray photoelectron spectrometer (XPS)	71
2.4.5	Nuclear Magnetic Resonance (NMR)	71
2.4.6	Powder X-ray diffraction (PXRD)	72
2.4.7	Field Emission Scanning Electron Microscopy (FESEM) and Energy Dispersive X-ray analysis (EDX)	72
2.4.8	Thermogravimetric analysis (TGA)	72

Table of Contents

	Particulars	Page No.
2.4.9	Atomic adsorption spectroscopy (AAS)	73
2.4.10	NH3-Temperature Programmed Desorption (NH_3-TPD)	73
2.4.11	Gas chromatography (GC)	73
2.4.12	Liquid Chromatography-Mass Spectroscopy (LC-MS)	74
2.4.13	Theoretical methods	74
2.5	**References**	77

Chapter 3: CO_2 to Cyclic Carbonate: A Mechanistic Insight of a Benign Route Using Zinc(II) Salophen Complexes

	Abstract	**80**
3.1	**Introduction**	**81**
3.2	**Results and discussions**	**82**
3.2.1	Fourier Transform Infrared (FT-IR) spectroscopy	82
3.2.2	X-ray Photoelectron Spectroscopy (XPS) studies	86
3.2.3	Thermogravimetric (TGA) analysis	92
3.2.4	Liquid Chromatography-Mass Spectrometry (LC-MS) and Structural Studies from DFT	94
3.2.5	Electronic Spectra: Experimental and Theoretical Approaches	98
3.2.6	^{1}H, ^{13}C NMR and Diffusion ordered spectroscopy (DOSY) studies	105
3.2.7	Catalytic Studies and mechanistic investigations using DFT	115
3.2.8	Discussions	118

Table of Contents

	Particulars	Page No.
3.3	**Conclusions**	**120**
3.4	**References**	**121**
Chapter 4: Importance of the Nature of Acidic Sites of Different Aluminosilicates on Fixation of Carbon Dioxide with Styrene Oxide		
	Abstract	**126**
4.1	**Introduction**	**127**
4.2	**Results and discussions**	**128**
4.2.1	Elemental analysis	128
4.2.2	Field Emission Scanning Electron Microscopy (FESEM)	129
4.2.3	Powder X-ray diffraction (XRD) studies	129
4.2.4	Fourier Transform Infrared (FT-IR) spectroscopy	130
4.2.5	Thermogravimetric (TGA) analysis	132
4.2.6	Brunauer–Emmett–Teller (BET) surface analysis	133
4.2.7	^{29}Si solid-state NMR	135
4.2.8	X-ray Photoelectron Spectroscopy (XPS) studies	135
4.2.9	Ammonia TPD (NH_3-TPD) studies	137
4.2.10	Catalytic Studies and discussions	140
4.3	**Conclusions**	**146**
4.4	**References**	**147**

Table of Contents

	Particulars	Page No.
Chapter 5: Zeolite-Y encapsulated Zinc(II) Schiff-base complexes for upcycling CO_2		
	Abstract	**152**
5.1	**Introduction**	**153**
5.2	**Results and Discussions**	**154**
5.2.1	Elemental Analysis	154
5.2.2	Powder X-ray Diffraction (PXRD) studies	155
5.2.3	Field Emission Scanning Electron Microscopy (FESEM) analysis	156
5.2.4	Fourier Transform Infrared (FT-IR) spectroscopy Study	158
5.2.5	Thermal analysis	160
5.2.6	Brunauer-Emmett-Teller (BET) surface area analysis	161
5.2.7	X-ray photoelectron Spectroscopy (XPS) analysis	163
5.2.8	Ultraviolet-Visible/Diffuse Reflectance Spectroscopy (UV-vis/DRS)	167
5.2.9	Ammonia TPD (NH_3-TPD) studies	169
5.2.10	Catalytic study for the coupling of styrene oxide to CO_2	171
5.3	**Conclusions**	**174**
5.4	**References**	**175**

Table of Contents

	Particulars	Page No.
Chapter 6: Zeolite-Y encapsulated Cobalt(II) Schiff-base complexes employed for upcycling CO_2		
	Abstract	**178**
6.1	**Introduction**	**179**
6.2	**Results and Discussions**	**180**
6.2.1	Theoretical studies and Diffuse Reflectance Spectroscopy (UV−Vis/DRS)	184
6.2.2	Catalytic study for the coupling of styrene oxide and CO_2	192
6.3	**Conclusions**	**195**
6.4	**References**	**197**
Chapter 7: Conclusion and Future Scope		
7.1	**Scope and nature of the present study**	**202**
7.2	**Overall conclusions of the present work**	**209**
7.3	**Future scope**	**209**
Appendices		
	Additional Information [A-1]	**213**
	List of Publications [A-2]	**215**
	Conferences and Workshops Attended [A-3]	**216**
	Brief Biography of the Candidate [A-4]	**217**
	Brief Biography of the Supervisor [A-5]	**218**

Acknowledgements

It is a pleasure to look back on the many special occasions and people who accompanied me on this long journey. Their unwavering support, encouragement, direction, and blessings at various points along the way enabled me to reach this important life milestone.

First and foremost, I would like to thank Dr. Saumi Ray, my research supervisor, for all her help and support during my doctoral studies. Without her passionate drive, my Ph.D. would have remained an unattainable goal. Her constant motivation, guidance, and support have been invaluable to me during my research tenure. I owe Dr. Saumi Ray a debt of gratitude for her fundamental knowledge, and proficiency in material chemistry, with every discussion becoming a new learning for me. She has always given me the freedom to operate in the lab without pressure. Her motivation and unending support during our conversations have been invaluable in my career as a researcher. Her suggestions on technical writing enabled me to publish in high-quality journals in such a short amount of time. In addition, I am also thankful to her for giving me the chance to tutor and guide undergraduate students in the lab, which gave me invaluable experience for my doctoral studies.

I am greatly thankful to the former and present Vice-Chancellors, Directors, Deans, and Associate Deans of Birla Institute of Technology & Science (BITS), Pilani for allowing me to pursue my doctoral studies by providing the necessary facilities and financial support. I extend my heartfelt appreciation to the office staff of AGSRD, whose secretarial assistance helped me in submitting the various evaluation documents on time. I would also like to acknowledge the former and current Head of the Chemistry Department, DRC Chemistry, BITS Pilani, Pilani Campus for their official support and encouragement.

I am profoundly grateful for the cooperation and affection extended by all the respected teachers: Dr. S. C. Sivasubramanian, Dr. R. K. Roy, Dr. Dalip Kumar, Dr. Anil Kumar, Dr. Bharti Khungar, Dr. Inamur R. Laskar, Dr. Rajeev Sakhuja, Dr. Indresh Kumar, Dr. Surojit Pande, Dr. Shamik Chakraborty, Dr. Madhushree Sarkar, Dr. Ajay K. Sah, Dr. Prashant U. Manohar, Dr. Paritosh Shukla, Dr. Bibhas R. Sarkar, Dr. Mrinmoyee Basu, Dr. Amrita Chakraborty, Dr. Pritam K. Jana, Dr, Satyajit Patra, Dr. Nitika Grover, Dr. Partha Sarathi Addy, Dr. Avik Kumar Pati, and staff members of Department of Chemistry, BITS Pilani, Pilani Campus for their constant guidance and substantial support at different stages during my research period.

Acknowledgements

I am grateful to the members of my Doctoral Advisory Committee, Dr. Bibhas R. Sarkar, and Dr. Madhushree Sarkar for their valuable suggestions and cooperation in refining my research proposal and thesis. I also thank them for their insightful discussions whenever I went to them with a query.

My special thanks are also extended to Mrs. Pushpalata, Mr. Suresh, and Mr. Nandlal for teaching me how to perform lab experiments in the General Chemistry Lab, and for allowing me to access the lab equipment and providing some required general chemicals.

I also acknowledge the Department of Chemistry, BITS Pilani for providing me Institute fellowship during the tenure of my Ph.D. Also, DST-FIST is sincerely acknowledged for providing instrumentation facilities in the department.

I would also like to thank Central Instrumentation Facility (CIF) BITS Pilani, Pilani campus, Sophisticated Instrumental Facility (SIF), BITS Pilani, Pilani campus, and Central Analytical Laboratory (CAL), BITS Pilani, Pilani campus, for providing me with state-of-art instrumentation facilities which helped me with the trouble-free characterization of my samples.

I would also like to extend my heartfelt thanks to the operators of various instruments in SIF and CAL, Mr. Abhishek Kumar Gautam (NMR), Mr. Sandip Ruidas (GC-MS, BET, and XPS), Mr. Om Prakash (FESEM), and Mr. Suman (GC-MS). I would also like to thank Mr. Naveen Rana, CAL, for providing me with technical help when working in the lab. Because of their punctuality, all the characterization of my compounds has been carried out smoothly.

I would also like to thank Mr. Kuldeep, Analytical Lab, Department of Chemical Engineering, BITS Pilani, for carrying out the TGA and AAS analysis. I also thank Mr. Dheeraj, University of Delhi for patiently performing and teaching me to perform the DOSY NMR. My thanks are also extended to Mr. Krishna Gopal from Toshvin Analytical Pvt. Ltd. whose technical conversations helped me to gain in-depth knowledge about the instrumentation and working of GC and TGA. I also like to thank Mr. Amarjeet Bagga and Mr. Jagdish for their help in setting the CO_2 cylinder. Without learning the technical and working knowledge from these people, my theoretical knowledge of these instruments could not have transferred to practical application.

My sincere thanks to Mr. Ranjan Sinha Thakur, Librarian, and other staff of library BITS Pilani for their support and help rendered while utilizing the library services.

Acknowledgements

I also thank our collaborators Dr. Bidisa Das (TCG-CREST, Kolkata) and Ms. Sharmistha De Dalui (IACS, Kolkata) for the theoretical studies.

I am also thankful to the Work Integrated Learning Program (WILP), BITS Pilani for financially supporting me after my fellowship was over.

I am highly thankful to my seniors Dr. Archana Choudhary and Dr. Susheela Kumari. I have learned a lot of essential things which are very important for my research and professional life. I also thank Dr. Dinesh Kumar for his guidance that made the initial phase of my Ph.D. life a bit easier in BITS Pilani.

My special thanks to my departmental seniors Dr. Pallavi Rao, Dr. Fayaz Baig, Dr. Sachin Choudhary, Dr. Santosh Khandagale, Dr. Saroj Budania, Dr. Vishal Kachwal, Dr. Moyna Das, Dr. Sonam Sharma, Dr. Dinesh Kumar, Dr. Vaishali Saini, Dr. Shiv Dhiman, Dr. Nitesh Kumar, Dr. Devesh Agarwal, Dr. Vimal Kumar Madduluri, Ms. Bijoya Das, Dr. Rishika Aggarwal, Dr. Aabid Hamid, Dr. Chavi Mahala, Dr. Vikki Shinde, Dr. Pidiyara Karishma, and Dr. Jagrity Choudhary for their unwavering support and welcoming environment, which have always motivated me to work hard.

I also thank my departmental juniors, Dr. Santosh Mishra, Dr. Pramod, Dr. Sonam Jaspal, Dr. Mahesha C.K., Ms. Soumana Joarder, Ms. Gurpreet Kaur, Mr. Sumit Agarwal, Ms. Divya Rathore, Ms. Neha Meena, Ms. Mamta Katewa, Mr. Prakash Taur, Mr. Narsimha Verma, Ms. Prakriti Saraf, Ms. Pragya, Mr. Dhananjay Nipate, Ms. Monika Malik, Mr. Ram Prasad Bhatta, Mr. Yadav Nagare, Ms. Shivani Thakkar, Ms. Vishakha Jaiswal, Ms. Anuvasita Parikh, Ms. Aarzoo, Mr. Ajeet Sisodia, Ms. Annu, Mr. Atul Dolas, Ms. Bhawani, Mr. Imtiyaz Ahmed, Ms. Manisha, Ms. Nandani Roy, Mr. Narendra, Ms. Nidhi, Mr. Prakash Swami, Ms. Priyanka Kumari, Ms. Sushma Naharwal, Ms. Karishma Prabhu, Mr. Bharat Kaushik, Ms. Sonika Sangwan, Mr. Sumit, Ms. Heena Charaya, Ms. Aastha Gupta, Mr. Prashant Choubey, Ms. Ritu Rani, Ms. Debrupa Banerjee, Mr. Jayesh Sarvaiya, Ms. Disha Tank, Mr. Somnath Borade, Mr. Saurajit Ghosh, Ms. Parmeshthi Parikh, Ms. Khushika, Ms. Nidhi, Mr. Amol Gadekar, Ms. Meenu Ganwall, Ms. Priyanka Bhardwaj, Ms. Ritu Kumari, Ms. Sneha Tailor, and Ms. Vineeta Chaturvedi whose encouragement and support never ceased to inspire me.

Acknowledgements

My acknowledgment can never be complete without the special mention of my batchmates and Ph.D. friends and Dr. Dhritabrata Pal, Dr. Bintu Kumar, Ms. Prachi Sharma, Dr. Jyothi Yadav, Dr. Amol Pawar, Dr. Mamta Devi Sharma for their continuous support in course work, brainstorming discussion and cheering me up all the time. They are the reason my doctoral journey has been simple and enjoyable. They constantly encouraged me to perform better every day, were there for me, and were a constant source of support.

I could not find enough words of gratitude for my dear juniors and lab mates Ms. Sakshi, Mr. Ajeet Singh, Ms. Sakshi Bajaj, Ms. Shruti Soni, and Ms. Susmita and Ms. Shubhangi for their continuous support and love. Working in the happy atmosphere that these wonderful people created in the lab was always enjoyable. I am grateful to BITS graduate students Ms. Pooja, Mr. Anusatya, Mr. Hemanth, Mr. Umang, Mr. Harshit, and Mr. Utkarsh for their patience and support during our interactions.

I want to particularly thank my friends, who were more like family during my Ph.D. tenure, Ms. Prachi Sharma, Dr. Kanika Monga, and Dr. G. Srividya. They have always been there throughout my ups and downs. My Ph.D. journey has been easy and memorable due to these lovely people. They were always there, continuously supporting me, full of positive energy, and motivating me to do better every day.

Some people made me feel at home during my stay in Pilani. A big thanks to my little circle of Telugu-speaking faculty and friends, Prof. B. Vani, Dr. K. Laxmi Swetha, Dr. Kavyashree, Dr. Karan Banoth, Ms. Karnam Ravali, Dr. Rajesh, Mrs. Urmila, and Mr. Omkar. I would also like to sincerely thank Ms. Soumana Joarder, Ms. Shivani Thakkar, Mr. Prabhjeet Singh, Dr. Arihant, Ms. Aryav Yadav, Dr. Nikhil Hatwar, and Dr. Pinki for their continuous support and charming company.

My thanks are also extended to my childhood friends Dr. Nupur Kumari, and Ms. Bhawna Sharad, for their motivation, and their positivity. They always encouraged me and gave me the support to overcome struggles.

I would also like to show gratitude to the staff of the Institute Canteen (IC), Pappu Ji (Skylab), Mr. Anil, and our cook, for providing me with well-nourished food.

Acknowledgements

A special thanks to my family. My heartfelt thanks to my grandfather Late Shri A. S. Lakshman and my grandmother Late Smt. Susheela Lakshman for their love, inspiration, and unconditional blessings. It is impossible for me to put into words how grateful I am to my parents Shri A.L. Ramesh and Smt. Kala Ramesh for their moral support, endless inspiration, and their faith in me and for making my education very comfortable and enjoyable from the very beginning till the end. Special thanks to my sweet little sister Ms. Akshaya for always encouraging me and always being there with me. I am also thankful to my dear husband, Shri V.A.R. Sudheer for his continued support towards the fag end of my degree.

My thanks are duly acknowledged to BITS Pilani, Pilani Campus for the support in the form of fellowship, infrastructure, and instrumental facilities during my research tenure.

Last but not least, I bow my head to Almighty who gave me enough strength to work hard and cross the toughest situations.

Aishwarya Ramesh

Abstract

The control of CO_2 emissions is of utmost importance as major environmental problems such as global warming and ocean acidification are due to the rising CO_2 concentrations in the atmosphere. CO_2 has the potential to become a C1 source for various compounds, and the 100 % atom economic synthesis of cyclic carbonates from CO_2 and epoxides has grabbed attention due to its numerous industrial applications. At the same time, the high thermodynamic stability of CO_2 makes the activation of CO_2 difficult, which is overcome by using a catalyst. Numerous homogeneous and heterogeneous catalysts have been developed for the synthesis of cyclic carbonates from CO_2 and epoxides, including metal-based complexes, ionic liquids, organocatalysts, silica-based catalysts, MOFs, COFs, and metal oxides. There are very few reports in the literature that utilize zeolites, and zeolite-encapsulated complexes as catalysts for the synthesis of cyclic carbonates. The encapsulation of a complex inside the supercage of zeolite-Y bestows site isolation and enforces it to undergo structural and geometrical modifications due to space constraints. These changes further lead to moderations in the electronic, magnetic, photophysical, and electrochemical properties, due to which the complex shows modified catalytic activity upon encapsulation.

The main object of the present thesis is to develop various homogeneous and heterogeneous catalysts for the upcycling of CO_2 to cyclic carbonates. The chapters in this thesis highlight the synthesis and application of various catalysts for cyclic carbonate synthesis. The current thesis is divided into seven chapters. **Chapter 1** is the introduction of the thesis, which provides the background of the research work carried out. The chapter includes comprehensive literature about the existing salen and salophen-type homogeneous catalysts for the synthesis of cyclic carbonates from CO_2. The various reports utilizing aluminosilicate-based heterogeneous catalysts, like zeolite, MCM-41, and ZSM-5, are also discussed. **Chapter 2** deals with the synthesis strategies employed for the preparation of the catalysts, the details of the catalysis reactions carried out and the characterization techniques used. **Chapter 3** explores the utility of zinc(II) salophen complexes as homogeneous catalysts for the synthesis of cyclic carbonates from epoxides and CO_2. Seven Zn(II) complexes with different electron-donating and withdrawing substituents at 5, 5' position are synthesized. Interestingly, the LC-MS studies of the complexes indicate that all the complexes are dimeric except ZnL4 (with $–NO_2$ substituent) which is coordinated with two water molecules. DFT studies also show the presence of ZnL4 with two water molecules. The mechanism studied using DFT, indicated a different rate-determining step for monomeric ZnL4 compared to monomeric ZnL1 (with –H substituent) and ZnL3 (with –Br substituent). The best yield was achieved by

monomeric ZnL4 for the synthesis of cyclic carbonates from CO_2. However, the comparative yields for the reaction with other complexes suggests that the dimeric complexes can also be efficient catalysts for this reaction and the use of the bulky *tert*-butyl (^{t}Bu) group may not be mandatory to prevent the dimerization. **Chapter 4** shows the utilization of the inherent acidity of commercially available zeolites like zeolite-Na-Y, and NH_4^+-ZSM-5, synthesized Al-MCM-41, and their applicability as catalysts for upcycling CO_2 to cyclic carbonates. The NH_3-TPD studies of these aluminosilicates indicate the increase in Lewis acidic sites with a decrease in the Si/Al ratio The yield of the cyclic carbonate obtained also directly correlates with the number of weak acidic sites and the Si/Al ratio. Interestingly, the drastic decrease in strong acidic sites as well as in the yield obtained with the calcined zeolite-Na-Y indicates that not only the weak Lewis acidic sites but also the strong Brønsted acidic sites appear to be crucial in the cycloaddition reaction. **Chapter 5** discusses the utilization of zeolite-Y encapsulated complexes for the synthesis of cyclic carbonates from CO_2 and epoxides. The homogeneous dimeric zinc(II) salophen complexes discussed in Chapter 3 are heterogenized by encapsulating them in the supercage of zeolite-Y. Upon encapsulation, the complex undergoes structural modifications from their dimeric to the monomeric form which lead to a change in the electronic environment around the metal. The red shift in the UV-vis spectrum compared to the "neat" analogues, and the shift in the XPS binding energy towards higher values point towards the changes around the metal center. The NH_3-TPD also shows an increase in the Brønsted acidity of the complex upon encapsulation. The structural modifications, along with the modified acidity upon encapsulation, lead to the fascinating catalytic activity shown by the encapsulated complexes. In **Chapter 6**, the correlation of the end-to-end distance of the cobalt(II) complex and its effect upon encapsulation is studied. Two complexes with varying end-to-end distances have been studied and the results indicate that the complex with a larger end-to-end distance (with –OMe group) undergoes more distortion upon encapsulation, which leads to the alteration of the electron density around the metal, and consequently modifies the catalytic activity of the encapsulated complex in comparison to its "neat" analogue. The modification in the electronic environment around the metal is established using characterization techniques like XPS, and solid-state UV-vis spectroscopy. Theoretical studies point towards the change in the spin states of the encapsulated and "neat" complexes, which lead to the fascinating catalytic activity of the encapsulated complexes. **Chapter 7** presents the overall conclusions and future scope from the work presented in this thesis.

List of Tables

Table No.	Table Caption	Page No.
1.1	Catalysts based on zinc salen and salophen-type complexes for cyclic carbonate synthesis	17
1.2	Catalysts based on cobalt salen and salophen-type complexes for cyclic carbonate synthesis	23
1.3	Zeolite-based catalysts for cyclic carbonate synthesis	34
1.4	ZSM-based catalysts for cyclic carbonate synthesis	36
1.5	MCM-41-based catalysts for cyclic carbonate synthesis	38
2.1	List of various chemicals and their suppliers used in the current thesis	63
2.2	Table showing the temperature program of the column oven of GC	73
2.3	List of various analytical instruments used in the current thesis	76
3.1	FT-IR peak positions of all the ligands and the prepared complexes (in cm^{-1})	83
3.2	XPS binding energies of all the complexes (in eV)	91
3.3	Observed and calculated weight loss from TGA for all the complexes	93
3.4	Important structural parameters of ZnL catalysts and HOMO-LUMO gaps calculated from DFT	96
3.5	Assignment of experimental UV peaks and comparison with calculated TD-DFT spectra	103
3.6	Catalytic activity of the complexes used	117
3.7	Control reactions	117
3.8	Activity of the catalyst ZnL4 with other epoxides	118
3.9	Table for yield, conversion, and selectivity	118
4.1	Si/Al ratios of the catalysts	129
4.2	FT-IR study of the catalysts	132
4.3	Weight loss profile from TGA	133
4.4	BET parameters for the catalysts	134

List of Tables

Table No.	Table Caption	Page No.
4.5	XPS profile of the catalysts	136
4.6	Acidic sites of the catalysts	139
4.7	Physicochemical properties of calcined zeolite Na-Y	140
4.8	Catalytic table for conversion of styrene oxide to styrene carbonate	142
4.9	Optimization of amount of catalyst using zeolite Na-Y	142
4.10	Substrate scope for the formation of cyclic carbonate using zeolite Na-Y	143
4.11	Comparison of yield, conversion, and selectivity	143
5.1	Concentration of zinc in the prepared complexes	155
5.2	Comparison of the elemental composition of ZnL2-Y before and after Soxhlet	155
5.3	FT-IR data of Zn(II) encapsulated complexes (in cm^{-1})	159
5.4	TGA weight loss of the encapsulated complexes	161
5.5	BET surface area and pore volume of the encapsulated complexes	162
5.6	XPS data of all the encapsulated complexes (in eV)	164
5.7	Solid UV values of all the “neat” and the encapsulated complexes (in nm)	169
5.8	NH_3-TPD data of all the encapsulated complexes (mmol/g)	170
5.9	Optimization of reaction conditions for coupling of styrene oxide to CO_2 using ZnL1-Y	172
5.10	Catalytic activity of the complexes used	172
5.11	Activity of the catalyst ZnL1-Y with different epoxides	173
6.1	Summary of characterization data for the prepared encapsulated and “neat” complexes	181
6.2	Structural parameters and molecular orbital energies of the complexes	186

List of Tables

Table No.	Table Caption	Page No.
6.3	Assignment of experimental UV-vis peaks and comparison with calculated TD-DFT spectra	190
6.4	Comparison of zinc and cobalt for the catalytic reaction	192
6.5	Optimization of reaction conditions of coupling of styrene oxide to CO_2	193
6.6	Activity of the catalysts for conversion of styrene oxide and CO_2 to styrene carbonate under optimized conditions	194
6.7	Comparison of activity of cobalt complexes at different reaction conditions	195

List of Figures

Figure No.	Figure Caption	Page No.
1.1	Global atmospheric CO_2 compared to annual emissions (1751-2022).	6
1.2	A few representative examples of a few reactions possible using CO_2 as a synthon.	8
1.3	Application of Schiff base complex for various reactions using CO_2 as a C1 source.	14
1.4	1st Schiff base chromium complex used for the cyclic carbonate synthesis from CO_2.	15
1.5	General representation of aluminosilicates.	29
1.6	Structure of aluminosilicates employed in this thesis.	30
1.7	Building units of **(A)** zeolite-Y, **(B)** ZSM-5, **(C)** MCM-41.	31
1.8	Representation of Brønsted acidic sites (BAS) and Lewis acidic site (LAS) in zeolites.	32
1.9	Schematic representation for the flexible ligand synthesis method.	41
1.10	Schematic representation for the template synthesis method.	42
1.11	Schematic representation for the zeolite synthesis method.	43
1.12	Change in electronic properties upon encapsulation as reported by Ray *et al.*	45
1.13	Metalloporphyrin in ZIF for cyclic carbonate synthesis reported by Du *et al.*	48
2.1	Calibration curve of product (left) and styrene oxide (right).	74
3.1	Full range FT-IR spectra of **(A)** (a) L1, (b) ZnL1, **(B)** (a) L2, (b) ZnL2, **(C)** (a) L3, (b) ZnL3, **(D)** (a) L4, (b) ZnL4, **(E)** (a) L5, (b) ZnL5, **(F)** (a) L6, (b) ZnL6, **(G)** (a) L7, (b) ZnL7.	84
3.2	Zoomed FT-IR spectra of **(A)** (a) L1, (b) ZnL1, **(B)** (a) L2, (b) ZnL2, **(C)** (a) L3, (b) ZnL3, **(D)** (a) L4, (b) ZnL4, **(E)** (a) L5, (b) ZnL5, **(F)** (a) L6, (b) ZnL6, **(G)** (a) L7, (b) ZnL7.	85

List of Figures

Figure No.	Figure Caption	Page No.
3.3	XPS survey spectra of **(A)** ZnL1, **(B)** ZnL2, **(C)** ZnL3, **(D)** ZnL4, **(E)** ZnL5, **(F)** ZnL6, **(G)** ZnL7.	87
3.4	XPS spectra of Zn (2p) of **(A)** ZnL1, **(B)** ZnL2, **(C)** ZnL3, **(D)** ZnL4, **(E)** ZnL5, **(F)** ZnL6, **(G)** ZnL7.	88
3.5	XPS profiles of **(A)** C (1s) of ZnL1, **(B)** N (1s) of ZnL1, **(C)** O (1s) of ZnL1, **(D)** C (1s) of ZnL2, (E) N (1s) of ZnL2, (F) O (1s) of ZnL2, (G) C (1s) of ZnL3, (H) N (1s) of ZnL3, (I) O (1s) of ZnL3, (J) Br (3d) of ZnL3.	89
3.6	XPS profiles of **(A)** C (1s) of ZnL4, **(B)** N (1s) of ZnL4, **(C)** O (1s) of ZnL4, **(D)** C (1s) of ZnL5, **(E)** N (1s) of ZnL5, **(F)** O (1s) of ZnL5, **(G)** C (1s) of ZnL6, **(H)** N (1s) of ZnL6, **(I)** O (1s) of ZnL6, **(J)** Cl (2p) of ZnL3, **(K)** C (1s) of ZnL7, **(L)** N (1s) of ZnL7, **(M)** O (1s) of ZnL7, **(N)** F (1s) of ZnL7.	90
3.7	TGA thermogram of (a) ZnL1, (b) ZnL2, (c) ZnL3, (d) ZnL4, (e) ZnL5, (f) ZnL6, (g) ZnL7.	94
3.8	LC-MS chromatogram of **(A)** ZnL1, **(B)** ZnL2, **(C)** ZnL3, **(D)** ZnL4, **(E)** ZnL5, **(F)** ZnL6, **(G)** ZnL7.	95
3.9	Optimized structures of **(A)** ZnL1, **(B)** ZnL2, **(C)** ZnL3 and **(D)** ZnL4 are shown in front and side views. Colour scheme: green balls: C, red balls: O, Blue balls: N, small white balls: H.	97
3.10	Structures of **(A)** dimeric complexes and **(B)** monomeric complex with two water molecules used for the synthesis of styrene carbonate.	98
3.11	Solution UV-vis spectrum of **(A)** (a) L1, (b) ZnL1, **(B)** (a) L2, (b) ZnL2, **(C)** (a) L3, (b) ZnL3, **(D)** (a) L4, (b) ZnL4, **(E)** (a) L5, (b) ZnL5, **(F)** (a) L6, (b) ZnL6, **(G)** (a) L7, (b) ZnL7, **(H)** Expansion of MLCT peaks of all complexes.	99
3.12	Calculated TD-DFT spectra for **(A)** ZnL1monomer, **(B)** ZnL1 dimer.	101
3.13	Calculated TD-DFT spectra for **(A)** ZnL2 monomer, **(B)** ZnL2 dimer.	101
3.14	Calculated TD-DFT spectra for **(A)** ZnL3 monomer, **(B)** ZnL3 dimer.	102
3.15	Calculated TD-DFT spectra for **(A)** ZnL4, **(B)** ZnL4 with two water molecules.	102

List of Figures

Figure No.	Figure Caption	Page No.
3.16	Comparison of experimental electronic spectra with DFT calculated TD-DFT spectra of the dimer for **(A)** ZnL1, **(B)** ZnL2, **(C)** ZnL3 and **(D)** Comparison of experimental electronic spectra with DFT calculated TD-DFT spectra ZnL4 with two water molecules.	103
3.17	DOSY NMR of **(A)** ZnL1 and **(B)** ZnL4.	105
3.18	Representative ^{1}H NMR of **(A)** L4, **(B)** ZnL4, **(E)** L5, **(F)** ZnL5, **(I)** L7, **(J)** ZnL7, and representative ^{13}C NMR of **(C)** L4, **(D)** ZnL4, **(G)** L5, **(H)** ZnL5, **(K)** L7, **(L)** ZnL7. The DMSO-d_6 residual peak in ^{1}H NMR appears at 2.5 ppm, and the solvent peak of DMSO-d_6 is at 3.3 ppm. In ^{13}C NMR, the solvent peak appears at 40 ppm. Trace solvent impurities in ^{1}H NMR include acetone at 2.09 ppm and methanol at 3.16 ppm and 4.01 ppm. In ^{13}C NMR, acetone appears at 30.14 ppm and methanol at 48.59 ppm.	109-114
3.19	**(A)** Reaction mechanism for the catalytic cycle. **(B)** The calculated Gibbs free energy profile diagram for ZnL1, ZnL3 and ZnL4 in monomeric state. along with the intermediates and activation free energies (E_a) marked.	116
3.20	The structure of Complex 1.	120
4.1	SEM images of **(A)** Zeolite NH_4^+ZSM-5, **(B)** Al-MCM-41, **(C)** Zeolite Na-Y.	129
4.2	XRD spectrum of the catalysts **(A)** Zeolite NH_4^+-ZSM-5 **(B)** Al-MCM-41 **(C)** Zeolite Na-Y.	130
4.3	FT-IR spectra of the catalysts **(A)** Zeolite NH_4^+-ZSM-5 **(B)** Al-MCM-41 **(C)** Zeolite Na-Y.	131
4.4	TGA profile of **(A)** Zeolite NH_4^+-ZSM-5 **(B)** Al-MCM-41 **(C)** Zeolite Na-Y	133
4.5	BET isotherms of the **(A)** Zeolite NH_4^+-ZSM-5 **(B)** Al-MCM-41 **(C)** Zeolite Na-Y.	134
4.6	^{29}Si solid-state NMR of zeolite Na-Y.	135
4.7	XPS survey graphs of **(A)** Zeolite NH_4^+-ZSM-5 **(B)** Al-MCM-41 **(C)** Zeolite Na-Y.	136

List of Figures

Figure No.	Figure Caption	Page No.
4.8	XPS profiles of **(A)** Al (2p) of Zeolite NH_4^+-ZSM-5, **(B)** Si (2p) of Zeolite NH_4^+-ZSM-5, **(C)** O (1s) of Zeolite NH_4^+-ZSM-5, **(D)** Al (2p) of Al-MCM-41, **(E)** Si (2p) of Al-MCM-41, **(F)** O (1s) of Al-MCM-41, **(G)** Al (2p) of Zeolite Na-Y, **(H)** Si (2p) of Zeolite Na-Y and **(I)** O (1s) of Zeolite Na-Y.	137
4.9	NH_3-TPD profiles of **(A)** Zeolite NH_4^+-ZSM-5 **(B)** Al-MCM-41 **(C)** Zeolite Na-Y **(D)** Calcined zeolite Na-Y.	140
4.10	Physicochemical properties of calcined zeolite Na-Y showing **(A)** XRD, **(B)** TGA, **(C)** FT-IR, **(D)** BET, **(E)** XPS of Al (2p), **(F)** XPS of Si (2p), and **(G)** XPS of O (1s).	141
4.11	HR-MS spectra of the crude reaction mixture.	144
4.12	^{1}H NMR spectra of the crude reaction mixture.	144
4.13	Recycle studies using zeolite-Na-Y.	145
5.1	Synthesis of zinc encapsulated complexes using flexible ligand approach.	154
5.2	Powder XRD patterns of **(A)** JCPDS reference pattern of zeolite-Y (JCPDS card number 00-043-0168, **(B)** Zeolite Na-Y, **(C)** Zinc(II) exchanged-Y, **(D)** ZnL1-Y, **(E)** ZnL2-Y, **(F)** ZnL3-Y, **(G)** ZnL4-Y.	156
5.3	FESEM images of **(A)** ZnL1-Y before Soxhlet extraction, **(B)** ZnL1-Y after Soxhlet extraction, **(C)** ZnL2-Y before Soxhlet extraction, **(D)** ZnL2-Y after Soxhlet extraction.	157
5.4	FESEM images of **(E)** ZnL3-Y before Soxhlet extraction, **(F)** ZnL3-Y after Soxhlet extraction **(G)** ZnL4-Y before Soxhlet extraction, **(H)** ZnL4-Y after Soxhlet extraction.	157
5.5	FT-IR peaks of **(A)** Zeolite Na-Y, **(B)** Zn(II) exchanged-Y, **(C)** ZnL1-Y, **(D)** ZnL2-Y, **(E)** ZnL3-Y, **(F)** ZnL4-Y (left) and zoomed view of the region 1200-1800 cm^{-1} (right).	159
5.6	TGA thermogram of **(A)** Zeolite Na-Y, **(B)** Zinc(II) exchanged-Y, **(C)** ZnL1-Y, **(D)** ZnL2-Y, **(E)** ZnL3-Y, **(F)** ZnL4-Y.	160
5.7	BET isotherms for **(A)** Zeolite Na-Y, **(B)** Zinc(II) exchanged-Y, **(C)** ZnL1-Y, **(D)** ZnL2-Y, **(E)** ZnL3-Y, **(F)** ZnL4-Y.	162
5.8	XPS survey spectra for **(A)** ZnL1-Y, **(B)** ZnL2-Y, **(C)** ZnL3-Y, **(D)** of ZnL4-Y.	164

List of Figures

Figure No.	Figure Caption	Page No.
5.9	XPS profiles for Zn (2p) for **(A)** ZnL1-Y, **(B)** ZnL2-Y, **(C)** ZnL3-Y, **(D)** ZnL4-Y	165
5.10	XPS profiles for **(A)** C (1s) of ZnL1-Y, **(B)** N (1s) of ZnL1-Y, **(C)** O (1s) of ZnL1-Y, **(D)** Si (2p) of ZnL1-Y, **(E)** Al (2p) of ZnL1-Y, **(F)** Na (1s) of ZnL1-Y, **(G)** C (1s) of ZnL2-Y, **(H)** N (1s) of ZnL2-Y, **(I)** O (1s) of ZnL2-Y, **(J)** Si (2p) of ZnL2-Y, **(K)** Al (2p) of ZnL2-Y, **(L)** Na (1s) of ZnL2-Y.	166
5.11	XPS profiles for **(A)** C (1s) of ZnL3-Y, **(B)** N (1s) of ZnL3-Y, **(C)** O (1s) of ZnL3-Y, **(D)** Si (2p) of ZnL3-Y, **(E)** Al (2p) of ZnL3-Y, **(F)** Na (1s) of ZnL3-Y, **(G)** Br (3d) of ZnL3-Y, **(H)** C (1s) of ZnL4-Y, **(I)** N (1s) of ZnL4-Y, **(J)** O (1s) of ZnL4-Y, **(K)** Si (2p) of ZnL4-Y, **(L)** Al (2p) of ZnL4-Y, **(M)** Na (1s) of ZnL4-Y.	167
5.12	Solid state UV of **(A)** (a) ZnL1-Y, (b) ZnL1, **(B)** (a) ZnL2-Y, (b) ZnL2, **(C)** (a) ZnL3-Y, (b) ZnL3, **(D)** (a) ZnL4-Y, (b) ZnL4.	168
5.13	NH_3-TPD profiles of **(A)** Zeolite Na-Y, **(B)** Zinc(II) exchanged-Y, **(C)** ZnL1-Y, **(D)** ZnL2-Y, **(E)** ZnL3-Y, **(F)** ZnL4-Y.	170
5.14	Recycle studies of the ZnL1-Y complex.	173
6.1	Schematic representation of the synthesized cobalt(II) Schiff-base complexes.	180
6.2	SEM images of **(A)** (a) and (b) CoL1-Y before Soxhlet at different resolutions, (c) and (d) CoL1-Y after Soxhlet at different resolutions, **(B)** PXRD patterns of (a) JCPDS reference of zeolite-Y (card number 00-043-0168), (b) Zeolite Na-Y, (c) Cobalt(II) exchanged-Y, (d) CoL1-Y, (e) CoL2-Y, **(C)** FT-IR spectra of (a) CoL1, (b) Zeolite Na-Y, (c) CoL1-Y, **(D)** BET isotherm of CoL2-Y, **(E)** XPS spectra for cobalt of CoL2, **(F)** XPS spectra for cobalt of CoL2-Y, **(G)** TGA curves of (a) Zeolite Na-Y, (b) CoL1, (c) CoL1-Y, (d) CoL2, (e) CoL2-Y.	183
6.3	Optimized doublet ground-state structures for **(A)** CoL1 and **(B)** CoL2; Optimized triplet ground-state structures for **(C)** CoL1 and **(D)** CoL2; **(E)** The encapsulated and extracted quartet state of CoL1-Y complex **(F)** The encapsulated and extracted quartet state of CoL2-Y complex **(G)** The CoL1 complex is shown encapsulated within model zeolite pore. The C atoms marked by black arrows are considered to measure the angle ∠C-Co-C as reported in Table 6.2.	185

List of Figures

Figure No.	Figure Caption	Page No.
6.4	Solid state UV-vis spectra of **(A)** (a) CoL1, (b) CoL1-Y, **(B)** (a) CoL2, (b) CoL2-Y, **(C)** (a) Experimental CoL1, (b) DFT simulated triplet of CoL1, **(D)** Experimental CoL1-Y, (b) DFT simulated quartet of CoL1-Y, **(E)** (a) Experimental CoL2, (b) DFT simulated triplet of CoL2, **(F)** Experimental CoL2-Y, (b) DFT simulated quartet of CoL2-Y.	191
7.1	Zn(II) salophen complex used for the synthesis of styrene carbonate at 80° C at ~1 atm pressure.	204
7.2	Utilization of commercially available aluminosilicates as catalysts for the synthesis of styrene carbonate from CO_2 and styrene oxide.	205
7.3	Application of "neat" and zeolite-Y encapsulated Zn(II) Schiff base complexes for the synthesis of styrene carbonate.	207
7.4	Application of "neat" and zeolite-Y encapsulated Co(II) Schiff base complexes for the synthesis of styrene carbonate.	208
A1	Calibration curve using zinc standards.	213

List of Schemes

Scheme No.	Scheme Caption	Page No.
1.1	Mechanism of formation of cyclic carbonate *via* the epoxide activation.	10
1.2	Mechanism of formation of cyclic carbonates *via* the CO_2 activation.	11
1.3	Mechanism of formation of cyclic carbonates *via* dual activation.	12
2.1	Synthesis of the Schiff base ligands.	66
2.2	Synthesis of the Schiff base "neat" or free-state metal complexes.	66
2.3	Synthesis of metal exchange zeolite Na-Y.	67
2.4	Synthesis of cyclic carbonates from CO_2 and epoxides using different catalysts.	69
3.1	Synthesis of zinc(II) salophen complexes.	82

List of Abbreviations and Symbols

Abbreviation/ Symbol	Description
α	Alpha
β	Beta
δ	Delta
ΔG^o	Standard Gibbs free energy
θ	Theta
λ	Lambda
ν	Nu
μ_B	Bohr Magneton
μm	Micrometer
φ	Psi
ε	Epsilon
°C	Degree centigrade
3D	Three Dimensional
Å	Angstrom
AAS	Atomic Absorption Spectroscopy
acac	Acetylacetonate
ACN	Acetonitrile
Asymm	Asymmetric
atm	Atmosphere
B3LYP	Becke Lee, Yang and Parr
BE	Binding energy
BET	Brunauer-Emmett-Teller
BINOL	1,1′-Bi-2-naphthol
BJH	Barrett-Joyner-Halenda
BM	Bohr Magneton
bmim	1-Butyl-3-methylimidazolium
bpy	Bipyridyl
Bu_4NCl	Tetrabutylammonium chloride
cat	Catalyst

List of Abbreviations and Symbols

Abbreviation/ Symbol	Description
$CDCl_3$	Deuterated chloroform
CO_2	Carbon dioxide
Co-cat	Co-catalyst
COF	Covalent Organic Framework
CS	Chitosan
DBU	1,8-Diazabicyclo(5.4.0)undec-7-ene
DCM	Dichloromethane
dd	Doublet of doublet
ddd	Doublet of doublet of doublet
DFT	Density Functional Theory
DMAP	4-Dimethylaminopyridine
DMF	Dimethyl formamide
DMSO	Dimethyl sulphoxide
DMSO-d_6	Deuterated dimethyl sulphoxide
DOSY	Diffusion Ordered Spectroscopy
DRS	Diffuse Reflectance Spectroscopy
ECH	Epichlorohydrin
ECHC	Epichlorohydrin carbonate
EDX	Energy dispersive X-ray
ee	Enantiomeric excess
Et_3N	Triethylamine
eV	Electron volts
FAU	Faujasite
FESEM	Field Emission Scanning Electron Microscopy
FID	Flame Ionization Detector
FT-IR	Fourier Transform Infrared
GC	Gas Chromatography
GC-MS	Gas Chromatography-Mass Spectrometry
h	Hour

List of Abbreviations and Symbols

Abbreviation/ Symbol	Description
HOMO	Highest Occupied Molecular Orbital
HR-MS	High Resolution- Mass Spectrometry
HS	High spin
Hz	Hertz
J	Coupling constant
JCPDS	Joint Committee on Powder Diffraction Standards
KBr	Potassium bromide
kcal	Kilocalorie
KI	Potassium iodide
kJ	Kilojoules
L1	*N, N'*-bis(salicylidene)-1,2-phenylenediamine
L2	*N, N'*-bis(5-methoxysalicylidene)-1,2-phenylenediamine
L3	*N, N'*-bis(5-bromosalicylidene)-1,2-phenylenediamine
L4	*N, N'*-bis(5-nitrosalicylidene)-1,2-phenylenediamine
L5	*N, N'*-bis(5-methylsalicylidene)-1,2-phenylenediamine
L6	*N, N'*-bis(5-chlorosalicylidene)-1,2-phenylenediamine
L7	*N, N'*-bis(5-(trifluoromethoxy)salicylidene)-1,2-phenylenediamine
LC-MS	Liquid Chromatography-Mass Spectrometry
LS	Low spin
LUMO	Lowest Unoccupied Molecular Orbital
M	Molar
m	Multiplet
MCM-41	Mobil Composite Material-41
MHz	Mega hertz
MLCT	Metal to Ligand Charge Transfer
MOF	Metal organic framework
mmol	millimoles
mol%	Mole percentage

List of Abbreviations and Symbols

Abbreviation/ Symbol	Description
MPa	Mega pascal
NaCl	Sodium chloride
Na-Y	Sodium zeolite-Y
NH_3-TPD	Ammonia- Temperature Programmed Desorption
NMR	Nuclear Magnetic Resonance
OAc	Acetate group
PC	Propylene carbonate
Pc	Phthalocyanine
PhBr	Bromobenzene
Phen 1,10	1, 10-Phenanthroline
PPh_3	Triphenylphosphine
PO	Propylene oxide
PPNCl	Bis(triphenylphosphoranylidene)ammonium chloride
PPNF	Bis(triphenylphosphoranylidene)ammonium fluoride
PTAT	Phenyltrimethylammonium tribromide
PXRD	Powder X-ray diffraction
RT	Room temperature
s	Singlet
Salen	Salicylidene ethylenediamine
Salophen	Salicylidene phenylenediamine
SBA-15	Santa Barbara Amorphous-15
sc	Super critical
SC	Styrene carbonate
SD	Standard Deviation
Si/Al	Silicon-to-Aluminium ratio
SO	Styrene Oxide
Str	Structure
Symm	Symmetric
T	Si or Al in aluminosilicate

List of Abbreviations and Symbols

Abbreviation/ Symbol	Description
t	Triplet
t	Tertiary
TBAB	Tetrabutylammonium bromide
TBACl	Tetrabutylammonium chloride
TBAI	Tetrabutylammonium iodide
TBHP	Tertiary Butyl Hydrogen Peroxide
^{t}Bu	Tertiary butyl group
TD-DFT	Time-Dependent Density Functional Theory
TEABr	Tetraethylammonium bromide
TEM	Transmission Electron Microscope
TGA	Thermo Gravimetric Analysis
TMPyP	5,10,15,20-Tetrakis(1-methyl-4-pyridinio)porphyrin tetra(p-toluenesulfonate)
TOF	Turn Over Frequency
Tol	*p*-tolyl group
TON	Turn Over Number
TPAB	Tetrapropylammonium bromide
UHV	Ultra-High Vacuum
UV-vis	Ultraviolet-Visible
wt%	Weight percent
XPS	X-ray Photoelectron Spectroscopy
ZIF	Zeolite Imidazole Framework
ZSM-5	Zeolite Socony Mobil–5

Chapter 1

Introduction

1.1 Introduction

To accomplish the goal towards a sustainable society, it is crucial to employ renewable energy resources. It can be argued that carbon dioxide, CO_2, is one of the cheapest and the most abundant renewable resources. However, being a greenhouse gas, CO_2 is also responsible for global climate change. According to the Intergovernmental Panel on Climate Change (IPCC), the atmospheric CO_2 concentration, which was about 280 ppm in the early 1800s, reached 410 ppm in April 2018 and has been predicted to almost double by 2100.[1] Hence, reducing CO_2 levels in the atmosphere has gained immense attention of the scientific community in the past few years. In this direction, researchers have developed three main ways to reduce atmospheric CO_2: (i) controlled emissions of CO_2, (ii) CO_2 capture and storage, and (iii) chemical conversion and utilization of CO_2. Although all the above-said methods are efficient ways of regulating atmospheric CO_2, the chemical society is generally interested in the chemical conversion of CO_2. CO_2 is a non-toxic, cheap, and readily available synthon, which is used as a C1 source for the production of a large number of industrially important chemicals. One such chemical is cyclic carbonate, generally formed by the cycloaddition reaction of epoxide and CO_2 in the presence of a catalyst and generally a nucleophilic co-catalyst. Apart from being a 100% atom economic reaction, the synthesis of organic cyclic carbonates is valuable because of their numerous industrial applications. Cyclic carbonates are the precursors for polycarbonates, which have optical transparency and outstanding impact resistance and are used to manufacture CDs, DVDs, aircraft windows,[2] etc. Cyclic carbonates have significant relevance in the industrial sector as electrolyte solvents for lithium batteries, polar aprotic solvents, solvents in the production of pharmaceuticals, degreasers, and fuel additives.[3] Therefore, it is necessary to design simple and efficient catalysts that activate the chemically inert and thermodynamically stable CO_2 (ΔG_f° = -394.4 kJ/mol)[4] and produce value-added chemicals such as cyclic carbonates.

Apart from the reaction conditions, the choice of catalyst is crucial for any reaction as it plays an important role in lowering the activation energy barrier. Likewise, the synthesis of cyclic carbonate from CO_2 and epoxides requires the use of a catalyst. A co-catalyst, which plays a dual role as the nucleophile and the leaving group, is also used in most cases. A few broad categories of catalysts that have been previously used to achieve this transformation include homogeneous metal-based complexes,[5] ionic liquid-based complexes,[6] organocatalysts,[7] heterogeneous silica-

based catalysts,[8] organic polymer-based catalysts, metal-organic framework (MOF),[9] covalent organic framework (COF),[10] metal oxides,[11] and zeolite imidazolate framework (ZIF).[12]

Prominently known for their exceptional catalytic activity, the N_2O_2 coordinated Schiff base metal complexes have the unique ability to stabilize different metals in various oxidation states and, hence, control the performance of the metal towards various catalytic transformations. A straightforward synthetic approach usually favours the Schiff base complexes as the ideal choice of catalysts. In the case of cycloaddition reactions, there is evidence of the metal complex activating the epoxide[13] in some instances and the CO_2[14] in others. Typically, the Lewis acidic metal complex activates the epoxide through M-O coordination, followed by the nucleophilic attack and the subsequent ring opening. On the other hand, for CO_2 activation, the Lewis basicity of the terminal oxygen atom or the weak Lewis acidity of the central carbon is exploited by the catalyst.

In the pursuit of sustainable catalysts, heterogeneous catalysts play a significant role in the field of catalysis. Simple catalyst separation and reusability are the prime advantages of a heterogeneous catalyst. The development of a heterogeneous catalyst can be categorized into three broad ways: (i) using solid material that has intrinsic catalytic activity, (ii) immobilizing a catalytically active unit onto a solid support, and (iii) immobilizing the solid with intrinsic catalytic activity onto catalytically active solid support. Silicon and aluminium-based microporous and mesoporous aluminosilicates like zeolite-Y, ZSM-5, and MCM-41 have potential applications as heterogeneous catalysts in many organic transformations. The variable Si/Al ratio of these aluminosilicates renders them with inherent acidity, making them an ideal candidate for the cycloaddition reaction. MCM and ZSM are also used as solid support for the heterogenization of a homogeneous catalyst. In contrast, the supercage of zeolite-Y has a suitable size (12.7 Å) that allows small organic molecules of appropriate dimensions to fit within it, leading to heterogenization. The process, known as encapsulation, leads to a change in the electronic and structural properties of the guest complex, providing the complex with unique catalytic activity.

With the above background, the present thesis aims to explore various homogeneous and heterogeneous catalysts for the synthesis of cyclic carbonate from CO_2 and epoxides. Homogeneous zinc(II) and cobalt(II) Schiff base complexes have been studied as catalysts for the cycloaddition reaction. The primary emphasis is on the role of the substituent at the 5, 5’ position of the complex. The reaction of the Schiff base ligand with the metal salt leads to complex

formation. The Schiff base ligands are synthesized using the simple condensation reaction of substituted hydroxybenzaldehyde and 1,2-phenylene diamine. The Schiff base ligands with the general names *N, N'*-bis(salicylidene)-1,2-phenylenediamine (L1), *N, N'*-bis(5-methoxysalicylidene)-1,2-phenylenediamine (L2), *N, N'*-bis(5-bromosalicylidene)-1,2-phenylenediamine (L3), *N, N'*-bis(5-nitrosalicylidene)-1,2-phenylenediamine (L4), *N, N'*-bis(5-methylsalicylidene)-1,2-phenylenediamine (L5), *N, N'*-bis(5-chlorosalicylidene)-1,2-phenylenediamine (L6), and *N, N'*-bis(5-(trifluoromethoxy)salicylidene)-1,2-phenylenediamine (L7), are used. The successful synthesis of the complexes and their purity is investigated using different techniques such as NMR (Nuclear magnetic resonance), LC-MS (Liquid chromatography-mass spectrometry), FT-IR (Fourier transform infrared spectroscopy), XPS (X-ray photoelectron spectroscopy), UV-vis (Ultraviolet-visible spectroscopy) and TGA (Thermogravimetric analysis).

Further, heterogeneous aluminosilicates with different Si/Al ratios have been used as catalysts. The inherent acidity of the aluminosilicates, measured by NH_3-TPD (Temperature programmed desorption), plays a vital role in the cycloaddition reaction along with the co-catalyst. The aluminosilicates include commercially available zeolite Na-Y, NH_4^+-ZSM-5 and synthesized Al-MCM-41. In addition, towards heterogenization, the zinc and cobalt complexes with the above-mentioned ligands are encapsulated in the supercage of zeolite-Y. The encapsulation is carried out *via* the flexible ligand approach, wherein the metal-ions present in metal-exchanged zeolite-Y and the corresponding ligands react together. The encapsulation is confirmed by indirect methods, including PXRD (Powder X-ray diffraction), FESEM (Field emission scanning electron microscopy), BET (Brunauer-Emmett-Teller) surface analysis, XPS and solid-state UV-vis spectroscopy, in addition to FT-IR and TGA analysis. The encapsulation renders the complexes with different structural and electronic changes, which causes the difference in the activity of the complexes. The encapsulation also enforces the dimeric neat Zn-complexes to acquire the monomeric form, which leads to site isolation and, subsequently, different activity than the corresponding neat complexes. The following sections will focus on the details of the existing catalysts used for the synthesis of cyclic carbonates. Particular emphasis will be given to various categories of the catalysts used, including the Schiff base type complexes, aluminosilicates, and metal encapsulated complexes, to comprehend the mechanism in more detail. This acquired knowledge will pave the route to achieving the most efficient capture of CO_2 and its conversion into cyclic carbonates.

1.1.1 Carbon Dioxide as a synthon

CO_2 is the fourth most abundant gas, constituting 0.04% of the Earth's atmosphere. It plays a crucial role in regulating the Earth's temperature by absorbing harmful infrared radiation. However, an imbalance in the natural levels of CO_2 due to human-induced activities like deforestation, industrialization, and over-exploitation of fossil fuels has led to major environmental concerns like the greenhouse effect and ocean acidification. Figure 1.1 clearly indicates that since the beginning of the industrial revolution in the 1950s, the increase in atmospheric CO_2 (blue line) has been analogous with human emissions (grey line). Intergovernmental Panel on Climate Change (IPCC) has predicted that CO_2 concentration might double by the 2100s.

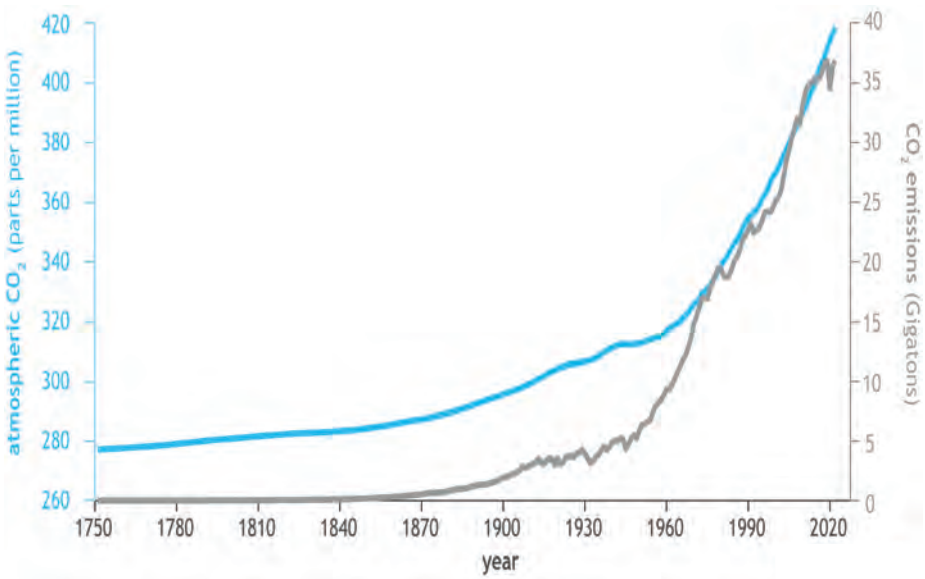

Figure 1.1: Global atmospheric CO_2 compared to annual emissions (1751-2022).[15]

While on the one hand, the greenhouse effect leads to an increase in the global temperature; on the other hand, ocean acidification affects the oceanic biosystems. CO_2 is also considered an industrial waste released directly into the atmosphere along with other harmful compounds like SO_x and NO_x. Hence, using renewable energy resources such as wind, water and solar energy and reducing CO_2 concentrations are the solutions towards sustainability. As mentioned earlier, for the chemical society, the most efficient way of upcycling CO_2 is the valorisation of CO_2 into more valuable chemicals and fuels. Being abundant and non-toxic, the applicability of CO_2 in reactions which directly utilize it as a C1 source is significant.

1.1.1.1 Stability of CO_2

At room temperature, CO_2 is an odourless and colourless gas with high thermodynamic stability, having a standard enthalpy of formation ΔG_f° value of -394.4 kJ/mol. The carbon present in its most oxidised form results in its high stability. The bond dissociation energy of the C=O bond in CO_2 is 750 kJ/mol.[16] This value is higher than the dissociation energy for C=O, C=C and C-H, which are 743 kJ/mol (in formaldehyde), 721 kJ/mol (in ethene) and 432 kJ/mol (in methane), respectively.[17] As a result of its high stability, CO_2 is not very reactive, and a substantial amount of energy is required to transform it into useful chemicals.

1.1.1.2 Reactions with CO_2

The high energy demand for the activation of CO_2 has rendered the commercial production of only a few chemicals which utilize CO_2 as a C1 source. To overcome this challenge, commercially produced chemicals such as urea, salicylic acid, methanol, dimethyl carbonate (DMC), and cyclic carbonates utilize CO_2 at high temperatures and pressures. These harsh reaction conditions and subsequent energy consumption can be refrained by introducing a catalyst that can efficiently and effectively activate CO_2. Presently, the synthesis of urea is carried out by the reaction of ammonia with CO_2 at 12.5-25 MPa and 170-220 °C.[18] The reaction of phenol and CO_2 at 125 °C and 4-7 atm in a strongly basic medium produces salicylic acid.[19] DMC is produced by the reaction of methanol with CO_2 at 190 °C and 40 bar.[20] Bulk production of around 100 million tons of methanol takes place annually by utilizing 2 million tons of CO_2. A few other reactions possible using CO_2 as a C1 source are shown in Figure 1.2.[16] Amongst these reactions, the pivotal point of the present thesis is the focus on the development of homogeneous and heterogeneous catalysts for the synthesis of cyclic carbonates.

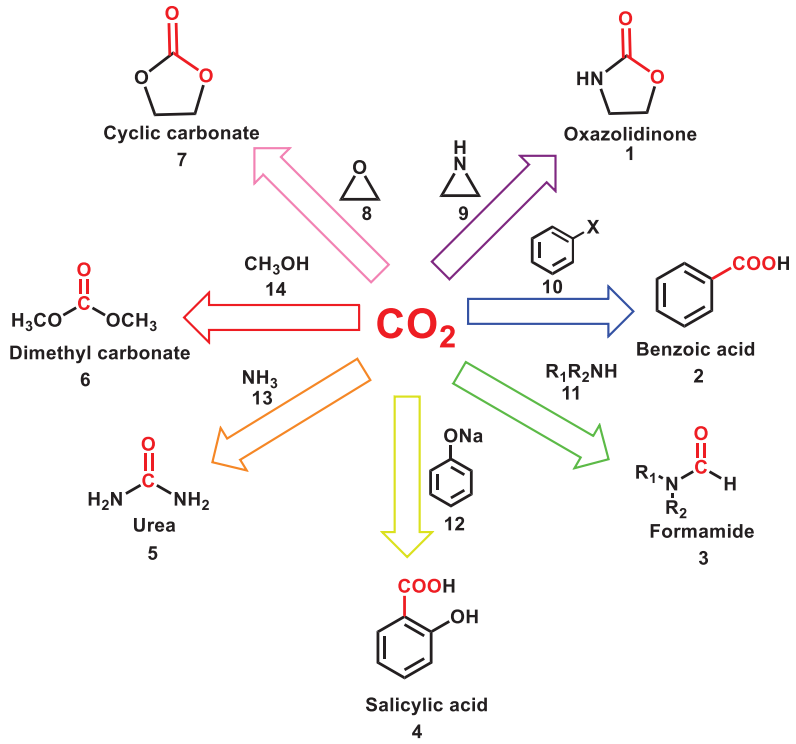

Figure 1.2: A few representative examples of a few reactions possible using CO_2 as a synthon.

1.1.2 Mechanisms of cyclic carbonate synthesis

The conversion of CO_2 to cyclic carbonates is of great interest due to its benefits in the upcycling of CO_2 and the added value of the cyclic carbonate product. The present thesis emphasises on the different catalysts used in the cycloaddition reaction. To comprehend the impact of the catalyst, it is essential to gain a-cut-above understanding of the mechanism of the reaction. In general, the mechanism of the insertion of CO_2 into epoxide falls into three broad categories.

i. Activation of the epoxide: Requiring a Lewis/Brønsted acid to activate the epoxide, followed by the attack of a base/nucleophile for the ring opening of the epoxide and then CO_2 insertion.[21, 22] (Scheme 1.1)

ii. Activation of the carbon dioxide: Requiring a base/nucleophile which is nucleophilic only to CO_2 and not to epoxide, followed by ring opening of the inactive epoxide by the activated CO_2.[23, 24] (Scheme 1.2)

iii. Dual activation of both epoxide and CO_2: Requiring acid and base, wherein CO_2 and epoxide are activated by the acid and base, respectively, followed by the attack of the activated CO_2 on the activated epoxide, leading to the ring opening.[25, 26] (Scheme 1.3)

A given reaction can be driven to any of the pathways with the choice of catalyst and the co-catalyst (if present).[3] A Lewis or Brønsted acid is required if the epoxide is to be activated, and to activate the CO_2, the presence of a base becomes important. Metal-based catalysts generally act as Lewis acids. On the other hand, hydrogen bond donors (HBD), acting as Brønsted acid, bind with the oxygen atom through hydrogen bond, thus polarizing the C-O bond of the epoxide. HBD catalysts comprise the recently developed silica-based catalysts having -OH groups and the catalysts having -NH group or the -COOH group.[27] On the other hand, there are two main types of bases or co-catalysts used for the cycloaddition reaction: (i) Carbene and nitrogen-based bases like DMAP, guanidines and amidines (Lewis base) and, (ii) Halide containing bases like quaternary ammonium halides (Bu_4NX) and metal halides (MX) (Brønsted base). In general, DMAP is used as a co-catalyst for the dual activation mechanism; carbene, guanidines and amidines are used as catalysts for the CO_2 activation pathway, while the ammonium salts and metal-based bases such as TBAB, TBAI and KI acts as a nucleophile/co-catalyst for the epoxide activation.

1.1.2.1 Epoxide activation

In the epoxide activation pathway, the epoxide is activated by the Lewis/Brønsted acid, and the nucleophile (from the co-catalyst or anionic part of the acid) attacks the less sterically hindered β-C of the epoxide to open the ring, forming the haloalkoxide intermediate, **17**. The formed alkoxide reacts with CO_2 to form the carbonate intermediate, **19**, which undergoes intramolecular (5-exo-tet cyclisation) ring closing to form the cyclic carbonate, **20**. (Scheme 1.1)

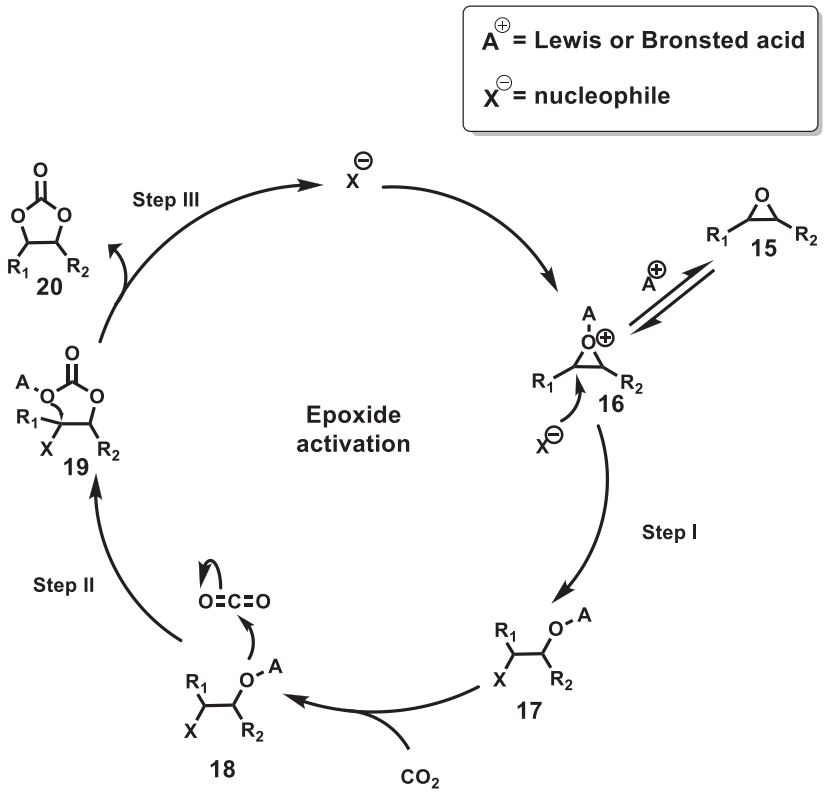

Scheme 1.1: Mechanism of formation of cyclic carbonate *via* the epoxide activation.[8]

One important aspect of this mechanism is that the same carbon undergoes two substitution reactions (step I and step III). Generally, the first substitution follows the S_N2 mechanism and, hence, takes place at the least-hindered carbon of the epoxide. The second is an intramolecular substitution. Both these reactions occur with the inversion of the stereochemistry, hence maintaining the retention of the stereochemistry of the epoxide. In this mechanism, metal-based catalysts act as the Lewis acid, while organocatalysts generally behave as the Brønsted acid. The nucleophile is most commonly a halide, which may be part of the Lewis/Brønsted acid catalyst or maybe from a tetraalkylammonium salt.

1.1.2.2 CO_2 activation

In the CO_2 activation, the catalyst reversibly reacts with CO_2, forming a carboxylate ion, **21**, which acts as a nucleophile to the epoxide. This nucleophilic attack of the epoxide leads to the ring opening. Subsequent ring-closing produces the desired cyclic carbonate. (Scheme 1.2)

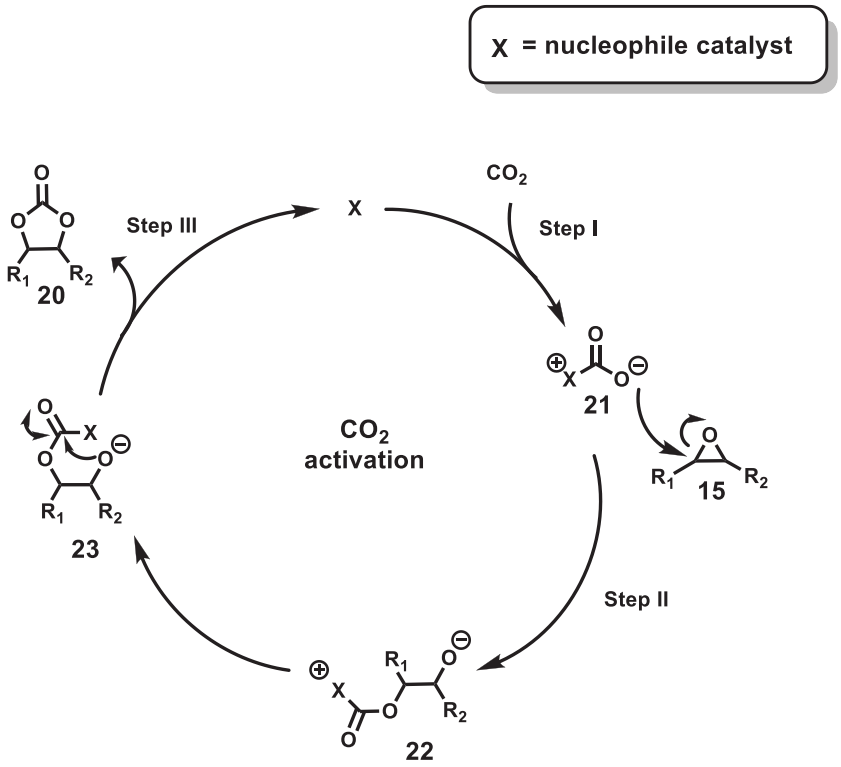

Scheme 1.2: Mechanism of formation of cyclic carbonates *via* the CO_2 activation.[8]

In this mechanism, the most common catalysts are the organic bases, including DMAP, tertiary amines, guanidines and amidines. This mechanism differs from the epoxide activation by virtue of the stereochemistry of the product. This mechanism accompanies the inversion in the stereochemistry of the product.

1.1.2.3 Dual activation

In the dual activation pathway, the epoxide is activated by the Lewis/Brønsted acid, and the nucleophile activates the CO_2, making it more nucleophilic. This nucleophile then attacks the epoxide to open the ring. Finally, the closing of the ring takes place to form the required product.[28]

The Lewis acid and the nucleophile can be part of the same catalyst[25] or be distinct species.[29] This mechanism generally leads to the inversion of the stereochemistry of the product.

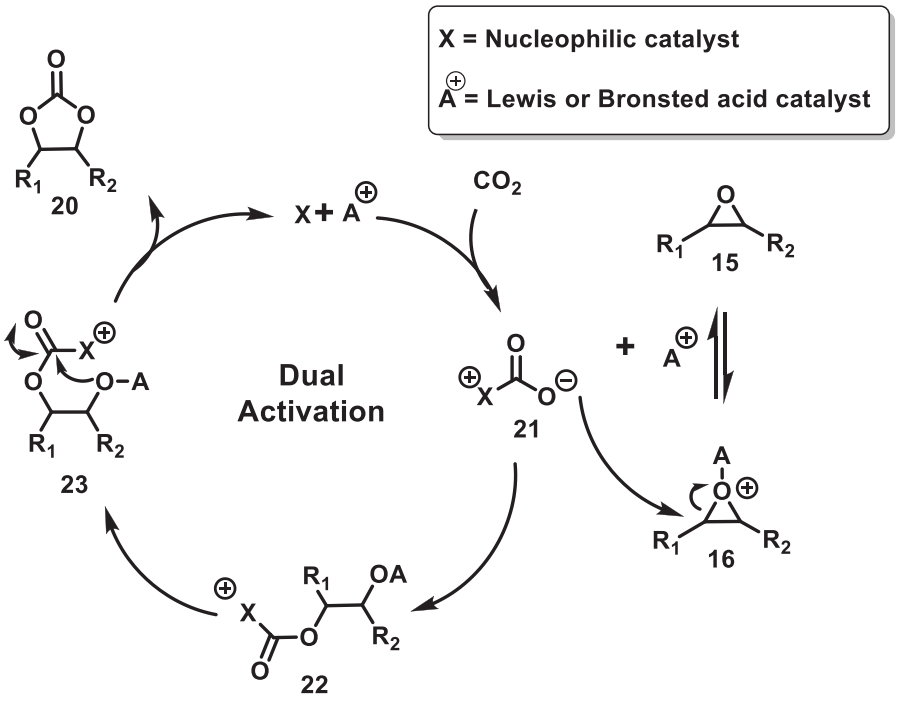

Scheme 1.3: Mechanism of formation of cyclic carbonates *via* dual activation.[8]

1.1.3 Homogeneous Schiff base complexes as catalysts for cyclic carbonate synthesis

Since their discovery, N_2O_2 coordinating Schiff base ligands and their complexes have exhibited utility as catalysts, dyes, polymer stabilizers, and organic synthesis intermediates. These "privileged" ligands and their complexes have been particularly explored in the fields of catalysis for organic transformations,[30] analytical chemistry,[31] and corrosion inhibitors,[32] photo-luminescence,[33] microelectronics,[34] optoelectronics[35] and biological sensors.[36] These complexes also show important applications in the field of biology as antibacterial,[37] antitumor,[38] antifungal,[39] antioxidant,[40] anti-inflammatory,[41] antimalarial,[42] and antiviral agents.[43] Hence, it can be surmised that with such prolific applications in various fields, these complexes can also be utilized as catalysts for the cycloaddition reaction of CO_2 and epoxide.

1.1.3.1 Versatile nature and activity of Schiff base transition metal complexes

Two of the most studied N_2O_2 coordinating Schiff base ligands, namely salen and salophen ligands, are formed by the simple condensation of salicylaldehyde (or its derivatives) with ethylene diamine (salen) or phenylene diamine (salophen). N_2O_2 Schiff base ligands, also called auxiliary ligands, generally have four free-coordinating sites and two axial sites open to ancillary ligands.[44] These are called auxiliary ligands because of their ability to control the structure and the reactivity of the metal ion while they themselves do not undergo irreversible transformations.[45] The donor atoms, i.e., nitrogen and oxygen, can exert two opposite electronic effects. The phenolic oxygen, being a hard donor, stabilizes the metal present in higher oxidation. On the other hand, nitrogen, being a soft donor, stabilizes metals in the lower oxidation state.[46] Complexation modifies the steric and electronic environment of the metal, leading to stabilization and regulation in the activity, especially of the metal ions at higher oxidation states. The structure of these complexes can also be tuned according to the accessibility of the catalytic sites based on the lability of the ligand system and the metal center.[47]

These ligands and their complexes are known for their versatility and wide range of applicability. In fact, salophen has an inherent precedence over its salen analogues because of the extended π-conjugation provided by the phenyl ring. The π-conjugation enables salophen to have more tuneable photophysical properties and provides a rigid geometry around the metal center, which in turn leads to the enhancement of properties like Lewis acidity and hence, improved reactivity of the complex.[48] This enhanced acidity plays a crucial role in cycloaddition reactions that are catalysed in the presence of a Lewis acid catalyst.

1.1.3.2 Schiff base transition metal complexes as catalysts for upcycling CO_2

Schiff base transition metal complexes have been explored as catalysts for polymerization reactions, oxidation and reduction reactions, aldol reactions, epoxidation reactions, and Henry reactions. In addition, these complexes have also been utilized for the production of various compounds that use CO_2 as the C1 source. Upcycling of CO_2 includes reactions like cycloaddition of CO_2 to epoxide, oxazolidinones form aziridines, oxidative carboxylation of alkenes, reductive formylation of amines, and carboxylation of aryl halides, etc. (shown in Figure 1.3) Schiff base complexes including phthalocyanine, porphyrins, salen and salophen complexes have shown good catalytic activities for these reactions.

One of the earliest reports described for the formation of oxazolidinones using Schiff base metal complex in 2004 was by Nguyen *et al.*,[49] wherein they utilized chromium (III) salen complex along with DMAP as an effective catalyst system. The same group developed another similar complex and studied the mechanism in detail.[50] Other reports using salen-based complexes include the bifunctional aluminium complex developed by Lu *et al.*[51] in 2014 and the bimetallic aluminium salophen complex designed by Whitewood *et al.* in 2019. [52] In the context of salen/salophen complexes as catalysts for the reductive formylation of amines, Ji *et al.* developed zinc phthalocyanine and salen systems and utilized them successfully as catalysts for the reaction.[53, 54,55]

Another reaction that has been investigated for CO_2 valorisation is oxidative carboxylation. It is the formation of cyclic carbonates directly by the oxidation of alkenes. In 2009, Jing *et al.*[56] reported the formation of cyclic carbonates from alkenes at ambient temperature and low pressure using Ru porphyrin and O_2 as the green oxidant. In 2011, Hu *et al.*[57] reported the formation of cyclic carbonate using $Mo(acac)_2$, using TBHP as the oxidant. In 2015, Ghosh *et al.*[58] developed an approach for cyclic carbonates using a N4 coordinating manganese complex. In 2023, Launay *et al.*[59,60] developed a catalyst similar to the Jacobsen's catalyst. Inspired by the Mukaiyama oxidation, they reported a route for the production of styrene carbonate from styrene.

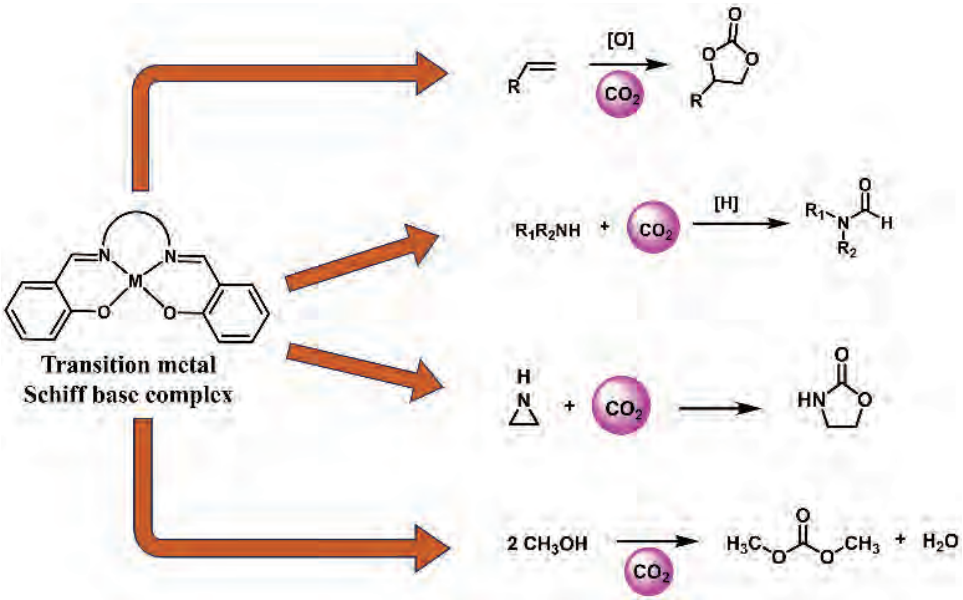

Figure 1.3: Application of Schiff base complex for various reaction using CO_2 as a C1 source.

Although these reports show that cyclic carbonates can be produced using the more stable alkenes compared to epoxides, this approach still suffers from the difficulty of obtaining low yield and low carbonate selectivity. Hence, this present thesis aims to improve the selectivity and yield of the carbonate product by using epoxide as the substrate. The thesis also endeavours to use milder conditions, including lower temperature and pressure, compared to the present literature.

Since the discovery of CO_2 activation using triphenylphosphine-based nickel(0) complexes in 1973,[61] the use of transition metal complexes as catalysts for cyclic carbonate production has witnessed an exceptional growth in the past two decades. In a pioneering work, Inoue *et al.*, in 1983, reported the cyclic carbonate synthesis using a homogeneous metalloporphyrin catalyst,[62] One of the initial works on the conversion of epoxides to carbonates using Schiff base as a metal complex was done by Nguyen *et al.*[63] They reported an efficient and straightforward route for the cycloaddition of CO_2 to epoxides using the Cr(III) salophen catalyst, **24** (shown in Figure 1.4) and dimethylaminopyridine (DMAP) as the co-catalyst. The catalyst could produce up to 100% yields with different epoxides under ambient conditions (6.8 bar, 100 °C, 1 h, 0.075 mol% catalyst, 5.72 × 10^{-2} mol DMAP). They studied the reaction mechanism and reported it to follow the dual activation pathway. Since the discovery of the above-said chromium-based complex, many salen and salophen complexes have been reported for the synthesis of cyclic carbonates. The following section will discuss the application of environmentally benign Schiff base metal complexes used for the synthesis of cyclic carbonates.

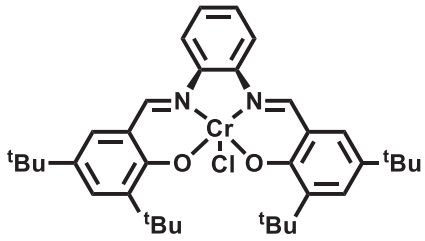

24

Figure 1.4: 1st Schiff base chromium complex used for the cyclic carbonate synthesis from epoxide and CO_2.[63]

1.1.3.3 Schiff base metal complexes of zinc and cobalt as catalysts for the synthesis of cyclic carbonates

There is plethora of reports catalyzed by various Schiff base metal complexes using metals including Nickel (Ni),[64] Cobalt (Co),[65] Iron (Fe),[66] Tin (Sn),[67] Zinc (Zn),[68] Chromium (Cr),[63] Vanadium (V),[69] Manganese (Mn),[70] Aluminium (Al),[71] Copper (Cu),[72] Molybdenum (Mo),[73] Ruthenium (Ru),[74] and Titanium (Ti).[75] The complexes of Zn, Co, Al, and Fe are widely studied owing to their environmental compatibility. Apart from being bio-compatible, these metal complexes also show reasonable catalytic activity, mainly due to their variable oxidation state, tuneable properties, and unique *d*-electronic configurations.

In the context of non-toxic, earth-abundant metals, zinc and cobalt-based salen and salophen-type complexes have been explored as catalysts in the literature. The pioneering work using cobalt-based salen complex was carried out by Nguyen *et al.*, and Darensbourg *et al.*[65] In 2004, Nguyen *et al.*[76] developed the cobalt catalyst, **40.** which showed promising activity towards several substrates, including aliphatic, aromatic, electron-withdrawing and donating epoxides with almost 100% yields. They used two equivalents of DMAP for its dual role. While one equivalent was for coordination with the Lewis acid, facilitating CO_2 insertion, the other equivalent of DMAP acts as a nucleophile to ring open the epoxide. A lot of research has been carried out using cobalt complexes since the report by Nguyen. Zinc, on the other hand, is a metal with inherent Lewis acidity, which is essential in the cycloaddition reaction. The reported zinc Schiff base-type complexes used for the fixation of CO_2 are tabulated in Table 1.1. The cobalt-based salen/salophen and similar systems reported in the literature for the conversion of CO_2 to cyclic carbonates are shown in Table 1.2.

Table 1.1: Catalysts based on zinc salen and salophen-type complexes for cyclic carbonate synthesis

Catalyst [Ref]	Reaction conditions (Yields with respect to styrene oxide)	Remarks
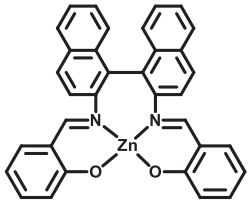 **25** [77]	**Reaction Conditions** 34.4 bar, 100 °C, 16 h, 1 mol% catalyst, 2 mol % Et_3N **Yield** 90%	• First report of use of Zn(II) salen-type complex for cyclic carbonate formation. • Substituted binaphthyl diamino salen-type Zn(II) complexes afforded the cyclic carbonate in lower yields. • In the presence of a large excess of Lewis bases, such as DBU or DMAP, the effectiveness of this reaction was lowered. • The mechanism was based on the epoxide activation pathway.
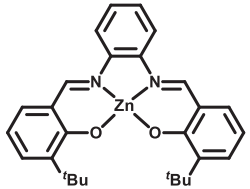 **26** [78]	**Reaction Conditions** 10 bar, 45 °C, 18 h, 2.5 mol% catalyst, 2.5 mol% TBAI **Yield** 66%	• Both the Zn (salophen) and co-catalyst are essential for the activity and the reaction follows the epoxide activation pathway. • The presence of ^{t}Bu assists in maintaining a rigid backbone of the complex, emphasizing the importance of a stable backbone. • The activity against internal epoxides is almost negligible.
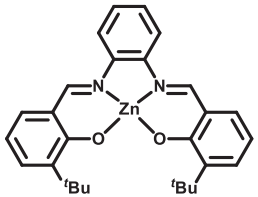 **26** [79]	**Reaction Conditions** 2 bar, 25 °C, 18 h, 2.5 mol% catalyst, 2.5 mol% TBAI **Yield** 15%	• 19 Zn(II) Schiff base complexes with different functionalization at 3, 3' positions and bridging groups were tested and electronic withdrawing groups at the bridging position favour cyclic carbonate production. • The presence of ^{t}Bu at the 3,3' position resulted in good yields, but lack of steric bulk decreased yields. • Effects of different solvents were studied, and 2-butanone was selected as the best solvent owing to its higher local concentration of CO_2.

Catalyst [Ref]	Reaction conditions (Yields with respect to styrene oxide)	Remarks
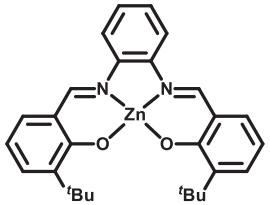 **26** [80]	**Reaction Conditions** 80 bar (sc-CO_2), 45 °C, 3 h, 2.5 mol% catalyst, 2.5 mol% TBAI **Yield** 96%	• A significant increase in the catalytic activity was accomplished in solvent-free and CO_2-rich environment (sc-CO_2) • The coordination of zinc metal and epoxide plays a vital role. • Sterically hindered epoxides and internal epoxides give no conversion.
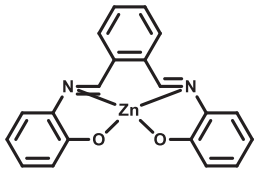 **27** [81]	**Reaction Conditions** 30 bar, 110 °C, 3 h, 0.046 mol% catalyst, 0.11 mol% TBAB **Yield** 92.4% (using propylene oxide)	• An increase in temperature from 70 °C to 110 °C is favourable for converting quaternary ammonium salt into amine, which forms carbamate salt with CO_2 and positively affects the reaction. • There was a significant loss in activity after the 10th cycle, due to the decomposition of some of the TBAB to form tributylamine.
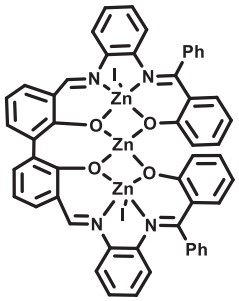 **28** [82]	**Reaction Conditions** 10 bar, 85 °C, 18 h, 2.5 mol% catalyst **Yield** 96% (using glycidyl methyl ether)	• Using the trinuclear bifunctional complexes, the initial step was halide dissociation, followed by epoxide activation. • The catalyst could be recovered and used up to 5 times. • This work showed a highly promising supramolecular approach towards catalyst immobilization.

Catalyst [Ref]	Reaction conditions (Yields with respect to styrene oxide)	Remarks
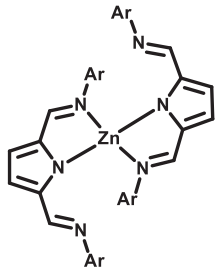 **29** [83]	**Reaction Conditions** 1 bar, 105 °C, 2 h, 2.5 mol% catalyst, 0.5 mol% TBAB **Yield** 80%	• 4 catalysts were prepared, and catalyst **29** was found to be versatile, highly stable and recyclable for 10 cycles. • Reactions were carried at mild reaction temperatures of 30-60 °C, and a 73% yield for internal epoxide, cyclohexene oxide, with *cis* isomer as the major product was obtained. • From time-dependent ^{1}H NMR studies, the diol formation was concluded to be a degradation product of the cyclic carbonate.
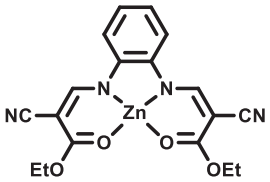 **30** [68]	**Reaction Conditions** 50 bar, 100 °C, 20 h, 0.2 mol% catalyst, 0.2 mol% TBAI **Yield** 99% (using Propylene oxide)	• The study catalyst is one of the earliest reports involving zinc and an N_2O_2 ligand with amine and ester functions. • Various co-catalysts were tested, and TBAI was found to be the best. • Utilization of co-catalysts containing chloride as a harder Lewis base (PPNCl and Bu_4NCl) led to the formation of pure alternating polycarbonates
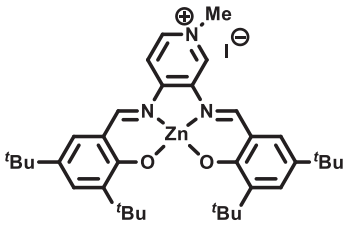 **31** [84]	**Reaction Conditions** 10 bar, 80 °C, 18 h, 0.5 mol% catalyst **Yield** 88%	• The catalyst has a framework that can be alkylated at the pyridyl-N atom, providing a complex with a built-in nucleophile. • The synergistic effect of Lewis acid and the nucleophile improves the catalytic activity.

Catalyst [Ref]	Reaction conditions (Yields with respect to styrene oxide)	Remarks
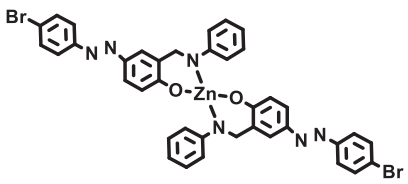 **32** [85]	**Reaction Conditions** 16 bar, 100 °C, 2 h, 0.1 mol% catalyst, 0.2 mol% DMAP **Yield** 2.4%	• Ionic liquid had a positive effect and showed the most active performance with (bmim)PF_6 in presence of **32** as an overall binary catalytic system. • The azo moiety plays an important role in the catalyst
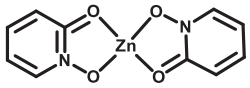 **33** [86]	**Reaction Conditions** 10 bar, 80 °C, 6 h, 0.15 mol% catalyst, 0.5 mol% TBAI **Yield** 97%	• Due to the steric factors, internal epoxides like cyclohexene oxide and isobutylene oxide exhibited lower activity. • The homogeneous catalyst could be recycled up to 5 times. • Polycarbonate formation did not occur.
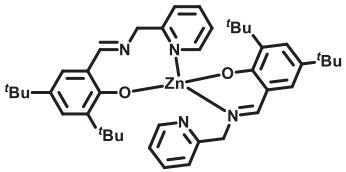 **34** [87]	**Reaction Conditions** 1 bar, 100 °C, 24 h, 0.14 mol% catalyst, 0.2 mol% TBAB **Yield** 71%	• Sterically hindered substrates were transformed selectively at lower conversion than terminal epoxides. • The reaction followed the epoxide activation pathway.

Catalyst [Ref]	Reaction conditions (Yields with respect to styrene oxide)	Remarks
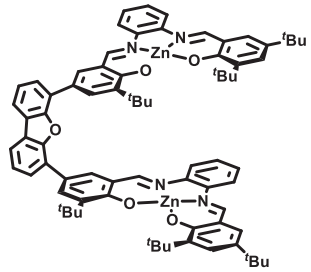 **35** [88]	**Reaction Conditions** 10 bar, 95 °C, 2 h, 0.01 mol% catalyst, 0.5 mol% TBAI **Conversion** 99% (using ethoxyoxirane)	• The catalyst displayed significant activity at low concentrations and produced high turnover frequencies (TOF) per Zn center using a large excess of the co-catalyst and at elevated temperatures.
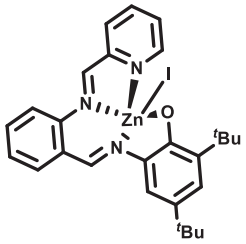 **36** [89]	**Reaction Conditions** 10 bar, 100 °C, 4 h, 0.5 mol% catalyst **Yield** 96%	• Nucleophilic activation of the axial ligand requires a high temperature of 100 °C. • Halide-derivative zinc complexes are the most active leaving groups on the zinc site for the homopolymerization of epoxides. • Small substituents like -OAc allowed CO_2 insertion to form a carbonate intermediate.
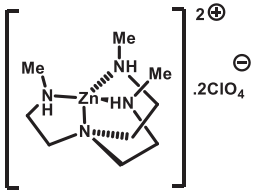 **37** [90]	**Reaction Conditions** 10 bar, 110 °C, 3 h, 0.25 mol% catalyst, 0.4 mol% TBAI **Yield** 75%	• One of the earliest reports of a C3 symmetric N4-chelated Zn complex. • The differences in reactivity followed the nucleophilicity and leaving ability of the halide anions in the tetrabutylammonium salt, i.e., $I^- > Br^- > Cl^-$ • A reaction time of 24 h is necessary to achieve sufficient conversion for the more challenging di-substituted terminal 1,2- epoxy-2-methylpropane and for the sterically hindered cyclohexene and cyclopentene oxides.

Catalyst [Ref]	Reaction conditions (Yields with respect to styrene oxide)	Remarks
38 [91]	**Reaction Conditions** 10 bar, 120 °C, 18 h, 0.033 mol% catalyst, 0.033 mol% TBAI **Yield** 100%	• Oxygen-containing glycidyl phenyl ether and resorcinol di-glycidyl ether with electron-withdrawing groups showed 100% conversion, while ECH and 1-hexene oxide resulted in yields of 16% and 10%, respectively. • The additional oxygen atom adjacent to the epoxide ring in the substrate facilitates the interaction of CO_2 with the catalyst.
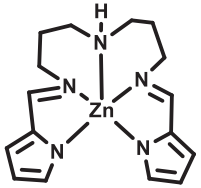 **39** [92]	**Reaction Conditions** 10 bar, 100 °C, 18 h, 1 mol% catalyst, 3 mol% TBAB **Yield** 91%	• The catalytic activity of 4 pyrrole-based Schiff base Zn complex series was tested against 7 different epoxides and related to their Lewis acidity: the more acidic being, the more active. • DFT studies showed that the penta-coordinated N5 ligand in complex **39** prevents the formation of dimeric species.

Table 1.2: Catalysts based on cobalt salen and salophen-type complexes for cyclic carbonate synthesis

Catalyst [Ref]	Reaction conditions (Yields with respect to styrene oxide)	Remarks
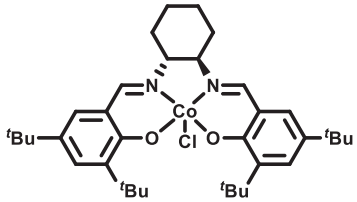 **40** [76]	**Reaction conditions** 20.6 bar, 100 °C, 1.5 h, 1 mol% catalyst, 2 mol% DMAP **Yield** 98%	• First report of cyclic carbonate using cobalt Schiff base complex. • Co(III) was more active than the Co(II) complex, and two equivalents of DMAP were required owing to its dual role. • The epoxide activation pathway was followed, Dual role of DMAP in activating the Lewis acid as well as epoxide ring opening.
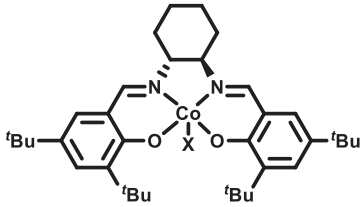 X = O_2CCCl_3 **41** [93]	**Reaction conditions** 0.32-0.35 bar, 25 °C, 2 h, 0.1 mol% catalyst, 0.1 mol% TBAB **Conversion** 48.2% (Using Propylene oxide)	• TBACl was more beneficial for improving the enantiomeric purity of the products, with a pronounced negative effect on the rate. • Enantiomerically pure carbonates were synthesized, obtaining ee values up to 70.2% for PC.

Catalyst [Ref]	Reaction conditions (Yields with respect to styrene oxide)	Remarks
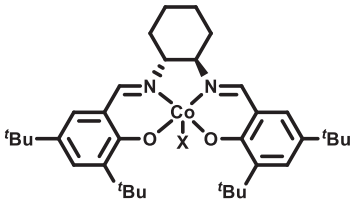 X = $OCOCF_3$ **42** [94]	**Reaction conditions** 1 bar, -20 °C, 18 h, 0.1 mol% catalyst, 0.2 mol% PPNF **Yield** 39% (Using propylene oxide)	• The enantioselectivity of the product formed was studied. • The metal had a pronounced effect on the reaction, and the choice of the counter ion influenced the activity but not the enantioselectivity. • The formation of side products was less.
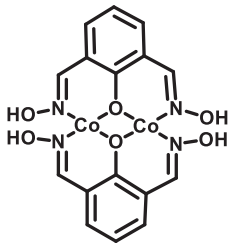 **43** [95]	**Reaction conditions** 6.89 bar, 25 °C, 15 h, 0.01 mol% catalyst, 0.04 mol% PTAT **Yield** 89.3%	• The bi-cobalt complex in the presence of PTAT is an excellent catalyst for CO_2 upcycling. • The reaction conditions used were extremely mild. • The reaction follows the epoxide activation pathway.
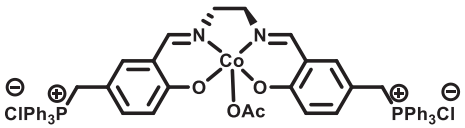 **44** [96]	**Reaction conditions** 40 bar, 100 °C, 2 h, 1 mol% catalyst **Yield** 97%	• A complex containing two functional groups in one molecule, a Lewis acidic metal center, and a quaternary phosphonium salt unit anchored on the ligand was developed. • The presence of axial ligands has a great effect on the catalytic performance. • The catalyst shows low toxicity and unique solubility and is easily recovered and reused at least four times without loss of its catalytic activity.

Catalyst [Ref]	Reaction conditions (Yields with respect to styrene oxide)	Remarks
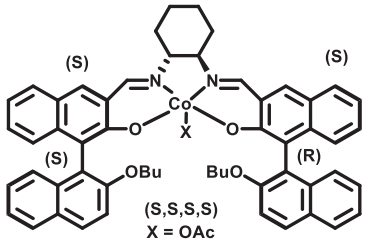 **45** [97]	**Reaction conditions** 5 bar, 0 °C, 48 h, 0.05 mol% catalyst, 0.1 mol% PTAT **Conversion** 5%	• The chiralities of BINOL-frame and the backbone of the Schiff base have some synergic effects. • The same absolute configuration has a positive effect, giving a higher ee value of propylene carbonate. Conversely, the opposite absolute configuration has a negative effect, giving a lower ee value of propylene carbonate. • 5 different epoxides were tested with good enantiomeric excess.
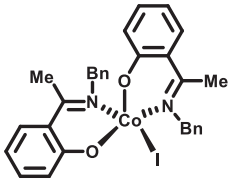 **46** [98]	**Reaction conditions** 10 bar, 145 °C, 1 h, 0.1 mol% catalyst, 0.6 mol% TBAB **TOF** 640 h^{-1}	• The Co(III) complex **46** co-catalyzed with Bu_4NBr produced only cyclic carbonate, while with DMAP, minor traces of oligomers were formed along with cyclic carbonate. • 5 epoxides were studied, with TON reaching up to 760. • The reaction mechanism was reported to follow epoxide activation pathway.
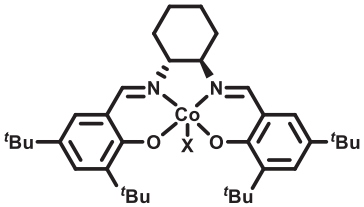 **47** [99]	**Reaction conditions** 6.67 bar, 40 °C, 24 h, 0.2 mol% catalyst, 0.4 mol% of **48** **Yield** **56%** 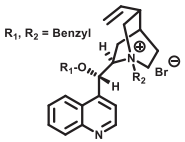 **48**	• The anions of the catalyst and co-catalyst affect the activity and the enantioselectivity of the reaction. • The structure of the co-catalyst also influences the activity of the reaction. • The mechanism follows the epoxide activation pathway.

Catalyst [Ref]	Reaction conditions (Yields with respect to styrene oxide)	Remarks
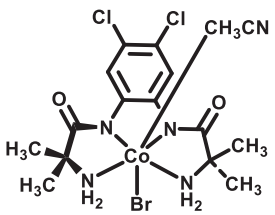 **49** [100]	**Reaction conditions** 20.6 bar, 130 °C, 5 h, 0.1 mol% catalyst, 0.2 mol% DMAP **Yield** 71%	• A new class of cobalt complexes bearing various substituents were prepared and characterized. • Improved catalytic activity was observed with high Lewis acidic metal complexes bearing electron-withdrawing groups. • Both cobalt(III) catalyst and DMAP in a 1 : 2 molar ratio are necessary to obtain high catalytic activity.
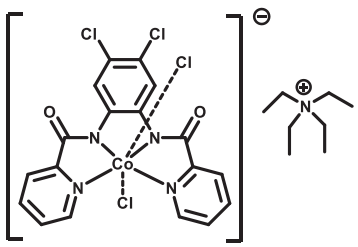 **50** [101]	**Reaction conditions** 50 bar, 80 °C, 20 h, 0.2 mol% catalyst **Conversion** 60%	• 8 epoxides were screened for the activity. • Internal epoxide like cyclohexene oxide gave a good conversion of 76% • The catalyst could not convert epoxide with bulky substrates on both sides. • The catalyst could be recycled up to 5 times with no loss in activity.
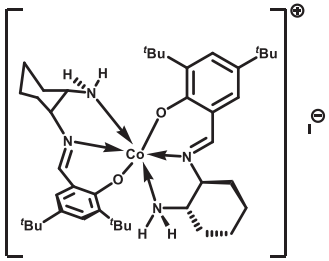 **51** [102]	**Reaction conditions** 50 bar, 50 °C, 24 h, 2 mol% catalyst **Yield** 85%	• The mechanism follows epoxide activation, where the complex activates the epoxide through hydrogen bonding. • 7 epoxides were tested for the scope. • The catalyst could be recycled up to 4 times.

Catalyst [Ref]	Reaction conditions (Yields with respect to styrene oxide)	Remarks
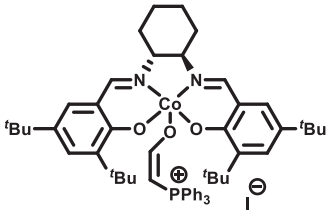 **52** [103]	**Reaction conditions** 1 bar, 25 °C, 36 h, 1 mol% catalyst, 1 mol% co-cat **Yield** 95%	• A phosphorane co-catalyst activates the complex. • It enhanced the Lewis acidity of the Co(III) center for electrophilic activation by generating an iodide to facilitate the ring-opening of the epoxide.
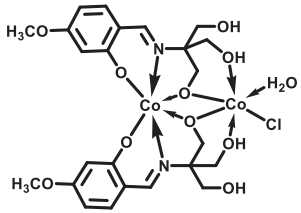 **53** [104]	**Reaction conditions** 1 bar, 120 °C, 8 h, 0.1 mol% catalyst, 0.1 mol% TBAB **Conversion** 94%	• The reaction follows the epoxide activation mechanism. TBAB was found to be the best amongst several other co-catalysts. • 11 epoxides with different substituents were tested with the catalyst, and most epoxides provided conversions up to 100%. • The catalyst showed good stability and could be used up to 5 cycles.

Inspired by the above reports, we observe that there is scope to synthesize simple homogeneous salophen complexes of zinc and cobalt metals and to study them for their potential application for the valorization of CO_2 by its cycloaddition with epoxides. There are limited reports which use mild conditions for the reaction.[57, 93] Rather, there are reports using pressure as high as 50 bar and temperatures up to 145 °C.[51, 91] The use of salen and salophen-based catalysts for reactions using CO_2 as the synthon has also inspired researchers to keep improving the already existing metal-based catalysts. Thus, in this present thesis, we focus mainly on cobalt and zinc Schiff base complexes, which not only effectively catalyse the cycloaddition reaction but also open the way towards sustainable and green chemistry. Hence, with our objective towards sustainability, there is a possibility of employing milder temperatures and pressures for cyclic carbonate synthesis using environmentally compatible metals with substantial Lewis acid characteristics.

1.1.4 Heterogeneous aluminosilicates as catalysts for cyclic carbonate synthesis

Homogeneous Schiff base complexes are attractive as robust catalysts, though they still suffer from drawbacks and disadvantages of often being irrecoverable from the reaction mixture. In some cases, homogenous complexes also suffer from drawbacks such as harsh reaction conditions,[105, 106] high catalyst loading[107] and metal content.[108] This has led to the development of heterogeneous catalysts, which, besides having better recyclability, promote environmentally benign catalytic processes and have a better and more efficient catalytic activity than their homogeneous counterparts. Inorganic heterogeneous catalysts have become a fascinating choice for upcycling CO_2 owing to their superior functionality, simple preparation, and the advantage of using aqueous media, avoiding organic solvents.[109] Some of the heterogeneous catalysts used for the cycloaddition reaction include encapsulated metal complexes, metal-organic frameworks (MOFs), covalent-organic frameworks (COFs), zeolite imidazole frameworks (ZIFs), organic polymers, silica-based catalysts, and metal oxides. All these catalysts show superior activities when compared with the homogenous catalysts. Hence, it is vital to prepare heterogeneous catalysts that are cost-effective, easy to synthesize, and efficient.

Porous aluminosilicates are one of the naturally occurring, abundant, and promising materials that can act as catalysts with adequate competence. These widespread minerals account for about 50% of the mass of Earth's crust.[110] They are generally porous materials with tuneable

chemical and physical properties, which render them with the requisite characteristics of a heterogeneous catalyst.

1.1.4.1 What are aluminosilicates?

Aluminosilicates are a family of compounds containing aluminium (Al), silicon (Si) and oxygen (O) atoms in their chemical composition. These materials comprise anionic Si-O-Al linkages associated with cations like Na^+, K^+ and H^+. Based on the microstructure, aluminosilicates are classified as (i) phyllosilicates (extended planar and layered structure) and (ii) tectosilicates (network of extended 3D covalent bonds).[111] Zeolites belong to the tectosilicate category of the aluminosilicates, which comprises a 3D framework of TO_4 (T=Si, Al) tetrahedrally linked by sharing the oxygen atom, which forms a uniform pore. (shown in Figure 1.5). Based on their pore size, aluminosilicates are majorly classified as (i) microporous (pore size less than 2 nm in diameter), (ii) mesoporous (pore size between 2 nm and 50 nm in diameter) and (iii) macroporous (pore size more than 50 nm in diameter). MCM-41 is an example of mesoporous aluminosilicate having an ordered hexagonal structure with uniform cylindrical pores.

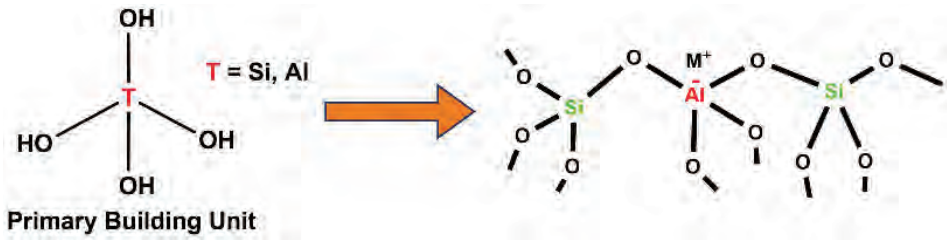

Figure 1.5: General representation of aluminosilicates.[112]

1.1.4.2 Structure and nature of aluminosilicates

One of the objectives of the present thesis is to study the properties and application of three aluminosilicates *viz* zeolite Na-Y, ZSM-5 and MCM-41 as catalysts for the cycloaddition reaction. While zeolite Na-Y and ZSM-5 primarily belong to the class of zeolites, MCM-41 belongs to the class of ordered mesoporous silica (shown in Figure 1.6).

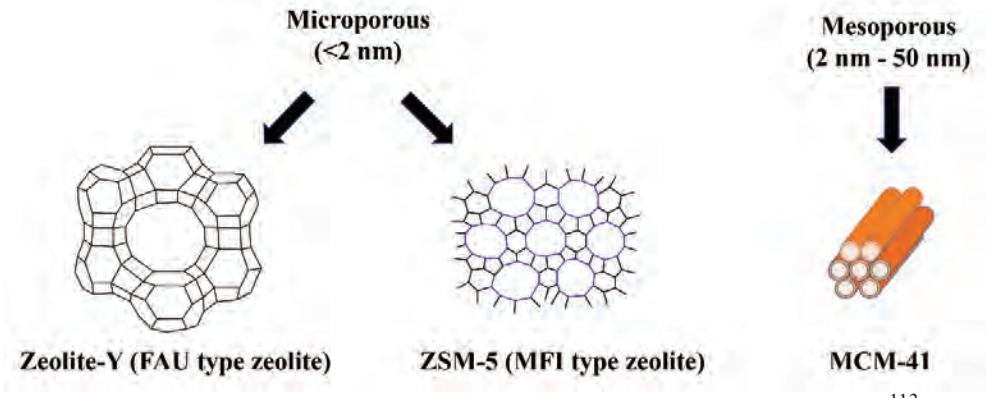

Figure 1.6: Structure of aluminosilicates employed in this thesis.[113]

Zeolites are molecular sieves of robust crystalline silica-alumina framework structure formed by a continuous network of oxygen-sharing SiO_4 or AlO_4^- tetrahedra. The framework of the zeolite consists of cross-linked TO_4 (T = Si or Al) units linked together with the O-T-O bond angle nearly equal to the tetrahedral angle. The T-O-T angle is more flexible and is close to 140°-165°. The presence of Al^{3+} in the tetrahedral position makes the zeolite bear a negative charge balanced by mobile alkali metals or alkaline earth metal cations, thus preserving the electro-neutrality of the zeolite. The TO_4 tetrahedra are often referred to as the primary building units of the zeolite structures. These primary units condense together to form the secondary units. This arrangement provides a unique architecture consisting of internal voids and regular-shaped windows with precise size, channels, and cages at the nanoscale.[114] These channels are naturally occupied by water molecules. The basic framework structure of the zeolite can be characterized by the pore opening, channel, and cages of specific sizes and shapes (shown in Figure 1.7). Other parameters, such as the influence of framework composition, extra-framework cations, organic species, and sorbed molecules, also play a vital role in describing the chemical behaviour of a given zeolite.

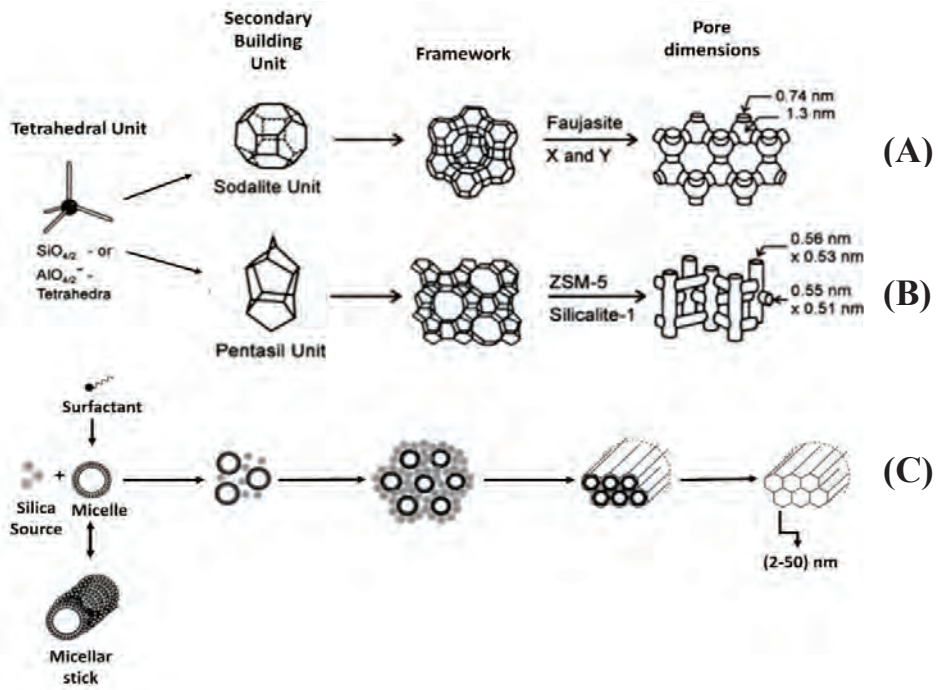

Figure 1.7: Building units of **(A)** zeolite-Y, **(B)** ZSM-5, **(C)** MCM-41.[111, 115]

Zeolites have both acidic and basic sites within the framework, which makes their study even more attractive. When the negative framework of the zeolite is balanced by a proton, a bridging hydroxyl group coordinated tetrahedrally between Si and Al atoms is formed, which results in the formation of Brønsted acidic sites.[116] Lewis acidic sites in the framework can be generated by the introduction of heteroatoms such as titanium, zirconium, tin, etc. In addition, the aluminium can also give rise to the Lewis acidity. Calcination at high temperatures or steaming of the zeolites results in the hydrolysis of the framework Si-O-Al bonds, generating the extra-framework aluminium with Lewis acidity (shown in Figure 1.8). The Lewis acidity can also be due to the tri-coordinated framework aluminium.[117] This acidity of zeolites is responsible for different catalytic activity. However, unlike Brønsted acidity, the concept of Lewis acidic aluminium in zeolites is still a grey area.[116] Brønsted acid strength depends on the protons present with the bridging hydroxyl groups of SiO(H)Al in zeolite frameworks. In contrast, the aluminium in the framework primarily controls the strength of the Lewis acidity. The acidity of zeolites can be altered by varying the Si/Al ratio. Regarding the basic nature of the zeolites, the negative lattice oxygens contribute to some basicity in cationic zeolites.[118] The basic strength of zeolites depends on the

charge of the oxygen atom.[119] Having such unique structural properties allows these porous materials to have extensive and efficient applications in the field of catalysis.

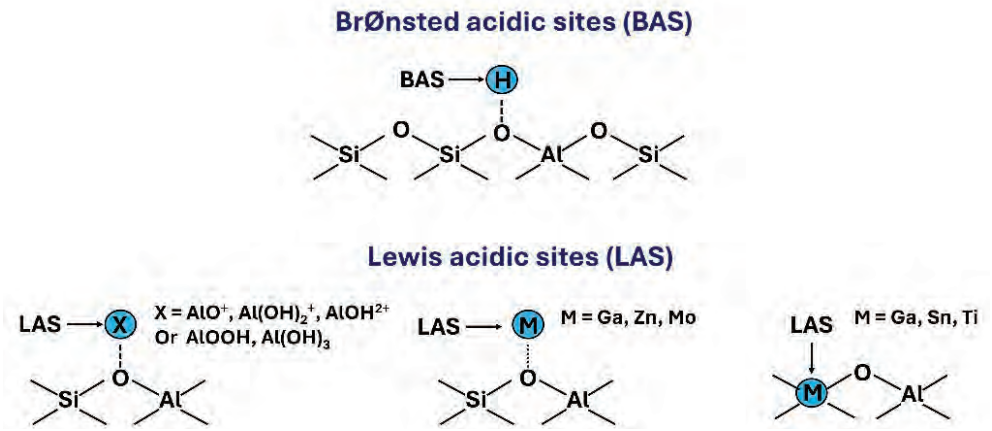

Figure 1.8: Representation of Brønsted acidic sites (BAS) and Lewis acidic site (LAS) in zeolites.[120]

Zeolite-Y belongs to the family of zeolite framework called the faujasite (FAU). FAU has a general formula $X^{m+}{}_{y/m}[(SiO_2)_x(AlO_2)^-{}_y].zH_2O$.[121] The FAU framework consists of 24 sodalite cages arranged analogously to the carbons in diamond. The sodalite cages are connected *via* hexagonal prisms or double six rings. The 3D pore called the supercage, formed by these hexagonal prisms, has an opening of 0.74 nm, and the supercage has an aperture of approximately 12.7 Å.[122] Due to its large windows, large void volume, inherent surface acidity, and high thermal stability, zeolite-Y is one of the most preferred zeolites for various catalytic reactions.[123] The ability to adsorb CO_2 and the presence of acidic sites have motivated many researchers to use zeolite-Y as a potential catalyst for the conversion of CO_2 to cyclic carbonates.

Zeolite Socony Mobil-5 (ZSM-5) is an MFI-type zeolite with a tuneable Si/Al ratio, crystalline framework, hydrothermal stability, high surface area, and flexible framework. ZSM-5 is generally synthesized from aluminium and silicate sources via hydrothermal methods.[124] It is a zeolite in which the content of silicon is more than aluminium. The aluminium and Si/Al ratio of ZSM-5 causes it to have acidic properties. It has a pore diameter range of 5 Å and a pore size (0.54 nm-0.56 nm). Its structure has two intersecting three-dimensional channels, defined by 10-membered ring openings.[125] ZSM-5 in its hydrogen form (HZSM-5) or metal-modified MHZSM-5 can acquire many functional, active sites like Brønsted acidity and Lewis acidity and basicity. The acidic properties of ZSM-5 and porous structure make it an excellent catalyst. HZSM-5 or

MHZSM-5 can also undergo reversible physical and chemical absorption of CO_2 at its channel/surface. The interaction between the electric field of ZSM-5 and the quadrupole moment of CO_2 gives ZSM-5 an excellent CO_2 adsorption capacity.[126] Due to its CO_2 adsorption capacities, it can be used to convert CO_2 to useful chemicals and the cycloaddition of CO_2 and epoxide to form cyclic carbonate is one such reaction.

MCM-41 (Mobil Composition of Matter-41) belongs to the family of ordered mesoporous silica, M41S and was developed in the early 1990s by Mobil oil research and development company. It was first synthesized by Beck *et al.* in 1992.[127] The building blocks of MCM are amorphous silica arranged in hexagonal tubes with uniform mesopores of diameters approximately 3 nm. Using template molecules of different lengths, the width of the tubes can be controlled to be in the range of 2 nm to 10 nm (shown in Figure 1.7). These tubes are connected by the sharing of silica walls.[128] Unlike FAU-type zeolites, MCM-41 shows mild Lewis acidity and does not exhibit desired Brønsted acid sites.[129] However, the acidity of aluminium-doped MCM-41 is similar to amorphous silica–alumina and researchers have developed methods to synthesize Al-MCM-41 to tune its acidity.[130] Due to attractive properties like homogeneity of the pores, high surface area of over 700 m^2g^{-1} and good thermal stability,[131] MCM-41 are used as attractive mesoporous materials with versatile applications in various fields including catalysis, sorption of large organic molecules, chromatographic separations etc. MCM-41 works as an excellent support material. Moreover, it contains few active sites on its surfaces, which can be functionalised easily. The catalytic properties of MCM-41 can be enhanced by incorporating additional functional groups in the silica walls, by deposition of active species on the inner surface of the material, or by carrying out post-synthetic functionalization, called grafting. Such modified MCM-41 have been widely used for the capture of CO_2[132] gas and is also being explored as a catalyst in the conversion of epoxides and CO_2 to cyclic carbonate.

1.1.4.3 Aluminosilicates as catalysts for cyclic carbonate synthesis

There are only a few reports in the literature that use the intrinsic activity of aluminosilicates. The incorporation of zeolite-Y as a catalyst for the conversion of CO_2 to cyclic carbonate was first reported by Davis *et al.*[133] in 2000. Even after two decades, limited reports are available which utilize the intrinsic properties of aluminosilicates for the synthesis of cyclic carbonates. The reports using zeolite-based, ZSM-based, and MCM-41-based catalysts are tabulated in Tables 1.3, 1.4 and 1.5, respectively.

Table 1.3: Zeolite-based catalysts for cyclic carbonate synthesis

Catalyst System [Ref]	Reaction conditions (Yield with respect to styrene oxide)	Remarks
Zeolite N-660 [134]	**Reaction conditions** 20 bar, 100 °C, 24 h, 100 mg catalyst, 50 mg TBAB **Conversion** 99%	• Commercial β-zeolite, N-660, with a high Si/Al ratio, catalysed the cycloaddition reaction with high selectivity. • Zeolite beta, N-625, with low Si/Al ratio, promotes the homopolymerization of propylene oxide to produce polyethers and polyols in the absence of CO_2 and a co-catalyst. • The Brønsted acid center (Al−OH), under the action of the hydrogen bond, activates the epoxide.
KI/KY [135]	**Reaction conditions** 50 bar, 100 °C, 6 h, 5 mol% of catalyst **Yield** 100%	• The yield depends on the halide's nature: $I^- > Br^-$ or Cl^-. • The zeolite system is more active than the pure metal halide. In the presence of zeolite, 100% styrene carbonate was formed within 6 hours, whereas in the absence of zeolite, the same reaction took 15 hours. • Higher yields using an impregnated KI/KY system than KI+KY suggested that the reaction occurs inside the zeolite pores and cavities.
LZ 276 [136]	**Reaction conditions** 5 bar, 140 °C, 10 h, 20 mg catalyst, 30 mg KI **Yield**	• NH_3 and CO_2 TPD confirm the presence of both acidic and basic sites. • The Lewis basic sites provided by Si atoms in the zeolite framework contribute to the activation of CO_2 and promote the catalytic reaction.

Catalyst System [Ref]	Reaction conditions (Yield with respect to styrene oxide)	Remarks
	77% (Using styrene)	• Nucleophile I^- anions and the aluminium atoms in the zeolite framework synergistically attacked the less sterically hindered β-carbon atom of epoxide, contributing to the ring-opening.
Zeolite chitosan composite [137]	**Reaction conditions** 10 bar, 100 °C, 6 h, 50 mg catalyst, 45 mg TBAI **Yield** 77%	• ZY-CS composite has enhanced CO_2 adsorption due to the nitrogen atom mesoporous structure and interaction sites, which play an essential role in the fixation of CO_2.
Zeolite beta [138]	**Reaction conditions** 6.9 bar, 120 °C, 8 h, 150 mg catalyst **Conversion** 98%	• Carbonate selectivity improved when the reaction was conducted in solvents like DMF, CH_3CN and CH_2Cl_2. CH_3OH suppressed the selectivity of cyclic carbonates. • The activity increased from 27% to 71% upon increasing the temperature from 100 °C to 110°C. • The catalyst was tested successfully using 4 epoxides with excellent yields and showed recyclability up to 8 times without loss in activity.
Cs/KX [133]	**Reaction conditions** 38 bar, 150 °C, 3 h, 2g catalyst **Yield** 14% (Using ethylene oxide)	• The deposition of zeolite KX with caesium acetate led to the formation of basic sites, which improved the reactivity. • The improved catalytic activity with the system Cs/Al_2O_3 indicated the importance of the acidic and basic sites. • Small amount of water positively affects the catalysis without forming side products.

Table 1.4: ZSM-based catalysts for cyclic carbonate synthesis

Catalyst System [Ref]	Reaction conditions (Yield with respect to styrene oxide)	Remarks
Seed-assisted sZSM-5 [139]	**Reaction conditions** 20 bar, 150 °C, 8 h, 100 mg catalyst **Yield** 81.8% (Using epichlorohydrin)	• ZSM of different sizes was prepared by changing the amount of water, where a lesser amount of water in the seed precursor led to a larger size of zeolite. • XRD patterns showed that the amount of water does not affect the final crystallinity. • The ZSM with the smallest size showed the best catalytic activity for cycloaddition.
Gallium-silicate based ZSM-5 [140]	**Reaction conditions** 5.5 bar, 75 °C, 6 h, 300 mg catalyst, 0.1 mg TEABr **Yield** 57.6% (Using propylene oxide)	• The calcination temperature played a vital role. An increase in the calcination temperature from 500 °C to 550 °C during the synthesis of the catalyst decrease the conversion of PO from 63.7% to 20.6%. • The surface area increased from 96.1 m^2g^{-1} to 103.8 m^2g^{-1} on removing gallium oxide from the zeolite framework, indicating that the conversion depended on gallium content rather than surface area. • The reaction follows the epoxide activation mechanism, and the co-catalyst attacks on the less hindered site to facilitate the ring-opening of the epoxide.

Catalyst System [Ref]	Reaction conditions (Yield with respect to styrene oxide)	Remarks
ZnHZSM-5(Zn 3%) [108]	**Reaction conditions** 10 bar, 160 °C, 4 h, 50 mg catalyst, 0.5 mol% of TPAB **Yield** 98%	• Shifting of strong acidic sites to higher temperature values for ZnZSM-5 compared to HZSM-5 in NH_3-TPD indicates interaction between the metal and the ZSM-5. • SEM and XRD indicate that high metal content lead to aggregation. • The reaction followed the epoxide activation pathway where the epoxide is activated by Lewis acidic Zn^{2+} and Al^{3+}. Brønsted acidic ($ZnOH^{+}$) sites, and Br^{-} from TPAB assists in the ring opening.
Basic meso ZSM-5 [141]	**Reaction conditions** 8 bar, 120 °C, 4 h, 100 mg catalyst, 10 mg DMAP **Conversion** 71.6% (Using epichlorohydrin)	• The calcined form of the mesoporous zeolite was treated with NH_4OH to obtain basic mesoporous ZSM-5. • TEM studies show that the base treatment influences the outer surface of large crystals, whereas the inside nanosheet architecture is preserved. • The low activity of Basic-Meso-ZSM-5 is not due to the low basicity of the catalyst, rather due to the inactivation of CO_2. Activation of CO_2 is essential for this reaction.

Table 1.5: MCM-41-based catalysts for cyclic carbonate synthesis

Catalyst System [Ref]	Reaction conditions (Yield with respect to styrene oxide)	Remarks
$KI_{35\%}$/MCM-41 [142]	**Reaction conditions** 30 bar, 130 °C, 5 h, 250 mg catalyst **Yield** 94.7%	• Negligible yield with only MCM-41. 35% weight % of KI was required for maximum yield. • In the mechanism, the -OH of the MCM activates the epoxide, and the iodide facilitates the ring opening. • The catalyst showed good stability and could be reused without loss in activity even after the fourth cycle.
As synthesized MCM-41 [143]	**Reaction conditions** 6.9 bar, 120 °C, 8 h, 50 mg catalyst **Conversion** 93.7%	• Using as-synthesized MCM-41 yielded cyclic carbonate as the main product and diol and ethers as minor products. • The cyclic carbonate selectivity improved in solvents like DMF and ACN, but CH_2Cl_2 and MeOH lowered the selectivity. • The reduced activity of MCM-41 after the fifth recycle was due to the partial loss in crystallinity/long-range ordering of the catalyst as detected by XRD.

With only a handful of reports showcasing the utilization of modified zeolites and MCM-41 as complexes for the synthesis of cyclic carbonates, there is a lot of scope to explore the inherent acidity and basicity of these heterogeneous aluminosilicates further for their catalytic activity.

1.1.5 Metal complexes encaged in zeolite as heterogeneous catalysts for cyclic carbonate synthesis

Zeolites are microporous materials formed by the tetrahedral linkage of alumina (AlO_4^-) and silica (SiO_4), having the innate ability to act as catalysts. The presence of the supercage (12.7 Å diameter) in zeolite-Y enables it to function as a host for the entrapment of relatively large molecules. The zeolite-Y framework, comprising open cage-like channels, offers it with a robust architecture ideal for appropriate guest molecules and ligands to diffuse inside the supercage. The process of encapsulation leads to the heterogenization of the guest catalyst inside the zeolite. Although homogeneous catalysts possess the advantage of high selectivity, they still suffer from the drawback of harsh reaction conditions, lack of reusability and loss of activity. Upon encapsulation, the properties of the guest molecule inside the zeolite supercage, coupled with the characteristic properties provided by the specific architecture and the environment of the host material, often lead to remarkable catalytic activity. Metal-salen, metal-salophen, metal tris(bipyridyl), and metallophthalocyanine (MPc) encaged in zeolite-Y are some important examples of encapsulated complexes widely known as "*ship-in-a-bottle*" complexes. These encapsulated complexes have been used as catalysts for various organic transformations, asymmetric synthesis, photocatalysis, redox reactions, and as sensors. The efficiency of transition metal complexes and aluminosilicates as catalysts for the conversion of CO_2 to cyclic carbonates has already been established separately. The combination of the activity of these homogeneous metal complexes with the inherent activity and the robustness of the zeolite is contemplated by the possibility of steering a new domain of heterogeneous catalysis for CO_2 upcycling. The cycloaddition of CO_2 using heterogeneous zeolite-encapsulated transition metal complexes is a lesser-studied area, and the present thesis aims to bridge the existing gap.

1.1.5.1 Heterogenization of transition metal complexes and methods of encapsulation

In recent years, there has been an upsurge in the demand for heterogeneous catalysts. The various advantages offered by the heterogeneous catalysts include simplification of the reaction procedures, recyclability of expensive catalysts, ease of separation of products, etc. These

advantages have piqued the interest of researchers towards the synthesis of heterogeneous catalysts. Generally, a homogeneous complex can be heterogenized using methods such as immobilization, grafting, anchoring and encapsulation.[144] Immobilization leads to the formation of the covalent bonding, hence changing the conformation of a molecule.[145] To prevent such conformational modifications, encapsulation is preferred. Zeolite-Y is often preferred as a host for encapsulation because of its elegant framework architecture, regular shape and size of cavities, windows and micropores, in addition to its stability. These encapsulated complexes are also known for their potential to mimic the biological systems and exhibit structural and functional analogy with cytochrome P-450 and are termed 'zeozymes'.[146] The structural rigidity of the framework confines the guest molecule inside the supercage, not allowing it to escape. The synthesized complex cannot be removed from the supercage without destroying the host framework. This specific architecture of the host-guest system is sometimes referred to as a "*ship-in-a-bottle*" complex. To synthesize these "*ship-in-a-bottle*" complexes, the molecular dimensions of the complex should be appropriate as not to exceed the size of the supercage of 12.7 Å. There are three basic methods of the synthesis of zeolite-encaged metal complexes.

(a) Flexible ligand method
(b) Template synthesis method
(c) Zeolite synthesis method

In the flexible ligand method, the mobile cations in zeolite are exchanged with the target metal using the ion-exchange method as the first step. The salen or salophen ligands of appropriate molecular dimensions, having the ability to rotate freely around the single bond (also known as flexible ligands), are often allowed to diffuse through the pores of the metal-exchanged zeolite. This leads to the *in-situ* complexation of the ligand with the metal. Once synthesized within the cavity of the host, due to its rigid structure and larger dimension compared to that of the pore openings of the cavity, the complex is immobilized. The unreacted ligands and the surface impurities are removed using Soxhlet extraction, and finally, the unreacted metal is again exchanged with Na^+ ions by treating it with NaCl solution. This method was first reported by Herron *et al.*[147] The general method for the flexible ligand synthesis method is shown in Figure 1.9.

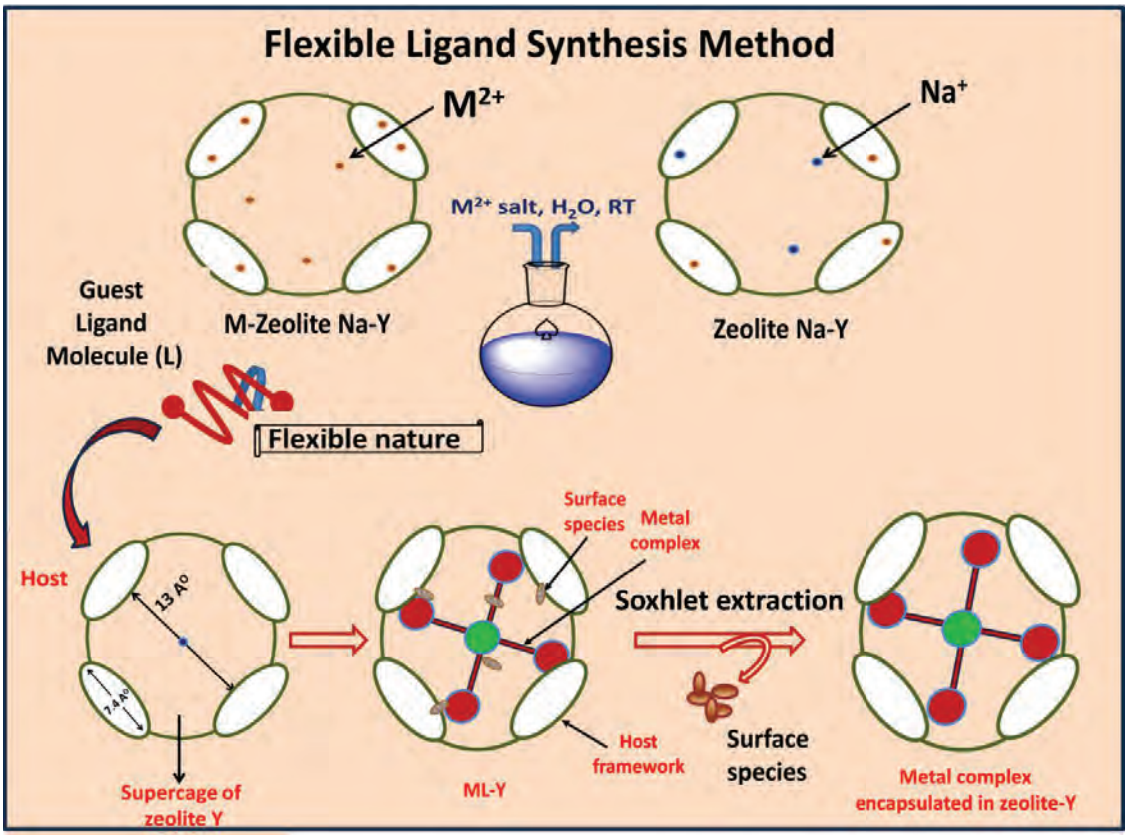

Figure 1.9: Schematic representation for the flexible ligand synthesis method.

The template synthesis (Figure 1.10) is used for the complexes having molecular dimensions comparable with that of the pore of the zeolite. In this method, the complex precursors or the building blocks of the ligand are allowed to diffuse through the pores of the metal-exchanged zeolites. The formation of the ligand, as well as the complex, takes place *in situ* in this method. Metal-phthalocyanine and metal-tris(bipyridyl) complexes encapsulated in zeolite-Y are generally prepared by this method. This method was first reported by Lunsford *et al.*[148]

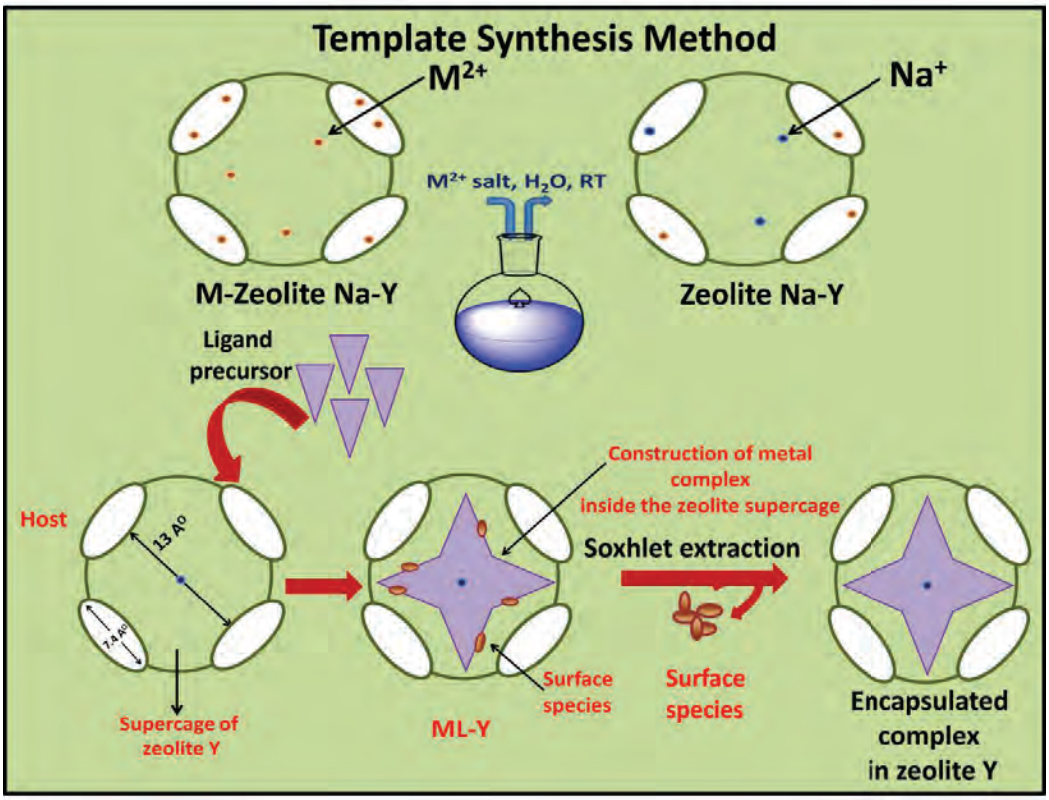

Figure 1.10: Schematic representation for the template synthesis method.

As the name suggests, in the zeolite synthesis method, the zeolite is synthesized around the metal complex. This method can only be applicable when the metal complex sustains the condition of zeolite synthesis. The metal complex to be encapsulated is added during the crystallization of the zeolite, such that, eventually, when the zeolite crystalizes, the metal complex is trapped inside the zeolite. This is a method where the building of the 'bottle' takes place around the 'ship'. One of the advantages of this method is that only distinct metal complexes are encapsulated without the contamination of excess ligands or uncomplexed metal ions.[149] (shown in Figure 1.11)

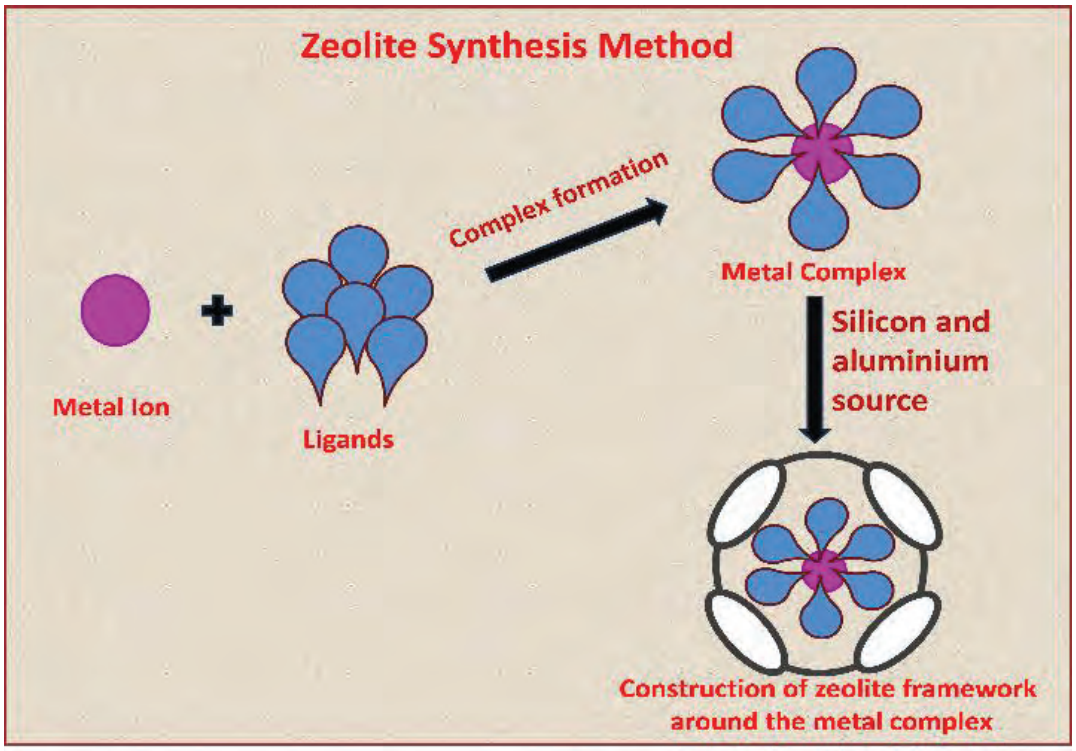

Figure 1.11: Schematic representation for the zeolite synthesis method.

1.1.5.2 Importance and effects of encapsulation on the structure and property of the guest metal complexes

The comparable sizes of the metal complex and the pore size of the supercage of zeolite-Y suggests the possibility of structural and chemical modifications of the metal complex upon encapsulation. Indeed, it is well established that on encapsulation inside the supercage of zeolite Y, a complex is forced to undergo structural and geometrical modifications, especially when the topology of the host cavities imposes space constraints on the guest complex. Therefore, the encapsulated complex modifies its geometry to remain inside the zeolite. The structural modification of the encapsulated complex leads to numerous other modifications in its electronic, photophysical and chemical properties. There are reports which indicate the change in the magnetic, electronic, photophysical, and electrochemical properties upon encapsulation.[150] Reports also indicate the global hardness and softness values (polarizability) change upon encapsulation. The modified functionality and the improved catalytic activity of the encapsulated system are a direct consequence of these changes in the structure and properties that the complex undergoes upon encapsulation.

In one of the earliest reports by Lunsford *et al.*,[148] they found that encapsulated Co(II) tris(bipyridyl) showed different spin-states compared to its "free" form. The authors reported that the encapsulated complex undergoes thermally driven spin-conversion from low to high spin-state. Vasudevan *et al.*[151] conducted detailed magnetic and spectroscopic studies of the complex. Their results revealed that the magnetic moment of the "free" complex remains constant at a wide range of temperatures. However, the encapsulated complex showed a gradual increase of magnetic moment from 1.9 μ_B (S = 1/2) at low temperature to a value intermediate between the high spin (HS) (S = 3/2) and low spin (LS) (S = 1/2) at higher temperatures. Modelling studies also showed that the complex adopts a less distorted octahedral geometry upon encapsulation as compared to the free state. Vasudevan *et al.*[152] also studied the effect of size and topology of the host supercage on the magnetic and electronic properties of the encapsulated Co phthalocyanine (CoPc) complex. They concluded that the complex adopts saddle-type distortion after the encapsulation, the consequence of which is the change in the magnetic moment of the encapsulated complex compared to the "free" complex.

The effect of electronic properties upon encapsulation was recently reported by Ray *et al.*[153] Their studies reveal the interesting difference in the optical spectra of 1, 2 and 1, 3 complexes of Ni(salophen) complexes. Upon encapsulation, all the 1, 2 Ni(salophen) complexes underwent a blue shift compared to their neat counterparts, while the 1, 3 Ni(salophen) complexes showed a red shift. (shown in Figure 1.12) This difference in optical spectra is attributed to the bridging phenyl ring, which experiences opposing structural modification on entrapment. Diffuse reflectance spectroscopy and DFT studies revealed that for 1, 3 systems, the bridging phenyl ring lies out of the plane in the "neat" form, leading to loss of conjugation. Upon encapsulation, the phenyl ring is forced to adopt a more planar geometry with enhanced conjugation and eventually experiences a red shift. On the other hand, the planar 1, 2 Ni(salophen) complex in "neat" form undergoes distortion upon encapsulation, leading to the loss of conjugation and, hence, a substantial blue shift observed in the electronic spectrum compared to the neat complex. A similar observation was reported by Ray *et al.*[154] for 1, 3 Pd(salen), which undergoes red shift upon encapsulation. However, in the case of 1, 3 Pd(salen), the red shift is dependent on the substituent present on the 5, 5' of the phenyl ring. Electron-donating substituents like -OH and -CH_3 assist in a red shift while electron-withdrawing -Br shows a blue shift compared to the "neat" complex.

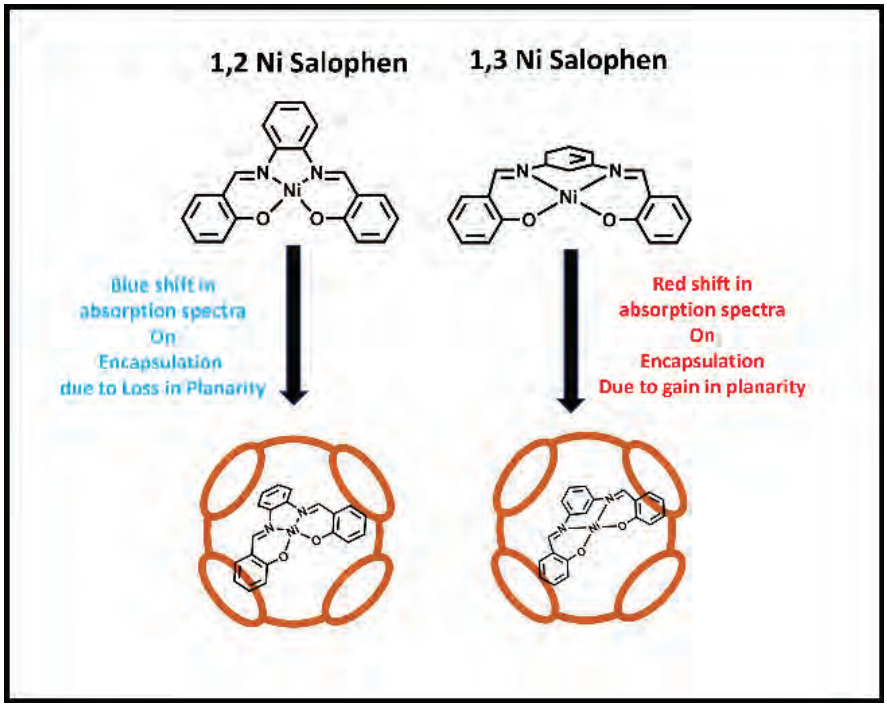

Figure 1.12: Change in electronic properties upon encapsulation as reported by Ray *et al.*[153]

The change in photophysical properties of iron complexes upon encapsulation was reported by Keyes *et al.*[155] They observed that in "free" state $[Fe(tpy)_2]^{2+}$ quenched $[Ru(bpy)_3]^{2+}$ through the radiative mechanism. However, upon encapsulation, the symmetry about the metal in the coordination sphere reduces, which enhances a $^1T_2 \leftarrow {}^1A_1$ ligand field transition in the complex. Hence, in the encapsulated state, $[Fe(tpy)_2]^{2+}$ quenches $[Ru(bpy)_3]^{2+}$ through a non-radiative mechanism

The effect of redox potential and polarizability was studied by Deka *et al.*[156] They studied salen and salophen complexes of iron(III) in "neat" and encapsulated form for the oxidation of naphthol. The authors report that Fe-Schiff-base complexes encapsulated in zeolite KY have more negative reduction potential as compared to other alkali metal exchanged zeolite. The encapsulation further leads to a decrease in global hardness and an increase in global softness, factors controlling polarizability. The changes in the redox potential and the polarizability of the encapsulated complex make it an efficient catalyst for oxidation compared to the "neat" complex.

Encapsulation of a metal complex inside zeolite also leads to site isolation.[153] Schiff base complexes of Zn, Co, and Al are also known to display dimerization,[157, 158] and these dimeric complexes show less catalytic activity than monomers. Di Bella and co-workers have extensively studied, theoretically[159] and experimentally,[160] the behaviour of zinc salen and salophen complexes in various coordinating and non-coordinating solvents. Their results showed that zinc salen and salophen complexes tend to form dimers, oligomers, and higher aggregates in the presence of non-coordinating solvents. To prevent dimerization, researchers have used bulky groups like *tert*-butyl (^{t}Bu) at the 3,3' and 5,5' positions). Encapsulation leads to the formation of the monomeric complex due to the size constraint of the zeolite pore.

The above studies indicate that the size constraints of the pore of the zeolite lead to various structural and functional modifications that have a direct impact on the catalytic activity of the encapsulated complex. There is vast scope to explore this remarkable property of the host-guest systems for the fixation of CO_2 to cyclic carbonates.

1.1.5.3 Applications of zeolite encapsulated complexes as catalysts

The encapsulated "*ship-in-a-bottle*" complexes with modified structural and functional properties have been studied for their application as catalysts for reactions, including organic transformations, photocatalysis, redox reactions, and sensors. There are many reports by Ray *et al.*, Deka *et al.*, and others on the organic transformations using encapsulated complexes. The studies report the activity of various complexes like 1, 2 Cu(salophen), 1, 2 Pd(salen), 1, 3 Ni(salophen), 1, 3 Pd(salophen) entrapped in zeolite-Y for different oxidation reactions like styrene oxidation,[161] sulfoxidation,[154] and phenol oxidation,[153] and Heck coupling[162] reactions respectively. The major conclusions from all these reports pointed out that the complexes studied undergo optical and geometric modifications upon encapsulation, leading to enhancement in the catalytic activity of the encapsulated complexes. Deka *et al.*[163] studied the oxidation of phenol using complex bis(picolinato) complexes of cobalt, nickel, and copper in both solution and encapsulated states. Their study revealed that on encapsulation, the walls of zeolite impart changes in the electronic, structural, and catalytic behaviour of the catalysts. The catalyst Cu(II) bis(picolinato) in the encapsulated state produces catechol selectively, while the "neat" complexes yield benzoquinone as the side product. Mohammed *et al.*[164] developed platinum metallated porphyrin (Pt(II)TMPyP) encapsulated in a rho-type zeolite-like metal-organic framework (rho-ZMOF) and a applied the complex for anion-selective sensing. The authors report that photo-induced triplet-state electron transfer of "neat" Pt(II)TMPyP showed a very low detection limit for anions with no selectivity. On the other hand, the Pt(II)TMPyP

encapsulated in the rho-ZMOF framework possessed a unique chemical structure to overcome such limitations. Tris(2,2'-bipyridine) ruthenium(II) ($[Ru(bpy)_3]^{2+}$) complex, a redox-active photosensitizer, was studied inside zeolite-Y.[165] Upon encapsulation, the complex undergoes strong distortion from its octahedral geometry, which leads to an increase in the intensity of the phosphorescence emission of the complex. It was also observed that the complex undergoes a blue shift of the luminescence maxima, termed "rigid chromism". The rigid environment after encapsulation gives rise to reduced relaxation, which results in the spectral blue shift.

Apart from the oxidation-reduction reactions, sensing and photochemical application, encapsulated complexes have also been used for the conversion of CO_2 to cyclic carbonates. Ratnasamy *et al.*[166] reported the utilization of aluminium phthalocyanine complexes encapsulated in zeolite-Y for the cycloaddition of CO_2 to ECH and PO in the presence of DMAP as a co-catalyst to yield their corresponding carbonates. A conversion of 97.3% with a selectivity of 99.7% for ECH was obtained at 120 °C, 4 hours, a CO_2 pressure of 6.9 bar, using the dual catalytic system of aluminium phthalocyanine (AlPc-Y) and DMAP. The catalyst was easily separated from the reaction mixture and reused with little loss in activity. The zeolite-Y-encapsulated complex, CuPc-Y, exhibited superior activity (TOF=12326 h^{-1}) compared to the "neat" (TOF=502 h^{-1}) and silica-supported phthalocyanine complexes (TOF=478 h^{-1}). They reported the higher activity of the encapsulated complexes as a result of the isolation of the complexes in the supercage of zeolite-Y and the consequent changes in the electronic structure. Du *et al.*[167] encapsulated manganese porphyrin complex, $[TMPyPMn\mathbf{(I)}]^{4+}(I^-)_4$, into ZIF-8 assembled from Zn(II) and 2-methylimidazole (Figure 1.13). The confinement of the porphyrin in ZIF, along with the Lewis acidity from the metals in the composite and the nucleophilicity of the halide ion, enhanced the activity through synergistic host-guest catalysis. The encapsulated system gave 99% yield of ECHC at 1 bar, 100 °C, and 36 h, as compared to 53% and 27% by only the ZIF and only the porphyrin, respectively. In one report by Luo *et al.*[168], they reported zeolite NaX supported cobalt porphyrin rather than encapsulation for the conversion of CO_2 to cyclic carbonate. They reported that the catalytic performance of the heterogeneous catalyst was better than the homogeneous counterpart. At 30 bar, 120 °C, and 5 h, they reported a 90.4% yield of propylene carbonate using PTAT as the co-catalyst. The mechanism followed epoxide activation, where the Lewis acidic site is the hydroxy group of the zeolite NaX of the supported catalyst system and the Br_3^- from PTAT aids in the ring opening.

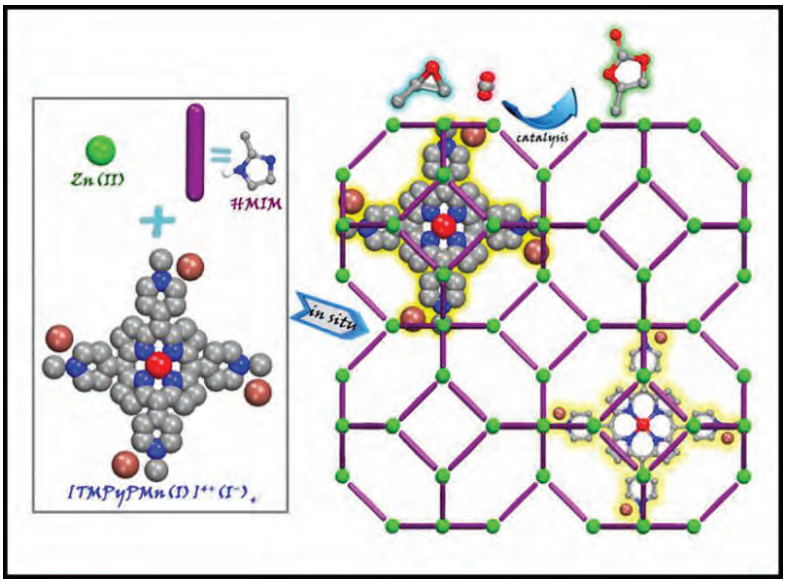

Figure 1.13: Metalloporphyrin in ZIF for cyclic carbonate synthesis reported by Du *et al.*[167] (Adapted with permission form John Wiley and Sons)

Hence, the vast range of applications of zeolite encapsulated complexes and the conversion of CO_2 to cyclic carbonates using encapsulated phthalocyanine and porphyrin complexes paves the way towards using zeolite encapsulated Schiff base metal complex for the upcycling of CO_2. The structural and functional modification of a complex upon encapsulation might lead to interesting catalytic activities.

1.2 Gaps in the literature and scope of the present thesis

After carefully studying the literature available for the synthesis of cyclic carbonates from CO_2 and epoxide, the following gaps were found:

- There are very few reports involving aluminosilicates as catalysts for the conversion of CO_2 to carbonates.
- Zeolite Y encapsulated salen and salophen type complex has not been explored for the conversion mentioned above.
- Encapsulation can deliver different electronic parameters to metal complexes *via* structural distortion, and this area is relatively less explored for cyclic carbonate synthesis.

The main motive of the present thesis is to discern the role of various homogeneous and heterogeneous complexes as catalysts for the valorization of CO_2 to industrially relevant cyclic carbonates, preferably with milder reaction conditions. The catalysts employed in this thesis transition progressively from a homogeneous to a heterogeneous state. Firstly, homogeneous N_2O_2 coordinating, Schiff base complexes of zinc(II) salophen (*N, N'*-bis(salicylidene)-1,2-phenylensediamine), with various substituents on the 5, 5' position, varying from the election donating methyl (-Me) group to electron-withdrawing nitro group (-NO_2) have been synthesized. The effect of the substituents has been compared, and the complexes have been studied for their utility as catalysts for the synthesis of styrene carbonate from CO_2 under ambient reaction conditions. Towards the use of heterogeneous catalysts, the relevance of commercially available aluminosilicates, such as Na-zeolite-Y, NH_4^+ZSM-5, and synthesized Al-MCM-41 have been studied for the cycloaddition reaction. The effect of the Si/Al ratio, and thus, the Lewis acidity of these heterogeneous catalysts, has been explored. Finally, the activity of the homogeneous complexes and the properties of the heterogeneous aluminosilicates have been integrated to form the zeolite-Y encapsulated complexes. The encapsulated complexes of non-toxic, earth-abundant metals Zn, Co, e.g.,1, 2 zinc(II) salophen and 1, 2 cobalt(II) salophen have been employed for the formation of styrene carbonate, and their activity compared with their homogeneous counterparts. The heterogeneous encapsulated complexes show superior activity compared to their homogeneous analogues due to the various structural and electronic modifications experienced by the complexes upon encapsulation.

The Schiff base complexes were synthesized by the simple condensation of diamine and substituted salicylaldehyde. The formation of the "neat" complexes was confirmed by NMR and LC-MS spectroscopic methods. Other spectroscopic techniques like electronic and vibrational spectroscopy were used to comprehend the electronic environment upon complexation. XPS spectroscopy and thermal analysis were carried out to study the oxidation state and the stability of the complex, respectively. The mechanism was investigated using theoretical methods. The zeolites, Na-zeolite-Y and NH_4^+-ZSM-5 were commercially purchased, but their comparative spectroscopic analysis was carried out along with synthesized Al-MCM-41. These aluminosilicates were characterized by powder XRD, FT-IR, TGA, BET and XPS. Temperature programmed desorption was carried out to discern the acidic sites present in these aluminosilicates. The encapsulated complexes were prepared by the flexible ligand method. Characterization techniques, including electronic, vibrational, XPS, BET and XRD, give us indirect proof of the

encapsulation of the complex inside the pores of zeolite. The DFT studies are carried out for the encapsulated complexes to understand the electronic transitions better. The reactions at ambient pressures were carried out using a balloon filled with CO_2, while those at slightly higher pressures were carried out in an autoclave.

1.3 References

1. A. Glikson, *Energy Procedia*, 2018, **146**, 3.
2. M. North, R. Pasquale and C. Young, *Green Chemistry*, 2010, **12**, 1514.
3. P. P. Pescarmona, *Current Opinion in Green and Sustainable Chemistry*, 2021, **29**, 100457.
4. T. Yan, H. Liu, Z. X. Zeng and W. G. Pan, *Journal of CO_2 Utilization*, 2023, **68**, 102355.
5. D. Prasad, K. N. Patil, N. K. Chaudhari, H. Kim, B. M. Nagaraja and A. H. Jadhav, *Catalysis Reviews: Science and Engineering*, 2022, **64**, 356.
6. Q. He, J. W. O'Brien, K. A. Kitselman, L. E. Tompkins, G. C. T. Curtis and F. M. Kerton, *Catalysis Science & Technology*, 2014, **4**, 1513.
7. M. Cokoja, M. E. Wilhelm, M. H. Anthofer, W. A. Herrmann and F. E. Kühn, *ChemSusChem*, 2015, **8**, 2436.
8. L. Guo, K. J. Lamb and M. North, *Green Chemistry*, 2021, **23**, 77.
9. T. K. Pal, D. De and P. K. Bharadwaj, *Coordination Chemistry Reviews*, 2020, **408**, 213173.
10. Y. Li, J. Zhang, K. Zuo, Z. Li, Y. Wang, H. Hu, C. Zeng, H. Xu, B. Wang and Y. Gao, *Catalysts*, 2021, **11**, 1133.
11. K. Yamaguchi, K. Ebitani, T. Yoshida, H. Yoshida and K. Kaneda, *Journal of the American Chemical Society*, 1999, **121**, 4526.
12. L. Hu, L. Chen, X. Peng, J. Zhang, X. Mo, Y. Liu and Z. Yan, *Microporous and Mesoporous Materials*, 2020, **299**, 110123.
13. C. Martín, G. Fiorani and A. W. Kleij, *ACS Catalysis*, 2015, **5**, 1353.
14. N. A. Tappe, R. M. Reich, V. D'Elia and F. E. Kühn, *Dalton Transactions*, 2018, **47**, 13281.
15. R. Lindsey, Climate Change: Atmospheric Carbon Dioxide, https://www.climate.gov/news-features/understanding-climate/climate-change-atmospheric-carbon-dioxide.
16. S. Samanta and R. Srivastava, *Materials Advances*, 2020, **1**, 1506.
17. B. Ruscic, *The Journal of Physical Chemistry A*, 2015, **119**, 7810.
18. J. Ding, R. Ye, Y. Fu, Y. He, Y. Wu, Y. Zhang, Q. Zhong, H. H. Kung and M. Fan, *Nature Communications*, 2023, **14**, 4586.
19. I. Omae, *Coordination Chemistry Reviews*, 2012, **256**, 1384.

20. F. F. T. de Groot, R. R. G. J. Lammerink, C. Heidemann, M. P. M. van der Werff, T. C. Garcia, L. A. G. J. van der Ham and H. van den Berg, *Chemical Engineering Transactions*, 2014, **39**, 1561.
21. T. Wang, D. Zheng, Y. Ma, J. Guo, Z. He, B. Ma, L. Liu, T. Ren, L. Wang and J. Zhang, *Journal of CO_2 Utilization*, 2017, **22**, 44.
22. Y. Toda, Y. Komiyama, H. Esaki, K. Fukushima and H. Suga, *The Journal of Organic Chemistry*, 2019, **84**, 15578.
23. J. Gao, L. Li, C. Cui, M. A. Ziaee, Y. Gong, R. Sa and H. Zhong, *RSC Advances*, 2019, **9**, 13122.
24. L. Muniandy, F. Adam, N. R. A. Rahman and E.-P. Ng, *Inorganic Chemistry Communications*, 2019, **104**, 1.
25. F. Xu, W. Cheng, X. Yao, J. Sun, W. Sun and S. Zhang, *Catalysis Letters*, 2017, **147**, 1654.
26. T. Hirose, S. Qu, K. Kodama and X. Wang, *Journal of CO_2 Utilization*, 2018, **24**, 261.
27. R. Khatun, P. Bhanja, R. A. Molla, S. Ghosh, A. Bhaumik and S. M. Islam, *Molecular Catalysis*, 2017, **434**, 25.
28. Y. Song, Q. Jin, S. Zhang, H. Jing and Q. Zhu, *Science China Chemistry*, 2011, **54**, 1044.
29. V. B. Saptal and B. M. Bhanage, *ChemSusChem*, 2017, **10**, 1145.
30. V. K. Juyal, A. Pathak, M. Panwar, S. C. Thakuri, O. Prakash, A. Agrwal and V. Nand, *Journal of Organometallic Chemistry*, 2023, **999**, 122825.
31. P. Kaur, R. Singh, V. Kaur and D. Talwar, *Analytical Sciences*, 2021, **37**, 553.
32. S. K. Saha, M. Murmu, N. C. Murmu and P. Banerjee, *Journal of Molecular Structure*, 2021, **1245**, 131098.
33. Z.-G. Zhao, T. Kodaira, N. Nagai, Y. Hakuta, K. K. Bando, H. Takashima and F. Mizukami, *Journal of Materials Chemistry*, 2012, **22**, 9738.
34. L. Yan-Yan, Y. Yu-Xi, H. Sha-Sha, L. Yao, Y. Zhi, Z. Bin-Yu, S. Jian-Po and W. Li, *Chinese Journal of Analytical Chemistry*, 2021, **49**, e21118.
35. K. Upendranath, T. Venkatesh, Y. Arthoba Nayaka, M. Shashank and G. Nagaraju, *Inorganic Chemistry Communications*, 2022, **139**, 109354.
36. J. Kumar, M. J. Sarma, P. Phukan and D. K. Das, *Dalton Transactions*, 2015, **44**, 4576.
37. O. A. El-Gammal, F. S. Mohamed, G. N. Rezk and A. A. El-Bindary, *Journal of Molecular Liquids*, 2021, **326**, 115223.

38. S. Daravath, A. Rambabu, N. Ganji, G. Ramesh and P. A. Lakshmi, *Journal of Molecular Structure*, 2022, **1249**, 131601.
39. L. Wei, J. Zhang, W. Tan, G. Wang, Q. Li, F. Dong and Z. Guo, *International Journal of Biological Macromolecules*, 2021, **179**, 292.
40. M. A. Ali, S. A. Musthafa, G. Munuswamy-Ramanujam and V. Jaisankar, *Carbohydrate Polymers*, 2022, **290**, 119501.
41. S. J. Hamid and T. Salih, *Drug Design, Development and Therapy*, 2022, **16**, 2275.
42. A. Ibezim, M. N. Ofokansi, X. Ndukwe, C. S. Chiama, B. C. Obi, O. N. Isiogugu, P. E. Ikechukwu, A. M. Onwuka, S. A. Ihim, J. N. Asegbeloyin and N. J. Nwodo, *Malaria Journal*, 2022, **21**, 243.
43. S. Kaushik, S. K. Paliwal, M. R. Iyer and V. M. Patil, *Medicinal Chemistry Research*, 2023, **32**, 1063.
44. P. G. Cozzi, *Chemical Society Reviews*, 2004, **33**, 410.
45. M. Stradiotto and R. J. Lundgren, in *Ligand Design in Metal Chemistry: Reactivity and Catalysis*, eds. M. Stradiotto and R. J. Lundgren, John Wiley and Sons, Chichester, UK, 2016, Ch. 1, pp. 1.
46. A. A. Varghese, Doctor of Philosophy, *Zeolite Encapsulated Complexes of Ruthenium: Synthesis, Characterization and Catalytic Activity Studies*, Cochin University of Science and Technology, 2008.
47. D. Prasad, K. N. Patil, N. K. Chaudhari, H. Kim, B. M. Nagaraja and A. H. Jadhav, *Catalysis Reviews*, 2022, **64**, 356.
48. C. J. Whiteoak, G. Salassa and A. W. Kleij, *Chemical Society Reviews*, 2012, **41**, 622.
49. A. W. Miller and S. T. Nguyen, *Organic Letters*, 2004, **6**, 2301.
50. D. Adhikari, A. W. Miller, M.-H. Baik and S. T. Nguyen, *Chemical Science*, 2015, **6**, 1293.
51. W.-M. Ren, Y. Liu and X.-B. Lu, *The Journal of Organic Chemistry*, 2014, **79**, 9771.
52. M. Sengoden, M. North and A. C. Whitwood, *ChemSusChem*, 2019, **12**, 3296.
53. W. Zhang, R. Luo, Q. Xu, Y. Chen, X. Lin, X. Zhou and H. Ji, *Chinese Journal of Catalysis*, 2017, **38**, 736.
54. R. Luo, X. Lin, Y. Chen, W. Zhang, X. Zhou and H. Ji, *ChemSusChem*, 2017, **10**, 1224.
55. R. Luo, X. Lin, J. Lu, X. Zhou and H. Ji, *Chinese Journal of Catalysis*, 2017, **38**, 1382.
56. D. Bai and H. Jing, *Green Chemistry*, 2010, **12**, 39.
57. F. Chen, T. Dong, T. Xu, X. Li and C. Hu, *Green Chemistry*, 2011, **13**, 2518.

58. P. Ramidi, C. M. Felton, B. P. Subedi, H. Zhou, Z. R. Tian, Y. Gartia, B. S. Pierce and A. Ghosh, *Journal of CO_2 Utilization*, 2015, **9**, 48.
59. M. Balas, A. Mayoufi, R. Villanneau and F. Launay, *Reaction Chemistry & Engineering*, 2023, **8**, 345.
60. M. Balas, R. Villanneau and F. Launay, *Journal of CO_2 Utilization*, 2023, **72**, 102497.
61. R. J. De Pasquale, *Journal of the Chemical Society, Chemical Communications*, 1973, 157.
62. T. Aida and S. Inoue, *Journal of the American Chemical Society*, 1983, **105**, 1304.
63. R. L. Paddock and S. T. Nguyen, *Journal of the American Chemical Society*, 2001, **123**, 11498.
64. S. Muthuramalingam, M. Sankaralingam, M. Velusamy and R. Mayilmurugan, *Inorganic Chemistry*, 2019, **58**, 12975.
65. X.-B. Lu and D. J. Darensbourg, *Chemical Society Reviews*, 2012, **41**, 1462.
66. I. Sinha, Y. Lee, C. Bae, S. Tussupbayev, Y. Lee, M.-S. Seo, J. Kim, M.-H. Baik, Y. Lee and H. Kim, *Catalysis Science & Technology*, 2017, **7**, 4375.
67. H. Jing, S. K. Edulji, J. M. Gibbs, C. L. Stern, H. Zhou and S. T. Nguyen, *Inorganic Chemistry*, 2004, **43**, 4315.
68. M. A. Fuchs, S. Staudt, C. Altesleben, O. Walter, T. A. Zevaco and E. Dinjus, *Dalton Transactions*, 2014, **43**, 2344.
69. A. Coletti, C. J. Whiteoak, V. Conte and A. W. Kleij, *ChemCatChem*, 2012, **4**, 1190.
70. F. Jutz, J.-D. Grunwaldt and A. Baiker, *Journal of Molecular Catalysis A: Chemical*, 2008, **279**, 94.
71. Y. Ren, O. Jiang, H. Zeng, Q. Mao and H. Jiang, *RSC Advances*, 2016, **6**, 3243.
72. R. Srivastava, T. H. Bennur and D. Srinivas, *Journal of Molecular Catalysis A: Chemical*, 2005, **226**, 199.
73. M. Bagherzadeh and M. Zare, *Journal of Coordination Chemistry*, 2013, **66**, 2885.
74. H. Ullah, Z. Ullah, Z. A. K. Khattak, M. A. Marwat, B. Yu, H. W. Kwon, H. Y. Kim and F. Verpoort, *Energy & Fuels*, 2023, **37**, 2178.
75. S. A. Kuznetsova, I. V. Gorodishch, A. S. Gak, V. V. Zherebtsova, I. S. Gerasimov, M. G. Medvedev, D. K. Kitaeva, E. A. Khakina, M. North and Y. N. Belokon, *Tetrahedron*, 2021, **82**, 131929.
76. R. L. Paddock and S. T. Nguyen, *Chemical Communications*, 2004, 1622.
77. Y.-M. Shen, W.-L. Duan and M. Shi, *The Journal of Organic Chemistry*, 2003, **68**, 1559.

78. A. Decortes, M. Martínez Belmonte, J. Benet-Buchholz and A. W. Kleij, *Chemical Communications*, 2010, **46**, 4580.
79. A. Decortes and A. W. Kleij, *ChemCatChem*, 2011, **3**, 831.
80. M. Taherimehr, A. Decortes, S. M. Al-Amsyar, W. Lueangchaichaweng, C. J. Whiteoak, E. C. Escudero-Adán, A. W. Kleij and P. P. Pescarmona, *Catalysis Science & Technology*, 2012, **2**, 2231.
81. Z. Wang, Z. Bu, T. Cao, T. Ren, L. Yang and W. Li, *Polyhedron*, 2012, **32**, 86.
82. M. V. Escárcega-Bobadilla, M. Martínez Belmonte, E. Martin, E. C. Escudero-Adán and A. W. Kleij, *Chemistry – A European Journal*, 2013, **19**, 2641.
83. H. Vignesh Babu and K. Muralidharan, *Dalton Transactions*, 2013, **42**, 1238.
84. C. Martín, C. J. Whiteoak, E. Martin, M. Martínez Belmonte, E. C. Escudero-Adán and A. W. Kleij, *Catalysis Science & Technology*, 2014, **4**, 1615.
85. M. İkiz, E. İspir, E. Aytar, M. Ulusoy, Ş. Karabuğa, M. Aslantaş and Ö. Çelik, *New Journal of Chemistry*, 2015, **39**, 7786.
86. R. Ma, L.-N. He and Y.-B. Zhou, *Green Chemistry*, 2016, **18**, 226.
87. L. Cuesta-Aluja, A. Campos-Carrasco, J. Castilla, M. Reguero, A. M. Masdeu-Bultó and A. Aghmiz, *Journal of CO2 Utilization*, 2016, **14**, 10.
88. S. He, F. Wang, W.-L. Tong, S.-M. Yiu and M. C. W. Chan, *Chemical Communications*, 2016, **52**, 1017.
89. Z. Alaji, E. Safaei and A. Wojtczak, *New Journal of Chemistry*, 2017, **41**, 10121.
90. B. Bousquet, A. Martinez and V. Dufaud, *ChemCatChem*, 2018, **10**, 843.
91. I. Karamé, S. Zaher, N. Eid and L. Christ, *Molecular Catalysis*, 2018, **456**, 87.
92. M. Alonso de la Peña, L. Merzoud, W. Lamine, A. Tuel, H. Chermette and L. Christ, *Journal of CO2 Utilization*, 2021, **44**, 101380.
93. X.-B. Lu, B. Liang, Y.-J. Zhang, Y.-Z. Tian, Y.-M. Wang, C.-X. Bai, H. Wang and R. Zhang, *Journal of the American Chemical Society*, 2004, **126**, 3732.
94. A. Berkessel and M. Brandenburg, *Organic Letters*, 2006, **8**, 4401.
95. J. Wang, J. Wu and N. Tang, *Inorganic Chemistry Communications*, 2007, **10**, 1493.
96. C.-X. Miao, J.-Q. Wang, Y. Wu, Y. Du and L.-N. He, *ChemSusChem*, 2008, **1**, 236.
97. L. Jin, Y. Huang, H. Jing, T. Chang and P. Yan, *Tetrahedron: Asymmetry*, 2008, **19**, 1947.
98. A. Sibaouih, P. Ryan, K. V. Axenov, M. R. Sundberg, M. Leskelä and T. Repo, *Journal of Molecular Catalysis A: Chemical*, 2009, **312**, 87.

99. S. Zhang, Y. Song, H. Jing, P. Yan and Q. Cai, *Chinese Journal of Catalysis*, 2009, **30**, 1255.

100. P. Ramidi, N. Gerasimchuk, Y. Gartia, C. M. Felton and A. Ghosh, *Dalton Transactions*, 2013, **42**, 13151.

101. M. Adolph, T. A. Zevaco, C. Altesleben, O. Walter and E. Dinjus, *Dalton Transactions*, 2014, **43**, 3285.

102. Y. A. Rulev, V. A. Larionov, A. V. Lokutova, M. A. Moskalenko, O. g. L. Lependina, V. I. Maleev, M. North and Y. N. Belokon, *ChemSusChem*, 2016, **9**, 216.

103. F. Zhou, S.-L. Xie, X.-T. Gao, R. Zhang, C.-H. Wang, G.-Q. Yin and J. Zhou, *Green Chemistry*, 2017, **19**, 3908.

104. Z. A. K. Khattak, H. A. Younus, N. Ahmad, H. Ullah, S. Suleman, M. S. Hossain, M. Elkadi and F. Verpoort, *Chemical Communications*, 2019, **55**, 8274.

105. A. Zhang, C. Chen, C. Zuo, X. Xu, T. Cai, X. Li, Y. Yuan, H. Yang and G. Meng, *Green Chemistry*, 2022, **24**, 7194.

106. T. Wang, D. Zheng, J. Zhang, B. Fan, Y. Ma, T. Ren, L. Wang and J. Zhang, *ACS Sustainable Chemistry & Engineering*, 2018, **6**, 2574.

107. H.-S. Seo and H.-J. Kim, *Bulletin of the Korean Chemical Society*, 2019, **40**, 169.

108. Q.-N. Zhao, Q.-W. Song, P. Liu, Q.-X. Zhang, J.-H. Gao and K. Zhang, *Chinese Journal of Chemistry*, 2018, **36**, 187.

109. W. Wang, S. Wang, X. Ma and J. Gong, *Chemical Society Reviews*, 2011, **40**, 3703.

110. O. Kotova, S. Sun, E. Kotova, A. Ponariaydov and R. Brodskaya, *Journal of Physics: Conference Series*, 2022, **2315**, 012003.

111. A. C. Lopes, P. Martins and S. Lanceros-Mendez, *Progress in Surface Science*, 2014, **89**, 239.

112. V. Yadav, M. Rani, L. Kumar, N. Singh and V. Ezhilselvi, *Water, Air, & Soil Pollution*, 2022, **233**, 465.

113. A. Ojuva, Undergraduate Diploma Thesis, *Quantification of crystallinity in zeolites: PXRD with and without an internal standard and IR spectroscopy*, Stockholm University, 2009.

114. K. J. Balkus and A. G. Gabrielov, in *Inclusion Chemistry with Zeolites: Nanoscale Materials by Design*, eds. N. Herron and D. R. Corbin, Springer Netherlands, Dordrecht, 1995, pp. 159.

115. D. Branković, R. A. Zarubica, D. Andjelković and H. D. Andjelkovic, *Advanced technologies*, 2017, **6**, 50.
116. M. Ravi, V. L. Sushkevich and J. A. van Bokhoven, *Nature materials*, 2020, **19**, 1047.
117. M. Ravi, V. L. Sushkevich and J. A. van Bokhoven, *Chemical Science*, 2021, **12**, 4094.
118. V. Verdoliva, M. Saviano and S. De Luca, *Foundations*, 2023, **3**, 72.
119. E. J. Doskocil, S. V. Bordawekar, B. G. Kaye and R. J. Davis, *The Journal of Physical Chemistry B*, 1999, **103**, 6277.
120. X. Zhao, J. Xu and F. Deng, *Frontiers of Chemical Science and Engineering*, 2020, **14**, 159.
121. C. Baerlocher, L. B. McCusker and D. H. Olson, in *Atlas of Zeolite Framework Types (Sixth Edition)*, eds. C. Baerlocher, L. B. McCusker and D. H. Olson, Elsevier Science B.V., Amsterdam, 2007, pp. 140.
122. A. Julbe and M. Drobek, in *Encyclopedia of Membranes*, eds. E. Drioli and L. Giorno, Springer Berlin Heidelberg, Berlin, Heidelberg, 2016, pp. 2060.
123. Jack H. Lunsford, *Reviews in Inorganic Chemistry*, 1987, **9**, 1.
124. R. J. White, A. Fischer, C. Goebel and A. Thomas, *Journal of the American Chemical Society*, 2014, **136**, 2715.
125. W. Widayat and A. N. Annisa, *IOP Conference Series: Materials Science and Engineering*, 2017, **214**, 012032.
126. Q. Liu, P. He, X. Qian, Z. Fei, Z. Zhang, X. Chen, J. Tang, M. Cui, X. Qiao and Y. Shi, *Energy & Fuels*, 2017, **31**, 13933.
127. C. T. Kresge, M. E. Leonowicz, W. J. Roth, J. C. Vartuli and J. S. Beck, *Nature*, 1992, **359**, 710.
128. M. Zhu and M. A. Carreon, *Journal of Applied Polymer Science*, 2014, **131**, 39738.
129. M.-C. Silaghi, C. Chizallet and P. Raybaud, *Microporous and Mesoporous Materials*, 2014, **191**, 82.
130. H. Kosslick, G. Lischke, B. Parlitz, W. Storek and R. Fricke, *Applied Catalysis A: General*, 1999, **184**, 49.
131. H. Zhou, Y.-M. Wang, W.-Z. Zhang, J.-P. Qu and X.-B. Lu, *Green Chemistry*, 2011, **13**, 644.
132. M. B. Yue, L. B. Sun, Y. Cao, Y. Wang, Z. J. Wang and J. H. Zhu, *Chemistry – A European Journal*, 2008, **14**, 3442.

133. M. Tu and R. J. Davis, *Journal of Catalysis*, 2001, **199**, 85.
134. R. Duan, C. Hu, Y. Zhou, Y. Huang, Z. Sun, H. Zhang and X. Pang, *Industrial & Engineering Chemistry Research*, 2021, **60**, 1210.
135. L. P. Ozorio, F. J. S. Henrique, J. W. Comerford, M. North and C. J. A. Mota, *Reaction Chemistry & Engineering*, 2021, **6**, 672.
136. B. Gu, T. Xu, G. Xu, J. Bai and C. Li, *Microporous and Mesoporous Materials*, 2020, **293**, 109779.
137. S. Kumar, K. Prasad, J. M. Gil, A. J. F. N. Sobral and J. Koh, *Carbohydrate Polymers*, 2018, **198**, 401.
138. R. Srivastava, D. Srinivas and P. Ratnasamy, *Applied Catalysis A: General*, 2005, **289**, 128.
139. W. Liu, T. Xu, C. Li and J. Bai, *Inorganic and Nano-Metal Chemistry*, 2020, **50**, 1087.
140. A. Aouissi, D. Aldhayan, N. A. Y. Abduh and A. A. Kahtani, *Green Processing and Synthesis*, 2020, **9**, 440.
141. B. Sarmah, B. Satpati and R. Srivastava, *Journal of Colloid and Interface Science*, 2017, **493**, 307.
142. L. Zhou, G. Cai, L. Zhang, Y. Luo, Z. He and W. Eli, *Synthesis and Reactivity in Inorganic, Metal-Organic, and Nano-Metal Chemistry*, 2014, **44**, 1545.
143. R. Srivastava, D. Srinivas and P. Ratnasamy, *Tetrahedron Letters*, 2006, **47**, 4213.
144. A. K. Chandrakar, D. G.P., N. Chandraker and R. S. Thakur, *International Journal of Advanced Research in Chemical Science*, 2015, **2**, 1.
145. J. Cejka, H. v. Bekkum, A. Corma and S. Ferdi, in *Introduction to Zeolite Molecular Sieves*, eds. J. Cejka, H. v. Bekkum, A. Corma and S. Ferdi, Elsevier Science, 2007.
146. D. R. Corbin and N. Herron, *Journal of Molecular Catalysis*, 1994, **86**, 343.
147. N. Herron, *Inorganic Chemistry*, 1986, **25**, 4714.
148. K. Mizuno and J. H. Lunsford, *Inorganic Chemistry*, 1983, **22**, 3484.
149. K. J. Balkus, Jr., C. D. Hargis and S. Kowalak, in *Supramolecular Architecture*, American Chemical Society, 1992, Vol. 499, Ch. 24, pp. 347.
150. M. Jafarian, M. Rashvand avei, M. Khakali, F. Gobal, S. Rayati and M. G. Mahjani, *The Journal of Physical Chemistry C*, 2012, **116**, 18518.
151. S. K. Tiwary and S. Vasudevan, *Inorganic Chemistry*, 1998, **37**, 5239.
152. S. Ray and S. Vasudevan, *Inorganic Chemistry*, 2003, **42**, 1711.

153. S. Kumari and S. Ray, *New Journal of Chemistry*, 2020, **44**, 14953.
154. A. Choudhary, S. Kumari and S. Ray, *ACS Omega*, 2017, **2**, 6636.
155. G. Sewell, R. J. Forster and T. E. Keyes, *The Journal of Physical Chemistry A*, 2008, **112**, 880.
156. K. K. Bania, D. Bharali, B. Viswanathan and R. C. Deka, *Inorganic Chemistry*, 2012, **51**, 1657.
157. D. Anselmo, G. Salassa, E. C. Escudero-Adán, E. Martin and A. W. Kleij, *Dalton Transactions*, 2013, **42**, 7962.
158. M. A. Hitchman, *Inorganic Chemistry*, 1977, **16**, 1985.
159. G. Forte, I. P. Oliveri, G. Consiglio, S. Failla and S. Di Bella, *Dalton Transactions*, 2017, **46**, 4571.
160. G. Consiglio, S. Failla, P. Finocchiaro, I. P. Oliveri and S. Di Bella, *Inorganic Chemistry*, 2012, **51**, 8409.
161. S. Kumari, A. Choudhary and S. Ray, *Applied Organometallic Chemistry*, 2019, **33**, e4765.
162. S. Kumari, K. Maddipoti, B. Das and S. Ray, *Inorganic Chemistry*, 2019, **58**, 1527.
163. K. K. Bania and R. C. Deka, *The Journal of Physical Chemistry C*, 2013, **117**, 11663.
164. D. Masih, V. Chernikova, O. Shekhah, M. Eddaoudi and O. F. Mohammed, *ACS Applied Materials & Interfaces*, 2018, **10**, 11399.
165. K. Mori, M. Kawashima, K. Kagohara and H. Yamashita, *The Journal of Physical Chemistry C*, 2008, **112**, 19449.
166. R. Srivastava, D. Srinivas and P. Ratnasamy, *Catalysis Letters*, 2003, **89**, 81.
167. H. He, Q.-Q. Zhu, C. Zhang, Y. Yan, J. Yuan, J. Chen, C.-P. Li and M. Du, *Chemistry – An Asian Journal*, 2019, **14**, 958.
168. F. Zhang, Y. Xie, P. Liu, F. Hao, Z. Yao and H. Luo, *Catalysis Letters*, 2014, **144**, 1894.

Chapter 2

Materials and Methods

2.1 Introduction

In this chapter, all the materials, the synthetic processes, methodologies, analytical instruments used, their parameters during the measurement, and their working principles are discussed in detail. Analytical tools, understanding of the underlying principles of these instruments, the interpretation of data and extracting vital conclusions are an integral part of research. Particularly, in the case of zeolite chemistry, the properties of the synthesized encapsulated complexes require the undoubted use of different analytical techniques. The encapsulations are generally proven by indirect methods to confirm the presence of the complex inside the pores of zeolites. The "neat" or the free state complexes also need to be characterized to ensure their purity.

All the above-mentioned instruments and the characterization techniques will be discussed in detail in the next section. A brief discussion about the working principles of these instruments, and the relevance of the data obtained from these analytical tools for this thesis, will also be discussed.

2.2 Materials

All the chemicals used and the companies from where those were procured, to carry out the work of this thesis are listed in Table 2.1.

Table 2.1: List of various chemicals and their suppliers used in the current thesis

S. No.	Chemical	Name of supplier
1.	2-Hydroxy-5-(trifluoromethoxy)benzaldehyde	Sigma Aldrich, India
2.	2-Hydroxy-5-bromobenzaldehyde	Sigma Aldrich, India
3.	2-Hydroxy-5-chlorobenzaldehyde	Alfa Aesar, India
4.	2-Hydroxy-5-methoxybenzaldehyde	Sigma Aldrich, India
5.	2-Hydroxy-5-methylbenzaldehyde	Sigma Aldrich, India
6.	2-Hydroxy-5-nitrobenzaldehyde	Sigma Aldrich, India
7.	2-Hydroxybenzaldehyde	Merck, India
8.	Acetone	Merck, India
9.	Acetonitrile (HPLC grade)	Sigma Aldrich, India
10.	Aluminium isopropoxide	Spectrochem, India

S. No.	Chemical	Name of supplier
11.	Ammonium ZSM-5	Alfa Aesar, India
12.	Barium sulphate	Merck, India
13.	Bromobenzene	Central Drug House, India
14.	Carbon Dioxide (CO_2)	Sigma Gases (99% purity)
15.	$CDCl_3$	Sisco Research Laboratories, India
16.	Cetyltrimethylammonium bromide	Spectrochem, India
17.	Cobalt acetate.5 H_2O	Qualikems, India
18.	Cyclohexene oxide	Thermo Fisher scientific, India
19.	Diethyl ether	Molychem, India
20.	DMSO-d_6	Sisco Research Laboratories, India
21.	Epichlorohydrin	Spectrochem, India
22.	Ethanol	Changshu Song Sheng Fine Chemical, China
23.	Methanol	Merck, India
24.	Nitric Acid	Emplura, India
25.	*o*-phenylenediamine	S D Fine Chemical Limited, India
26.	Parent zeolite Na-Y	Sigma Aldrich, India
27.	Potassium bromide (Spectroscopy grade)	Merck, India
28.	Propylene oxide	Sigma Aldrich, India
29.	Silver nitrate	Molychem, India
30.	Sodium chloride	Molychem, India
31.	Sodium metasilicate	Central Drug House, India
32.	Styrene oxide	TCI, India
33.	Sulphuric acid	Spectrochem, India
34.	Tetrabutylammonium bromide	Merck, India
35.	Tetrabutylammonium iodide	Spectrochem, India
36.	UV grade chloroform	Spectrochem, India
37.	UV grade DMSO	Spectrochem, India
38.	Zinc acetate.2 H_2O	Merck, India

2.3 Experimental Methods

This section deals with the details of the methods and the methodologies used for the synthesis of the complexes used. The procedure for upcycling CO_2, i.e., the cycloaddition reaction of epoxide with CO_2, using various catalysts is also discussed.

2.3.1 Synthesis of Al-MCM-41

For the preparation of Al-MCM-41, sodium metasilicate was taken as the silicon source, and aluminium isopropoxide was taken as the aluminium source maintaining their ratio as 1:20. The synthesis was carried out according to the procedure reported in the literature.[1] In a typical reaction setup, sodium metasilicate (44-47% SiO_2,12.2 g, 1 mol, dissolved in 50 g of deionized water) was mixed with aluminium isopropoxide (1.1 g, 0.05 mol, dissolved in 10 g of deionized water) and stirred for 30 minutes. After the stipulated time, 100 ml of 1 N sulphuric acid was added until the gel formation takes place. Consequently, cetyltrimethylammonium bromide (7.2 g, 0.2 mol) was added drop-by-drop to the solution till the gel changed to suspension. Ultimately, the suspension was transferred to a polypropylene bottle, after which it was heated in a furnace at 100 °C for four days. The material was cooled to room temperature, recovered, and repeatedly washed with deionized water and ethanol. It was finally subjected to calcination overnight at 540 °C for 12 hours.

2.3.2 Synthesis of Schiff-base ligands[2]

For the synthesis of the salophen ligands (*N, N'*-bis(salicylidene)-1,2-phenylenediamine), the benzaldehyde precursor (**54 A-G,** shown in Scheme 2.1) was dissolved in ethanol by heating. To this solution, *o*-phenylenediamine was added. The ratio of aldehyde and amine was taken as 2:1, and the reaction temperature was maintained at 80 °C. The reaction mixture was then refluxed for 3-5 hours. After the completion of the reaction, the synthesized ligand was filtered and thoroughly washed with cold ethanol and diethyl ether. The product (**L1-L7,** shown in Scheme 2.1) was finally collected and dried in the air.

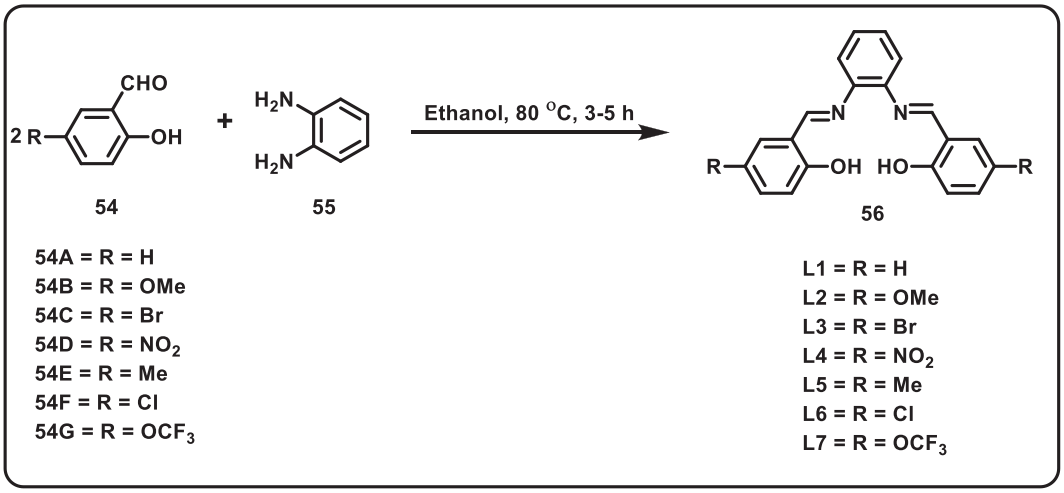

Scheme 2.1: Synthesis of the Schiff base ligands.

2.3.3 Synthesis of metal (Co, Zn) Schiff-base complexes[3, 4]

For the preparation of the metal complex (**57 ML1-ML7, M´L1-M´L3,** shown in Scheme 2.2), the synthesized ligand (L1-L7) was dissolved in ethanol by heating. After the complete dissolution of the ligand, an equimolar amount of metal acetate salt was added to the solution. The temperature was maintained at 80 °C, and the reaction was then refluxed for 3-5 hours. After the completion of the reaction, the solid was filtered by simple filtration. The product was washed thoroughly with cold diethyl ether and ethanol. Finally, the solid product was dried in an oven at 85 °C.

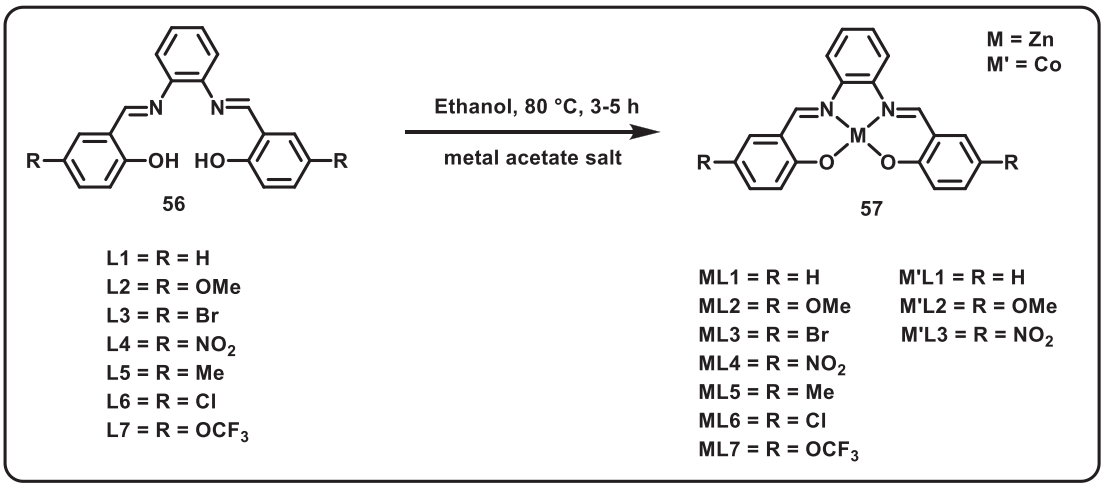

Scheme 2.2: Synthesis of the Schiff base "neat" or free-state metal complexes.

2.3.4 Synthesis of metal [M(II)] exchanged zeolite-Y[5, 6]

To exchange the mobile Na^+ ions of zeolite-Y framework by the desired metal ions to prepare the M(II) exchanged zeolite-Y (M-Y), a particular concentration of the metal salt was added to the parent zeolite Na-Y. To prepare Co-Y, 0.01 M $Co(CH_3COO)_2 \cdot 4H_2O$ in 100mL milli-Q water was to 10g of zeolite Na-Y, and for Zn-Y, 0.015 M $Zn(CH_3COO)_2.2H_2O$ in 100 mL of milli-Q water was added to the 5g of zeolite-Na-Y (Scheme 2.3) . The mixture was stirred at room temperature for 24 h to obtain the required loading level of metal ions. The slurry was filtered, washed repeatedly with milli-Q water, and then kept in a muffle furnace for 12 h at 150 °C.

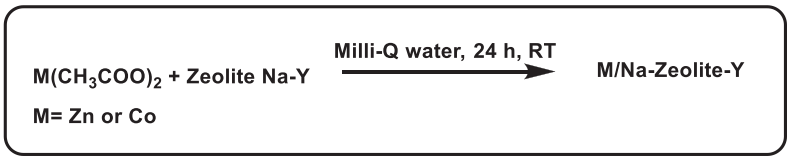

Scheme 2.3: Synthesis of metal exchange zeolite Na-Y.

2.3.5 Synthesis of encapsulated M(II)-Schiff base complexes in zeolite-Y[7]

The metal encapsulated complex was prepared as per the flexible ligand approach (Figure 1.9). Initially, the flexible Schiff-base ligand was allowed to diffuse inside the pores of zeolite-Y. For this to occur, the Schiff-base ligand with M(II)-zeolite-Y was taken in a particular ratio, and the reaction mixture was heated at 150-200 °C for 24 hours. Then the ligand was allowed to react with the metal ions present in the supercage. To prepare zinc(II) encapsulated complex, the ligand : Zn-Y ratio was kept at 0.75:1 and for cobalt(II) encapsulated complexes, the ratio was maintained at 1:1. Upon reaction, the colour of solid reaction mass changed from yellowish to dark brown. The resultant product was further purified by Soxhlet extraction to remove unreacted ligands and the metal complex formed/adsorbed on the surface. The choice of the solvent for Soxhlet was based on the ability of the solvent to solubilize the unreacted ligand and the surface-adsorbed complex, i.e., acetone, followed by methanol and diethyl ether. The product was then allowed to react with 0.01M NaCl solution to remove the unreacted metal ions. The product was filtered and washed with distilled water thoroughly until the filtrate was negative for the chloride ion test. Finally, the obtained product was dried in a muffle furnace at 150 °C for 12 h. The final product was obtained as a brown powder.

2.3.6 Synthesis of cyclic carbonate from epoxide using different aluminosilicates as catalysts at high pressure[8]

In a teflon container, 25 mg of the aluminosilicate catalyst, 0.05 mmol (16.1 gm) of TBAB, and 10 mmol (1.13 mL) of styrene oxide were added sequentially. The teflon container was put in the stainless-steel vessel of the pressure reactor under solvent-free conditions, and the reactor was sealed. The temperature was first increased to 120 °C, and once the temperature was constant, CO_2 was introduced at a pressure of 4 bar. The reaction was carried out for 2 hours with a continuous flow of CO_2 (Scheme 2.4(b)). The flow of CO_2 was stopped after the reaction, and the excess gas was vented out. The reactor was allowed to cool down and then opened. The reaction mixture was then diluted with 10 mL of acetonitrile and transferred to a glass vial. From this vial, 1.5 ml of the reaction mixture was taken in a 2 ml eppendorf tube, and 0.45 ml of internal standard, i.e., PhBr, was added. This mixture was centrifuged and was used for gas chromatographic study. For the recycling experiments, the zeolite Na-Y was separated using simple filtration. Then it was further washed using various organic solvents such as ACN, methanol, acetone, and hexane. The catalyst was dried and again used for the next cycle under the same conditions.

2.3.7 Synthesis of cyclic carbonate from epoxide using cobalt(II) free state and encapsulated catalysts at high pressure

25 mg of the encapsulated complex (CoL1-Y or CoL2-Y), or 0.05 mmol of the free state complex, 0.05 mmol (16.1 mg) of TBAB and 10 mmol (1.13 ml) of styrene oxide, were added sequentially in a teflon container. The teflon container was put in the stainless-steel chamber of the pressure reactor and was sealed. This reaction mixture was supplied with a continuous flow of CO_2 to maintain the pressure at 5 bar. Following the optimized reaction condition, the reaction was carried out for 1.5 hours at 130 °C (Scheme 2.4(d)). After the specified time, the excess CO_2 was released, and the reactor was allowed to cool down to room temperature and then opened. The reaction mixture was diluted with 10 ml of acetonitrile and transferred to a glass vial. From this vial, 1.5 ml of the reaction mixture was taken in a 2 ml eppendorf tube, and 0.45 ml of internal standard, i.e., PhBr, was added. This mixture was centrifuged and was used for gas chromatography.

2.3.8 Synthesis of cyclic carbonate from epoxide using zinc(II) Schiff base complexes.[9]

In a typical experimental setup for the synthesis of cyclic carbonate, zinc salophen complex (0.05 mmol), TBAB (0.05 mmol, 16.1 mg), and styrene oxide (10 mmol, 1.13 mL) were

sequentially added in a two-neck round bottom flask and evacuated. CO_2 was then introduced into the system using a rubber gas sample bladder. The reaction mixture was stirred for 5 hours at 80 °C (Scheme 2.4 (a)). Once the reaction was complete, the reaction mixture was diluted with 10 mL acetonitrile. From the diluted solution, 1.5 ml of the reaction mixture was taken in presence of 0.45 ml of internal standard, i.e., PhBr. After centrifuging the mixture, it was proceeded for gas chromatography.

2.3.9 Synthesis of cyclic carbonate from epoxide using zinc(II) encapsulated complexes.

In a typical experimental setup for the synthesis of cyclic carbonate, 25 mg of the zinc(II) encapsulated complex, TBAB (0.05 mmol, 16.1 mg), and styrene oxide (10 mmol, 1.13 mL) were sequentially added in a two-neck round bottom flask and evacuated. CO_2 was then introduced into the system using a rubber gas sample bladder. The reaction mixture was stirred for 14 hours at 80 °C. (Scheme 2.4 (c)) Once the reaction was complete, the reaction mixture was diluted with 10 mL acetonitrile. From the diluted solution, 1.5 ml of the reaction mixture was taken in presence of 0.45 ml of internal standard, i.e., PhBr. After centrifuging the mixture, it was proceeded for gas chromatography. For the recycling experiments, the ZnL1-Y complex was separated using simple filtration. Then it was further washed using various organic solvents such as ACN, methanol, acetone, and hexane. The catalyst was dried and again used for the next cycle under the same conditions.

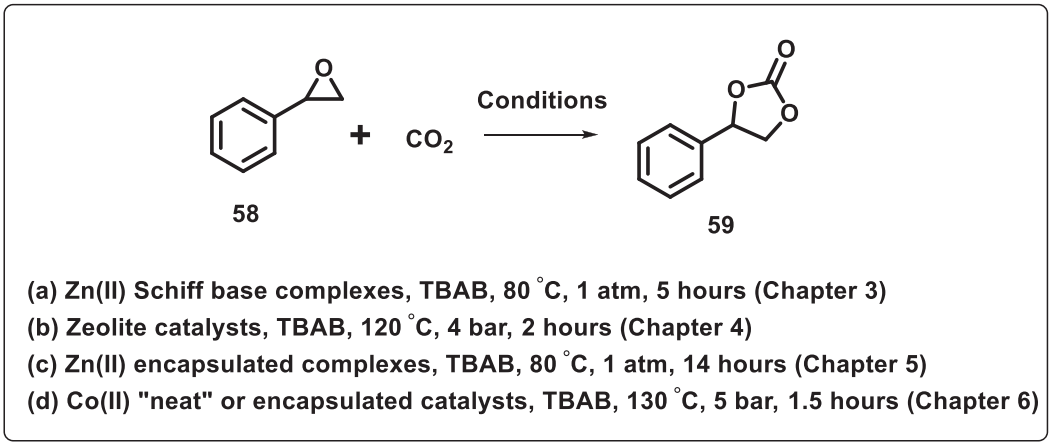

Scheme 2.4: Synthesis of cyclic carbonates from CO_2 and epoxides using different catalysts.

2.4 Characterization techniques

This section explains, in detail, the various analytical instruments used to characterize the encapsulated and the free-state complexes synthesized.

2.4.1 UV-visible/Diffuse Reflectance Spectroscopy (DRS)[10]

In the case of diffuse reflectance spectroscopy (or solid UV), the absorbance is measured by taking the ratio of the reflected light samples rather than the transmitted light.

However, in most cases, due to the inhomogeneity of the sample, it undergoes scattering instead of reflection. The Kubelka-Munk equation provides a good approximation description for the calculation of the scattering coefficient s. The diffuse reflectance, R_∞, is given as

$$k/s = (1-R_\infty)^2 / 2 R_\infty$$

where k is the absorption coefficient of the sample ($k=4\pi \kappa/\lambda$), and s is the scattering coefficient.

In the present thesis, the solution-state UV-vis measurement has been done for all the ligands and the "neat" complexes. All spectra of the cobalt(II) complexes and their ligands have been recorded using chloroform as the solvent, while the UV-vis spectra of zinc(II) complexes and their ligands have been carried out in DMSO as the solvent. All the solution-state UV-vis absorption spectra have been recorded using a JASCO V-650 spectrophotometer. Most measurements have been carried out between the wavelength range of 190-900 nm. The spectrophotometer is fitted with two lamps, i.e., a tungsten (W-lamp) lamp for the measurement between the wavelength range 900-350 nm and a deuterium (D^2-lamp) lamp for the measurement between the wavelength range 350-190 nm. Photodiodes consisting of silicon crystals is used as a detector. The solid UV spectra have been recorded using a Shimadzu UV-2450 spectrophotometer in the diffuse reflectance mode. The sample was mixed with barium sulphate ($BaSO_4$), which was used as the reference material. To measure the diffuse reflectance, the spectrophotometer is equipped with an integrating sphere of 60 mm inner diameter

2.4.2 Fourier Transform Infrared spectroscopy (FT-IR)[11]

In this thesis, the FT-IR measurements have been carried out for the zeolites, zeolite Na-Y and NH_4^+-ZSM-5, and the mesoporous silica, Al-MCM-41. All the ligands, metal complexes, and encapsulated complexes also have been characterized by FT-IR. The FT-IR spectra has

been recorded using a SHIMADZU IR AFFINITY-1S FT-IR spectrometer in the range of 450–4000 cm^{-1} by making pellets using potassium bromide.

2.4.3 Brunauer-Emmett-Teller (BET) surface analysis

In the present thesis, the Brunauer–Emmett–Teller (BET) analysis has been carried out to study surface area, pore volume of the zeolites, zeolite Na-Y and NH_4^+-ZSM-5, and the mesoporous silica, Al-MCM-41. The N_2 absorption isotherms have also been carried out for all the encapsulated complexes of cobalt and zinc. The BET measurements of the zeolites have been done using the Microtrac Bel BEL SORP mini II model machine. The same instrument was used for the surface area analysis of the zinc(II) encapsulated complexes. The adsorption studies were carried out after the pretreatment of the samples at 200 °C for 4 hours. The BET surface area, pore volume and pore size of the cobalt(II) encapsulated complexes were measured using Quantachrome instruments along with a volumetric adsorption setup at -196 °C.

2.4.4 X-ray photoelectron Spectroscopy (XPS)[12]

The complexes that have been characterized using XPS in this present thesis include the zeolites, the mesoporous silica, Al-MCM-41. and all the cobalt(II) and zinc(II) encapsulated complexes. The XPS study of all the cobalt(II) and zinc(II) free-state complexes has also been carried out for comparison. The XPS analysis was carried out by Omicron EA 125 source using Al Kα radiation having energy 1486.7 eV. During the measurement, base pressure was maintained at < 10^{-9} m bar in the UHV. High-resolution XPS traces were deconvoluted using the Gaussian statistical analysis in Origin-9 software.

2.4.5 Nuclear Magnetic Resonance (NMR)[13]

All the zinc(II) "neat" complexes used in the present thesis, were characterized using the solution NMR. The ^1H and the ^{13}C NMR were recorded on a Bruker Avance 400 spectrometer using DMSO as the solvent. The operating frequency for recording the proton NMR was 400 MHz, while that for carbon NMR was 100 MHz. The ^{29}Si MAS-NMR was recorded on JEOL-JNM-ECA Series (Delta V4.3)-400 MHz-FT-NMR instrument with a spinning frequency of 6KHz, 512 scans and 10 sec of relaxation delay. A single pulse sequence was used. Chemical shifts are reported relative to tetramethylsilane (TMS).

The DOSY experiment was performed to determine the diffusion constant of ZnL1 and ZnL4 on a Bruker Ascend 400 NMR instrument at a constant temperature of 300 K. The Z-gradient probe with the stebpgp1s pulse sequence was used. The diffusion period (d20, Δ) was 0.1 sec, and

the gradient pulse duration (p30, δ) was 1000 μs. Initial and final gradient strengths (GPZ6) were set at 5% or 95%, respectively. The data were analyzed using the MestReNova 12.0 software using the Peak Heights Fit method.

2.4.6 Powder X-ray diffraction (PXRD)[14]

Small-angle XRD has been used to characterize Al-MCM-41. All other complexes have been characterized by wide-angle XRD. In the present thesis, for small angle XRD of Al-MCM-41, Xeuss C HP100 fm instrument was used with 2θ values ranging from 0° to 4°. The XRD patterns for zeolite NH_4^+-ZSM-5 and zeolite Na-Y have been recorded by a RIGAKU MINIFLEX II X-ray diffractometer using a Cu Kα X-ray source (λ = 1.542 Å). The analysis of zeolite Na-Y was carried out with 2θ values from 8° to 50° at a scanning rate of 2° min^{-1}, while 2θ values from 5° to 80° at a scanning rate of 2° min^{-1} was used for zeolite NH_4^+-ZSM-5. For all the encapsulated complexes and metal exchanged zeolite-Y, the analysis was carried out with 2θ values from 8° to 40° at a scanning rate of 2° min^{-1}.

2.4.7 Field Emission Scanning Electron Microscopy (FESEM) and Energy Dispersive X-ray analysis (EDX)[15]

The FESEM and EDX analysis technique was employed on all the encapsulated complexes, metal exchanged zeolite-Y, zeolite Na-Y, zeolite NH_4^+- ZSM-5 and Al-MCM-41. For the encapsulated complexes, FESEM imaging was performed to perceive the proper washing after Soxhlet extraction. The Si/Al ratio in the zeolites and the metal loading in the Zn(II) and Co(II) encapsulated complexes and the metal exchange complexes were calculated by EDX analysis. In the present thesis, the FESEM imaging of the zeolites was carried out using a ThermoFisher Scientific APERO 2S model. FEI Apreo LoVac instrument with an accelerated voltage of 5–20 kV was used for the FESEM and EDX imaging of the Co(II) and Zn(II) encapsulated complexes and the metal exchange zeolites. The imaging and the EDX of the complexes were carried out after coating the samples with gold.

2.4.8 Thermogravimetric analysis (TGA)[16]

The TGA analysis in the present thesis was conducted to study the thermal stability of all three zeolite catalysts, cobalt and zinc "neat" complexes and all the encapsulated complexes. The analysis was performed in an inert (nitrogen) atmosphere within the temperature range of 25 °C - 800 °C using a TGA-60, SHIMADZU equipment at a heating rate of 10 °C min^{-1}.

2.4.9 Atomic absorption spectroscopy (AAS)

The AAS spectroscopy in the present thesis was conducted to quantify the metal, i.e., zinc, present in the complex after encapsulation. The AAS study was carried out using a SHIMADZU AA-7000 spectrophotometer.

2.4.10 NH_3-Temperature Programmed Desorption (NH_3-TPD)[17]

The NH_3-TPD analysis presented in the present thesis was performed for the zeolite catalysts using BEL Microtrac BEL crop. Bel cat II instrument. The sample was first pretreated at 400 °C for one hour in a helium stream (50 mL/min), and at the same rate, the sample was pretreated at 300 °C for another hour and finally cooled to 50 °C. Saturated adsorption of ammonia was obtained by purging NH_3 gas at 50 mL/min for 30 minutes. The sample was heated to 800 °C with a ramp rate of 10 °C/min to get the TPD profile.

2.4.11 Gas chromatography (GC)[19]

In the present thesis, the GC was done to analyze the yield obtained from the various catalysis reactions. GC analysis was carried out using GC 2014, Shimadzu fitted with column Rtx@-5MS using a flame ionization detector (FID). The calibration curves for the product and the starting material are presented in Figure 2.1. The following parameters were used in the method for the detection of the styrene carbonate:

Injector temperature: 200 °C
Injection mode: Split
Flow control mode: Pressure
Total flow: 99.5 mL/min
Linear velocity: 31.1 cm/sec
Detector temperature: 250 °C

Column temperature: 80 °C
Split ratio: 80.0
Pressure: 100.0 kPa
Column flow: 1.19 mL/min
Purge flow: 3.0 mL/min

Table 2.2: Table showing the temperature program of the column oven of GC

	Rate (°C/min)	Temperature (°C)	Hold Time (min)
0	-	80.0	0.00
1	14.00	150.0	2.00
2	20.0	240.0	2.00

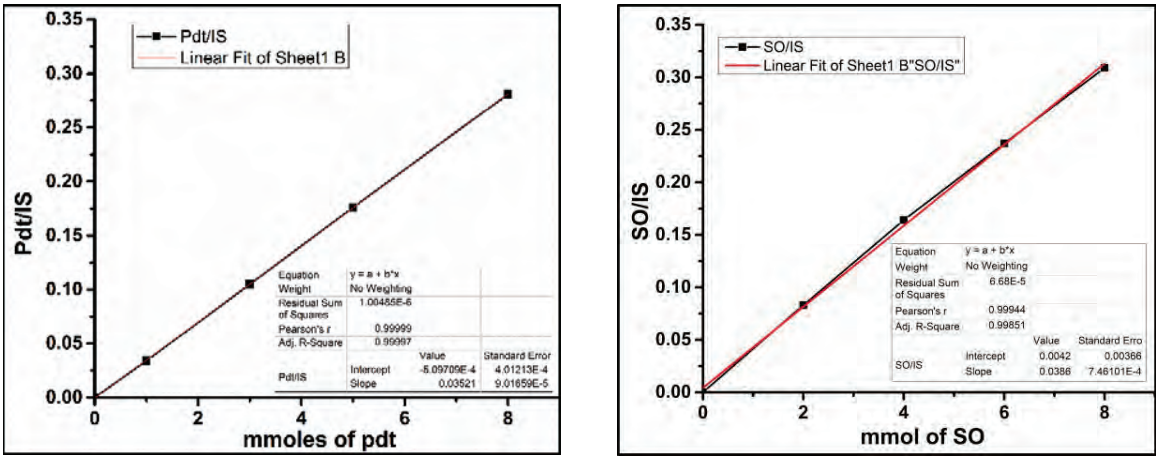

Figure 2.1: Calibration curve of product (left) and styrene oxide (right).

2.4.12 Liquid Chromatography-Mass Spectroscopy (LC-MS)

In the present thesis, all the zinc(II) free-state complexes were analyzed using the LC-MS technique. The LC-MS model Waters Acquity-H-class UPLC-MS/MS equipped with a XEVO TQD analyzer has been used for the analysis. The column used is an Acquity UPLC BEH C18 column (50mm X 2.1 mm X 1.7 µm). The solvent system used is Acetonitrile : Methanol : Ammonium acetate (pH 3.6), with their flow being 49:49:2. The column temperature was maintained at 35 °C while the sample temperature was 10 °C. The probe used was an ESI probe in both positive and negative modes.

2.4.13 Theoretical methods

In the present thesis, the electronic structure studies of all the cobalt and zinc complexes were performed using Density Functional Theory (DFT). Detailed analyses of the structural and optical properties of all the complexes were carried out. In the case of zinc "neat" complexes, theoretical studies were applied to probe the reaction mechanism and the catalysis also. For both "neat" cobalt and zinc, all results presented were obtained using the GAUSSIAN 16 suite of *ab initio* quantum chemistry programs.[20] For the structural optimizations, hybrid B3PW91 exchange[21, 22] and correlation functional with the double-zeta 6-31++G** basis set for all atoms were used. Vibrational frequencies were calculated without any symmetry constraints to ascertain the stable structures of the Zn-complexes. The optical spectra of the complexes were calculated using time-dependent density functional (TD-DFT) methods, and we used B3PW91/6-31++G** for all atoms. The closed shell singlet electronic state was used in all calculations, and the results correspond to

the gas phase. The molecular orbitals have been defined with respect to the highest occupied molecular orbital (HOMO) and lowest unoccupied molecular orbital (LUMO) as HOMO-n and LUMO+n.

To evaluate the catalytic properties of ZnL complexes, theoretically modelled reaction mechanism of the catalysis process was selected. The structures of all intermediates and the transition states were optimized to calculate the respective free energies of activation. The transition state (TS) structures found during the reaction pathway were confirmed with one imaginary vibrational frequency, and the course of the reaction was modelled using the reaction path concept using the intrinsic reaction coordinate (IRC) analysis, which verifies that the transition state connects the correct reactants and products on the potential energy surface.[23, 24] For catalysis studies, we have used hybrid meta-functional M05-2X/6-311G** as it is known to predict thermochemical data with greater accuracy.[25, 26]

In the studies involving encapsulation of cobalt and zinc complexes within zeolite pore, we have modelled only a portion zeolite-Y supercage. All the unsatisfied valencies of silicon atoms were terminated by hydrogen atoms. During the study of encapsulated complexes, the structure of the zeolite supercage was kept fixed without any relaxations, however the positions of the terminal hydrogen atoms were allowed to change. Cobalt(II) being a d^7 system, we studied the doublet, neat and quartet, encapsulated states of the cobalt complexes, and the optical spectra were calculated using time-dependent density functional (TD-DFT) methods. For these studies we used B3PW91/6-31++G** for all atoms on B3PW91/6-31G** optimized structures. In case of quartet encapsulated complexes, the optical spectra were calculated without the zeolite supercage, *i.e.* after extracting the encapsulated cobalt complexes from zeolite and keeping its geometry fixed. The optical spectra was then analysed in terms of the molecular orbitals of the cobalt complexes in free or encapsulated states. Similar protocol was followed for the zinc encapsulated complexes as well. Since the cobalt(II) and zinc(II) complexes are commonly known to dimerize, we also looked into dimerization of these complexes. The binding energy for the dimer formation is calculated as:

$$E_{bind} = 2(E_{monomeric\ Co\text{-}complex}) - E_{dimeric\ Co\text{-}complex}$$

Table 2.3: List of various analytical instruments used in the current thesis

S. No	Name of the analytical instrument	Probed complex	Inference from the instrument
1	UV-visible/Diffuse Reflectance (DR) spectrometer	"Neat" complex and encapsulated complex	To study the electronic environment of the complex
2	Fourier-Transform Infrared spectrometer (FT-IR)	"Neat" complex, encapsulated complex and zeolite-complexes	To identify the different types of functional groups present in the complexes
3	Brunauer–Emmett–Teller (BET)	Encapsulated complex and zeolite-based complex	To measure the surface area, the pore size, and the pore volume
4	X-ray photoelectron spectrometer (XPS)	"Neat" complex, encapsulated complex and zeolite-based complexes	To investigate the oxidation state of the metal, to study the electronic environment of the metal, and to calculate the Si/Al ratio of zeolites
5	Nuclear Magnetic Resonance (NMR)	"Neat" complex and zeolite-based complexes	To elucidate the structure of the complexes
6	Powder X-ray diffraction (PXRD)	Encapsulated complex and zeolite-based complexes	To study the various planes present in the molecule
7	FESEM and EDX	Encapsulated complex and zeolite-based complexes	To understand the microscopic structure and to ensure proper encapsulation
8	Thermogravimetric analysis (TGA)	"Neat" complex, encapsulated complex and zeolite-based complexes	To measure the stability of the complexes at high temperatures
9	NH_3-Temperature Programmed Desorption (NH_3-TPD)	Encapsulated complex and zeolite-based complexes	To identify the acidic sites of the complexes
10	Atomic absorption spectroscopy (AAS)	Encapsulated complexes	To quantify the metal content in the encapsulated complex
11	Gas chromatography (GC)	Reaction mixture	To analyze the result of the catalytic reaction
12	Liquid Chromatography-Mass Spectroscopy (LC-MS)	"Neat" complex	To elucidate the structure with the help of mass

2.5 References

1. M. Selvaraj, A. Pandurangan, K. S. Seshadri, P. K. Sinha, V. Krishnasamy and K. B. Lal, *Journal of Molecular Catalysis A: Chemical*, 2002, **186**, 173.
2. S. Di Bella, I. Fragalà, I. Ledoux, M. A. Diaz-Garcia and T. J. Marks, *Journal of the American Chemical Society*, 1997, **119**, 9550.
3. I. Giannicchi, R. Brissos, D. Ramos, J. d. Lapuente, J. C. Lima, A. D. Cort and L. Rodríguez, *Inorganic Chemistry*, 2013, **52**, 9245.
4. G. Pattenden and A. J. Clark, in *Encyclopedia of Reagents for Organic Synthesis (EROS)*, 2001.
5. N. Herron, *Inorganic Chemistry*, 1986, **25**, 4714.
6. K. Mori, M. Kawashima, K. Kagohara and H. Yamashita, *The Journal of Physical Chemistry C*, 2008, **112**, 19449.
7. K. K. Bania, D. Bharali, B. Viswanathan and R. C. Deka, *Inorganic Chemistry*, 2012, **51**, 1657.
8. Q.-N. Zhao, Q.-W. Song, P. Liu, Q.-X. Zhang, J.-H. Gao and K. Zhang, *Chinese Journal of Chemistry*, 2018, **36**, 187.
9. C. Martín, C. J. Whiteoak, E. Martin, M. Martínez Belmonte, E. C. Escudero-Adán and A. W. Kleij, *Catalysis Science & Technology*, 2014, **4**, 1615.
10. M. A. Zanjanchi, K. Tabatabaeian and F. Hosseinzadeh, *Russian Journal of Coordination Chemistry*, 2005, **31**, 585.
11. G. Coudurier, C. Naccache and J. C. Vedrine, *Journal of the Chemical Society, Chemical Communications*, 1982, 1413.
12. J. Azoulay, *Vacuum*, 1983, **33**, 211.
13. S. Li, L. Zhou, A. Zheng and F. Deng, *Chinese Journal of Catalysis*, 2015, **36**, 789.
14. D. J. C. Yates, *Canadian Journal of Chemistry*, 1968, **46**, 1695.
15. L. A. Bursill, E. A. Lodge and J. M. Thomas, *Nature*, 1980, **286**, 111.
16. C. Song, W.-C. Lai, A. D. Schmitz and K. M. Reddy, Spring national meeting of the American Chemical Society (ACS), United States, 1996.
17. M. Niwa and N. Katada, *The Chemical Record*, 2013, **13**, 432.
18. C.-A. Trujillo, N.-T. Ramírez-Marquez and J.-S. Valencia-Rios, *Thermochimica Acta*, 2020, **689**, 178651.

19. K. D. Bartle and P. Myers, *TRAC Trends in Analytical Chemistry*, 2002, **21**, 547.
20. M. J. Frisch, G. W. Trucks, H. B. Schlegel, G. E. Scuseria, M. A. Robb, J. R. Cheeseman, G. Scalmani, V. Barone, G. A. Petersson, H. Nakatsuji, X. Li, M. Caricato, A. V. Marenich, J. Bloino, B. G. Janesko, R. Gomperts, B. Mennucci, H. P. Hratchian, J. V. Ortiz, A. F. Izmaylov, J. L. Sonnenberg, Williams, F. Ding, F. Lipparini, F. Egidi, J. Goings, B. Peng, A. Petrone, T. Henderson, D. Ranasinghe, V. G. Zakrzewski, J. Gao, N. Rega, G. Zheng, W. Liang, M. Hada, M. Ehara, K. Toyota, R. Fukuda, J. Hasegawa, M. Ishida, T. Nakajima, Y. Honda, O. Kitao, H. Nakai, T. Vreven, K. Throssell, J. A. Montgomery Jr., J. E. Peralta, F. Ogliaro, M. J. Bearpark, J. J. Heyd, E. N. Brothers, K. N. Kudin, V. N. Staroverov, T. A. Keith, R. Kobayashi, J. Normand, K. Raghavachari, A. P. Rendell, J. C. Burant, S. S. Iyengar, J. Tomasi, M. Cossi, J. M. Millam, M. Klene, C. Adamo, R. Cammi, J. W. Ochterski, R. L. Martin, K. Morokuma, O. Farkas, J. B. Foresman and D. J. Fox, Gaussian 16 Rev. C.01, Wallingford, CT, 2016.
21. A. D. Becke, *Journal of Chemical Physics*, 1993, **98**, 5648.
22. A. D. Becke, *Physical Review A*, 1988, **38**, 3098.
23. K. Fukui, *The Journal of Physical Chemistry*, 1970, **74**, 4161.
24. K. Fukui, *Accounts of Chemical Research*, 1981, **14**, 363.
25. A. Sorkin, D. G. Truhlar and E. A. Amin, *Journal of Chemical Theory and Computation*, 2009, **5**, 1254.
26. E. A. Amin and D. G. Truhlar, *Journal of Chemical Theory and Computation*, 2008, **4**, 75.

Chapter 3

CO_2 to Cyclic Carbonate: A Mechanistic Insight of a Benign Route Using Zinc(II) Salophen Complexes

Abstract: *Zinc(II) Schiff base complexes with different substituents at 5, 5' positions have been synthesized to study the effect of the electronic environment of the metal towards the cycloaddition reaction between CO_2 and epoxide. The prepared complexes have been characterized by FT-IR, XPS, NMR, electronic spectroscopy, LC-MS, and TGA analysis. We have used density functional theory (DFT) to study the electronic structure of the Zn(II) complexes and modelled the electronic spectra and the mechanism of catalysis for selected complexes. Results from DFT and LC-MS data show the existence of all the complexes as dimers except ZnL4. The monomeric ZnL4 has the strongest electron withdrawing group, i.e., -NO_2 attached to it along two labile water molecules at the 5th and 6th coordination sites. The dimeric complexes exhibit good to moderate yield for cycloaddition reaction to styrene carbonate under solvent-free conditions and a relatively low reaction temperature of 80 °C, with CO_2 pressure of ~1 atm from a bladder. However, the best yield has been achieved by ZnL4. Different rate-determining steps are also captured by the DFT studies for dimeric and monomeric complexes. Without taking any preventing measure of dimerization by attaching the bulky ^{t}Bu groups, relatively lesser catalytic amounts of all the complexes have shown yields of cyclic carbonate between 53-74%, depending on the nature of the substituent present.*

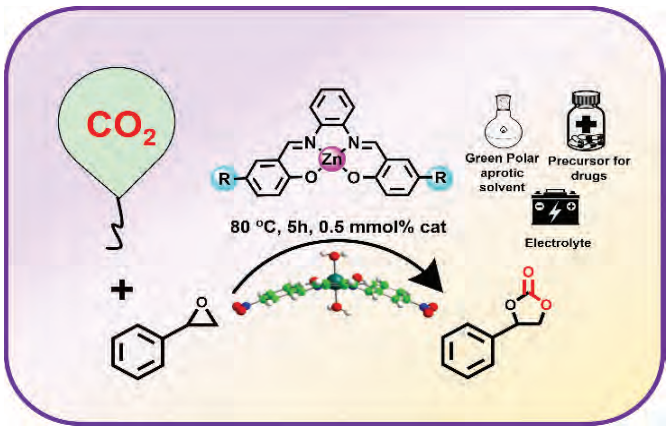

A. Ramesh, S. De, S. Bajaj, B. Das and S. Ray, *European Journal of Inorganic Chemistry*, 2024, **27**, e202300610.

3.1 Introduction

Over the past decade, an alarming increase of CO_2 in the atmosphere has led to unprecedented global warming, resulting in harsh climatic conditions and posing significant environmental as well as societal challenges.[1] To control and maintain the CO_2 levels in the atmosphere, upcycling CO_2 is one of the important focus of the scientific community. As previously discussed, CO_2 is an abundant, non-toxic, and readily available C1 source for useful chemical transformations. In the past two decades, numerous homogeneous and heterogeneous catalysts have been explored for synthesizing cyclic carbonates using epoxides and CO_2.[2-9] Most of the homogeneous catalysts used earlier require high pressure and temperature,[10, 11] with only a handful of reports available using homogeneous metal-based catalysts at ambient temperature and pressure.[12] In continuation to the discussion in scope of the thesis (Section 1.2), this chapter deals with N_2O_2-coordinating tetradentate Schiff base salophen complexes due to their straightforward synthesis process from cheap precursors, broad applicability, metal complexing ability combined with fascinating electronic properties.[13, 14]

Zinc salophen-type complexes are generally known to undergo dimerization.[15, 16] Among the reported zinc(II) salophen-type complexes, the bulky *tert*-butyl (^{t}Bu) group has been introduced at the 3, 3' and 5, 5' positions to prevent dimerization.

In the present chapter, we have synthesized simple zinc(II) salophen complexes, ZnL1-ZnL7 (shown in Scheme 3.1) and employed them as catalysts for the cycloaddition reaction of styrene oxide and CO_2. The report of the cycloaddition reaction with complex ZnL1 leaves the scope of exploring the structural variation driven by different substituents and their effects in catalytic activity along with mechanistic insight.[17] Zinc is an abundant, non-toxic, and inexpensive Lewis acidic metal.[10, 18] Zinc complexes are advantageous due to uncomplicated synthesis procedures, high thermal stability, and ligand coordination ability.[1] The prepared zinc(II) complexes were studied systematically to see the effects of different substituents at the para position to hydroxy group on the probe reaction. Moderate to good yields of styrene carbonate (SC) were attained with these synthesized catalysts at the temperature of 80 °C and CO_2 pressure of a little more than 1 atm using a rubber bladder filled with CO_2. (The pressure of a bladder is generally between 0.5-1.06 atm).

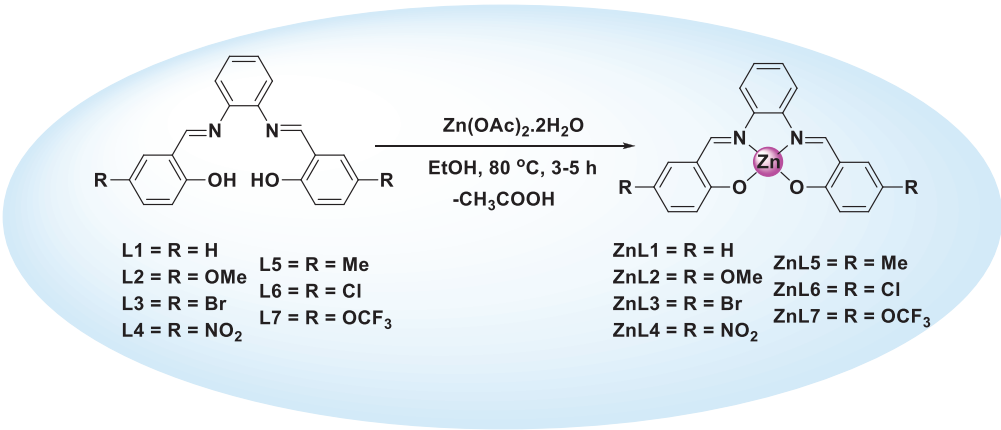

Scheme 3.1: Synthesis of zinc(II) salophen complexes.

3.2 Results and discussions

3.2.1 Fourier Transform Infrared (FT-IR) spectroscopy

FT-IR of all the prepared ligands and the corresponding zinc salophen complexes was carried out. The full range spectra are presented in Figure 3.1, while Figure 3.2 shows the zoomed spectra in the range 400-1800 cm^{-1}. The corresponding peak position values are tabulated in Table 3.1. The major peaks which we can observe in common for both ligands and corresponding zinc complexes are the functional groups C=C, C-H (deformation), C=N and C-O. All the ligands show the characteristic peak for the hydroxy group within the range of 3398-3490 cm^{-1}, which disappears upon complexation. The complexes show an identical spectra as compared to ligands, with the peaks for the major functional groups shifting at a lower wavenumber.[19] This is attributed to the increase in the mass of the complex upon complexation, which decreases the stretching frequency and hence the wavenumber. The C=C stretching frequency appears around ~1583-1561 cm^{-1} and ~1490-1473 cm^{-1} in the ligands, which is shifted to ~1550-1515 cm^{-1} and ~1487-1454 cm^{-1}, for the complexes. Similarly, all the other major peaks, i.e., C-O, C=N and C-H (deformation), are also shifted to lower wavenumber upon complexation (shown in Table 3.1).

Table 3.1: FT-IR peak positions of all the ligands and the prepared complexes (cm^{-1})					
Complex	**C=N**	**C=C**	**C-H deformation**	**C-O**	**O-H**
L1	1615	1562,1480	1402	1363	3498
ZnL1	1614	1527, 1463	1383	1321	-
L2	1616	1569, 1483	1378	1330	3479
ZnL2	1604	1531, 1471	1397	1306	-
L3	1611	1561, 1473	1382	1346	3482
ZnL3	1611	1515, 1454	1376	1312	-
L4	1619	1583, 1480	1339	1298	3440
ZnL4	1618	1550, 1487	1397	1320	-
L5	1616	1564, 1485	1389	1356	3465
ZnL5	1619	1528, 1468	1381	1320	-
L6	1611	1564, 1475	1384	1349	3309
ZnL6	1620	1517, 1459	1378	1305	-
L7	1619	1574, 1490	1360	1298	3482
ZnL7	1621	1531, 1470	1384	1264	-

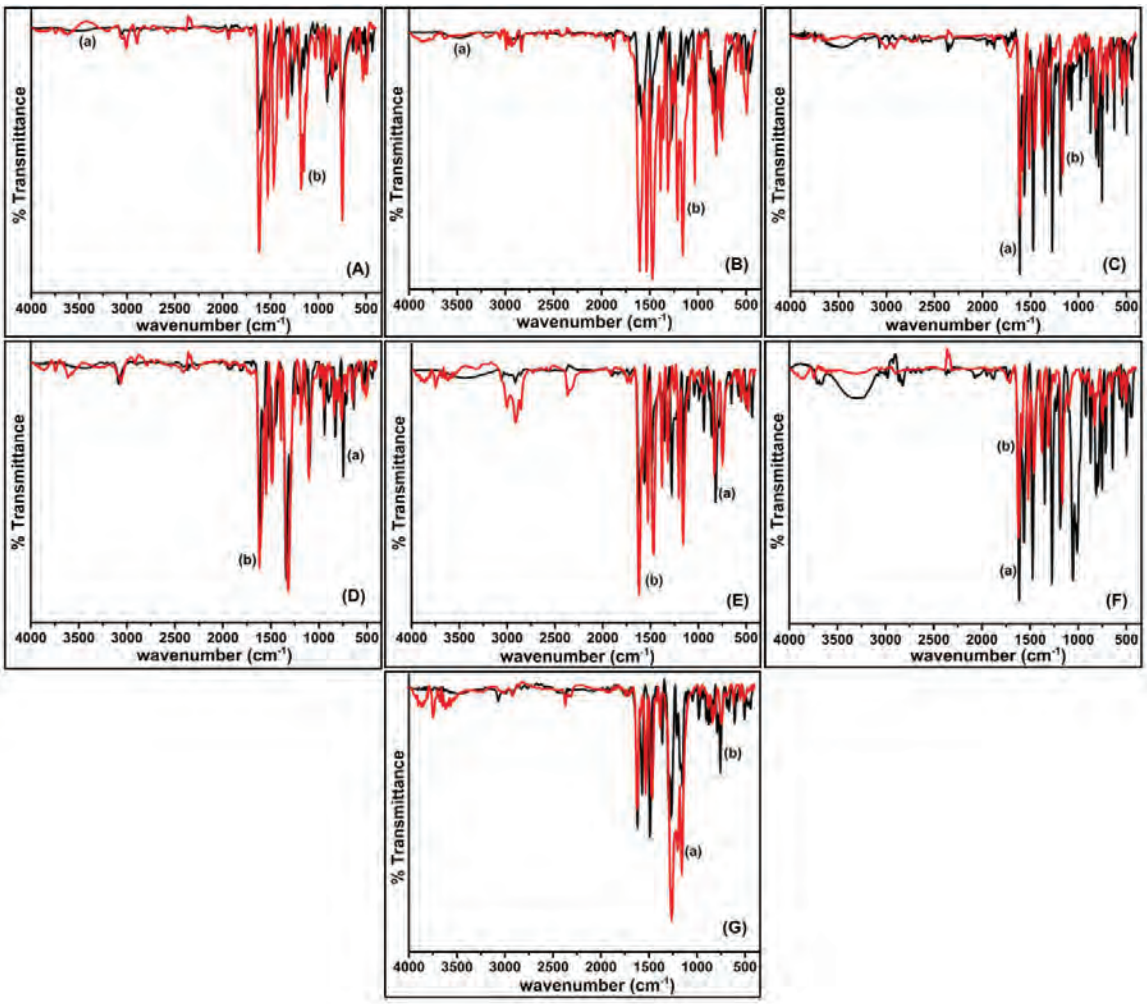

Figure 3.1: Full range FT-IR spectra of **(A)** (a) L1, (b) ZnL1, **(B)** (a) L2, (b) ZnL2, **(C)** (a) L3, (b) ZnL3, **(D)** (a) L4, (b) ZnL4, **(E)** (a) L5, (b) ZnL5, **(F)** (a) L6, (b) ZnL6, **(G)** (a) L7, (b) ZnL7.

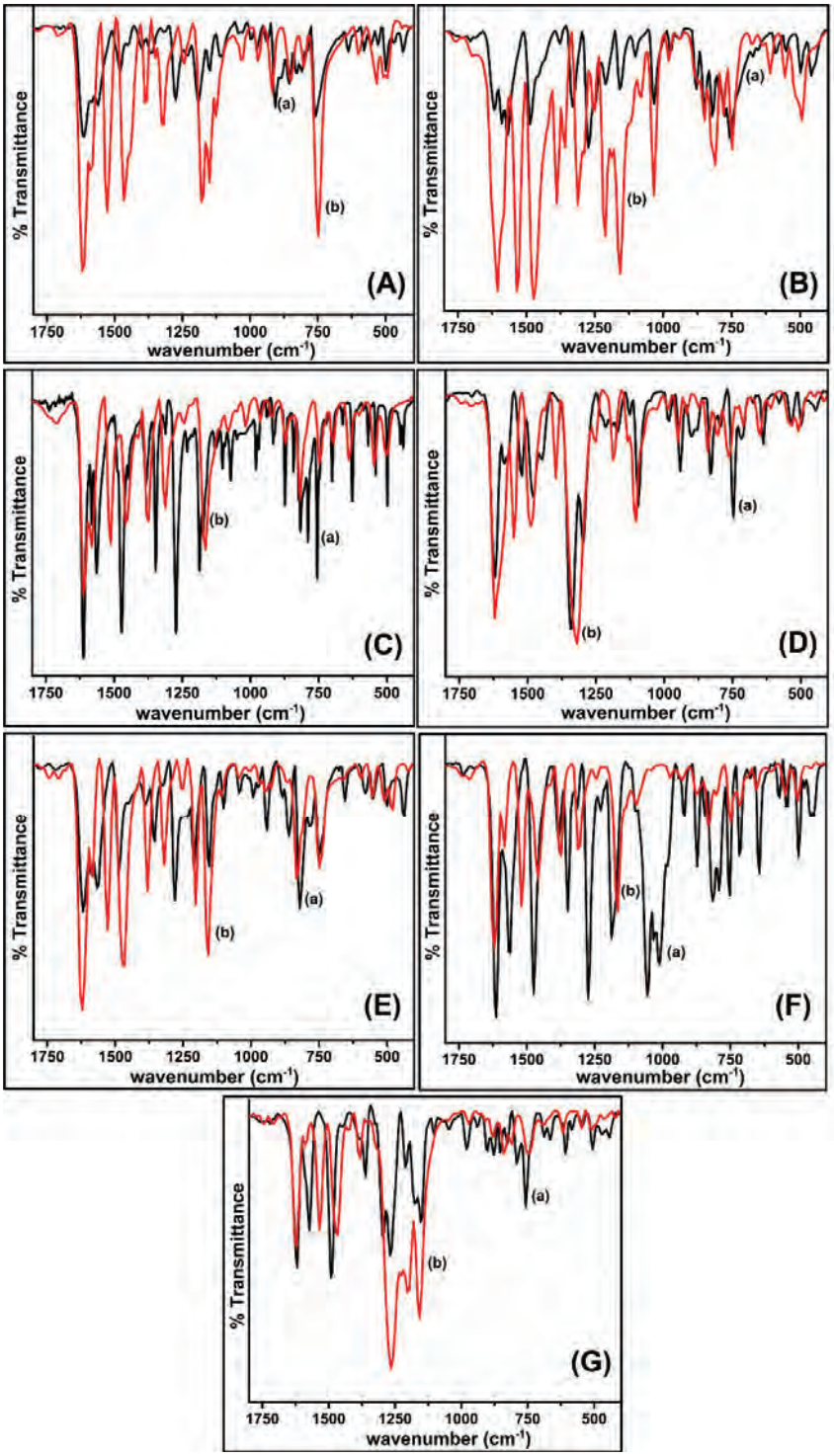

Figure 3.2: Zoomed FT-IR spectra of **(A)** (a) L1, (b) ZnL1, **(B)** (a) L2, (b) ZnL2, **(C)** (a) L3, (b) ZnL3, **(D)** (a) L4, (b) ZnL4, **(E)** (a) L5, (b) ZnL5, **(F)** (a) L6, (b) ZnL6, **(G)** (a) L7, (b) ZnL7.

3.2.2 X-ray Photoelectron Spectroscopy (XPS) studies

To understand the nature of the core metal, i.e., zinc, to ensure the presence of other elements and to investigate their chemical environment, XPS of all the zinc complexes was performed. The spectra for Zn (2p) for all the complexes is shown in Figure 3.4 and the spectra of C (1s), N (1s), and O (1s) are shown in Figure 3.5 and Figure 3.6. Figure 3.3 depicts the XPS survey spectra of all the complexes. The corresponding binding energy values are tabulated in Table 3.2. The presence of zinc in the +2 oxidation state is confirmed by the appearance of $2p_{3/2}$ and $2p_{1/2}$ peaks with a binding energy difference of ~23 eV.[20] Also, depending on the electron donating or withdrawing ability of the -R group of the complex, the binding energy of Zn $2p_{3/2}$ and Zn $2p_{1/2}$ for the complexes range from the values 1020.82-1022.29 eV and 1043.91-1045.38 eV, respectively; wherein the complexes with electron-donating groups like -OMe and -Me have lower binding energy while the electron-withdrawing groups are towards the higher binding energy side. The presence of an electron-withdrawing group on the complex makes the metal center electron deficient, and consequently making the binding energy appear at a higher value.[21]

The presence of other elements like carbon, nitrogen and oxygen is also confirmed by the XPS analysis. The different environment of C (1s) present in each complex differs with the substituent and is shown in Figure 3.5 and Figure 3.6. The three types of C (1s) atoms present commonly in all the complexes are in -C=C, -C=N and -C-O, and are in well agreement with the reported values for similar complexes.[22] Likewise, all the complexes show three peaks for oxygen. The O (1s) peak is deconvoluted into three peaks, which indicates the presence of the O-Zn bond in the molecular plane, the O-Zn bond of the dimeric zinc (except ZnL4) and the O-C bonds. The presence of oxygen bound with two different zinc centers indicates the complex in dimeric form. In the case of ZnL2, ZnL4, and ZnL7, apart from O-C and O-Zn, oxygen peaks for the respective substituent also appeared. Similarly, the deconvoluted spectra of N (1s) rendered two peaks corresponding to N=C and N-Zn. ZnL4 showed the N peaks for the NO_2 group as well, and the peak positions are in agreement with the values reported for complexes with analogous structures.[23, 24] The peaks typically of Br (3d),[25] Cl (2p)[26] and F (1s)[27] in complexes ZnL3, ZnL6, and ZnL7, respectively, are also observed, which confirm the presence of these elements in the corresponding complexes.

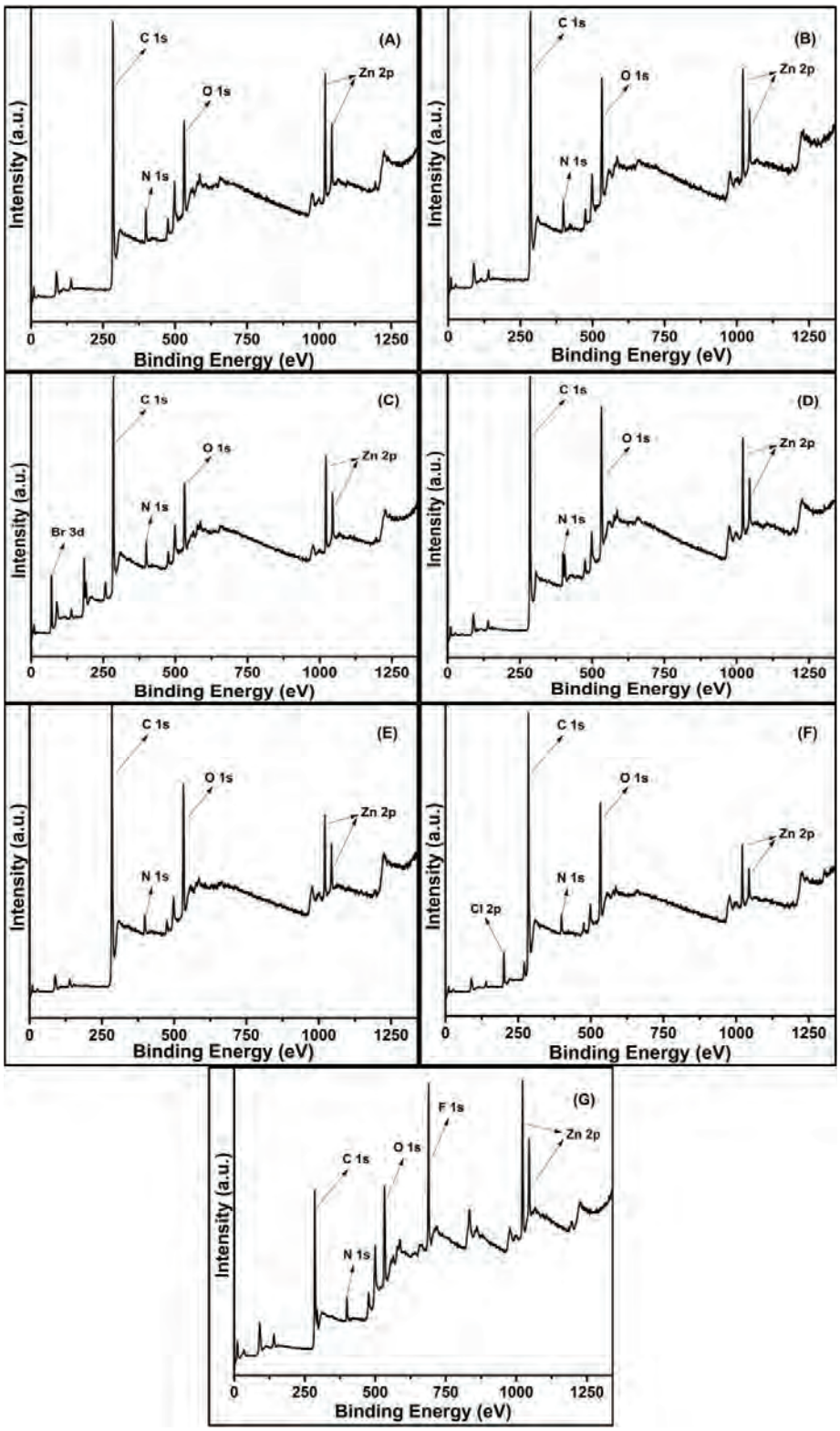

Figure 3.3: XPS survey spectra of **(A)** ZnL1, **(B)** ZnL2, **(C)** ZnL3, **(D)** ZnL4, **(E)** ZnL5, **(F)** ZnL6, **(G)** ZnL7.

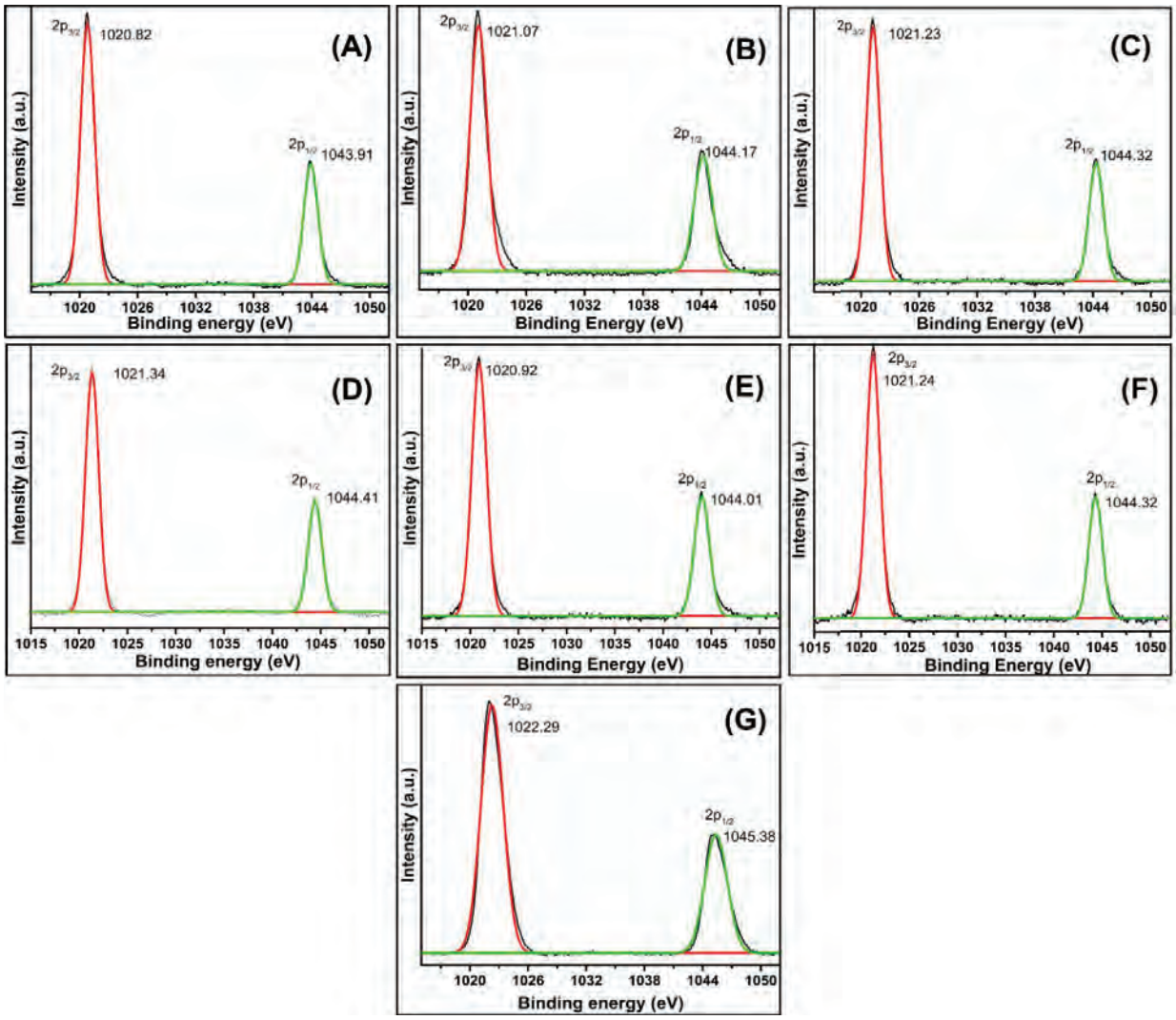

Figure 3.4: XPS spectra of Zn (2p) of **(A)** ZnL1, **(B)** ZnL2, **(C)** ZnL3, **(D)** ZnL4, **(E)** ZnL5, **(F)** ZnL6, **(G)** ZnL7.

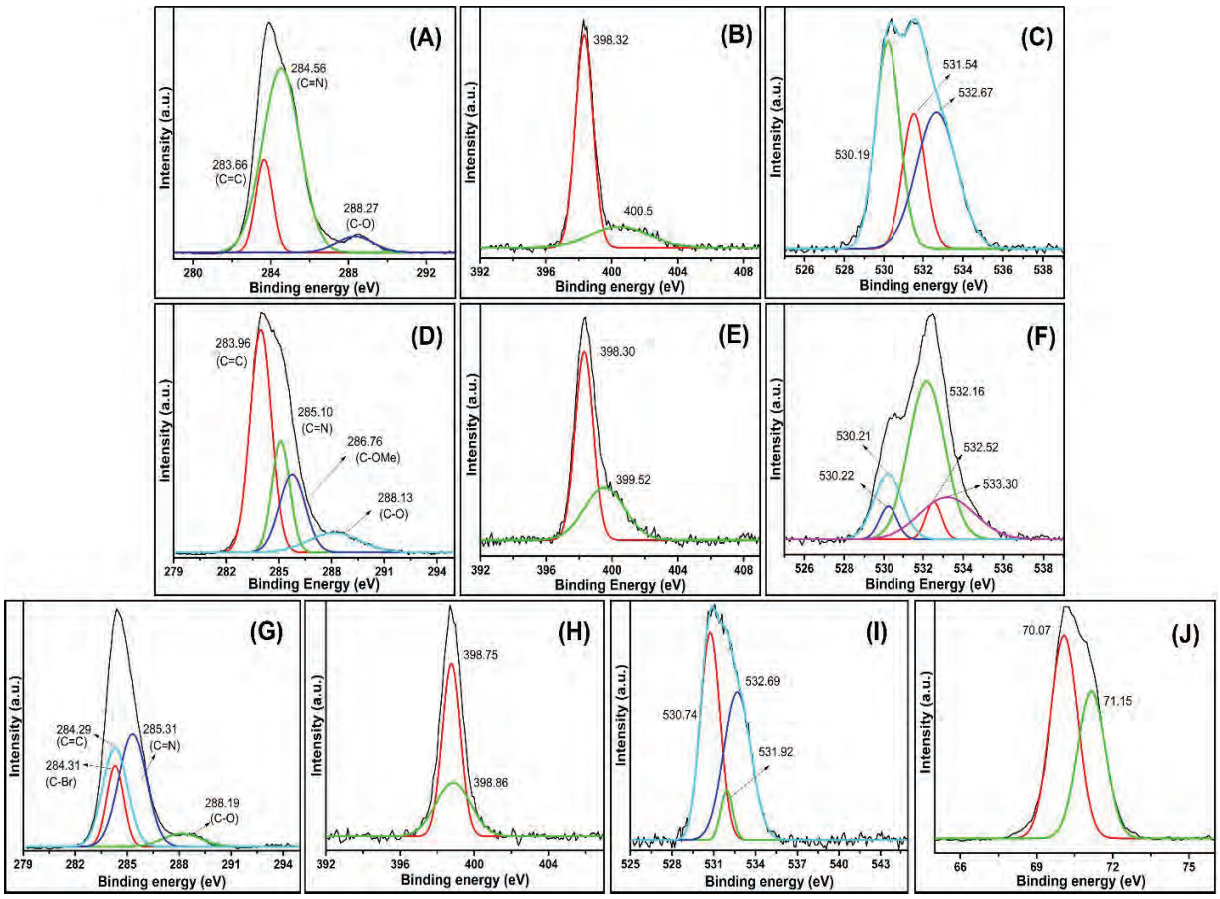

Figure 3.5: XPS profiles of **(A)** C (1s) of ZnL1, **(B)** N (1s) of ZnL1, **(C)** O (1s) of ZnL1, **(D)** C (1s) of ZnL2, **(E)** N (1s) of ZnL2, **(F)** O (1s) of ZnL2, **(G)** C (1s) of ZnL3, **(H)** N (1s) of ZnL3, **(I)** O (1s) of ZnL3, **(J)** Br (3d) of ZnL3.

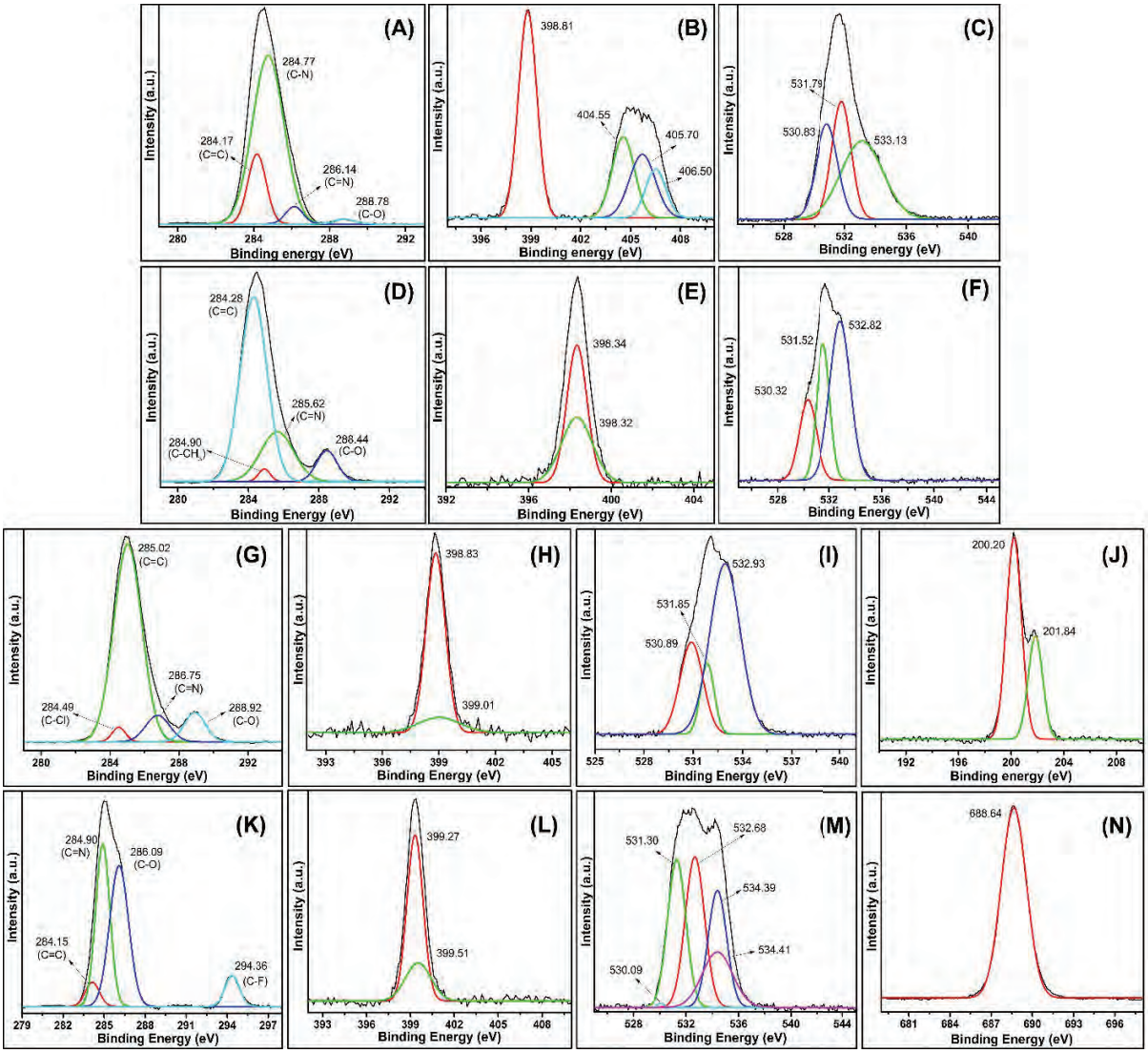

Figure 3.6: XPS profiles of **(A)** C (1s) of ZnL4, **(B)** N (1s) of ZnL4, **(C)** O (1s) of ZnL4, **(D)** C (1s) of ZnL5, **(E)** N (1s) of ZnL5, **(F)** O (1s) of ZnL5, **(G)** C (1s) of ZnL6, **(H)** N (1s) of ZnL6, **(I)** O (1s) of ZnL6, **(J)** Cl (2p) of ZnL3, **(K)** C (1s) of ZnL7, **(L)** N (1s) of ZnL7, **(M)** O (1s) of ZnL7, **(N)** F (1s) of ZnL7.

Table 3.2: XPS binding energies of all the complexes (eV)							
Complex	**C (1s)**	**N (1s)**	**O (1s)**	**Zn ($2p_{1/2}$)**	**Zn ($2p_{3/2}$)**	**ΔBE Zn**	**Other Peaks**
ZnL1	283.66 284.56 288.27	398.32 400.5	530.19 531.54 532.67	1043.91	1020.82	23.09	-
ZnL2	283.96 285.10 286.76 288.13	398.30 399.52	530.21 530.22 532.16 532.52 533.30	1044.17	1021.07	23.10	-
ZnL3	284.29 284.31 285.31 288.19	398.75 398.86	530.74 531.92 532.69	1044.32	1021.23	23.09	Br 3d 70.07 71.15
ZnL4	284.17 284.77 286.14 288.78	398.81 404.55 405.70 406.50	530.83 531.79 533.13	1044.41	1021.34	23.07	-
ZnL5	284.28 284.90 285.62 288.44	398.32 398.34	530.32 531.52 532.82	1044.01	1020.92	23.09	-
ZnL6	284.49 285.02 286.75 288.92	398.83 399.01	530.89 531.85 532.93	1044.32	1021.24	23.08	Cl 2p 200.20 201.84
ZnL7	284.15 284.90 286.09 294.36	399.27 399.51	530.09 531.30 532.68 534.39 534.41	1045.38	1022.29	23.09	F 1s 688.64

3.2.3 Thermogravimetric (TGA) analysis

The thermal stability of all the complexes was studied, and the thermogram is shown in Figure 3.7. The weight loss undergone by the complexes is tabulated in Table 3.3. All the complexes show a three-step weight loss before final decomposition. Notably, all the complexes are stable at the reaction temperature, i.e., 80 °C. The first weight loss, approximately between 3.5-5 weight % at temperatures higher than 150 °C, for all the complexes, is attributed to the removal of water molecules.[28] The subsequent decrease in weight, which is less than 10 weight % (except ZnL7) of the weight loss, is attributed to the loss of small organic fractions from the ligand moiety. The third and most major weight loss, in all the complexes, is ascribed to the disintegration of the salophen ligand molecules, after which the complex is completely degraded.[29, 30] From the TGA plots, it is clear that none of the complexes is completely degraded. It is possible that at the end of the decomposition, metallic zinc is left as the residue.[31]

From the TGA curve, the steep weight loss in complexes ZnL4 and ZnL5 is evident. These complexes exhibit a sudden weight loss of 60.5% and 70% in the third step, respectively, with comparatively lesser weight loss in step two. The substituent present in the 5, 5' position of the complex has vital role in the stability of the complex. Electron donating and electron withdrawing groups affect the thermal stability of the complex in different ways. It is observed that the thermogram of two similar substituents -Cl and -Br show similar degradation patterns. Electron withdrawing groups lower down the stability of the complex, while electron donating groups tend to stabilize the complex. From the TGA thermogram, we can see that withdrawing groups like -NO_2 and -OCF_3 have degraded almost completely (up to 85%), while the complexes with -H and electron donating -OMe have degraded only up to 30% and 40% respectively, indicating their higher stability. Moreover, of all the prepared ligands, L5 has the lowest melting point (118-120 °C), which is reflected in the comparatively lesser stability of its complex, ZnL5. As a result of the effect of the substituent group, It is also observed that the thermogram of the complexes having similar nature of substituents follow a similar trend.[32]

Table 3.3: Observed and calculated weight loss from TGA for all the complexes			
Complex	**Temperature (°C)**	**Weight loss (%) (obs)**	**Weight loss (%) (cal)**
ZnL1	164-214 366-383 515-800	5.1 2 28.5	4.7 32
ZnL2	202-231 301-517 517-800	3.9 10 46.5	4.1 51.8
ZnL3	145-210 417-432 432-800	5 8 77	3.3 79.2
ZnL4	150-215 413-541 454-460	5 16.5 60.5	3.8 65.3
ZnL5	172-213 365-382.5 394-513	4 3 70	4.4 73.3
ZnL6	158-195 460-472 474-735	3.5 9 66	4.0 69.2
ZnL7	163-192.5 355-420 421-605	3.5 36.5 34.6	3.2 32.6

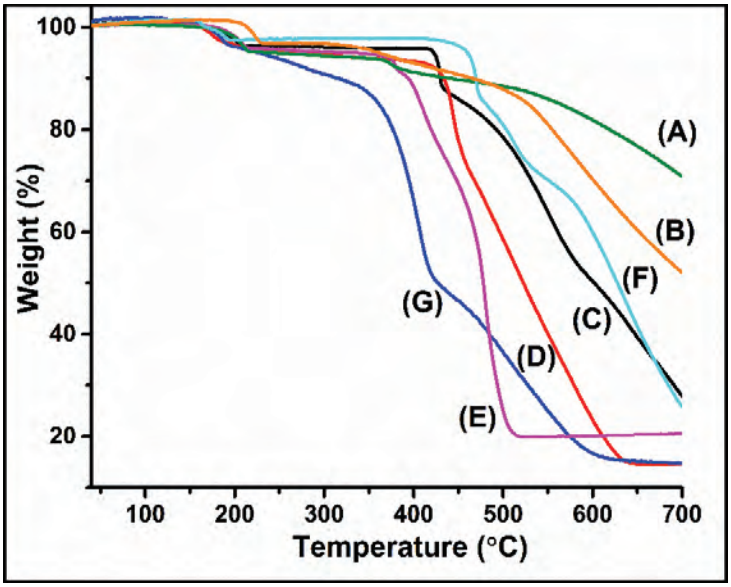

Figure 3.7: TGA thermogram of **(A)** ZnL1, **(B)** ZnL2, **(C)** ZnL3, **(D)** ZnL4, **(E)** ZnL5, **(F)** ZnL6, **(G)** ZnL7.

3.2.4 Liquid Chromatography-Mass Spectrometry (LC-MS) and Structural Studies from DFT

The formation of the complexes was confirmed through LC-MS analysis, and the results may be correlated to the catalytic performance of these complexes. It is known from the literature that salophen-type zinc complexes undergo dimerization,[33] and correspondingly, for the complexes, we observed the $[2M^{+}+H]$ peak. The notable $[2M^{+}+H]$ peak is observed for all the complexes except ZnL4. LC-MS data indicate the presence of the monomeric structure of ZnL4, possibly bonded with two water molecules $[M^{+}+2OH^{-}]$ (shown in Figure 3.8(D)). It is fascinating to note that ZnL4 is the only complex that has not undergone dimerization, reflected in its singular catalytic activity.

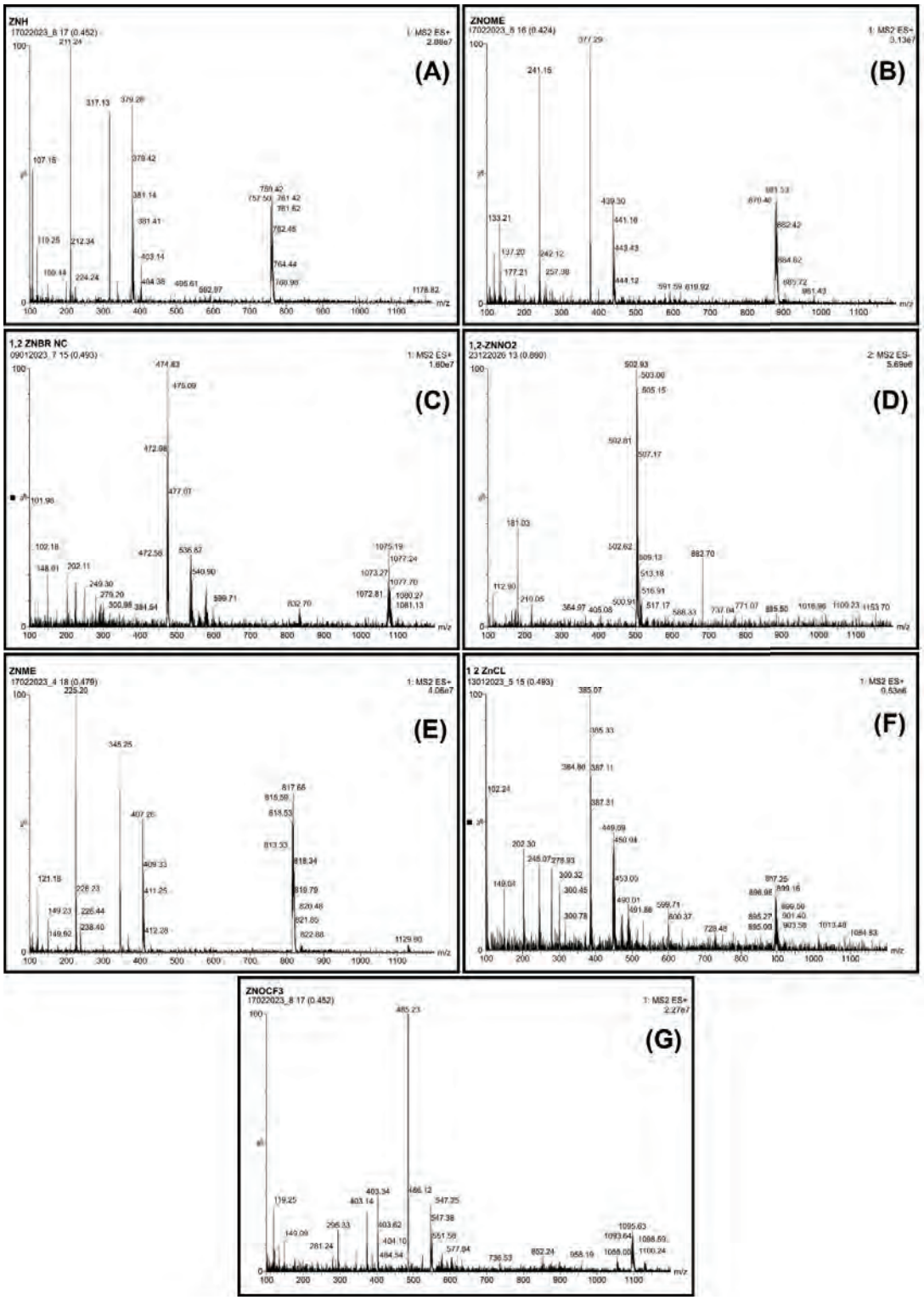

Figure 3.8: LC-MS chromatogram of **(A)** ZnL1, **(B)** ZnL2, **(C)** ZnL3, **(D)** ZnL4, **(E)** ZnL5, **(F)** ZnL6, **(G)** ZnL7.

DFT studies were used to investigate the structures of ZnL1, ZnL2, ZnL3 and ZnL4 and the. optimized structures are shown in Figure 3.9 and important parameters are given in Table 3.4. The methodology of DFT studies used for the structures and optical properties and the detailed discussions of the results are provided in reference,[47] while here we include important DFT results required for interpretation of the experimental spectra.

Table 3.4: Important structural parameters of ZnL catalysts and HOMO-LUMO gaps calculated from DFT

Bond distances /Bond angles	ZnL1	ZnL2	ZnL3	ZnL4
Zn-O (Å)	1.93	1.92	1.93	1.93
Zn-N (Å)	2.07	2.08	2.07	2.07
O-C (Å)	1.29	1.29	1.29	1.29
N-C (Å)	1.31	1.31	1.31	1.30
∠O-Zn-N (°)	91.2	91.0	91.7	91.4
∠C-Zn-C (°)	165.2	164.4	172.8	165.4
End-to-end distance (Å)	13.2	15.4	14.9	14.75
Atomic charge on Zn (MK)	0.99	1.00	0.96	1.02
HOMO (eV)	-5.81	-5.29	-5.97	-6.75
LUMO (eV)	-2.41	-2.36	-2.76	-3.23
HOMO-LUMO Gap (eV)	3.40	2.93	3.21	3.52

Atomic charges reported are calculated using Merz Kollman (MK) scheme

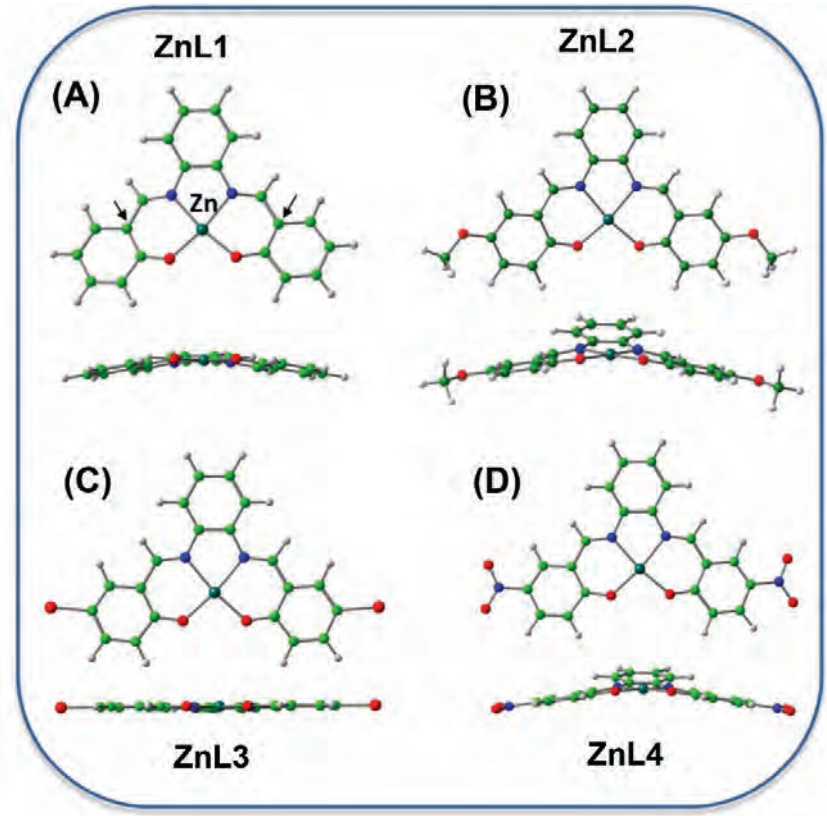

Figure 3.9: Optimized structures of **(A)** ZnL1, **(B)** ZnL2, **(C)** ZnL3 and **(D)** ZnL4 are shown in front and side views. Colour scheme: green balls: C, red balls: O, Blue balls: N, small white balls: H.

Zinc forms four bonds with salophen ligand in ZnL1-ZnL4 complexes but intends to increase the coordination to five or even six consequently, these complexes can coordinate with other ligands, such as water molecules easily and may also form dimeric. Indeed, earlier studies have shown that there is a strong tendency of metal salen and salophen complexes to aggregate by intermolecular interactions between the metal of one monomeric complex and the phenolic oxygen of a second monomeric complex in solution and in the solid state.[34, 35] This leads to a μ_2-phenoxo bridging and Zn_2O_2 central unit with penta-coordinated square-pyramidal Zn(II) metal centres involving Zn···O axial interactions. (schematically shown in Figure 3.10(A)) The water binding energy of complexes ZnL1-ZnL4 were studied using DFT and compared it to the corresponding dimerization energies to identify the complexes with greater dimerization tendencies. DFT results

show that for ZnL1, ZnL2 and ZnL3, dimerization is preferred while for, ZnL4 the coordination of two water molecules to the Zn(II) center is preferred compared to dimer formation. (schematically shown in Figure 3.10(B)).

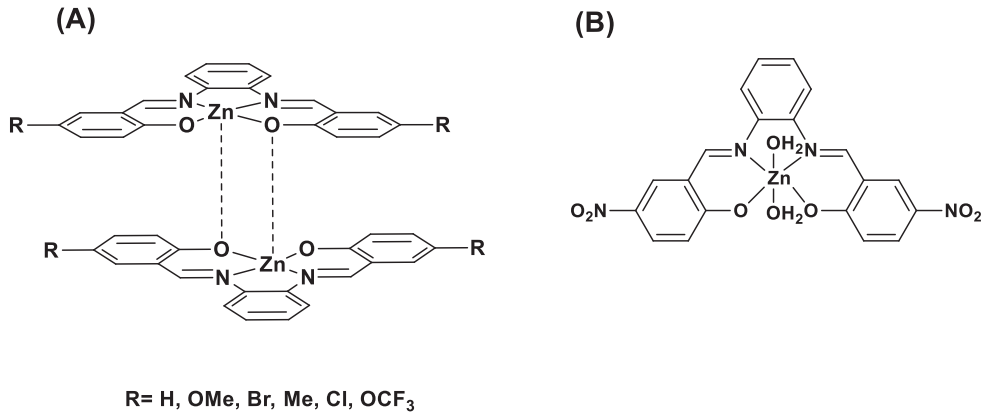

Figure 3.10: Structures of **(A)** dimeric complexes and **(B)** monomeric complex with two water molecules used for the synthesis of styrene carbonate.

3.2.5 Electronic Spectra: Experimental and Theoretical Approaches

UV-vis spectroscopy of all the ligands and the zinc complexes was carried out to probe the difference in the electronic environment of the different complexes. The UV-vis spectra of different ligands and complexes in DMSO are shown in Figure 3.11, and the values are tabulated in Table 3.5. The spectra of all the ligands predominantly show absorption in the range of 250-400 nm. It is reported in the literature that these are primarily $\pi \rightarrow \pi^*$ and $n \rightarrow \pi^*$ based transitions.[36] Upon complexation with zinc, all the peaks undergo a red shift with respect to the ligand, and there is the formation of a new peak around 430 nm. Similar observations were obtained for the complexes of other metals with structurally similar ligands.[19, 37-39] This appearance of the new peak is generally considered as an indication of the formation of the complex and is assigned to the metal-to-ligand charge transfer (MLCT).[40] On comparison of the MLCT peaks of all the complexes (Figure 3.11(H)), the apparent shift in peak positions with the different substituents is clearly visible. The electron-donating groups like -OMe and -Me facilitate conjugation and subsequently show the peak towards a higher wavelength. On the contrary, in the presence of electron-withdrawing groups like $-NO_2$ and $-OCF_3$, the peak appears at a lower wavelength.

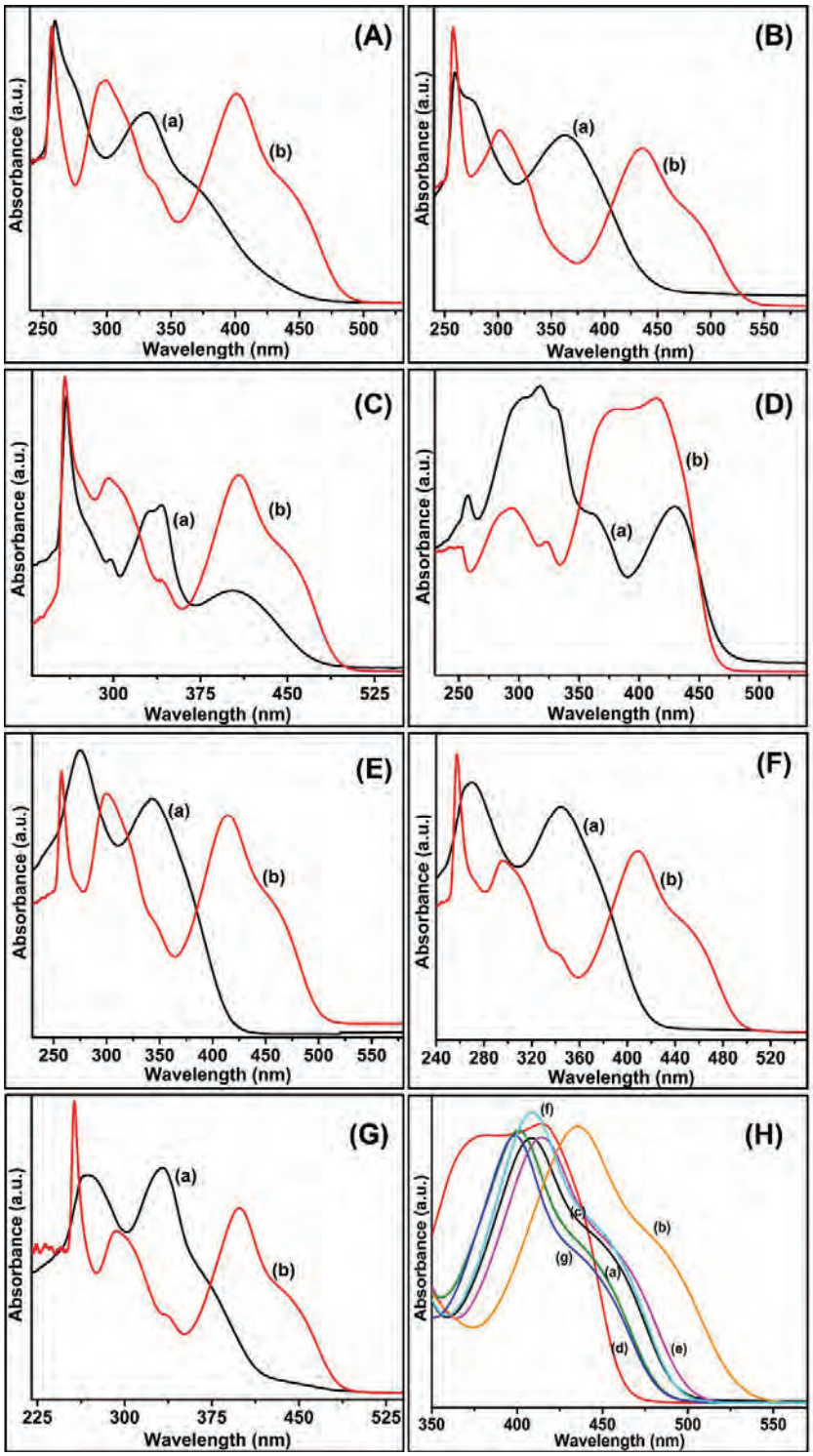

Figure 3.11: Solution UV-vis spectrum of **(A)** (a) L1, (b) ZnL1, **(B)** (a) L2, (b) ZnL2, **(C)** (a) L3, (b) ZnL3, **(D)** (a) L4, (b) ZnL4, **(E)** (a) L5, (b) ZnL5, **(F)** (a) L6, (b) ZnL6, **(G)** (a) L7, (b) ZnL7, **(H)** Expansion of MLCT peaks of all complexes.

To understand the optical properties and related transitions of the Zn(II) salophen complexes, it is imperative to investigate the nature of their frontier molecular orbitals obtained from DFT. The of frontier molecular orbitals show that the HOMO (Highest Occupied Molecular Orbital) of ZnL1 is comprised of ligand p orbitals hybridized with Zn p_z and d_{yz} orbital while the LUMO (Lowest Unoccupied Molecular Orbital) has ligand p-character only. The HOMO and LUMO energies for ZnL1 are -5.81 eV and -2.41 eV, respectively, with a HOMO-LUMO energy gap of 3.40 eV. For the ZnL1 dimer, molecular orbitals are split, and the HOMO, which becomes doubly degenerate, is shifted to -5.44 eV, and LUMO, also doubly degenerate, is shifted to -2.18 eV resulting in a lowered HOMO-LUMO gap of 3.26 eV, as expected for dimerization. For ZnL3, the HOMO-LUMO energy gap is 3.21 eV, which reduces to 3.08 eV for the corresponding dimer, and the nature of the molecular orbitals are similar to ZnL1. The HOMO and LUMO energies for ZnL4 are -6.75 eV and -3.23 eV, respectively, with a HOMO-LUMO energy gap of 3.52 eV. Therefore, an electron-withdrawing group like $–NO_2$ in ZnL4 stabilizes the HOMO and LUMO orbitals compared to ZnL1 strongly and increases the HOMO-LUMO gap. When two water molecules are coordinated to the Zn center of ZnL4, the HOMO-LUMO gap and the nature of the orbitals remain the same.

We have calculated the TD-DFT spectra for selected Zn(II) salophen complexes in monomeric and dimeric (Shown in Figure 3.12-3.15) The peaks obtained from TD-DFT have been correlated with the corresponding transitions from absorption spectra based on their frontier molecular orbitals. The transitions assigned for dimeric ZnL1-ZnL3 are in agreement to the experimental values obtained for these complexes. In the case of ZnL4, however, the calculated spectra with two water molecules more closely corresponds to the experimental values. The overlay of experimental and theoretical spectrum is shown in Figure 3.16 and corresponding absorption wavelengths are tabulated in Table 3.5.

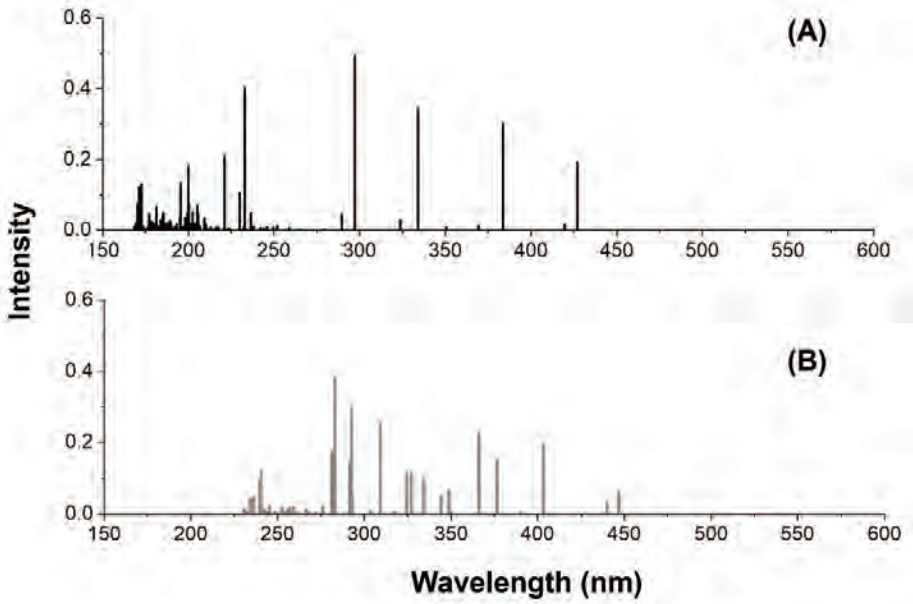

Figure 3.12: Calculated TD-DFT spectra for **(A)** ZnL1monomer, **(B)** ZnL1 dimer.

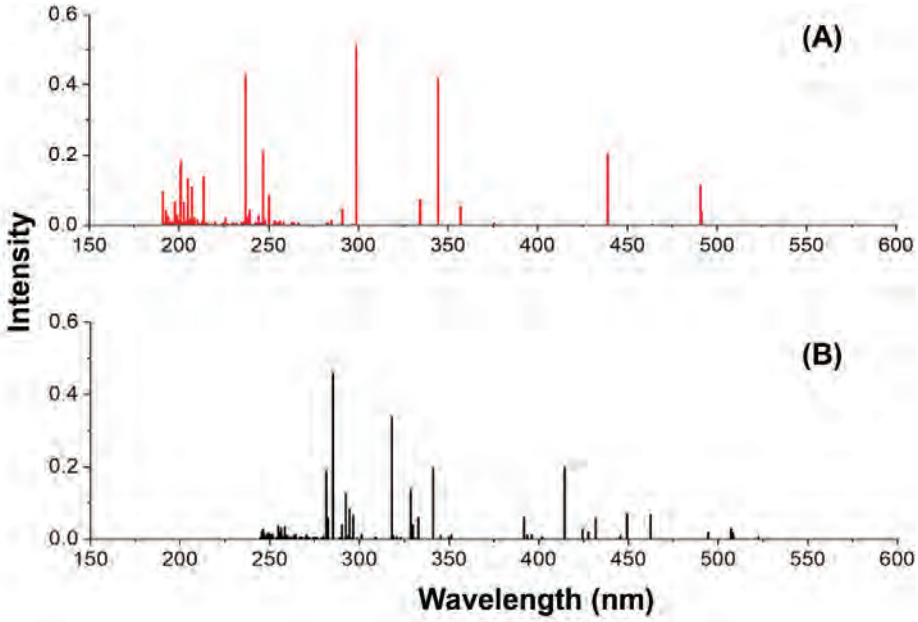

Figure 3.13: Calculated TD-DFT spectra for **(A)** ZnL2 monomer, **(B)** ZnL2 dimer.

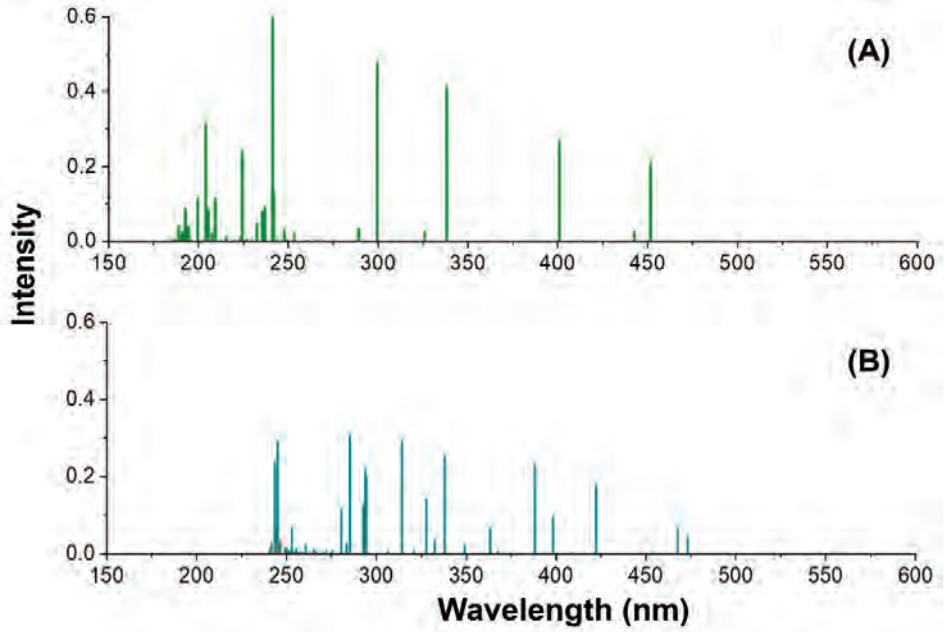

Figure 3.14: Calculated TD-DFT spectra for **(A)** ZnL3 monomer, **(B)** ZnL3 dimer.

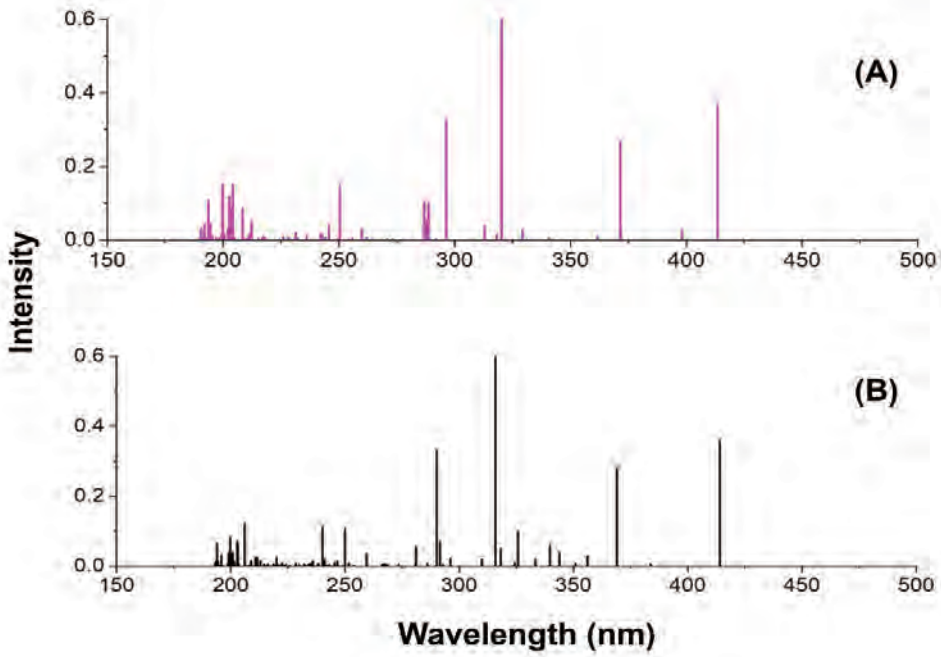

Figure 3.15: Calculated TD-DFT spectra for **(A)** ZnL4, **(B)** ZnL4 with two water molecules.

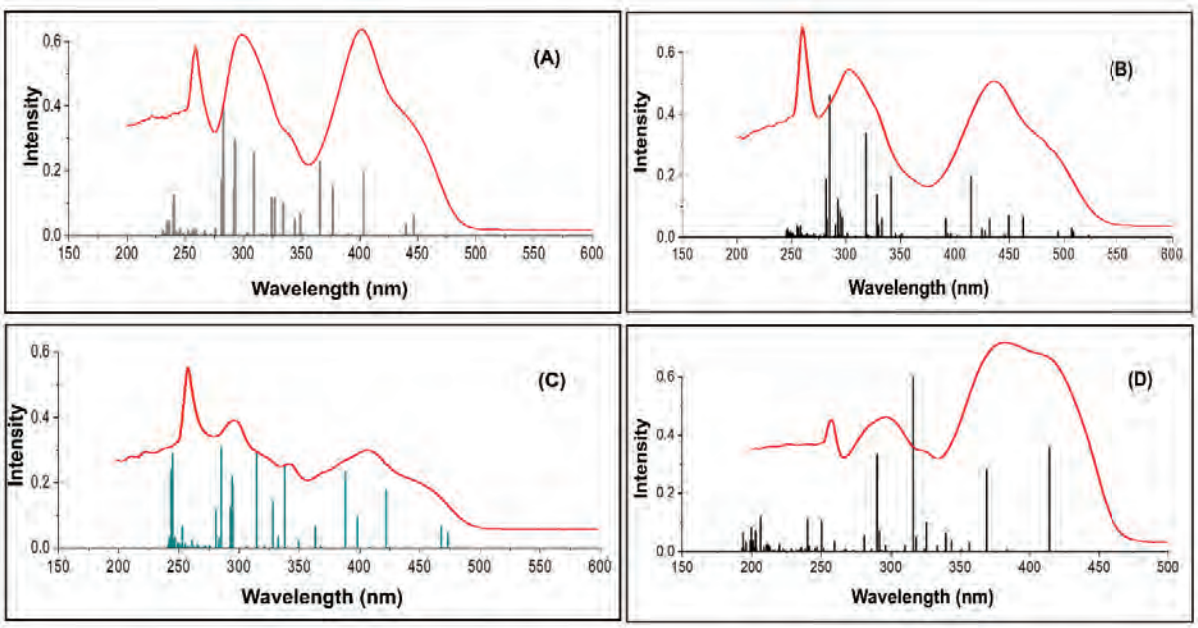

Figure 3.16: Comparison of experimental electronic spectra with DFT calculated TD-DFT spectra of the dimer for **(A)** ZnL1, **(B)** ZnL2, **(C)** ZnL3 and **(D)** Comparison of experimental electronic spectra with DFT calculated TD-DFT spectra ZnL4 with two water molecules.

Table 3.5: Assignment of experimental UV peaks and comparison with calculated TD-DFT spectra.

Ligand/ Complex	Peaks from experiment (nm)	Peaks from DFT (nm)	Assignment
L1	259, 277 (shoulder)	-	$\pi \rightarrow \pi^*$
	331, 374 (shoulder)	-	$n \rightarrow \pi^*$
ZnL1	257, 299	240,283,293	$\pi \rightarrow \pi^*$
	338 (shoulder)	325,327,377	$n \rightarrow \pi^*$
	401, 450 (shoulder)	403,447 (weak)	MLCT
L2	260, 277 (shoulder)	-	$\pi \rightarrow \pi^*$
	363	-	$n \rightarrow \pi^*$
ZnL2	258, 301, 330 (shoulder)	285, 328,341(strong)	$\pi \rightarrow \pi^*$
	-	414	$n \rightarrow \pi^*$
	436, 490 (shoulder)	449, 462 (weak)	MLCT

Ligand/ Complex	Peaks from experiment (nm)	Peaks from DFT (nm)	Assignment
L3	259, 297	-	$\pi \rightarrow \pi^*$
	330 (shoulder), 342, 403	-	$n \rightarrow \pi^*$
ZnL3	258, 273 (shoulder), 295	244,245,293,294,295	$\pi \rightarrow \pi^*$
	340 (shoulder)	338, 328,314	$n \rightarrow \pi^*$
	408, 460 (shoulder)	422, 467,473	MLCT
L4	256, 301	-	$\pi \rightarrow \pi^*$
	317.3, 364 (shoulder), 429.8	-	$n \rightarrow \pi^*$
ZnL4	282 (shoulder), 294	250, 290	$\pi \rightarrow \pi^*$
	323	315	$n \rightarrow \pi^*$
	381, 416 (shoulder), 439 (shoulder)	369, 414	MLCT
L5	274	-	$\pi \rightarrow \pi^*$
	342	-	$n \rightarrow \pi^*$
ZnL5	257, 299	-	$\pi \rightarrow \pi^*$
	349 (shoulder)	-	$n \rightarrow \pi^*$
	414, 465 (shoulder)	-	MLCT
L6	269	-	$\pi \rightarrow \pi^*$
	344	-	$n \rightarrow \pi^*$
ZnL6	257, 295	-	$\pi \rightarrow \pi^*$
	343	-	$n \rightarrow \pi^*$
	408, 456 (shoulder)	-	MLCT
L7	267	-	$\pi \rightarrow \pi^*$
	332, 376 (broad)	-	$n \rightarrow \pi$
ZnL7	256, 291	-	$\pi \rightarrow \pi^*$
	338	-	$n \rightarrow \pi$
	398, 452 (shoulder)	-	MLCT

3.2.6 ^{1}H, ^{13}C NMR and Diffusion ordered spectroscopy (DOSY) studies

^{1}H and ^{13}C NMR spectroscopy was carried out to confirm the structures of all the ligands and the prepared ligands and complexes. ^{1}H and ^{13}C NMR of few selected complexes and ligands is shown in Figure 3.18. DOSY NMR experiments were carried out for ZnL1 and ZnL4 to study their structural aspects in solution state. It is known that molecules with larger molecular mass diffuse more slowly in solution.[41, 42] From the DOSY experiments, we found that the value of diffusion coefficient, D for ZnL1 is 1.92×10^{-6} cm^2/sec while that of ZnL4 is found to be 3.32×10^{-6} cm^2/sec (Figure 3.17). The molecular mass of monomeric ZnL4 is more than that of monomeric ZnL1; ZnL4 is expected to have a lower diffusion coefficient as compared to ZnL1.[43, 44] However, our observation is just on the contrary. This suggests that the mass of ZnL1 should be more than ZnL4, which is possible only if ZnL1 exists as a dimer and ZnL4 exists as a monomer.[45, 46] The results obtained by LC-MS studies and theoretical studies are also in line with DOSY NMR, which indicates that ZnL1 exists as a dimer and ZnL4 exists as a monomer with two water molecules attached.

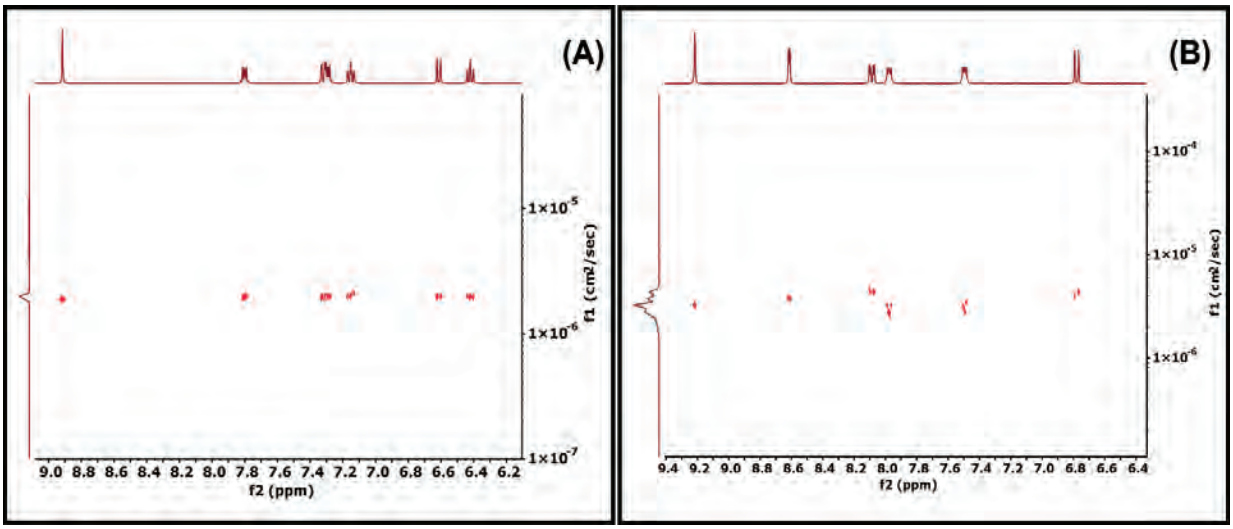

Figure 3.17: DOSY NMR of **(A)** ZnL1 and **(B)** ZnL4.

The NMR peak shifts of all the prepared ligands and complexes are presented below.

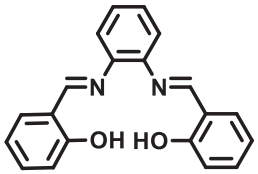

$C_{20}H_{16}N_2O_2$

L1

^{1}H NMR (400 MHz, DMSO-d_6) δ 12.97 (s, 1H), 8.95 (s, 1H), 7.68 (dd, J = 8.0, 1.7 Hz, 1H), 7.52 – 7.37 (m, 3H), 6.98 (t, J = 7.4 Hz, 2H). ^{13}C NMR (101 MHz, DMSO) δ 164.52, 160.86, 142.90, 133.91, 132.94, 128.29, 120.22, 119.95, 119.56, 117.15.

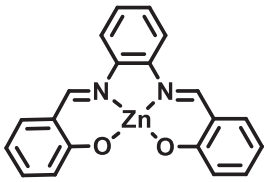

$C_{20}H_{14}N_2O_2Zn$

ZnL1

^{1}H NMR (400 MHz, DMSO-d_6) δ 9.00 (s, 1H), 7.89 (dd, J = 6.2, 3.5 Hz, 1H), 7.40 (ddd, J = 10.9, 7.0, 2.6 Hz, 2H), 7.25 (ddd, J = 8.7, 6.8, 2.0 Hz, 1H), 6.71 (dd, J = 8.6, 1.1 Hz, 1H), 6.53 (ddd, J = 7.9, 6.8, 1.2 Hz, 1H). ^{13}C NMR (101 MHz, DMSO) δ 172.72, 163.30, 139.83, 136.71, 134.81, 127.74, 123.56, 119.90, 116.95, 113.46.

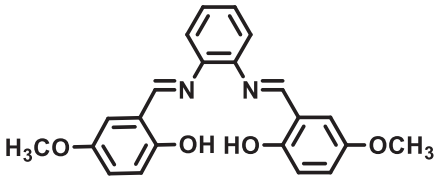

$C_{22}H_{20}N_2O_4$

L2

^{1}H NMR (400 MHz, DMSO-d_6) δ 12.30 (s, 1H), 8.92 (s, 1H), 7.47 – 7.39 (m, 2H), 7.30 (d, J = 3.1 Hz, 1H), 7.04 (dd, J = 8.9, 3.1 Hz, 1H), 6.90 (d, J = 9.0 Hz, 1H), 3.75 (s, 3H). ^{13}C NMR (101 MHz, DMSO) δ 163.31, 154.91, 152.29, 142.95, 128.24, 121.18, 119.99, 119.92, 118.05, 115.11, 56.00.

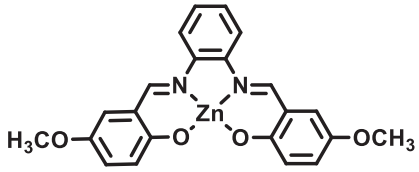

$C_{22}H_{18}N_2O_4Zn$

ZnL2

^{1}H NMR (400 MHz, DMSO-d_6) δ 9.03 (s, 1H), 7.89 (dd, J = 6.2, 3.5 Hz, 1H), 7.38 (dd, J = 6.2, 3.4 Hz, 1H), 6.98 (s, 2H), 6.70 – 6.64 (m, 1H), 3.71 (s, 3H). ^{13}C NMR (101 MHz, DMSO) δ 168.43, 162.60, 147.86, 139.83, 127.55, 125.11, 124.50, 118.08, 116.81, 116.36, 55.97.

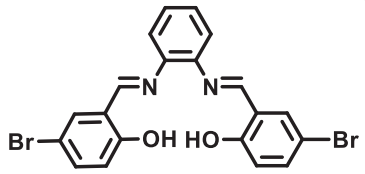

$C_{20}H_{14}Br_2N_2O_2$

L3

^{1}H NMR (400 MHz, DMSO-d_6) δ 12.93 (s, 1H), 8.93 (s, 1H), 7.91 (d, J = 2.6 Hz, 1H), 7.56 (dd, J = 8.8, 2.6 Hz, 1H), 7.48 – 7.43 (m, 2H), 6.96 (d, J = 8.8 Hz, 1H). ^{13}C NMR (101 MHz, DMSO) δ 162.71, 159.94, 142.50, 136.16, 134.25, 128.64, 121.91, 120.13, 119.65, 110.37.

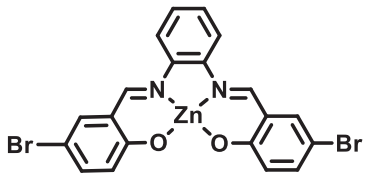

$C_{20}H_{12}Br_2N_2O_2Zn$

ZnL3

^{1}H NMR (400 MHz, DMSO-d_6) δ 9.02 (s, 1H), 7.89 (dd, J = 6.2, 3.5 Hz, 1H), 7.63 (d, J = 2.8 Hz, 1H), 7.43 (dd, J = 6.1, 3.3 Hz, 1H), 7.32 (dd, J = 9.1, 2.8 Hz, 1H), 6.68 (d, J = 9.1 Hz, 1H). ^{13}C NMR (101 MHz, DMSO) δ 171.42, 162.63, 139.67, 137.77, 136.91, 128.26, 125.95, 121.43, 117.22, 103.16.

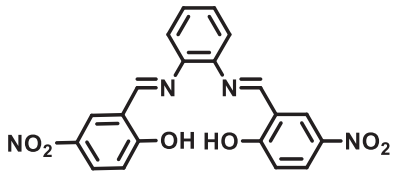

$C_{20}H_{14}N_4O_6$

L4

^{1}H NMR (400 MHz, DMSO-d_6) δ 14.15 (s, 1H), 9.14 (s, 1H), 8.27 (dd, J = 9.2, 2.8 Hz, 1H), 7.74 (dd, J = 6.0, 3.2 Hz, 2H), 7.36 (d, J = 9.2 Hz, 2H), 7.23 (d, J = 9.2 Hz, 1H). ^{13}C NMR (101 MHz, $CDCl_3$) δ 163.99, 149.75, 139.39, 136.51, 127.10, 123.55, 122.94, 118.35, 115.07, 112.68.

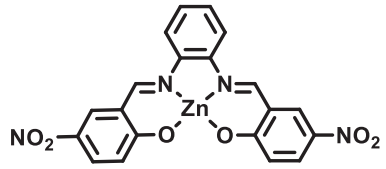

$C_{20}H_{12}N_4O_6Zn$

ZnL4

^{1}H NMR (400 MHz, DMSO-d_6) δ 13.70 (s, 0.31 H), 9.23 (s, 1H), 8.63 (d, J = 3.1 Hz, 1H), 8.09 (dd, J = 9.5, 3.1 Hz, 1H), 7.99 (dd, J = 6.2, 3.5 Hz, 1H), 7.50 (dd, J = 6.2, 3.4 Hz, 1H), 6.78 (d, J = 9.5 Hz, 1H). ^{13}C NMR (101 MHz, DMSO) δ 177.17, 163.13, 139.45, 134.90, 134.53, 129.04, 128.96, 124.24, 119.05, 117.75.

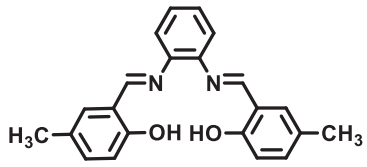

$C_{22}H_{20}N_2O_2$

L5

^{1}H NMR (400 MHz, DMSO-d_6) δ 12.67 (s, 1H), 8.87 (s, 1H), 7.47 – 7.38 (m, 3H), 7.24 (dd, J = 8.4, 2.3 Hz, 1H), 6.87 (d, J = 8.4 Hz, 1H), 2.28 (s, 3H). ^{13}C NMR (101 MHz, DMSO) δ 164.44, 158.70, 142.82, 134.67, 132.71, 128.21, 128.07, 120.20, 119.60, 116.99, 20.41.

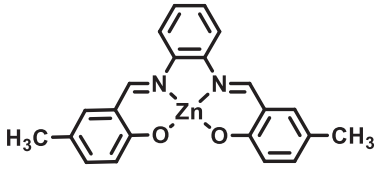

$C_{22}H_{18}N_2O_2Zn$

ZnL5

^{1}H NMR (400 MHz, DMSO-d_6) δ 8.96 (s, 1H), 7.88 (dd, J = 6.2, 3.5 Hz, 1H), 7.37 (dd, J = 6.1, 3.4 Hz, 1H), 7.23 – 7.17 (m, 1H), 7.09 (dd, J = 8.7, 2.5 Hz, 1H), 6.64 (d, J = 8.6 Hz, 1H), 2.20 (s, 3H). ^{13}C NMR (101 MHz, DMSO) δ 171.03, 162.94, 139.87, 136.37, 135.66, 127.59, 123.48, 121.27, 119.15, 116.82, 20.32.

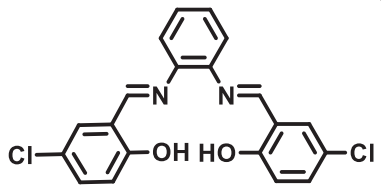

$C_{20}H_{14}Cl_2N_2O_2$

L6

^{1}H NMR (400 MHz, DMSO-d_6) δ 12.92 (s, 1H), 8.94 (s, 1H), 7.78 (d, J = 2.7 Hz, 1H), 7.49 – 7.42 (m, 3H), 7.01 (d, J = 8.8 Hz, 1H). ^{13}C NMR (101 MHz, DMSO) δ 162.77, 159.52, 142.54, 133.40, 131.27, 128.64, 123.00, 121.30, 120.13, 119.23.

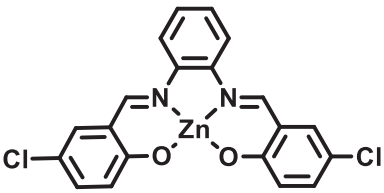

$C_{20}H_{12}Cl_2N_2O_2Zn$

ZnL6

^{1}H NMR (400 MHz, DMSO-d_6) δ 9.03 (s, 1H), 7.89 (dd, J = 6.2, 3.5 Hz, 1H), 7.51 (d, J = 3.0 Hz, 1H), 7.44 (dd, J = 6.1, 3.4 Hz, 1H), 7.23 (dd, J = 9.1, 3.0 Hz, 1H), 6.73 (d, J = 9.1 Hz, 1H). ^{13}C NMR (101 MHz, DMSO) δ 171.17, 162.67, 139.67, 134.68, 134.36, 128.25, 125.49, 120.45, 117.22, 116.08.

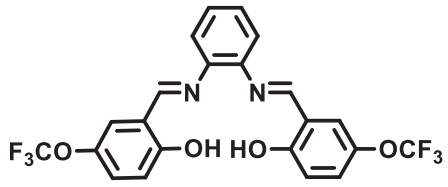

$C_{22}H_{14}F_6N_2O_4$

L7

^{1}H NMR (400 MHz, DMSO-$d6$) δ 12.97 (s, 1H), 8.99 (s, 1H), 7.78 – 7.75 (m, 1H), 7.52 – 7.41 (m, 3H), 7.06 (d, J = 9.0 Hz, 1H). ^{13}C NMR (101 MHz, DMSO) δ 171.32, 162.85, 146.81, 139.61, 135.95, 134.82, 128.32, 127.82, 124.75, 118.81, 117.31.

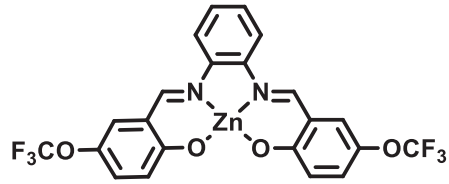

$C_{22}H_{12}F_6N_2O_4Zn$

ZnL7

^{1}H NMR (400 MHz, DMSO-d_6) δ 9.09 (s, 1H), 7.92 (dd, J = 6.2, 3.4 Hz, 1H), 7.53 – 7.39 (m, 2H), 7.24 (dd, J = 9.2, 3.2 Hz, 1H), 6.76 (d, J = 9.2 Hz, 1H). ^{13}C NMR (101 MHz, DMSO) δ 177.17, 176.31, 163.13, 161.73, 141.99, 139.45, 135.05, 134.89, 134.52, 133.52, 129.19, 129.03, 128.96, 128.57, 124.24, 123.71, 121.19, 119.04, 117.88, 117.75.

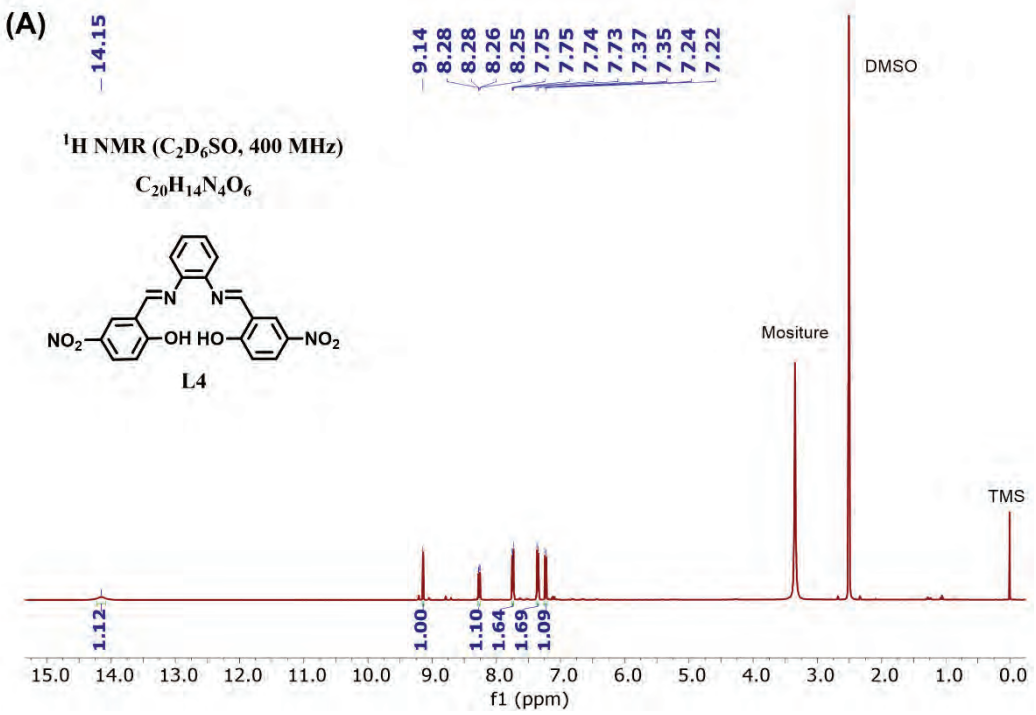
(A)
14.15
9.14
8.28
8.28
8.26
8.25
7.75
7.75
7.74
7.73
7.37
7.35
7.24
7.22
DMSO
^{1}H NMR (C_2D_6SO, 400 MHz)
$C_{20}H_{14}N_4O_6$
NO2
OH HO
NO2
L4
Mositure
TMS
1.12
1.00
1.10
1.64
1.69
1.09
15.0 14.0 13.0 12.0 11.0 10.0 9.0 8.0 7.0 6.0 5.0 4.0 3.0 2.0 1.0 0.0
f1 (ppm)

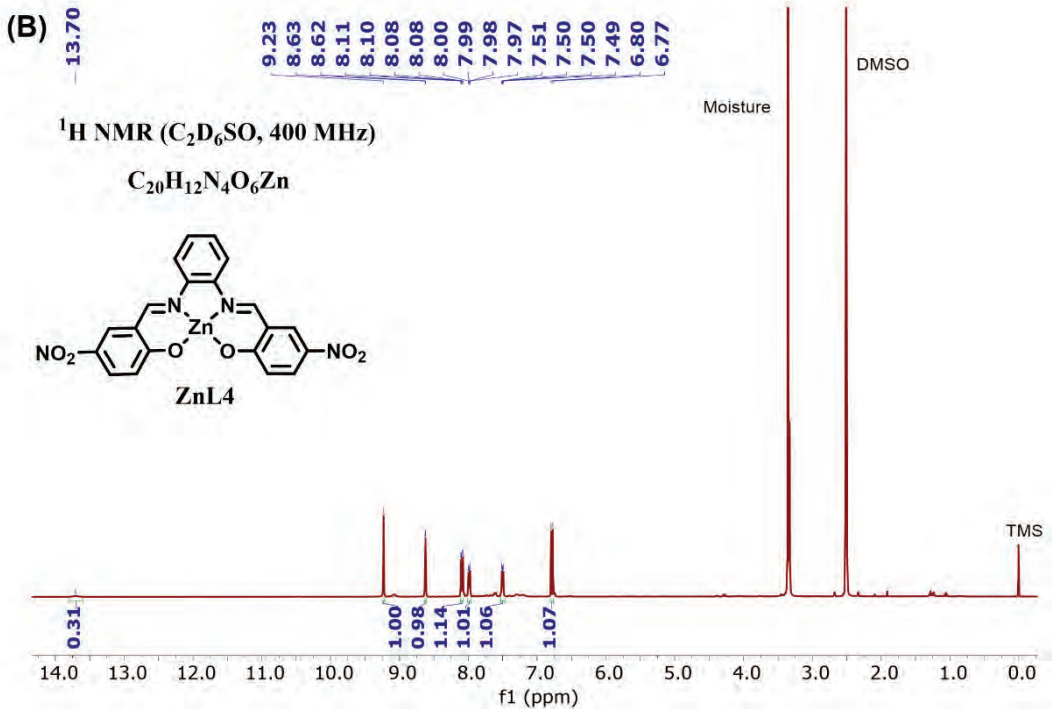
(B)
13.70
9.23
8.63
8.62
8.11
8.10
8.08
8.08
8.00
7.99
7.98
7.97
7.51
7.50
7.50
7.49
6.80
6.77
Moisture
DMSO
^{1}H NMR (C_2D_6SO, 400 MHz)
$C_{20}H_{12}N_4O_6Zn$
Zn
NO2
NO2
ZnL4
TMS
0.31
1.00
0.98
1.14
1.01
1.06
1.07
14.0 13.0 12.0 11.0 10.0 9.0 8.0 7.0 6.0 5.0 4.0 3.0 2.0 1.0 0.0
f1 (ppm)

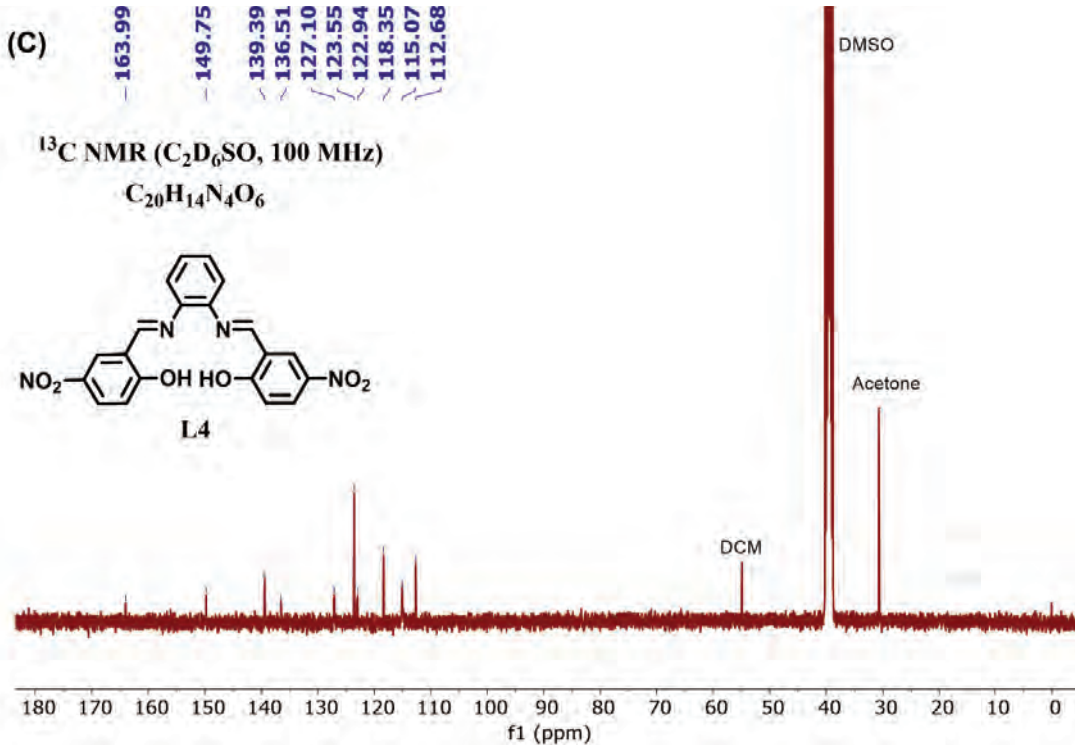
(C)
163.99
149.75
139.39
136.51
127.10
123.55
122.94
118.35
115.07
112.68
DMSO
^{13}C NMR (C_2D_6SO, 100 MHz)
$C_{20}H_{14}N_4O_6$
N
N
NO_2
OH HO
NO_2
L4
Acetone
DCM
180 170 160 150 140 130 120 110 100 90 80 70 60 50 40 30 20 10 0
f1 (ppm)

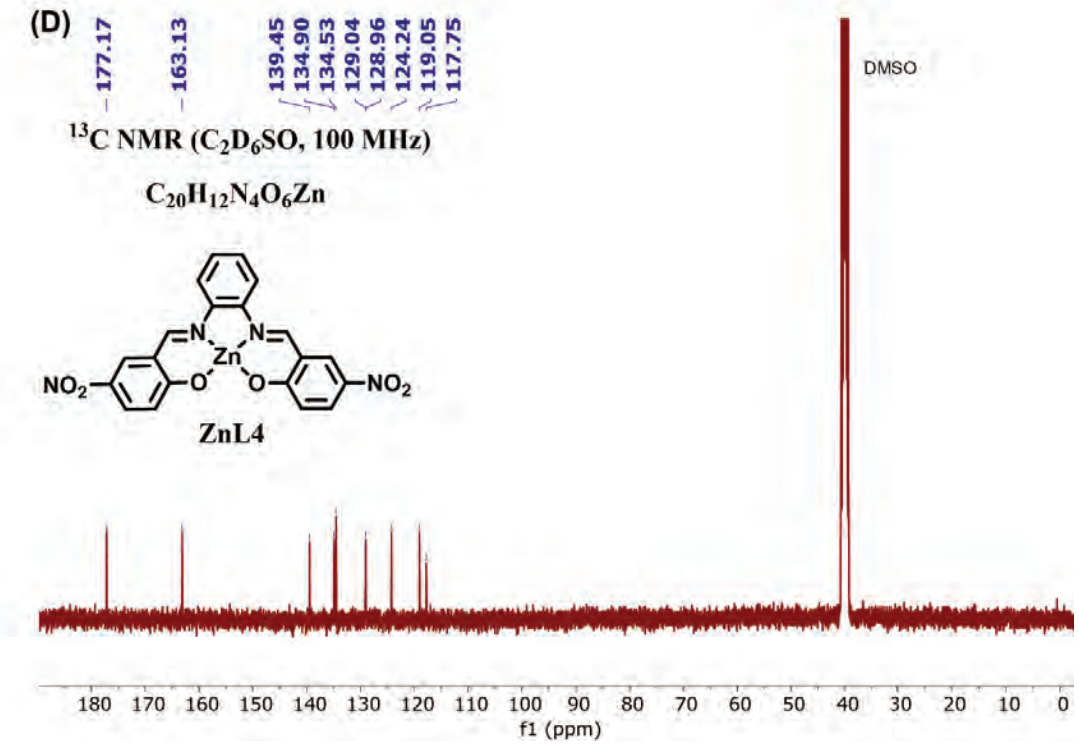
(D)
177.17
163.13
139.45
134.90
134.53
129.04
128.96
124.24
119.05
117.75
DMSO
^{13}C NMR (C_2D_6SO, 100 MHz)
$C_{20}H_{12}N_4O_6Zn$
N
N
Zn
O
O
NO_2
NO_2
ZnL4
180 170 160 150 140 130 120 110 100 90 80 70 60 50 40 30 20 10 0
f1 (ppm)

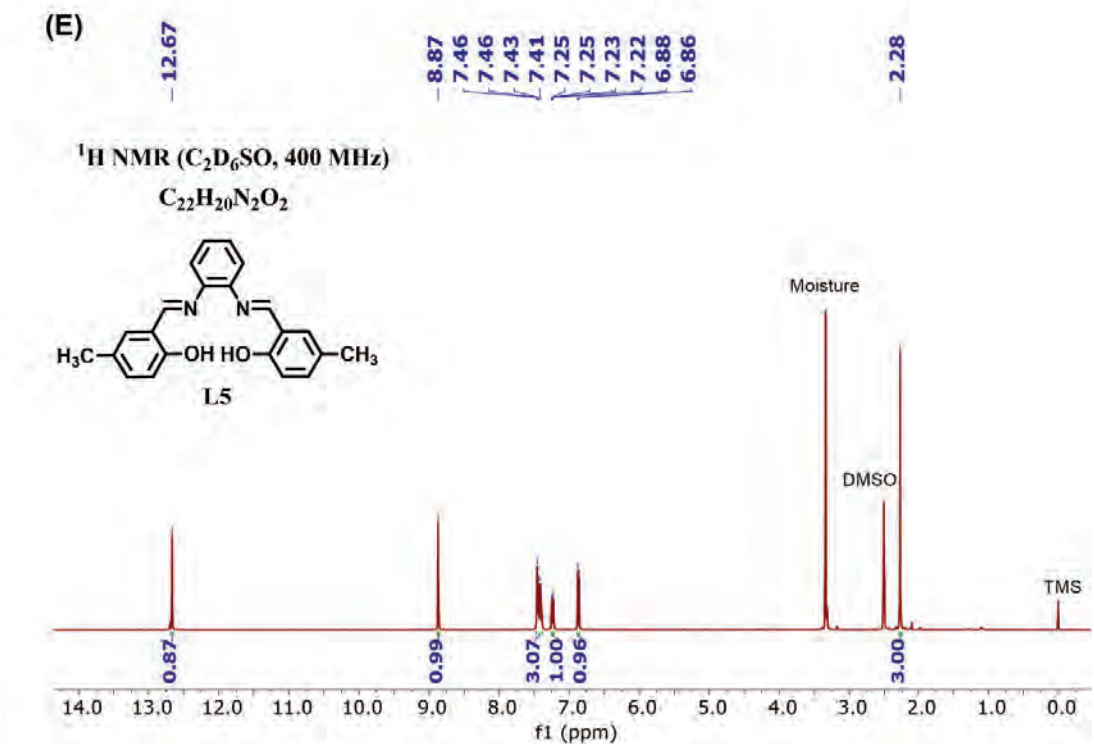
(E)
12.67
8.87
7.46
7.46
7.43
7.41
7.25
7.25
7.23
7.22
6.88
6.86
2.28
^{1}H NMR (C_2D_6SO, 400 MHz)
$C_{22}H_{20}N_2O_2$
L5
Moisture
DMSO
TMS
0.87
0.99
3.07
1.00
0.96
3.00
f1 (ppm)

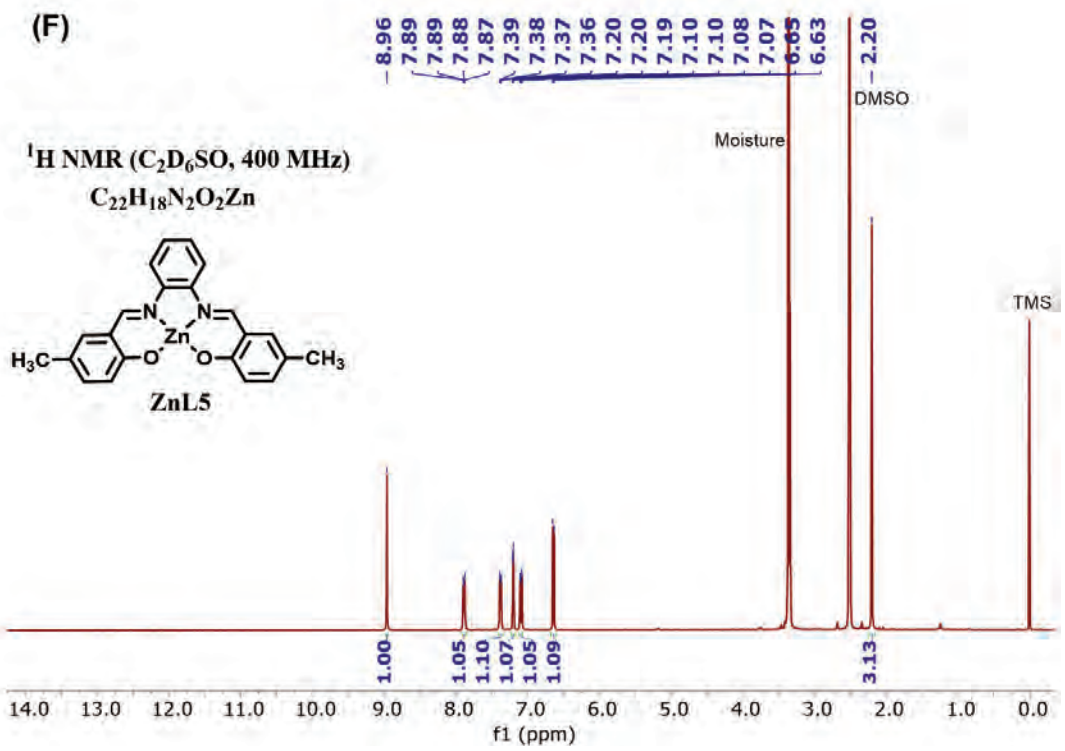
(F)
8.96
7.89
7.89
7.88
7.87
7.39
7.38
7.37
7.36
7.20
7.20
7.19
7.10
7.10
7.08
7.07
6.65
6.63
2.20
DMSO
Moisture
^{1}H NMR (C_2D_6SO, 400 MHz)
$C_{22}H_{18}N_2O_2Zn$
ZnL5
TMS
1.00
1.05
1.10
1.07
1.05
1.09
3.13
f1 (ppm)

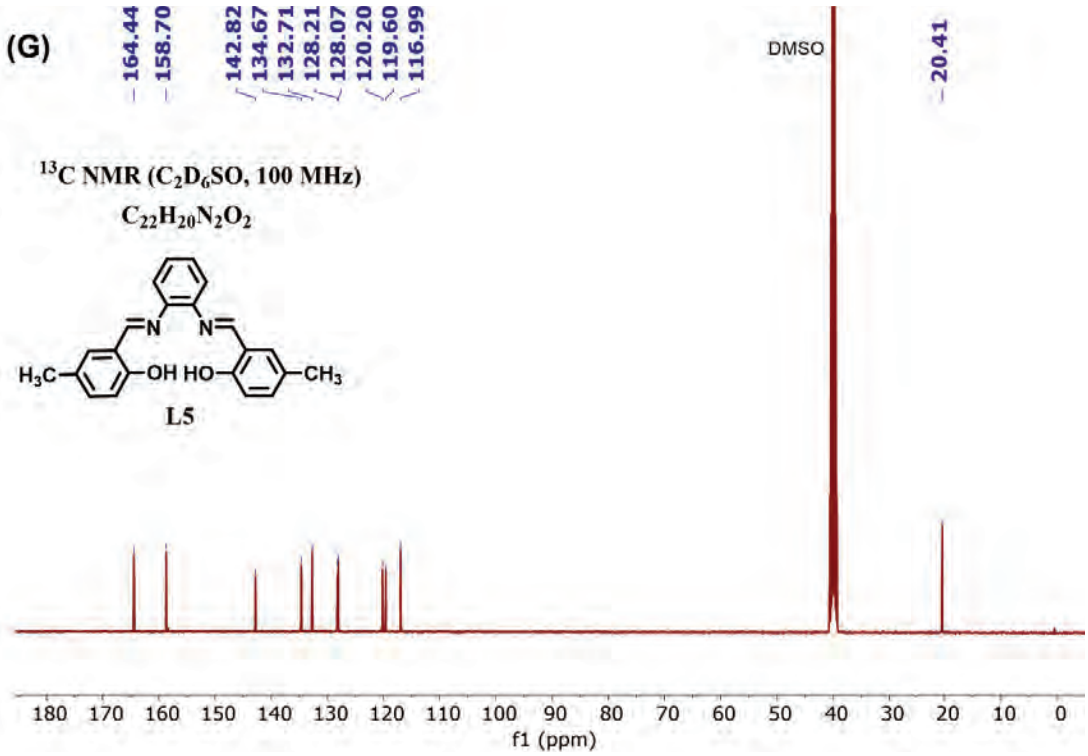
(G)
164.44
158.70
142.82
134.67
132.71
128.21
128.07
120.20
119.60
116.99
DMSO
20.41
13C NMR (C2D6SO, 100 MHz)
C22H20N2O2
H3C
OH HO
CH3
L5
180 170 160 150 140 130 120 110 100 90 80 70 60 50 40 30 20 10 0
f1 (ppm)

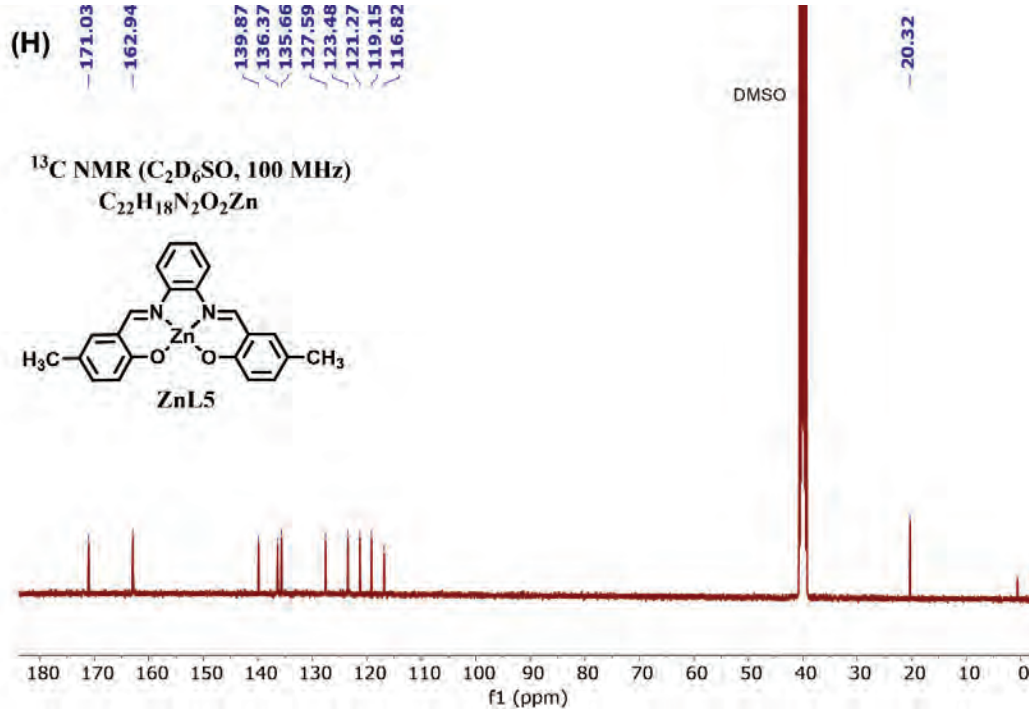
(H)
171.03
162.94
139.87
136.37
135.66
127.59
123.48
121.27
119.15
116.82
DMSO
20.32
13C NMR (C2D6SO, 100 MHz)
C22H18N2O2Zn
Zn
H3C
CH3
ZnL5
180 170 160 150 140 130 120 110 100 90 80 70 60 50 40 30 20 10 0
f1 (ppm)

(I)

^{1}H NMR (C_2D_6SO, 400 MHz)

$C_{22}H_{14}F_6N_2O_4$

L7

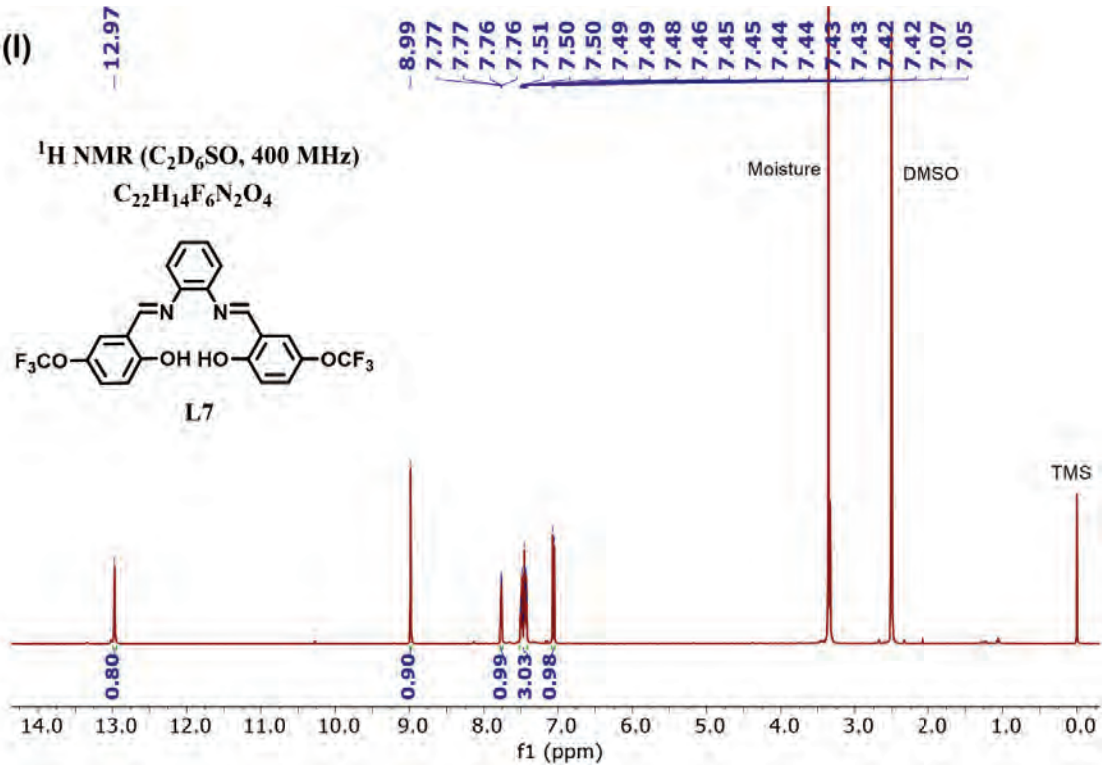

(J)

^{1}H NMR (C_2D_6SO, 400 MHz)

$C_{22}H_{12}F_6N_2O_4Zn$

ZnL7

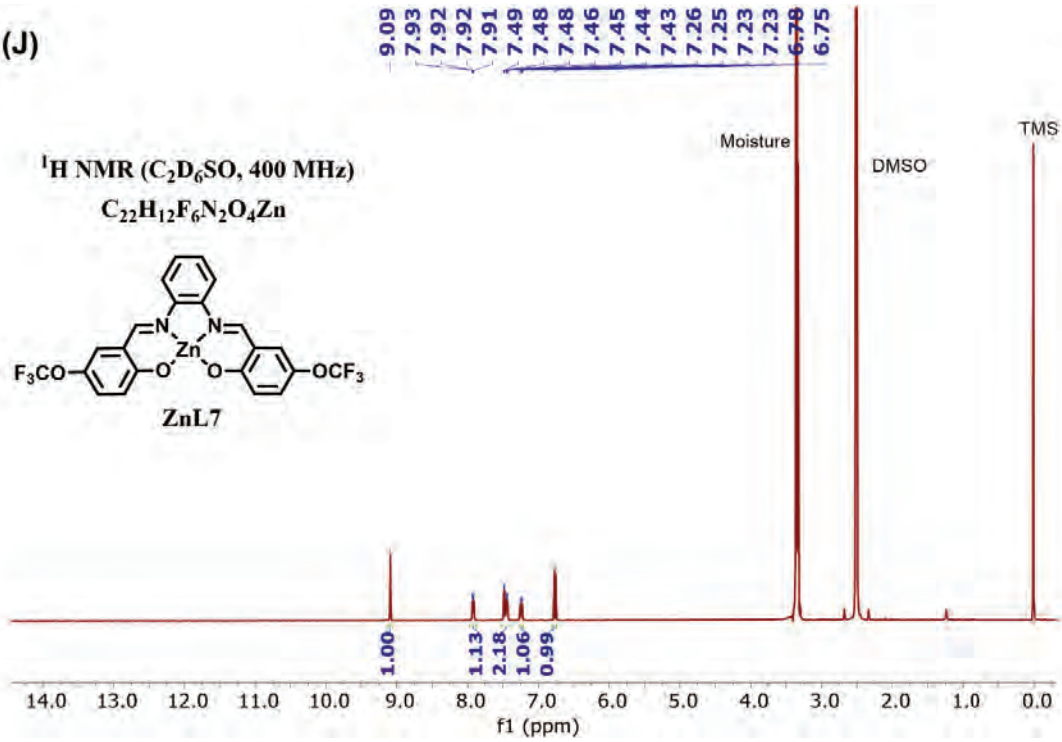

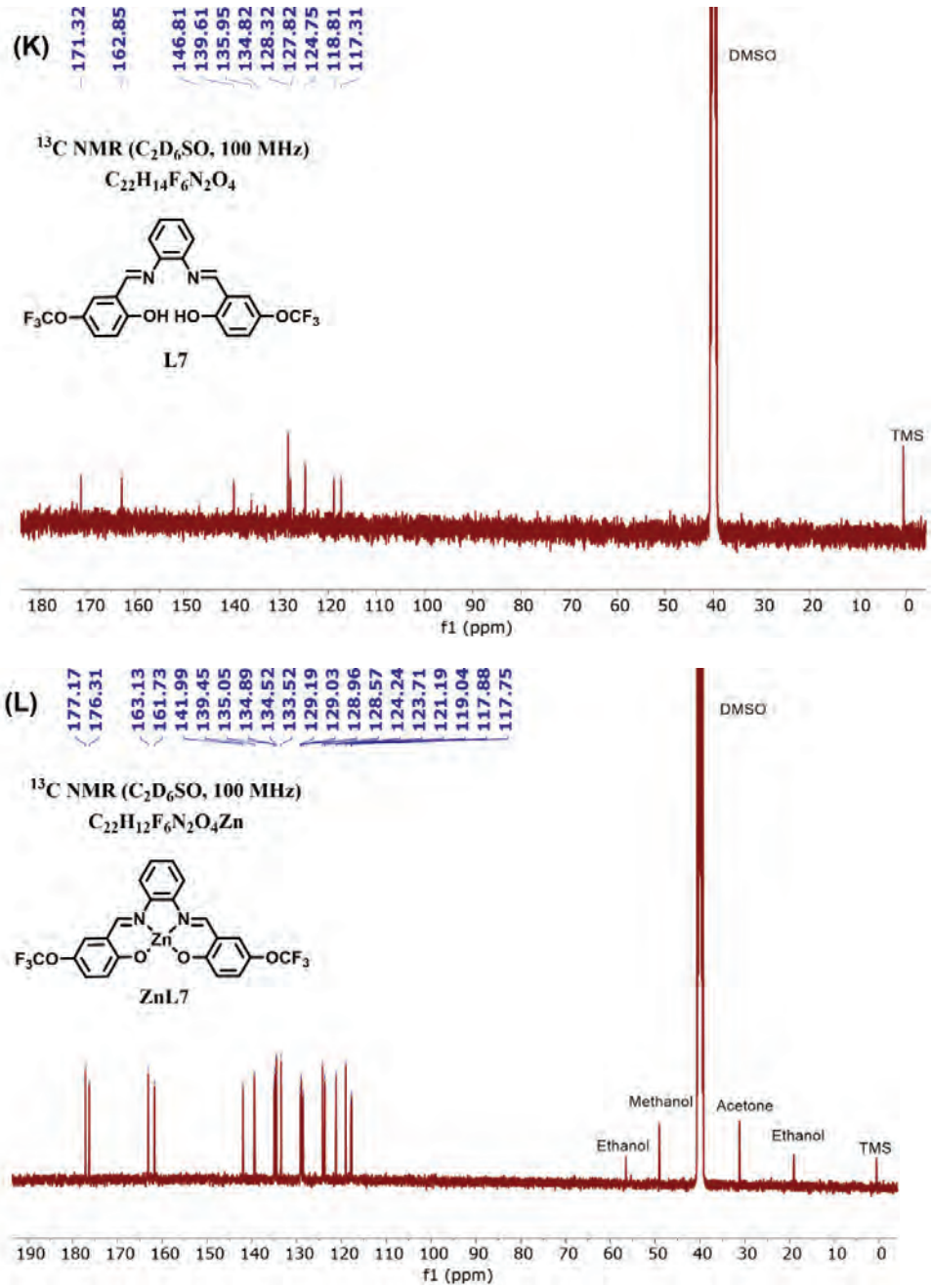

Figure 3.18: Representative ^{1}H NMR of **(A)** L4, **(B)** ZnL4, **(E)** L5, **(F)** ZnL5, **(I)** L7, **(J)** ZnL7, and representative ^{13}C NMR of **(C)** L4, **(D)** ZnL4, **(G)** L5, **(H)** ZnL5, **(K)** L7, **(L)** ZnL7. The DMSO-d_6 residual peak in ^{1}H NMR appears at 2.5 ppm, and the solvent peak of DMSO-d_6 is at 3.3 ppm. In ^{13}C NMR, the solvent peak appears at 40 ppm. Trace solvent impurities in ^{1}H NMR include acetone at 2.09 ppm and methanol at 3.16 ppm and 4.01 ppm. In ^{13}C NMR, acetone appears at 30.14 ppm and methanol at 48.59 ppm.

3.2.7 Catalytic Studies and mechanistic investigations using DFT

All the prepared complexes were used to study their efficiency as catalysts for the cycloaddition reaction of styrene oxide and CO_2 to form styrene carbonate. The yields obtained using the catalysts ZnL1-ZnL7 are shown in Table 3.6 and the selectivities and conversion shown in Table 3.9. The reaction was carried out at a temperature of 80 °C for 5 hours at a pressure of ~1 atm (using a bladder filled with CO_2). Although similar complexes have been reported, a systematic investigation of the effects of the substituent groups on the catalysis reaction was not studied earlier. To obtain a clear insight into the catalysis process in a stepwise manner, we modelled the reaction using DFT for unsubstituted ZnL1 and compared it with ZnL3 and ZnL4, where we observed the effects of both electron-donating and electron-withdrawing groups. The methodology of DFT studies for the catalysis reaction and the detailed discussions of the results are provided in reference,[47] while this chapter only contains important results required for interpretation of the experimental observations.

DFT studies of the catalytic process reveals that for ZnL1 and ZnL3 the activation free energy calculated for the rate determining step is 15.7 kcal/mol for ZnL1, and 13.9 kcal/mol for ZnL3, which shows ZnL3 to be the more efficient catalyst compared to ZnL1 in the monomeric state. In the case of ZnL4, the rate determining step is different and the activation free energy is 15.9 kcal/mol. This cycloaddition reaction was studied earlier using a substituted Zn-salen complex as a catalyst, and a similar activation barrier was obtained.[48] .The complexes in dimeric structures act as weaker catalysts due to the presence of penta co-ordinated Zn(II) in the structure. The mechanistic pathway for catalysis reaction involving the dimeric ZnL1 catalyst was also studied using DFT and the calculated activation barrier is 17 kcal/mol, which is higher than the monomeric case and, therefore, dimeric ZnL1 is indeed a weaker catalyst compared to monomeric ZnL1. (Shown in Figure 3.19) In the case of ZnL4, with the Zn site bound to water molecules, the activation free energy increases to 17.2 kcal and is comparable to the catalytic potential of dimeric ZnL1.

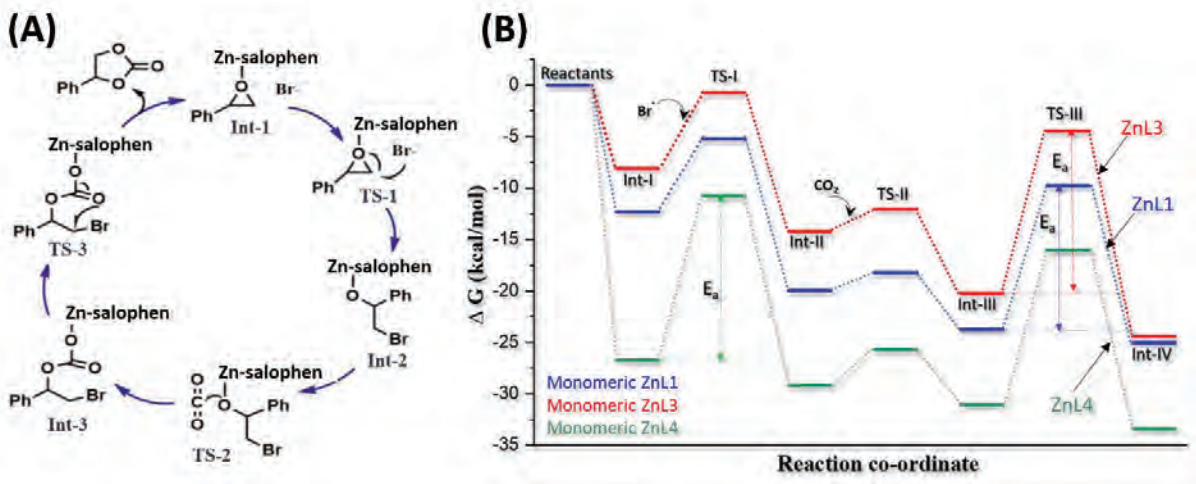

Figure 3.19: (A) Reaction mechanism for the catalytic cycle. **(B)** The calculated Gibbs free energy profile diagram for ZnL1, ZnL3 and ZnL4 in monomeric state along with the intermediates and activation free energies (E_a) marked.

Some control reactions were carried out to investigate the importance of the presence of the metal complex, and the significance of the metal complex was clearly evident from the results (shown in Table 3.7). The reaction when carried out using only TBAB, gives a yield of only 31%. The ligand precursor of the best-performing complex, i.e., L4, along with TBAB, gave a reaction yield of 41.7%. We have also tried the reaction with the metal salt, i.e., zinc acetate. Only the salt, along with TBAB, also performs poorly, giving a yield of 42.8%. It is also evident from the literature that the anion of the co-catalyst also plays an important role.[49, 50] We tried the reaction using ZnL4 and TBAI (tetrabutylammonium iodide), which showed improvement in activity with 62.8% yield. However, ZnL4, the best-performing complex, gives a 74.1% yield in the presence of TBAB. This shows the critical role that the complex can play in the reaction, either in terms of providing optimum electron density for the cycloaddition through the metal or resisting dimerization of the metal complex. Only the metal salt, TBAB and ligand, individually, are not very effective, however the binding of the epoxide to the metal present in the complex facilitates the reaction.

The catalyst system of ZnL4/TBAB was also investigated for its activity with different epoxides as shown in Table 3.8. The catalyst system performed better with epichlorohydrin, which can be due to the electronegativity of the chloromethyl group.[51] We also tried the activity with internal epoxide, i.e., cyclohexene oxide, but with no positive result. Generally, internal epoxides require

harsh conditions like higher temperature and pressure.[52, 53] Since our reaction is at 1 atm pressure, the internal epoxide could not be converted to its corresponding carbonate.

Table 3.6: Catalytic activity of the complexes used

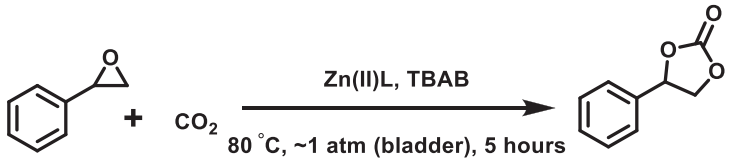

Complex	Yield[a] (%)
ZnL1	59.1
ZnL2	60.5
ZnL3	63.4
ZnL4	74.1
ZnL5	53.0
ZnL6	54.6
ZnL7	63.5

Reaction conditions - styrene oxide: 10 mmol, Tetrabutylammonium bromide (TBAB):0.05 mmol, Complex: 0.05 mmol, 80 °C, 5 hours, ~1 atm CO_2 (bladder), [a] Calculated by GC using bromobenzene as internal standard

Table 3.7: Control reactions

Catalyst	Yield[a] (%)
Only TBAB	31
TBAB + L4	41.7
$Zn(OAc)_2.2H_2O$+TBAB	42.8
ZnL4 + TBAI	62.8
ZnL4 + TBAB	74.1

Reaction conditions - styrene oxide: 10 mmol, TBAB:0.05 mmol, Complex: 0.05 mmol, 80 °C, 5 hours, ~1 atm CO_2 (bladder), [a] GC yield

Table 3.8: Activity of the catalyst ZnL4 with other epoxides	
Epoxide	**Conversion[a] (%)**
Styrene oxide	85.4
Propylene oxide[b]	93
Epichlorohydrin	91.4
Cyclohexene oxide[c]	0
Reaction conditions - epoxide: 5 mmol, TBAB:0.025 mmol, Complex: 0.025 mmol, 80 °C, 5 hours, ~1 atm CO_2 (bladder), [a] GC conversion, [b] Reaction carried out at room temperature for 5 h. [c] Reaction carried out at 120 °C for 10 h.	

Table 3.9: Table for yield, conversion, and selectivity			
Complex	**Yield (%)[a]**	**Conversion (%)[b]**	**Selectivity (%) (Y/C)**
ZnL1	59.1	75.6	78.1
ZnL2	60.5	75.7	79.9
ZnL3	63.4	79.7	82.0
ZnL4	74.1	85.4	86.7
ZnL5	53.0	67.6	78.4
ZnL6	54.6	77.5	70.4
ZnL7	63.5	94.2	67.4
Reaction conditions - styrene oxide: 10 mmol, Tetrabutylammonium bromide (TBAB):0.05 mmol, Complex: 0.05 mmol, 80 °C, 5 hours, ~1 atm CO_2 (bladder) [a] Calculated by GC using bromobenzene as internal standard			

3.2.8 Discussions

Our experimental studies involving ZnL1-ZnL7 complexes combined with theoretical results indicate that the complex with the strongest electron withdrawing -NO_2 substituent, ZnL4, is the most efficient catalyst for the cycloaddition of CO_2 to SO. The presence of a strong electron-withdrawing group in this complex is well supported by the electronic spectroscopic studies, which appropriately manifests in the red-shifted positioning of the MLCT band of the ZnL4 complex with respect to the other complexes (Figure 3.11(H)). Another striking observation indicated by mass (LC-MS) spectrometric analysis and theoretical studies is the presence of two water

molecules coordinated to monomeric ZnL4. In contrast, all the other complexes exist as dimers. On the one hand, the dimerization reduces the catalytic activity of the Zn centers in the complexes. On the other side, ZnL4, having a $–NO_2$ group attached to it, exists as a monomer with the Zn center bound to two labile water molecules. Consequently, ZnL4 exhibits quite an improved catalytic activity compared to the rest. DFT studies of the reaction mechanism also show a different rate-determining step for the catalytic reaction involving ZnL4, which has a lower activation barrier in comparison to dimeric ZnL1 (Figure 3.19(B)). Therefore, it may be summarized as the electronic environment around the metal in the ZnL4 complex prevents dimerization, which, in turn, leads to the highest reactivity towards the cycloaddition reaction of CO_2 to styrene oxide *via* a different rate-determining step.

To comprehend the electronic effect of the substituents, another complex with an electron-withdrawing group, i.e., $-OCF_3$, was prepared. Although both $-NO_2$ and $-OCF_3$ are electron withdrawing, the difference in their activity is evident. Among the dimeric complexes, the activity of ZnL7 is on the higher side. The inductive effect of $-OCF_3$ in ZnL7 dominates over the resonance effect, which is also evident in the UV-vis spectra in Figure 3.11(H)).

These observations are also in line with the studies of the mechanism, according to which the activation of the epoxide requires a lesser electron density on the metal. The lesser electron density around the metal center is also confirmed by the XPS studies, where the binding energy of ZnL4 is comparatively higher. The presence of electron-withdrawing $-NO_2$ makes the zinc center electron deficient, enabling the better activation of the epoxide.

Kleij *et al.* have extensively studied the zinc salophen systems and their application as catalysts in the cycloaddition reaction.[12, 54-57] They have shown the existence of the salophen complexes as dimers and, thus, added the bulky ^{t}Bu group as a substituent to prevent dimerization.[33, 58, 59] We observed the formation of dimers in similar types of complexes as well, and those dimeric complexes also are explored as catalysts for cycloaddition reaction. In the literature, complex 1 (shown in Figure 3.20), which is structurally quite similar to our complexes, has been widely utilized as a catalyst for the cycloaddition reaction using SO as the substrate. In one report,[12] using complex 1, the yield of SC obtained was reported as 15% with 18 hours of reaction time at room temperature of 25 °C and 2 bar pressure. In another report, supercritical CO_2 as a synthon and a solvent source has been employed for the cycloaddition reaction with the applied pressure of 80 bar.[54] In the third report, using the complex 1,[55] 66% of SC was reported at a comparatively higher

pressure and time of 10 bar and 18 hours, respectively, at 45 °C. However, in the current study, comparable yields have been achieved at much milder reaction conditions, even with the dimeric complexes. The dimeric ZnL7, at the ~1 atm within 5 hours of reaction time, yielded 63.5% of SC. Despite the fact that the temperature employed in this work seems to be relatively in the higher range, the literature with similar zinc complexes shows that the temperature used for the cycloaddition is mostly higher than 100 °C.[10, 11, 60-62]. There are reports utilizing catalyst loading as high as 25 mol%.[63] The reaction time reported in some reports is longer (20-24 h).[64-66] In comparison, our complexes, in synergy with tetrabutylammonium bromide (TBAB), are able to provide moderate to good yields for the SC at a lower reaction temperature of 80 °C, at 5 hours and an ambient pressure of ~1 atm using quiet low catalyst loading of 0.5 mol%. Instead of higher pressure, usage of CO_2 at ambient pressure of ~ 1 atm undoubtedly improves the reaction in terms of conversion efficiency and moulds the pathway further benign.

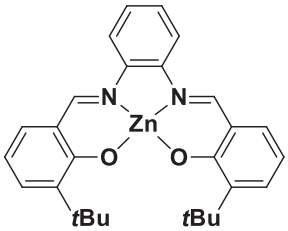

Complex 1

Figure 3.20: The structure of Complex 1.

3.3 Conclusions

Zinc(II) salophen complexes were synthesized and used as catalysts for the cycloaddition reaction between CO_2 and styrene oxide. All the catalysts afforded good to moderate yields (74.1-53%) of the product, i.e., styrene carbonate at comparatively milder conditions (80 °C, ~1 atm CO_2 pressure in 5 hours of reaction time The complex with the strongest electron withdrawing -NO_2 group (ZnL4) showed the best catalytic activity. LC-MS and DFT studies show that ZnL4 exists as a monomer with two coordinated water molecules, while the other complexes exist as dimers. Mechanistic studies of catalysis were performed using DFT, and the results indicate that the rate-determining step for ZnL4 is different in comparison to ZnL1 and ZnL3. These factors contribute to the singular activity of ZnL4. Although existing as dimers, the other complexes also show comparatively better activity, suggesting that the incorporation of the bulky ^{t}Bu group may not be mandatory to achieve similar catalytic activity of these complexes.

3.4 References

1. D. Prasad, K. N. Patil, N. K. Chaudhari, H. Kim, B. M. Nagaraja and A. H. Jadhav, *Catalysis Reviews*, 2022, **64**, 356.
2. X.-B. Lu, J.-H. Xiu, R. He, K. Jin, L.-M. Luo and X.-J. Feng, *Applied Catalysis A: General*, 2004, **275**, 73.
3. J.-Q. Wang, X.-D. Yue, F. Cai and L.-N. He, *Catalysis Communications*, 2007, **8**, 167.
4. K. Motokura, S. Itagaki, Y. Iwasawa, A. Miyaji and T. Baba, *Green Chemistry*, 2009, **11**, 1876.
5. R. Martín and A. W. Kleij *ChemSusChem*, 2011, **4**, 1259.
6. H. Vignesh Babu and K. Muralidharan, *Dalton Transactions*, 2013, **42**, 1238.
7. M. H. Beyzavi, C. J. Stephenson, Y. Liu, O. Karagiaridi, J. T. Hupp and O. K. Farha, *Frontiers in Energy Research*, 2015, **2**, 63.
8. J. Ozdemir, I. Mosleh, M. Abolhassani, L. F. Greenlee, R. R. Beitle and M. H. Beyzavi, *Frontiers in Energy Research*, 2019, **7**, 77.
9. S. Pappuru, D. Shpasser, R. Carmieli, P. Shekhter, F. C. Jentoft and O. M. Gazit, *ACS Omega*, 2022, **7**, 24656.
10. I. Karamé, S. Zaher, N. Eid and L. Christ, *Molecular Catalysis*, 2018, **456**, 87.
11. M. Alonso de la Peña, L. Merzoud, W. Lamine, A. Tuel, H. Chermette and L. Christ, *Journal of CO_2 Utilization*, 2021, **44**, 101380.
12. A. Decortes and A. W. Kleij, *ChemCatChem*, 2011, **3**, 831.
13. M. S. More, P. G. Joshi, Y. K. Mishra and P. K. Khanna, *Materials Today Chemistry*, 2019, **14**, 100195.
14. C. J. Whiteoak, G. Salassa and A. W. Kleij, *Chemical Society Reviews*, 2012, **41**, 622.
15. K. G. Vladimirova, A. Y. Freidzon, O. V. Kotova, A. A. Vaschenko, L. S. Lepnev, A. A. Bagatur'yants, A. G. Vitukhnovskiy, N. F. Stepanov and M. V. Alfimov, *Inorganic Chemistry*, 2009, **48**, 11123.
16. M. E. Germain, T. R. Vargo, P. G. Khalifah and M. J. Knapp, *Inorganic Chemistry*, 2007, **46**, 4422.
17. Y. Xu, M. Xiao, S. Wang, M. Pan and Y. Meng, *Polymer Chemistry*, 2014, **5**, 3838.
18. L. Cuesta-Aluja, A. Campos-Carrasco, J. Castilla, M. Reguero, A. M. Masdeu-Bultó and A. Aghmiz, *Journal of CO_2 Utilization*, 2016, **14**, 10.

19. A. Choudhary, S. Kumari and S. Ray, *ACS Omega*, 2017, **2**, 6636.
20. M. Rakibuddin and R. Ananthakrishnan, *RSC Advances*, 2015, **5**, 68117.
21. Z. Liu, G. Li, T. Cui, A. Lahiri, A. Borodin and F. Endres, *Physical Chemistry Chemical Physics*, 2017, **19**, 25989.
22. C. Boulechfar, H. Ferkous, S. Boufas, M. Berredjem, A. Delimi, S. Djellali, A. Djedouani, R. Bahadi, S. Laamari, K. K. Yadav, B.-H. Jeon, W. Bouchelaghem, M. Alam and Y. Benguerba, *Journal of Molecular Structure*, 2023, **1271**, 134007.
23. V. Haber and P. Ptáček, *Inorganica Chimica Acta*, 1991, **179**, 267.
24. S. Bhunia, R. A. Molla, V. Kumari, S. M. Islam and A. Bhaumik, *Chemical Communications*, 2015, **51**, 15732.
25. C. M. Doyle, C. McGuinness, A. P. Lawless, A. B. Preobrajenski, N. A. Vinogradov and A. A. Cafolla, *Physica Status Solidi B*, 2019, **256**, 1800349.
26. X. Zhang, T. Schiros, D. Nordlund, Y. C. Shin, J. Kong, M. Dresselhaus and T. Palacios, *Advanced Functional Materials*, 2015, **25**, 4163.
27. I. Palchan, M. Crespin, H. Estrade-Szwarckopf and B. Rousseau, *Chemical Physics Letters*, 1989, **157**, 321.
28. S. Solihah Khaidir, H. Bahron, A. Mohd Tajuddin and K. Ramasamy, *International Pharmacy Acta*, 2020, **3**, 1.
29. Z. Shaghaghi, N. Kalantari, M. Kheyrollahpoor and M. Haeili, *Journal of Molecular Structure*, 2020, **1200**, 127107.
30. M. S. More, S. B. Pawal, S. R. Lolage and S. S. Chavan, *Journal of Molecular Structure*, 2017, **1128**, 419.
31. G. Avsar, H. Altinel, M. Yilmaz and B. Guzel, *Journal of Thermal Analysis and Calorimetry*, 2010, **101**, 199.
32. M. Sharma, B. Das, G. V. Karunakar, L. Satyanarayana and K. K. Bania, *The Journal of Physical Chemistry C*, 2016, **120**, 13563.
33. A. W. Kleij, D. M. Tooke, A. L. Spek and J. N. H. Reek, *European Journal of Inorganic Chemistry*, 2005, **2005**, 4626.
34. T. Khan, S. Vaidya, D. S. Mhatre and A. Datta, *The Journal of Physical Chemistry B*, 2016, **120**, 10319.
35. M. Odoko, N. Tsuchida and N. Okabe, *Acta Crystallographica Section E*, 2006, **62**, m708.

36. I. Giannicchi, R. Brissos, D. Ramos, J. d. Lapuente, J. C. Lima, A. D. Cort and L. Rodríguez, *Inorganic Chemistry*, 2013, **52**, 9245.
37. S. Kumari and S. Ray, *New Journal of Chemistry*, 2020, **44**, 14953.
38. S. Kumari, A. Choudhary and S. Ray, *Applied Organometallic Chemistry*, 2019, **33**, e4765.
39. S. Kumari, B. Das and S. Ray, *Dalton Transactions*, 2019, **48**, 15942.
40. F. Dumur, E. Contal, G. Wantz and D. Gigmes, *European Journal of Inorganic Chemistry*, 2014, **2014**, 4186.
41. R. Evans, G. Dal Poggetto, M. Nilsson and G. A. Morris, *Analytical Chemistry*, 2018, **90**, 3987.
42. A.-K. Kreyenschmidt, S. Bachmann, T. Niklas and D. Stalke, *ChemistrySelect*, 2017, **2**, 6957.
43. G. Consiglio, I. P. Oliveri, S. Cacciola, G. Maccarrone, S. Failla and S. Di Bella, *Dalton Transactions*, 2020, **49**, 5121.
44. G. Consiglio, S. Failla, P. Finocchiaro, I. P. Oliveri and S. D. Bella, *Dalton Transactions*, 2012, **41**, 387.
45. I. Gerz, S. A. V. Jannuzzi, K. T. Hylland, C. Negri, D. S. Wragg, S. Øien-Ødegaard, M. Tilset, U. Olsbye, S. DeBeer and M. Amedjkouh, *European Journal of Inorganic Chemistry*, 2021, **2021**, 4762.
46. G. Consiglio, S. Failla, P. Finocchiaro, I. P. Oliveri and S. Di Bella, *Inorganic Chemistry*, 2012, **51**, 8409.
47. A. Ramesh, S. De, S. Bajaj, B. Das and S. Ray, *European Journal of Inorganic Chemistry*, 2024, **27**, e202300610.
48. T.-T. Wang, Y. Xie and W.-Q. Deng, *The Journal of Physical Chemistry A*, 2014, **118**, 9239.
49. F. D. Bobbink, D. Vasilyev, M. Hulla, S. Chamam, F. Menoud, G. Laurenczy, S. Katsyuba and P. J. Dyson, *ACS Catalysis*, 2018, **8**, 2589.
50. J. Martínez, F. de la Cruz-Martínez, M. A. Gaona, E. Pinilla-Peñalver, J. Fernández-Baeza, A. M. Rodríguez, J. A. Castro-Osma, A. Otero and A. Lara-Sánchez, *Inorganic Chemistry*, 2019, **58**, 3396.
51. W. F. Monteiro, M. O. Vieira, E. F. Laschuk, P. R. Livotto, S. M. O. Einloft, M. O. de Souza and R. A. Ligabue, *Journal of CO_2 Utilization*, 2020, **37**, 20.

52. R. B. Mujmule, M. P. Raghav Rao, P. V. Rathod, V. G. Deonikar, A. A. Chaugule and H. Kim, *Journal of CO_2 Utilization*, 2019, **33**, 284.
53. R. Ma, L.-N. He, X.-F. Liu, X. Liu and M.-Y. Wang, *Journal of CO_2 Utilization*, 2017, **19**, 28.
54. M. Taherimehr, A. Decortes, S. M. Al-Amsyar, W. Lueangchaichaweng, C. J. Whiteoak, E. C. Escudero-Adán, A. W. Kleij and P. P. Pescarmona, *Catalysis Science & Technology*, 2012, **2**, 2231.
55. A. Decortes, M. Martínez Belmonte, J. Benet-Buchholz and A. W. Kleij, *Chemical Communications*, 2010, **46**, 4580.
56. C. Martín, C. J. Whiteoak, E. Martin, M. Martínez Belmonte, E. C. Escudero-Adán and A. W. Kleij, *Catalysis Science & Technology*, 2014, **4**, 1615.
57. M. V. Escárcega-Bobadilla, M. Martínez Belmonte, E. Martin, E. C. Escudero-Adán and A. W. Kleij, *Chemistry – A European Journal*, 2013, **19**, 2641.
58. J. A. A. W. Elemans, S. J. Wezenberg, M. J. J. Coenen, E. C. Escudero-Adán, J. Benet-Buchholz, D. den Boer, S. Speller, A. W. Kleij and S. De Feyter, *Chemical Communications*, 2010, **46**, 2548.
59. M. M. Belmonte, S. J. Wezenberg, R. M. Haak, D. Anselmo, E. C. Escudero-Adán, J. Benet-Buchholz and A. W. Kleij, *Dalton Transactions*, 2010, **39**, 4541.
60. M. A. Fuchs, S. Staudt, C. Altesleben, O. Walter, T. A. Zevaco and E. Dinjus, *Dalton Transactions*, 2014, **43**, 2344.
61. Z. Wang, Z. Bu, T. Cao, T. Ren, L. Yang and W. Li, *Polyhedron*, 2012, **32**, 86.
62. Z. Alaji, E. Safaei and A. Wojtczak, *New Journal of Chemistry*, 2017, **41**, 10121.
63. J. Hu, J. Ma, H. Liu, Q. Qian, C. Xie and B. Han, *Green Chemistry*, 2018, **20**, 2990.
64. L. Wang, G. Zhang, K. Kodama and T. Hirose, *Green Chemistry*, 2016, **18**, 1229.
65. L. Wang, K. Kodama and T. Hirose, *Catalysis Science & Technology*, 2016, **6**, 3872.
66. S. Liu, N. Suematsu, K. Maruoka and S. Shirakawa, *Green Chemistry*, 2016, **18**, 4611.

Chapter 4

Importance of the Nature of Acidic Sites of Different Aluminosilicates on Fixation of Carbon Dioxide with Styrene Oxide

Abstract: *The nature of acidic sites in commercially available aluminosilicates, zeolite Na-Y, zeolite NH_4^+-ZSM-5, and synthesized Al-MCM-41 have been investigated by employing them as catalysts for capturing CO_2 by styrene oxide. TPD studies indicate the number of weak acidic sites of these materials is just in accordance with their Si/Al ratio and the yield of the cyclic carbonates obtained. The TPD data and the yield of the product carried out with calcined zeolite Na-Y indicate that not only the weak acidic sites but also the role of strong acidic sites might appear crucial in the cycloaddition reaction.*

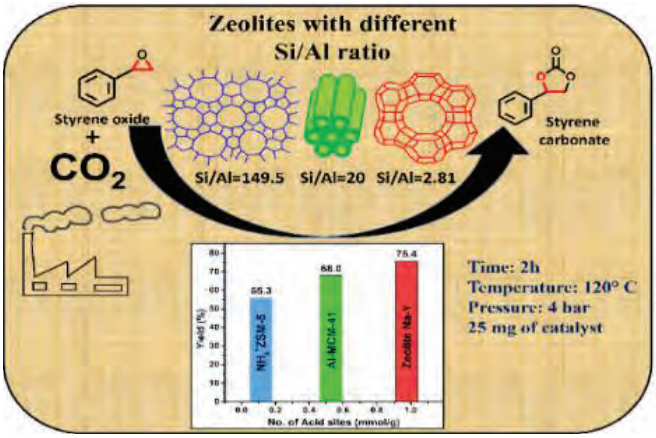

A. Ramesh and S. Ray, *ChemPlusChem* **2023**, 88, e202300086.

4.1 Introduction

In the previous chapter, we have explored the synthesis of styrene carbonate from CO_2 and styrene oxide using Zn-complexes as homogeneous catalysts. The studies aimed to explore the role of substituents present at 5,5' positions of the complex on the cycloaddition reaction to understand the electronic factors associated with the reaction. However, heterogeneous catalysts have a huge upper hand over the homogeneous catalysts. In this regard, zeolites, which are porous in nature and have inherent acidity, possess the ideal characteristics for an efficient catalyst for the cycloaddition reaction. As discussed in the introduction, the aluminosilicate framework consists of both Lewis acidity and Brønsted acidity. It is also known that the acidity of zeolites can be tweaked by varying the Si/Al ratio. The presence of these acidic sites in zeolites and mesoporous silica can be implemented as heterogeneous acid catalysts for reactions involving a Lewis or Brønsted acid catalyst.

It has already been highlighted that cyclic carbonates are industrially relevant materials which require an acid catalyst. Traditionally, cyclic carbonates were synthesized using toxic phosgene; however, recently, in the past two decades, many other homogeneous catalysts like Schiff base catalysts,[1] ionic liquids (ILs),[2, 3] and heterogeneous catalysts including covalent organic frameworks (COFs), metal-organic frameworks (MOFs),[4] porous organic polymers (POPs),[5] zeolitic imidazolate frameworks (ZIFs), metal oxides, polymer-supported ILs, silica-based[6] catalysts have been developed and have been used as catalysts.

Homogeneous catalysts face the drawback of catalyst separation, on the other hand, heterogeneous catalysts like MOFs and COFs require a tedious synthesis process. For the targeted cyclic carbonate to synthesize from CO_2, aluminosilicate catalysts, including zeolites and mesoporous Al-MCM-41, have been explored as solid support.[7, 8] Reports wherein zeolite has been used as catalyst include Cesium-exchanged zeolite-Y, [9] beta zeolite,[10] and zeolite-Y impregnated with metal halides.[11] However, there are fewer reports focusing on the use of ZSM-5 and MCM-41 as catalysts. The use of basic meso-ZSM-5 was reported by Sarmah *et al.*[12] and Zn-ZSM-5 was reported by Zhao *et al.*[13] Liu *et al.*[14] reported the use of different sized ZSM-5 for the synthesis of cyclic carbonates. In literature, there exist fewer reports utilizing MCM as catalysts like synthesized MCM-41,[15] and KI dispersed MCM-41[16] (discussed in detail in section 1.1.4.3). Apart from ZSM-5, MCM-41, and zeolite-Y, there are also reports of using other silica-based catalysts like functionalized SBA-15.[17-19] From the mechanism, it is quite evident that acidity plays a

significant role in the formation of cyclic carbonates. Initially, reports on the formation of cyclic carbonates mainly discussed the role of the Lewis acidity of the catalyst. Recently, Zhao *et al.*[13] and Wu *et al.*[20] were the first to report the role of Brønsted acidity of the catalyst. Zhao *et al.* highlighted the hydroxyl group of ZSM-5 as the source of Brønsted acidity, while Wu *et al.* attributed the Brønsted acidity to the hydroxyl group of the salophen ligand they used. Hence, in the limited amount of zeolite-related literature that is currently available, some papers highlight the Lewis acidity of the catalyst, while others have emphasized the crucial role that Brønsted acidity plays. However, there are very few reports of using synthesized or commercial zeolites directly as catalysts for the synthesis of cyclic carbonates. Zeolites have become a fascinating choice for the synthesis of cyclic carbonates since they include both Lewis and Brønsted acidic sites. Apart from the intrinsic acidity, zeolites also have a porous structure, which renders them with very good CO_2 adsorbing capacity[21-23] and hence, become a potential candidate as catalysts.

In this chapter, we have studied the catalytic activity of commercially available zeolites, zeolite NH_4^+-ZSM-5 and zeolite Na-Y, and the synthesized mesoporous silica, Al-MCM-41 for the cycloaddition reaction. The correlation between the acidity of the aluminosilicates and the yield of the cycloaddition product has been discussed. We have used aluminosilicates with different Si/Al ratio to compare the effect of the same. All the catalysts have different Si/Al ratios and hence, have variation in the acidic property. All these catalysts show moderate to good yields for the synthesis of styrene carbonate from styrene oxide without the use of any other metal. Utilizing commercially available zeolites as catalysts offers the obvious upper hand of avoiding the complicated synthesis process and the tedious characterization. However, since Al-MCM-41 has been synthesized, all the catalysts have been characterized for comparison. Also, there is no study reported using commercially available aluminosilicate catalysts for the conversion of CO_2 to cyclic carbonates.

4.2 Results and discussions

4.2.1 Elemental analysis

Energy Dispersive X-ray (EDX) analysis is performed to analyze the elements present in the zeolite samples. This technique has been mainly used to calculate the Si/Al ratio value. The Si/Al ratio values of the zeolites are presented in Table 4.1. The Si/Al ratio of commercially available FAU-type zeolite Na-Y and zeolite NH_4^+-ZSM-5 are 2.79 and 175, respectively. The Si/Al ratio of synthesized Al-MCM-41 is also consistent with the ratio of sodium silicate and aluminum isopropoxide used in synthesis. The different amounts of Si, Al, and O in all three zeolites are

indicative of their different framework structures. It could be preceded that the variable Si/Al ratio and the amount of oxygen accompany the difference in the acidity of these materials. It is quite explicit from Table 4.1 that the lesser content of the aluminium present in the zeolite NH_4^+-ZSM-5 leads to quite a high standard deviation (SD), i.e., 46.87. This high SD value indicates the non-homogeneous distribution of aluminium in the sample.

Table 4.1: Si/Al ratios of the catalysts

Catalyst	O	Si	Al	Si/Al Ratio	SD
Zeolite NH_4^+-ZSM-5	39.86	59.77	0.35	175	46.87
Al-MCM-41	48.45	49.08	2.55	19.55	0.36
Zeolite Na-Y	43.36	30.16	10.76	2.79	0.08

4.2.2 Field Emission Scanning Electron Microscopy (FESEM)

To study the morphology of the zeolites and MCM-41, Field Emission Scanning Electron Microscopy (FESEM) technique is used. Zeolite Na-Y and Zeolite NH_4^+-ZSM-5 are found to have morphology as reported previously.[24, 25] The SEM images of MCM-41 confirm its successful synthesis.[26] The SEM images of all the aluminosilicates is presented in Figure 4.1

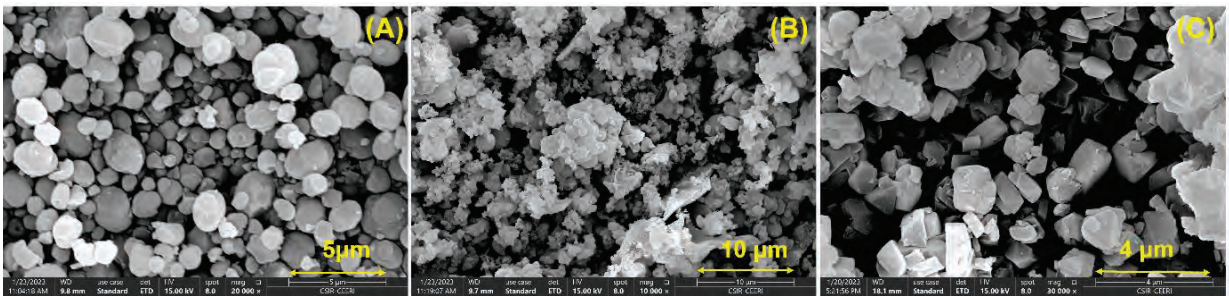

Figure 4.1: SEM images of **(A)** Zeolite NH_4^+ZSM-5, **(B)** Al-MCM-41, **(C)** Zeolite Na-Y.

4.2.3 Powder X-ray diffraction (XRD) studies

The XRD patterns of all three zeolites are presented in Figure 4.2. XRD analysis is carried out to probe the crystallinity of the zeolite structures. The XRD of all the zeolites, *i.e.*, commercial

zeolite Na-Y and zeolite NH_4^+-ZSM-5 and the synthesized Al-MCM-41, is well-matched with the literature,[14, 27, 28] showing the crystalline nature of all the three aluminosilicates.

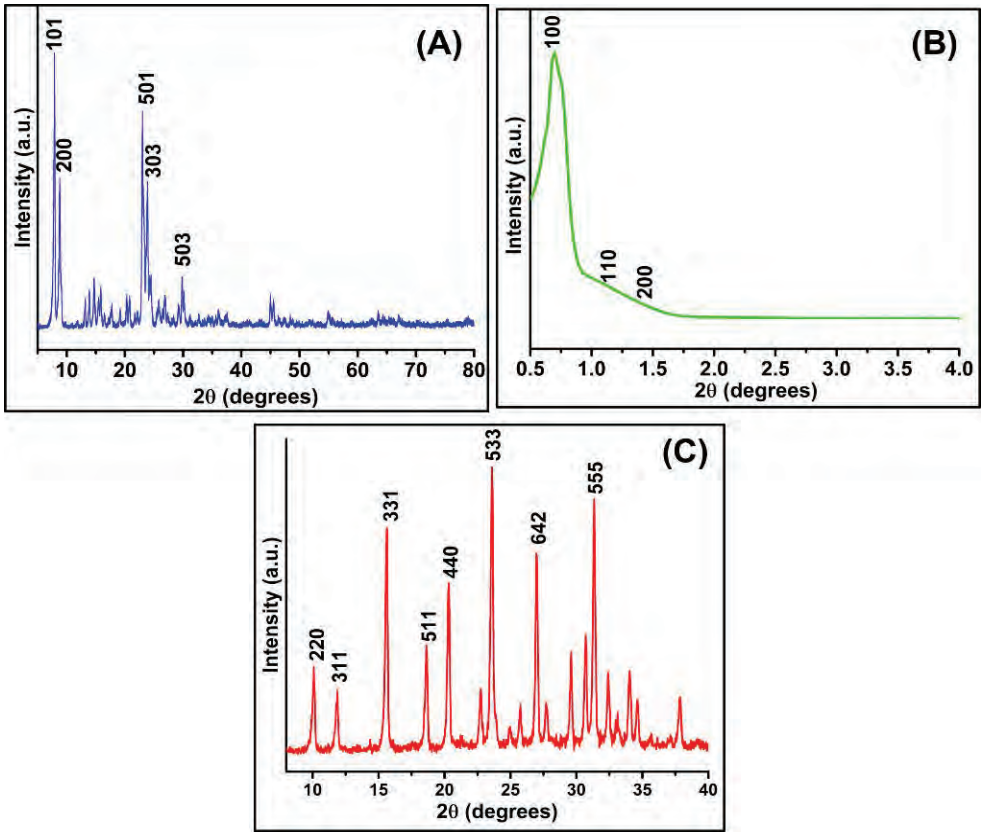

Figure 4.2: XRD spectrum of the catalysts **(A)** Zeolite NH_4^+-ZSM-5 **(B)** Al-MCM-41 **(C)** Zeolite Na-Y.

4.2.4 Fourier Transform Infrared (FT-IR) spectroscopy

The FT-IR spectroscopy of the catalysts has been performed (shown in Figure 4.3) to study the structural integrity of the catalysts and to assess the presence of the hydroxyl group, which is indicative of Brønsted acidity. There are a few distinctive peaks for all three different aluminosilicate frameworks used. All the important peaks have been tabulated in Table 4.2. For the commercially available zeolite NH_4^+-ZSM-5, the peaks are well-matched with the reported literature. We observe a broad peak around 3661 cm^{-1}, indicating the presence of the isolated silanol groups. The peak at 3533 cm^{-1} represents the presence of the Al-OH framework, which can be ascribed to the presence of Brønsted acidity.[28] The peak at 557 cm^{-1} is typical for MFI zeolites.[29]

In the case of the synthesized Al-MCM-41, all the characteristic peaks are well-matched with the literature. Some of the main peaks include 803 cm^{-1}, 1081 cm^{-1}, 1189 cm^{-1}, 1637 cm^{-1}, 3468 cm^{-1}, corresponding to symmetric and asymmetric Si-O stretching modes. The peak at 1637 cm^{-1} is due to the adsorbed water molecules, while the peak at 3468 cm^{-1} is due to surface silanol groups.[30, 31] Again, for the commercial zeolite Na-Y, the peaks are well agreed with the literature, with the main peaks at 577 cm^{-1}, 728 cm^{-1}, 789 cm^{-1}, 1049 cm^{-1}, and 1642 cm^{-1}. The broad peak at 3477 cm^{-1} indicates the existence of surface hydroxyl groups and adsorbed water molecules, while the peak at 1642 cm^{-1} represents the lattice water molecules.[27]

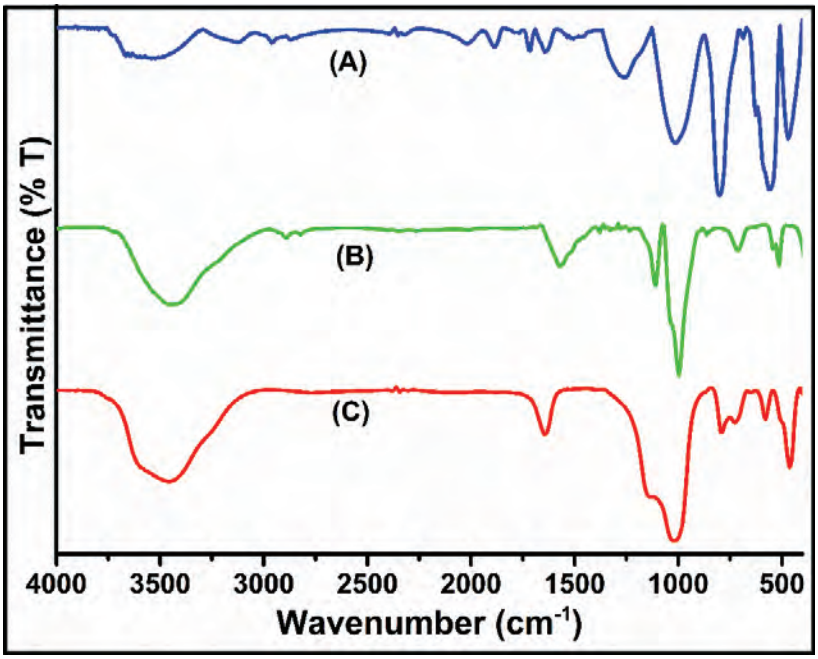

Figure 4.3: FT-IR spectra of the catalysts **(A)** Zeolite NH_4^+-ZSM-5 **(B)** Al-MCM-41 **(C)** Zeolite Na-Y.

Table 4.2: FT-IR study of the catalysts		
Catalyst	**Wavenumber (cm^{-1})**	**Inference**
Zeolite NH_4^+-ZSM-5	557	Typical for MFI-type zeolite
	800	T-O-T Symmetric stretching
	1015	T-O-T Internal Asymmetric stretching
	1258	T-O-T External Asymmetric stretching
	1642	Adsorbed water
	3533	Al-OH framework
	3661	Isolated silanol groups
Al-MCM-41	803	Symmetric Si-O stretching
	949	Symmetric stretching of silanol group
	1081	Internal Asymmetric Si-O stretching mode
	1189	External Asymmetric Si-O stretching mode
	1637	vibrations of adsorbed water molecules
	3468	Si-OH groups
Zeolite Na-Y	577	T-O bending vibrations
	728	T-O Double ring vibrations
	789	Symmetric T-O stretching vibrations
	1049	Asymmetric T-O stretching vibrations
	1642	Lattice water molecules
	3477	Surface hydroxyl group

4.2.5 Thermogravimetric (TGA) analysis

The TGA analysis of all three catalysts was carried out to study the thermal stability. From the thermogram depicted in Figure 4.4, it is evident that the catalysts show very high stability even at a temperature of 800 °C. The catalysts show one-step weight loss of 1.12%, 7.04%, and 18.06% (shown in Table 4.3) for zeolite NH_4^+-ZSM-5, Al-MCM-41, and zeolite Na-Y, respectively,

between the temperature range of 40-180 °C. The weight loss is attributed to the loss of water molecules that are physically adsorbed on the external surface or the water molecules trapped within the pores of the zeolites. Since the framework of Al-MCM-41 consists majorly of silanol groups, the relatively flat peak of Al-MCM-41 at higher temperature shows that there is probably negligible condensation of those silanol on the surface of the prepared catalyst.[32]

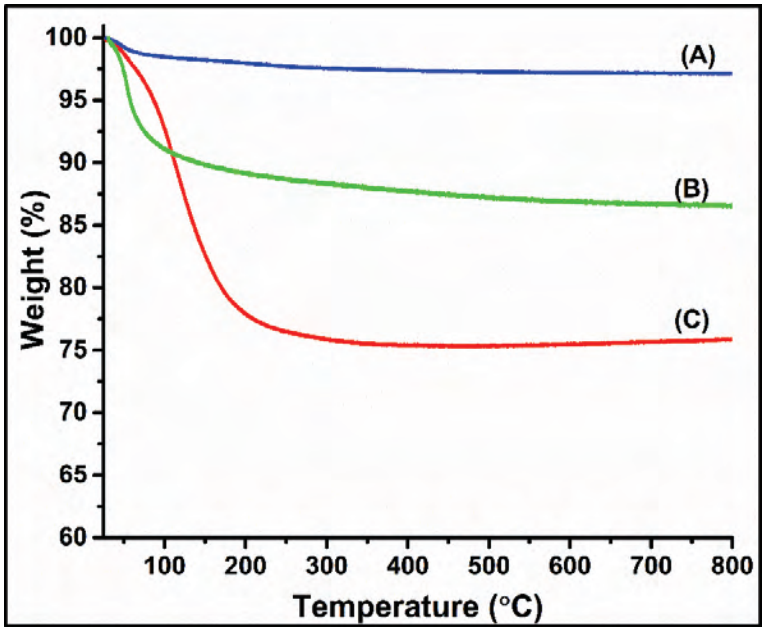

Figure 4.4: TGA profile of **(A)** Zeolite NH_4^+-ZSM-5 **(B)** Al-MCM-41 **(C)** Zeolite Na-Y.

Table 4.3: Weight loss profile from TGA		
Catalyst	**Temperature Range (°C)**	**Weight loss**
Zeolite NH_4^+-ZSM-5	43.94-86.71	1.12%
Al-MCM-41	40.48-80.05	7.04%
Zeolite Na-Y	65.74-178.38	18.06%

4.2.6 Brunauer–Emmett–Teller (BET) surface analysis

The BET surface analysis of the complexes was done to perceive the surface area and the pore volume of the complexes. The plots are shown in Figure 4.5 and the values reported in Table 4.4. From the BET plots, mesoporous nature of MCM-41 is confirmed as it follows the Type-IV

isotherm.[33] On the other hand, the Type I BET isotherm obtained for zeolite Na-Y indicates its microporous nature.[34]

Table 4.4: BET parameters for the catalysts

Catalyst	Surface Area ($A_{s\ BET}$) (m^2/g)	Total pore volume at p/p_0 =0.99 (cm^3/g)	Pore Diameter from BJH plot (nm)
Zeolite Na-Y	713	0.3607	1.61
Calcined zeolite Na-Y	723	0.3352	1.61
Al-MCM-41	425	0.596	4.90
NH_4^+-ZSM-5	323	0.2152	2.86

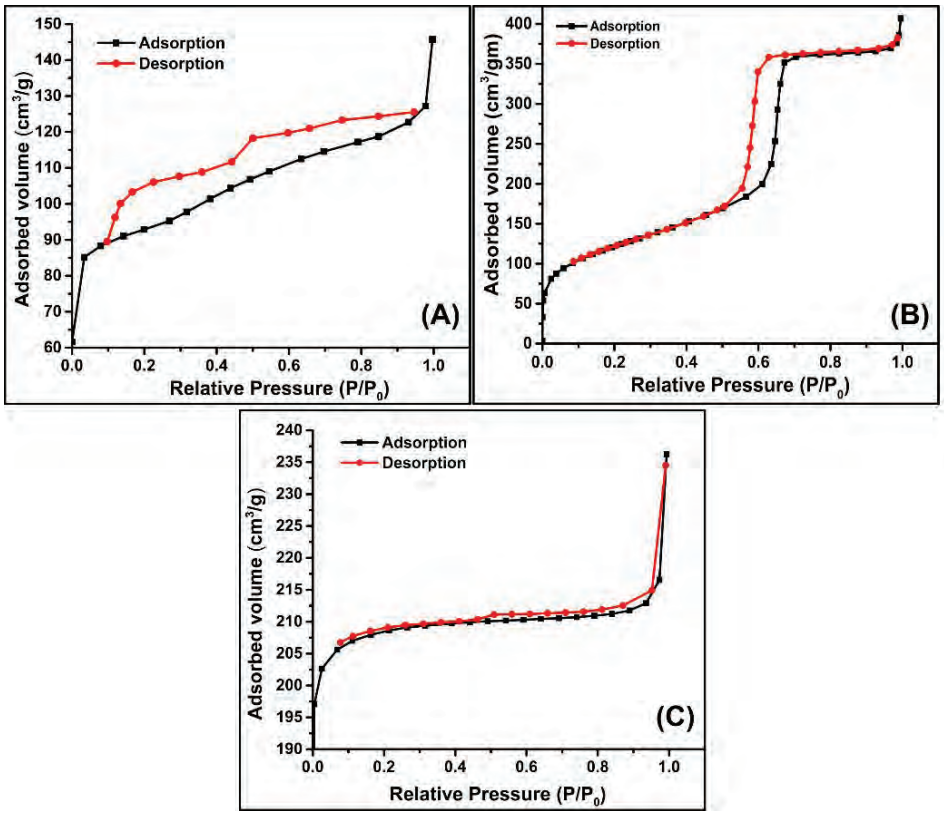

Figure 4.5: BET isotherms of the **(A)** Zeolite NH_4^+-ZSM-5 **(B)** Al-MCM-41 **(C)** Zeolite Na-Y.

4.2.7 ^{29}Si solid-state NMR

^{29}Si solid-state NMR of zeolite-Y was done to assess the Si/Al ratio of the zeolite Na-Y catalyst. The deconvoluted ^{29}Si solid-state NMR of zeolite-Y is shown in Figure 4.6. The NMR peaks show four different peaks in the range of -85 to -105 ppm. The peaks obtained are in good agreement with the literature.[35, 36] The peaks obtained at -88.73, -93.51, -98.84, and -104.72 correspond to Si(3Al), Si(2Al), Si(1Al), and Si(0Al), respectively. The Si/Al ratio was calculated from the ^{29}Si solid-state NMR and was compared with the Si/Al ratio calculated from EDX.[37, 38] The Si/Al_{NMR} ratio was found to be 2.48, while the Si/Al_{EDX} was 2.79. It is reported that the Si/Al ratio calculated from ^{29}Si solid-state NMR is generally found to be less than the Si/Al ratio calculated from quantitative analysis like EDX. The difference is because, in ^{29}Si NMR, the peaks due to Si(nAl) and Si(nOH) get overlapped, due to which the actual silicon present is decreased, while EDX detects the overall silicon present, which results in higher Si/Al ratio.[39]

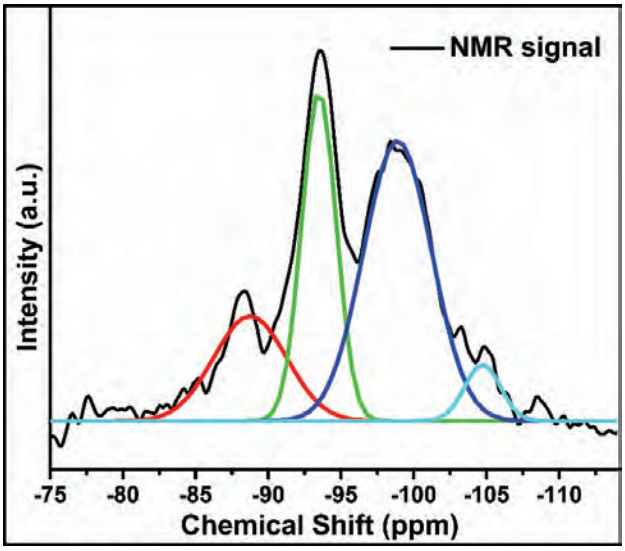

Figure 4.6: ^{29}Si solid-state NMR of zeolite Na-Y.

4.2.8 X-ray Photoelectron Spectroscopy (XPS) studies

XPS studies were also carried out to calculate the Si/Al ratio of the two zeolites and the prepared mesoporous silica, Al-MCM-41. The XPS profiles of the catalysts used are shown in Figure 4.7 and Figure 4.8. The binding energy values, and the Si/Al ratios are tabulated in Table 4.5. From the table, it is clear that the Si/Al ratio for zeolite Na-Y and Al-MCM-41 calculated from XPS and those obtained from EDX are comparable. According to a report by Huang *et al.*,[40] the binding energy of Al (2p), Si (2p), and O (1s) of the zeolites increase with the increase in the Si/Al ratio.

We also observe a similar trend in the case of zeolite Na-Y and zeolite NH_4^+-ZSM-5. The binding energy values of the O 1s for both the zeolites, zeolite NH_4^+-ZSM-5, and zeolite Na-Y are 532.63 eV and 531.71 eV, respectively. This may be attributed to the oxygen present in the form of Si-O-Al or Si-O-Si in the zeolite.[41] For Al-MCM-41, there are two peaks for O 1s. The peak at 533.34 eV corresponds to SiO_2 [42] and the peak at 534.26 eV corresponds to the adsorbed hydroxide.[43] The binding energy values at 103.38 eV and 102.41 eV corresponding to Si 2p for zeolite NH_4^+-ZSM-5 and zeolite Na-Y, respectively, indicate the presence of the aluminosilicate framework. The Si 2p peaks at 103.19 eV and 105.26 eV for Al-MCM-41 correspond to the Si-O-Al bond and SiO_2 network, respectively.[44] The Al 2p of Al-MCM-41 also has two peaks at 74.34 eV and 76.41 eV, corresponding to Al_2O_3 and $Al(OH)_3$, respectively.[42] The Al 2p peaks of both zeolites confirm the presence of the aluminosilicate framework.[45]

Table 4.5: XPS profile of the catalysts

Catalyst	Binding energies of (in eV)			Si/Al ratio (from XPS)	Si/Al ratio (from EDX)
	Si (2p)	Al (2p)	O (1s)		
Zeolite NH_4^+-ZSM-5	103.38	74.05	532.63	173	175
Al-MCM-41	103.19 105.26	74.34 76.41	533.34 534.55	25.3	19.55
Zeolite Na-Y	102.41	73.94	531.71	3.87	2.79

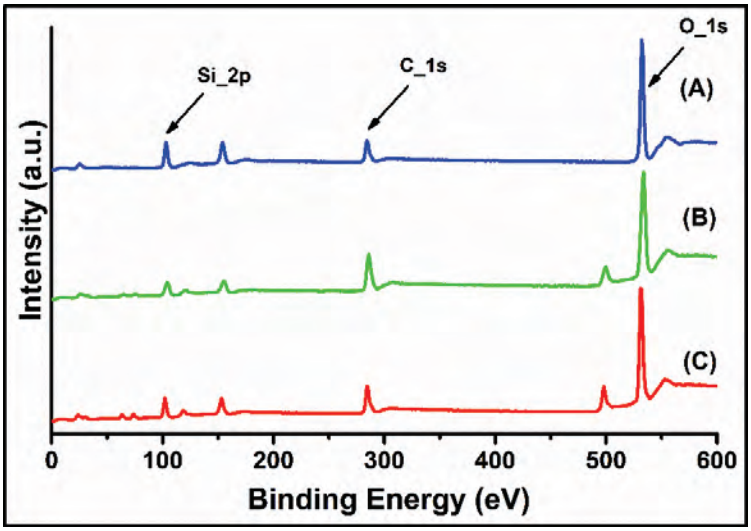

Figure 4.7: XPS survey graphs of **(A)** Zeolite NH_4^+-ZSM-5 **(B)** Al-MCM-41 **(C)** Zeolite Na-Y.

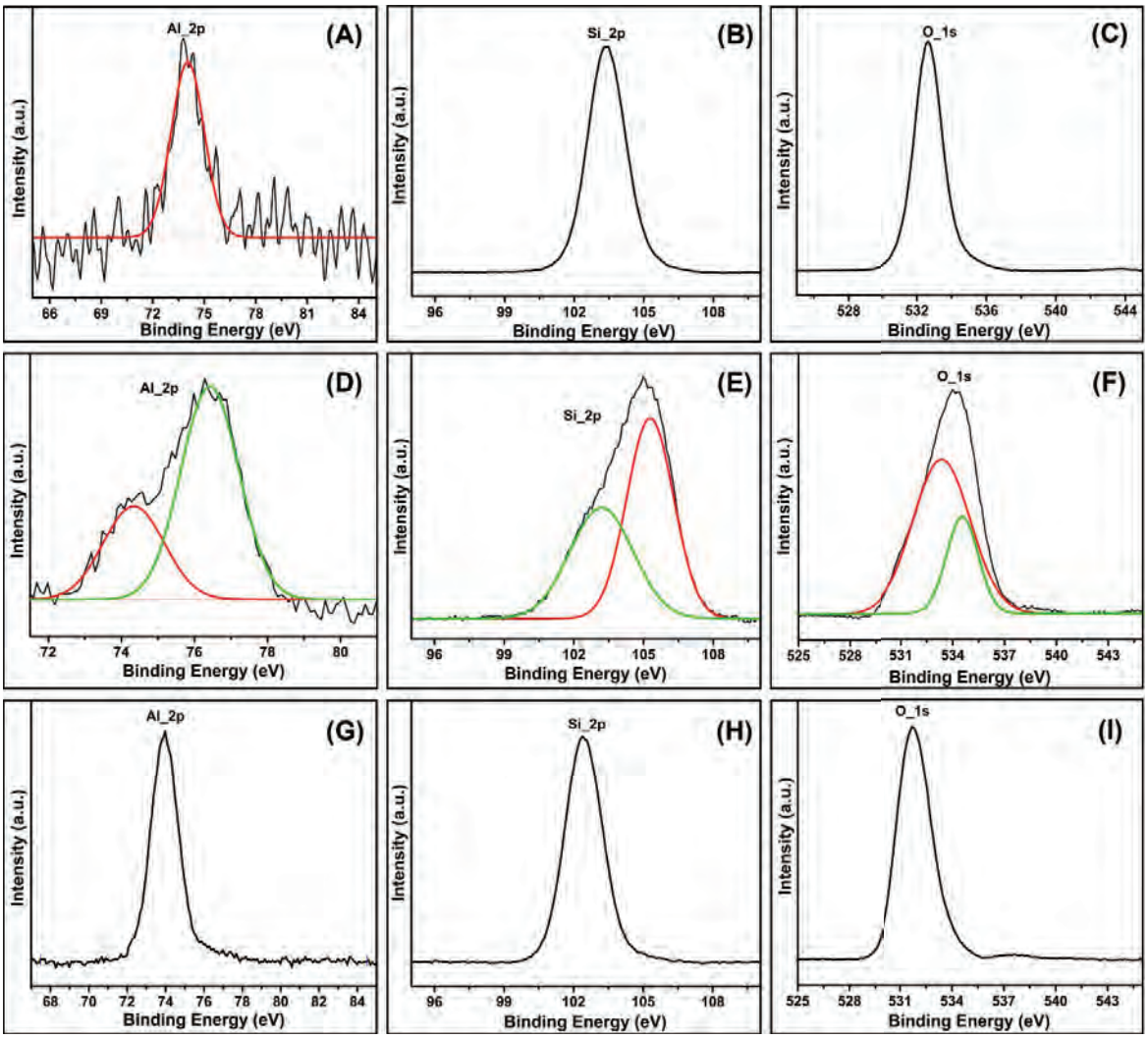

Figure 4.8: XPS profiles of **(A)** Al (2p) of Zeolite NH_4^+-ZSM-5, **(B)** Si (2p) of Zeolite NH_4^+-ZSM-5, **(C)** O (1s) of Zeolite NH_4^+-ZSM-5, **(D)** Al (2p) of Al-MCM-41, **(E)** Si (2p) of Al-MCM-41, **(F)** O (1s) of Al-MCM-41, **(G)** Al (2p) of Zeolite Na-Y, **(H)** Si (2p) of Zeolite Na-Y and **(I)** O (1s) of Zeolite Na-Y.

4.2.9 Ammonia TPD (NH_3-TPD) studies

The surface acidity of the catalysts utilized, determined using NH_3-TPD studies is depicted in Figure 4.9, and the number of acid sites is listed in Table 4.6. To further study the effect of the Si/Al ratio, zeolite Na-Y was calcined at 500 °C for 10 hours and was also studied using TPD. The catalyst, when exposed to ammonia, undergoes both physisorption and chemisorption of ammonia. Generally, one ammonia molecule is adsorbed on one acid site; hence, the concentration of

ammonia is equal to the number of surface acid sites of the catalyst.[46] Figure 4.9 shows that zeolite Na-Y and mesoporous Al-MCM-41 show two peaks, while zeolite NH_4^+-ZSM-5, NH_3-TPD mainly show three peaks. Previously carried out NH_3-TPD studies for ZSM-5 (MFI-type zeolite) by Topsøe *et al.*,[47] referred to the three peaks for ZSM-5 as α, β, and γ states in the temperature range of 60-100 °C, 150-200 °C and 320-500 °C respectively. They drew parallels between their results of Pyridine-IR and microcalorimetry with NH_3-TPD and associated the γ state peak with ammonia adsorption on strong Brønsted and/or Lewis acidic sites. They also correlated the α and the β states with lower acidity states. They pointed out that it is not always necessary that both α and the β states are present. The presence of the peak depends on the nature of the zeolite. Ahmadpour *et al.*[48] performed the NH_3-TPD of alkaline ZSM-5 and reported two peaks at 189 °C and 398 °C, respectively. They assigned the low-temperature peak to ammonia desorption from weak Lewis acid sites, while the high-temperature peak was attributed to ammonia desorbed from stronger Brønsted acid sites. In line with the literature, we have got three peaks for zeolite NH_4^+-ZSM-5 with the temperature peak position at 161.6 °C, 391.1 °C and 706.6 °C corresponding to α, β, and γ states, respectively, as referred by Topsøe *et al.*[47] Likewise, in the literature, we have also assigned the low-temperature peaks as weak acid sites and the high-temperature peaks as strong acid sites. The NH_3-TPD For MCM-41 has also been reported previously. Kosslick *et al.*[49] studied the NH_3-TPD of H-MCM-41 (Si/Al ratio = 24.4) and reported that it has peaks at two temperatures, i.e., around 150 °C and 600 °C. They reported that the peak with a higher desorption temperature corresponds to strong acidity. Similarly, Wang *et al.*[50] also studied the NH_3-TPD profiles and reported two peaks of Al-MCM-41 at approximately 200 °C and 650 °C, which they assigned to weak and strong acid sites, respectively. Our results for Al-MCM-41 also show similar nature with two peaks at 133 °C and 541 °C, which we have also assigned as weak and strong acid sites, respectively. Our TPD profile of zeolite-Y is consistent with that reported in the literature. The NH_3-TPD profile reported by Liu *et al.*[51] shows two peaks around 200 °C and 580 °C. Miessner *et al.*[52] also reported the TPD profile of different FAU-type zeolites. They reported temperature maxima around 250 °C and 420 °C for dealuminated FAU-type zeolite and reported that weakly bound NH_3 desorbs in the lower temperature range while strongly bound ammonia desorbs at higher temperature. We have observed two peaks at 163 °C and 692 °C. It is reported in a review by Niwa-Katada[53] that the temperature maximum also depends on the experimental conditions which cause some shift in the peak position. For FAU-type zeolite also, the lower

temperature peak is attributed to weak acid sites while higher temperature peaks correspond to the strong acid sites.

The comparison of the NH_3-TPD profiles and the Si/Al ratio for the catalysts used is in agreement with the well-known fact that the acidity of zeolites is governed by the Si/Al ratio.[54] It is also mentioned in the review by Ravi *et al.* [55] that with the increase of the Si/Al ratio, the number of Lewis acidic sites decreases. All our observations are quite in-line with the literature. According to our results, zeolite Na-Y has a greater number of weak acidic sites compared to that of zeolite NH_4^+-ZSM-5. The TPD data shown in Table 4.6 clearly indicates that the zeolite NH_4^+-ZSM-5 with the highest Si/Al ratio has the minimum weak acidic sites. In contrast, zeolite-Y, with the minimum Si/Al ratio, has the maximum number of weak acidic sites.[56] It is quite apparent from Figure 4.9 that for Al-MCM-41, strong acidic sites are relatively more in number. It can be attributed to the presence of a greater number of surface hydroxyl groups compared to zeolites. Hence it is evident that Si/Al ratio certainly has a significant impact on the acid strength of the catalysts, which in turn affects their catalytic activity.[49] It is a known fact that upon calcination of zeolite-Y, the Brønsted acidity decreases, and there is a formation of Lewis acidic sites.[57-59] From Table 4.6, it is quite apparent that there is an increase in the weak acidic sites in calcined zeolite Na-Y while the strong acidic sites have decreased.

Table 4.6: Acidic sites of the catalysts

Catalyst	**Acid sites (mmol/g)**			**Si/Al Ratio**
	Weak acid Sites (peak I)		**Strong Acid site (peak II)**	
Zeolite NH_4^+-ZSM-5	0.071	0.044	0.061	175
Al-MCM-41	0.197		0.331	19.55
Zeolite Na-Y	0.892		0.084	2.79
Calcined zeolite Na-Y	0.967		0.004	3.00

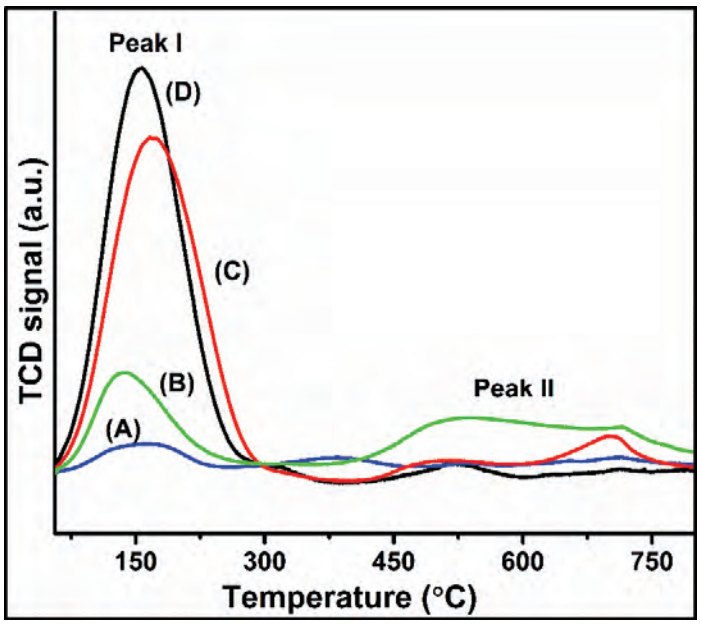

Figure 4.9: NH_3-TPD profiles of **(A)** Zeolite NH_4^+-ZSM-5 **(B)** Al-MCM-41 **(C)** Zeolite Na-Y **(D)** Calcined zeolite Na-Y.

4.2.10 Catalytic Studies and discussion

The commercially available zeolites, zeolite Na-Y and zeolite NH_4^+-ZSM-5, calcined zeolite Na-Y, and the prepared Al-MCM-41 have been tested as catalysts for the cycloaddition reaction of CO_2 and styrene oxide to investigate the role of Si/Al ratio. The characterization details of calcined zeolite Na-Y are provided in Figure 4.10 and Table 4.7. The Si/Al ratio of the calcined sample using EDX and XPS was found to be 3.00 and 4.25, respectively. According to our experimental findings, the maximum yield is for zeolite Na-Y followed by Al-MCM-41 and calcined zeolite Na-Y. Zeolite NH_4^+-ZSM-5 gives the least yield (presented in Table 4.8).

Table 4.7: Physicochemical properties of calcined zeolite Na-Y

Sample	Si/Al (EDX)	Si/Al (XPS)	TGA weight loss (%)	IR peaks (cm^{-1})
Calcined zeolite Na-Y	3.00	4.25	17.053%	3478, 1646, 1039, 789, 722, 578

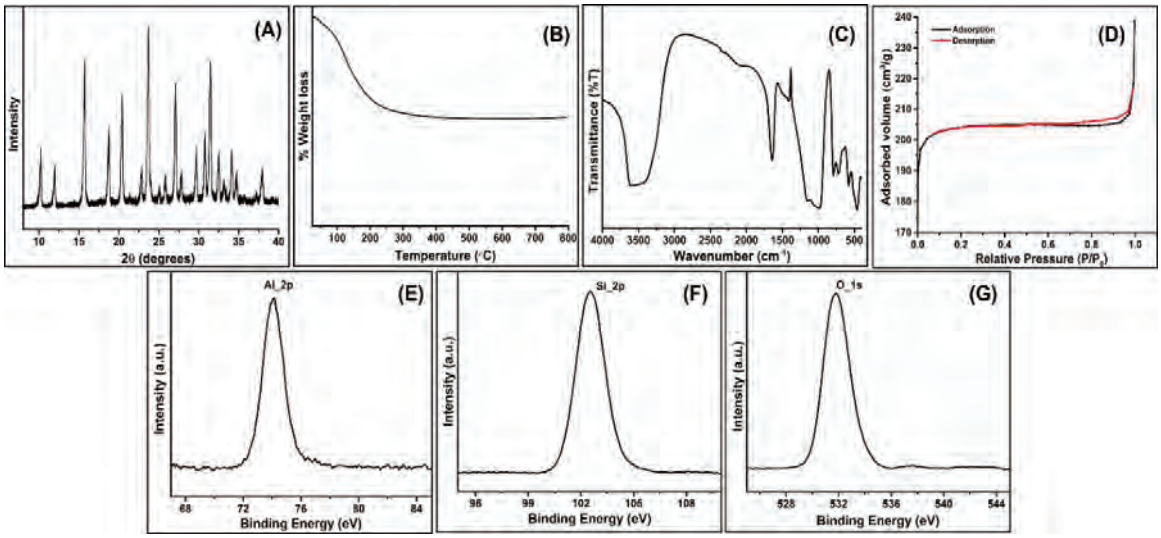

Figure 4.10: Physicochemical properties of calcined zeolite Na-Y showing **(A)** XRD, **(B)** TGA, **(C)** FT-IR, **(D)** BET, **(E)** XPS of Al (2p), **(F)** XPS of Si (2p), and **(G)** XPS of O (1s).

As discussed in section 1.1.2, the mechanism of the reaction is well established in the literature. In the present study, the cycloaddition reaction follows the epoxide activation pathway, (shown in figure 1.3) wherein a Lewis or Brønsted acid is required to activate the epoxide, followed by the ring-opening assisted by a co-catalyst, which is generally a nucleophile.[60, 61] Therefore, higher acidic sites make the reaction more feasible. This is followed by the insertion of CO_2, and finally, the product is formed. It is also proven in the literature that the ring-opening step is the rate-determining step in most cases.[62-64] In 2018, Zhao *et al.* [13] have shown a 57% yield using H-ZSM-5 and tetrabutylammonium bromide (TBAB) as a catalyst system for the conversion of propylene oxide to propylene carbonate at a temperature of 120 °C, pressure of 1 MPa and 8 hours reaction time with 50 mg of the catalyst. Herein, we report a very similar finding of the yield of styrene carbonate (55.3% using zeolite NH_4^+-ZSM-5 and TBAB), though at a lower pressure (4 bar) and with a lower reaction time (2 hours) and with a lesser amount (25 mg) of catalyst. More fascinating observation is with zeolite Na-Y; its higher acidic sites lead to the improved yield of styrene carbonate as 75.4% in the presence of TBAB.

According to the recent report by Wu *et al.,* [20] the hydroxy functional group of the salophen ligand acts very efficiently as a Brønsted acid, with one of the hydroxyl groups activating the epoxide while the second hydroxy group activating the CO_2. In the present study, the surface hydroxyl groups of the zeolites are the source of Brønsted acidity, and the aluminium present as the extra-framework aluminium is the source of Lewis acidity for the cycloaddition reaction. In

2006, Srinivas *et al.*[15] reported the conversion of CO_2 and epoxides to polycarbonates using MCM-41. They reported a conversion of 93.7% for styrene oxide under solvent-free reaction conditions of 6.9 bar pressure, 8 h of reaction time, and a temperature of 100 °C. With our catalyst, Al-MCM-41, we are getting a comparatively lesser yield of 68%, which could be due to the reaction conditions which utilizes lesser time and pressure (2 hours and 4 bar, respectively). Our observation of correlating the Si/Al ratio of the hosts with the obtained yield of carbonates has the support of literature by Duan *et al.*[10] According to their study, commercial beta-zeolites N-660 with higher Si/Al ratio could produce cyclic carbonates from epoxides and CO_2, while beta-zeolite with lower Si/Al ratio gave homopolymers, polyether, and polyols in the absence of CO_2. Hence, only a few reports in the literature show the conversion of CO_2 to carbonates utilizing the Brønsted and Lewis acidity of the zeolites. In the present study, the catalysts we have used, *i.e.*, the two commercially available zeolites and the synthesized Al-MCM-41 show comparative yields as reported in the literature (Optimization shown in Table 4.9 and yields shown in Table 4.8).

Table 4.8: Catalytic table for conversion of styrene oxide to styrene carbonate

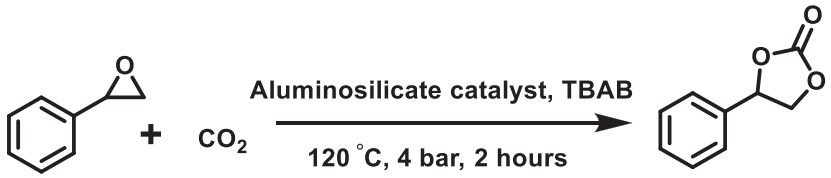

Catalyst	Yield (%)
Zeolite NH_4^+-ZSM	55.3
Al-MCM-41	68
Zeolite Na-Y	75.4
Calcined Zeolite Na-Y	57.8

Reaction conditions: Styrene Oxide: (10 mmol, 1.13 mL), TBAB: (0.05 mmol, 16.1 mg), Catalyst: 25 mg, Temperature: 120 °C, Pressure: 4 bar, Time: 2 hours

Table 4.9: Optimization of amount of catalyst using zeolite Na-Y

Catalyst	Amount (mg)	Yield (%)
Zeolite Na-Y	12.5	64
Zeolite Na-Y	**25**	**75.4**
Zeolite Na-Y	50	51.8
Zeolite Na-Y	100	65.3

Reaction conditions: Styrene Oxide: (10 mmol, 1.13 mL), TBAB: (0.05 mmol, 16.1 mg), Temperature: 120 °C, Pressure: 4 bar, Time: 2 hours

Apart from styrene oxide, we have tested the most successful catalyst i.e., zeolite Na-Y, for the conversion of other epoxides. The yield calculated from NMR (tabulated in Table 4.10) shows that the catalyst performs equally good with other substrates like electron withdrawing epichlorohydrin and electron donating propylene oxide.

Table 4.10: Substrate scope for the formation of cyclic carbonate using zeolite Na-Y

Substrate	NMR conversion (%)
Styrene Oxide	81
Epichlorohydrin	83
Propylene Oxide	76*

***Carried out the reaction at 30 °C owing to the low boiling point of propylene oxide**

Table 4.11: Comparison of yield, conversion, and selectivity

Catalyst	Yield (Y)* (%)	Conversion (C)* (%)	Selectivity (=Y/C) (%)
Zeolite Na-Y	75.4	91.0	82.75
Al-MCM-41	68.0	88.3	76.9
Zeolite NH_4^+ ZSM-5	55.3	91.6	60.3
Calcined zeolite Na-Y	57.8	79.8	72.4

***Both the yield and the conversion have been calculated by using calibration curve using GC**

It is also a well-known fact that in the presence of water, epoxide undergoes ring opening to form a diol.[65, 66] Since zeolites are very prone to absorb water molecules, it is possible that in this reaction, the styrene oxide has formed styrene glycol as the minor product. The mass spectra and the NMR spectra of the crude also support the formation of the diol [67] (Figure 4.11 and Figure 4.12).

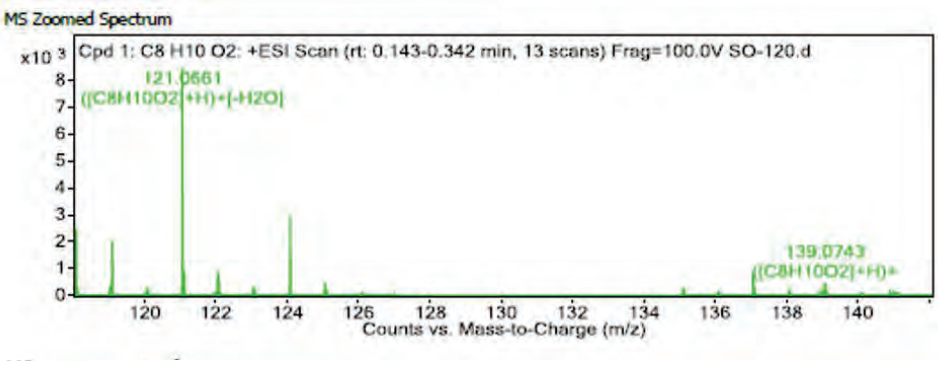

Figure 4.11: HR-MS spectra of the crude reaction mixture.

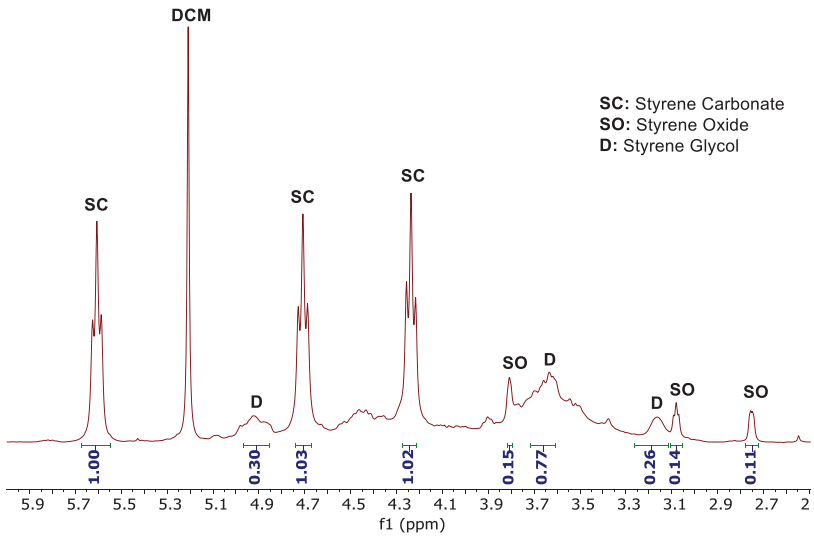

Figure 4.12: ^{1}H NMR spectra of the crude reaction mixture.

The aluminosilicate catalysts are superior in the sense that even with the inherent water molecules, the selectivity for carbonate product with the best-performing catalyst, i.e., zeolite-Na-Y, is 83%. Apart from the diol, the other side product might include the formation of polycarbonate.[68]

We can draw some parallels between the acidity obtained from TPD and the yield of the product obtained. The order of the yields of the cyclic carbonate formed is in accordance with the number of available weak acidic sites of the catalysts. The activities of zeolite Na-Y and zeolite NH_4^+-ZSM-5 differ significantly despite the number of strong acidic sites being comparable (0.061 and 0.084 mmol/g for zeolite NH_4^+-ZSM-5 and zeolite Na-Y, respectively). Furthermore, Al-MCM-41, with a substantially higher number of strong acidic sites, shows lesser activity as compared to

zeolite-Na-Y. Reduced activity of mesoporous Al-MCM-41 may be due to the presence of lesser weak acidic sites and larger pores in it (shown in Table 4.4).[69]

The calcination of zeolite Na-Y has enhanced the number of weak acidic sites at the expense of strong acidic sites, and it yields strong acid sites 15 times lower than that of zeolite NH_4^+-ZSM-5. This, possibly, is a reason that the yield obtained by the calcined zeolite Na-Y is comparable to that of the least active catalyst, i.e., zeolite NH_4^+-ZSM-5. This observation indicates that along with the weak acidic sites, strong acidic sites may play a role in catalysis. The decrease in the yield of the product in the case of calcined zeolite-Y compared to zeolite Na-Y is again indicative of the fact that along with weak acidic sites, the strong acid sites of zeolite Na-Y is responsible for the activity of the catalyst, as the weak acid sites are almost equal for both zeolite Na-Y and calcined zeolite Na-Y. It could be perceived that in all the above cases, it is the weak acidic sites that are dominant, but strong acid sites also have a contribution which cannot be neglected in the product formation. Furthermore, the introduction of metals like cobalt, zinc, copper, palladium, etc., in zeolite Na-Y would render the acidic sites along with the inherent aluminium, thus enabling it to show better catalytic activity.[13]

The best-performing catalyst, i.e., has been tested for recycling studies (Figure 4.13) and shows minimum loss of activity till three cycles.

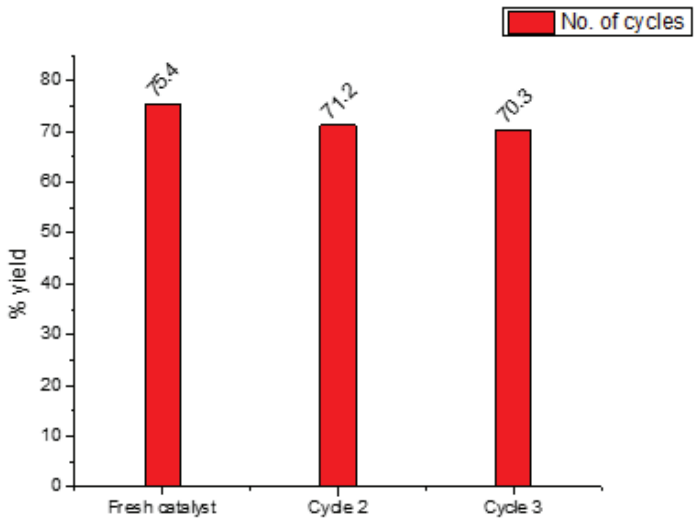

Figure 4.13: Recycle studies using zeolite-Na-Y.

4.3 Conclusions

Acidity plays a vital role in the formation of cyclic carbonates from epoxides and CO_2. We have shown in the present study that synthesized Al-MCM-41 and commercially available zeolites, without any post-modification, are able to convert the styrene oxide to styrene carbonate with the use of TBAB as a co-catalyst. The yields obtained are comparable to those reported in the literature with lesser reaction time, and the conditions used are milder. The activity of the catalysts is governed by their Si/Al ratio. The decrease in reactivity using calcined zeolite-Y, as compared to zeolite-Y, is indicative that not only Lewis acidity, but also, Brønsted acidity plays a vital role in the conversion of CO_2 and epoxides to its corresponding carbonates. The cycloaddition reaction has been used as a tool to systematically study the acidity difference of the utilized catalysts. The present literature majorly focuses on functionalization or the post-modification to make the catalyst acidic. We have explored the acidity of commercially available zeolites without any post-modification and utilized them for the cycloaddition reaction. The primary emphasis is to access the acidity of the catalysts and not to stand in line with the state-of-the-art materials. Although only good to medium yields have been reported, the parallels drawn between the acidity and the yield point out the fact that the acidity of zeolite itself plays a significant role in the cycloaddition reaction.

4.4 References

1. D. Prasad, K. N. Patil, N. K. Chaudhari, H. Kim, B. M. Nagaraja and A. H. Jadhav, *Catalysis Reviews: Science and Engineering*, 2022, **64**, 356.
2. Q. He, J. W. O'Brien, K. A. Kitselman, L. E. Tompkins, G. C. T. Curtis and F. M. Kerton, *Catalysis Science & Technology*, 2014, **4**, 1513.
3. H. Büttner, L. Longwitz, J. Steinbauer, C. Wulf and T. Werner, in *Chemical Transformations of Carbon Dioxide*, eds. X.-F. Wu and M. Beller, Springer International Publishing, Cham, 2018, pp. 89.
4. T. K. Pal, D. De and P. K. Bharadwaj, *Coordination Chemistry Reviews*, 2020, **408**, 213173.
5. V. B. Saptal and B. M. Bhanage, *Current Opinion in Green and Sustainable Chemistry*, 2017, **3**, 1.
6. L. Guo, K. J. Lamb and M. North, *Green Chemistry*, 2021, **23**, 77.
7. L. Muniandy, F. Adam, N. R. A. Rahman and E.-P. Ng, *Inorganic Chemistry Communications*, 2019, **104**, 1.
8. J. N. Appaturi and F. Adam, *Applied Catalysis B: Environmental*, 2013, **136-137**, 150.
9. M. Tu and R. J. Davis, *Journal of Catalysis*, 2001, **199**, 85.
10. R. Duan, C. Hu, Y. Zhou, Y. Huang, Z. Sun, H. Zhang and X. Pang, *Industrial & Engineering Chemistry Research*, 2021, **60**, 1210.
11. L. P. Ozorio, F. J. S. Henrique, J. W. Comerford, M. North and C. J. A. Mota, *Reaction Chemistry & Engineering*, 2021, **6**, 672.
12. B. Sarmah, B. Satpati and R. Srivastava, *Journal of Colloid and Interface Science*, 2017, **493**, 307.
13. Q.-N. Zhao, Q.-W. Song, P. Liu, Q.-X. Zhang, J.-H. Gao and K. Zhang, *Chinese Journal of Chemistry*, 2018, **36**, 187.
14. W. Liu, T. Xu, C. Li and J. Bai, *Inorganic and Nano-Metal Chemistry*, 2020, **50**, 1087.
15. R. Srivastava, D. Srinivas and P. Ratnasamy, *Tetrahedron Letters*, 2006, **47**, 4213.
16. L. Zhou, G. Cai, L. Zhang, Y. Luo, Z. He and W. Eli, *Synthesis and Reactivity in Inorganic, Metal-Organic, and Nano-Metal Chemistry*, 2014, **44**, 1545.
17. B. Chatelet, L. Joucla, J.-P. Dutasta, A. Martinez and V. Dufaud, *Journal of Materials Chemistry A*, 2014, **2**, 14164.

18. S. Ravi, R. Roshan, J. Tharun, A. C. Kathalikkattil and D. W. Park, *Journal of CO_2 Utilization*, 2015, **10**, 88.
19. S. Zhong, L. Liang, M. Liu, B. Liu and J. Sun, *Journal of CO_2 Utilization*, 2015, **9**, 58.
20. X. Wu, C. Chen, Z. Guo, M. North and A. C. Whitwood, *ACS Catalysis*, 2019, **9**, 1895.
21. B. Bonelli, B. Civalleri, B. Fubini, P. Ugliengo, C. O. Areán and E. Garrone, *The Journal of Physical Chemistry B*, 2000, **104**, 10978.
22. S. Loganathan, M. Tikmani and A. K. Ghoshal, *Langmuir*, 2013, **29**, 3491.
23. M. Sai Bhargava Reddy, D. Ponnamma, K. K. Sadasivuni, B. Kumar and A. M. Abdullah, *RSC Advances*, 2021, **11**, 12658.
24. S. Kumari, A. Choudhary and S. Ray, *Applied Organometallic Chemistry*, 2019, **33**, e4765.
25. W. Widayat and A. N. Annisa, *IOP Conference Series: Materials Science and Engineering*, 2017, **214**, 012032.
26. X. Wang, H. Wang, X. Jin, W. Kong, B. Shen and J. Yang, *Biomass Conversion and Biorefinery*, 2023, 1.
27. A. Choudhary, B. Das and S. Ray, *Dalton Transactions*, 2015, **44**, 3753.
28. S. Narayanan, J. J. Vijaya, S. Sivasanker, L. J. Kennedy and S. K. Jesudoss, *Powder Technology*, 2015, **274**, 338.
29. R. Sabarish and G. Unnikrishnan, *Journal of Porous Materials*, 2020, **27**, 691.
30. B. R. Jermy and A. Pandurangan, *Applied Catalysis A: General*, 2005, **288**, 25.
31. A. Palani, N. Gokulakrishnan, M. Palanichamy and A. Pandurangan, *Applied Catalysis A: General*, 2006, **304**, 152.
32. A. F. Hassan, S. A. Helmy and A. Donia, *Journal of the Brazilian Chemical Society*, 2015, **26**, 1367.
33. W. E. Rashwan, K. S. Abou-El-Sherbini, M. A. Wahba, S. A. Sayed Ahmed and P. G. Weidler, *Silicon*, 2020, **12**, 2017.
34. A. Mobinikhaledi, M. Zendehdel, S. M.-B. Hosseini-Ghazvini and P. Safari, *Transition Metal Chemistry*, 2015, **40**, 313.
35. E. Lippmaa, M. Maegi, A. Samoson, M. Tarmak and G. Engelhardt, *Journal of the American Chemical Society*, 1981, **103**, 4992.
36. J. Klinowski, S. Ramdas, J. M. Thomas, C. A. Fyfe and J. S. Hartman, *Journal of the Chemical Society, Faraday Transactions 2: Molecular and Chemical Physics*, 1982, **78**, 1025.

37. R. Deka, *Indian Journal of Chemical Technology*, 1998, **5**, 109.
38. A. G. Stepanov, in *Zeolites and Zeolite-Like Materials*, eds. B. F. Sels and L. M. Kustov, Elsevier, Amsterdam, 2016, pp. 137.
39. M. Müller, G. Harvey and R. Prins, *Microporous and Mesoporous Materials*, 2000, **34**, 281.
40. M. Huang, A. Adnot and S. Kaliaguine, *Journal of the American Chemical Society*, 1992, **114**, 10005.
41. M. Ojeda, N. Osterman, G. Dražić, L. Fele Žilnik, A. Meden, W. Kwapinski, A. M. Balu, B. Likozar and N. Novak Tušar, *Topics in Catalysis*, 2018, **61**, 1757.
42. A. Sterczyńska, A. Deryło-Marczewska, M. Zienkiewicz-Strzałka, M. Śliwińska-Bartkowiak and K. Domin, *Langmuir*, 2017, **33**, 11203.
43. H. Dong, M. Wei, J. Li, J. Fang, L. Gao, X. Li and A. Xu, *RSC Advances*, 2016, **6**, 70747.
44. J. C. Bedoya, R. Valdez, L. Cota, M. A. Alvarez-Amparán and A. Olivas, *Catalysis Today*, 2022, **388-389**, 55.
45. Y. Wang, W. Ma, B. A. Yoza, Y. Xu, Q. X. Li, C. Chen, Q. Wang, Y. Gao, S. Guo and Y. Zhan, *Journal*, 2018, **8**, 128.
46. A. Jankowska, A. Chłopek, A. Kowalczyk, M. Rutkowska, M. Michalik, S. Liu and L. Chmielarz, *Molecules*, 2020, **25**, 5651.
47. N.-Y. Topsøe, K. Pedersen and E. G. Derouane, *Journal of Catalysis*, 1981, **70**, 41.
48. J. Ahmadpour and M. Taghizadeh, *Comptes Rendus Chimie*, 2015, **18**, 834.
49. H. Kosslick, G. Lischke, B. Parlitz, W. Storek and R. Fricke, *Applied Catalysis A: General*, 1999, **184**, 49.
50. Z. Wang and S. Yu, *Advances in Chemical Engineering and Science*, 2016, **6**, 305.
51. S. Liu, L. Li, C. Li, X. Xiong and F.-S. Xiao, *Journal of Porous Materials*, 2008, **15**, 295.
52. H. Miessner, H. Kosslick, U. Lohse, B. Parlitz and V. A. Tuan, *The Journal of Physical Chemistry*, 1993, **97**, 9741.
53. M. Niwa and N. Katada, *The Chemical Record*, 2013, **13**, 432.
54. Y. Sang, H. Li, M. Zhu, K. Ma, Q. Jiao and Q. Wu, *Journal of Porous Materials*, 2013, **20**, 1509.
55. M. Ravi, V. L. Sushkevich and J. A. van Bokhoven, *Nature Materials*, 2020, **19**, 1047.
56. Z. Zhang, D. Liu, X. Zhu, H. Yu, S. Liu and L. Xu, *Journal of Natural Gas Chemistry*, 2008, **17**, 45.

57. M. Ravi, V. L. Sushkevich and J. A. van Bokhoven, *Chemical Science*, 2021, **12**, 4094.
58. J. W. Ward, *Journal of Catalysis*, 1968, **11**, 251.
59. B. Xu, F. Rotunno, S. Bordiga, R. Prins and J. A. van Bokhoven, *Journal of Catalysis*, 2006, **241**, 66.
60. X.-B. Lu and D. J. Darensbourg, *Chemical Society Reviews*, 2012, **41**, 1462.
61. F. Della Monica and A. W. Kleij, *Catalysis Science & Technology*, 2020, **10**, 3483.
62. M. Liu, K. Gao, L. Liang, J. Sun, L. Sheng and M. Arai, *Catalysis Science & Technology*, 2016, **6**, 6406.
63. M. Zhang, B. Chu, G. Li, J. Xiao, H. Zhang, Y. Peng, B. Li, P. Xie, M. Fan and L. Dong, *Microporous and Mesoporous Materials*, 2019, **274**, 363.
64. H. Büttner, L. Longwitz, J. Steinbauer, C. Wulf and T. Werner, *Topics in Current Chemistry*, 2017, **375**, 50.
65. Z. Wang, Y.-T. Cui, Z.-B. Xu and J. Qu, *The Journal of Organic Chemistry*, 2008, **73**, 2270.
66. W. Natongchai, J. A. Luque-Urrutia, C. Phungpanya, M. Solà, V. D'Elia, A. Poater and H. Zipse, *Organic Chemistry Frontiers*, 2021, **8**, 613.
67. H. Vignesh Babu and K. Muralidharan, *Dalton Transactions*, 2013, **42**, 1238.
68. P. P. Pescarmona, *Current Opinion in Green and Sustainable Chemistry*, 2021, **29**, 100457.
69. S. Kumar, R. Srivastava and J. Koh, *Journal of CO_2 Utilization*, 2020, **41**, 101251.

Chapter 5

Zeolite-Y encapsulated Zinc(II) Schiff-base complexes for upcycling CO_2

Abstract: *The presence of salophen complexes as dimers largely affects their lifetime and stability and thus can lead to decrease in the catalytic activity. Encapsulation prevents dimerization and leads to site isolation, hence improves the activity. These hybrid systems showcase the properties of their host, like nanocavity size, electrostatic potential, along with the electronic and stereochemical properties of the guest complex. In the present chapter, Zn(II)salophen complexes prepared in chapter 3 are encapsulated in the supercage of zeolite. The red shift in solid UV studies compared to "neat" complexes and the shift of Zn (2p) peak towards higher energy in XPS studies point towards the change in the electronic environment around the metal center. The Lewis acidity of the zinc metal in the complex along with the inherent acidity of the zeolite-Y and encapsulation driven structural modification of the metal complex lead to increased activity of the Zn(II) salophen encapsulated complexes for the synthesis of cyclic carbonates from CO_2. ZnL1-Y shows the best activity with an overall TOF of 150 h^{-1}, while the TOF of only the complex in ZnL1-Y is 96 h^{-1}, as compared to TOF of only 13.8 h^{-1} for "neat" ZnL1. The best performing monomeric ZnL4 gave a TOF of 16 h^{-1}, while the encapsulated ZnL4 complex in ZnL4-Y showed 3.2 times increase in the TOF with value of 52 h^{-1}.*

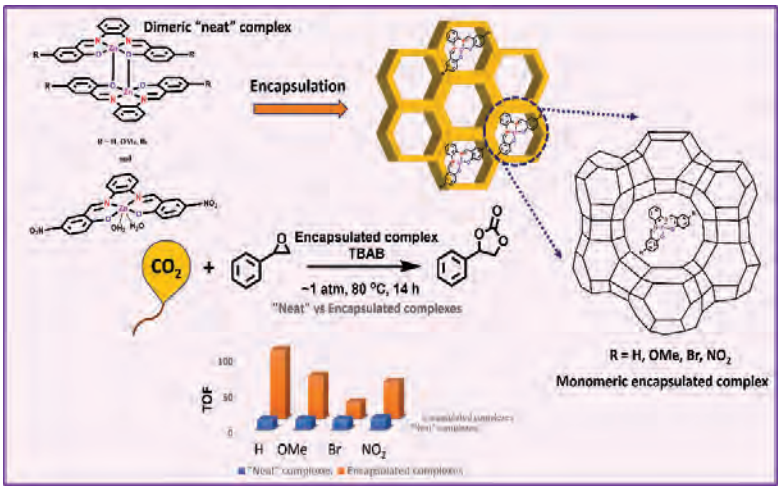

5.1 Introduction

Hitherto, the primary focus of this thesis has been the upcycling of CO_2 to cyclic carbonates utilizing environmentally benign reaction conditions and avoiding an elaborate synthetic methodology. Towards that direction, homogeneous zinc(II) salophen complexes and various commercially available heterogeneous catalysts including zeolite Na-Y, ZSM-5 and MCM-41 have been successfully attempted. The current chapter aims to unify both the above said catalytic approaches, with the objective of further improving the catalytic activity. The technique known as encapsulation is a well-known method of heterogenization of a homogeneous catalyst, simultaneously retaining the catalytic activity of the guest molecule. As already discussed in detail in the previous chapters, a plethora of homogeneous and heterogeneous catalysts have been reported for the conversion of epoxide to cyclic carbonates.[1-6] However, there are scarcely any reports using encapsulated complexes.[7-9] These reports utilize rather difficult-to-synthesize complexes such as porphyrin and phthalocyanine encapsulated in ZIF and zeolite-Y respectively. The utilization of simple N_2O_2 coordinating Schiff base complexes entrapped in zeolite-Y has been reported for various catalytic reactions.[10, 11] With the inspiration from these studies, this chapter aims to utilize the zeolite-Y encapsulated Zn(II) Schiff base complexes for the conversion of epoxide to cyclic carbonate.

The present chapter deals with the encapsulation of the zinc(II) complexes, ZnL1, ZnL2, ZnL3 and ZnL4 discussed in Chapter 3. The encapsulated heterogeneous catalysts, ZnL1-Y, ZnL2-Y, ZnL3-Y and ZnL4-Y have been synthesized using the flexible ligand method (shown in Figure 5.1). It is already discussed in Chapter 3 that most of the chosen homogeneous Zn(II) complexes exist as dimers. Hence, apart from the obvious advantage of heterogenization, encapsulation also induces site isolation, which can be further advantageous from a catalysis point of view. Additionally, the encapsulation leads to structural modifications which may impart improved catalytic activity to the encapsulated complexes towards the cycloaddition reaction of epoxide and CO_2.

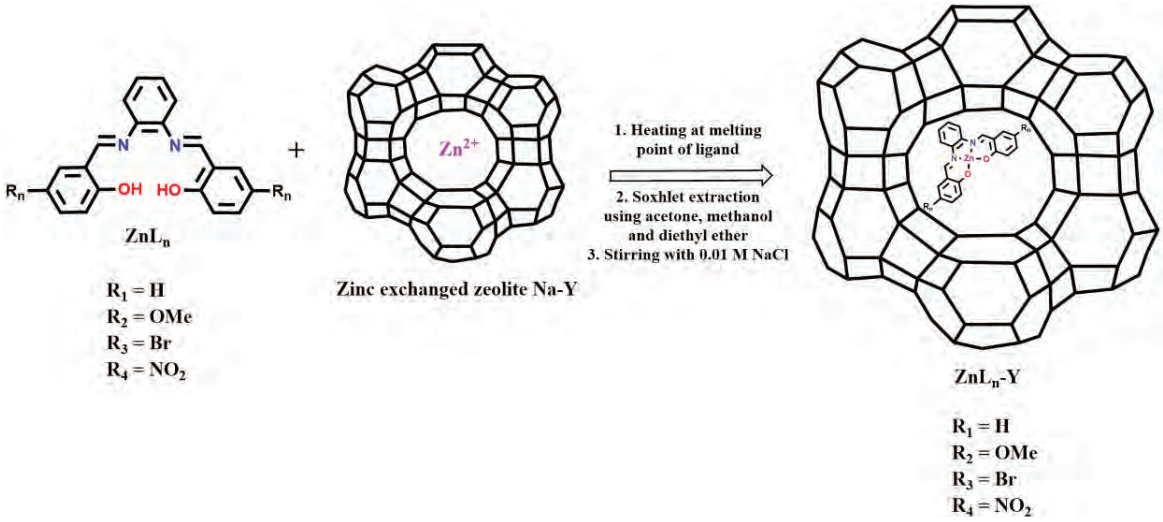

Figure 5.1: Synthesis of zinc encapsulated complexes using flexible ligand approach.

5.2 Results and Discussions

5.2.1 Elemental Analysis

The amount of zinc metal present in the zinc exchange zeolite-Y and the prepared zinc(II) encapsulated complexes was discerned using Energy Dispersive X-ray (EDX) spectroscopy and Atomic Absorption Spectroscopy (AAS). The results presented in Table 5.1 clearly indicate that the encapsulation process does not lead to the dealumination in the parent zeolite, which is reflected in the comparable Si/Al ratio of all the encapsulated complexes. This observation ensures zeolite-Y sustains with the process of encapsulation. The decrease in the metal content of the encapsulated complexes compared to zinc exchange zeolite-Y indirectly suggests the formation of the complex inside the supercage of the zeolite-Y.[12] The decrease in the weight percentage of the elements after Soxhlet extraction (shown in Table 5.2) is also indicative of the removal of the surface impurities.

Table 5.1: Concentration of zinc in the prepared complexes						
Complex	**Zinc (wt%)**		**Na (wt%) (from EDX)**	**Si (wt%) (from EDX)**	**Al (wt%) (from EDX)**	**Si/Al ratio (from EDX)**
	From EDX	**From AAS**				
Na-Y	-	-	8.12	30.16	10.76	2.79
Zn-Y	1.56	0.95	9.84	34.31	11.99	2.86
ZnL1-Y	0.44	0.48	4.29	11.36	4.57	2.48
ZnL2-Y	0.66	0.56	3.53	15.04	5.28	2.84
ZnL3-Y	0.53	0.65	3.35	16.16	4.67	3.46
ZnL4-Y	0.40	0.57	4.56	11.27	4.64	2.42

Table 5.2: Comparison of the elemental composition of ZnL2-Y before and after Soxhlet		
Element	**EDX data before Soxhlet (wt%)**	**EDX data after Soxhlet (wt%)**
C	32.85	40.82
N	2.69	1.75
O	33.66	32.90
Na	4.39	3.53
Al	6.41	5.28
Si	18.96	15.04
Zn	1.02	0.66
Si/Al	2.95	2.84

5.2.2 Powder X-ray Diffraction (PXRD) studies

The PXRD analysis was carried out to perceive changes occurring in the framework structure of zeolite-Y and the prepared complexes upon encapsulation. The XRD peaks shown in Figure 5.2 exhibit a similar pattern for the parent zeolite-Y and the encapsulated complexes, indicating the retention of the crystallinity and the integrity of the host framework. In addition, the apparent change in the diffraction intensities I_{220} and I_{311} at planes (220) and (311) appearing at 2θ value 10° and 12° respectively, indicate the successful encapsulation of the complex. The intensities of the

peaks diffracted from these planes hold the relation $I_{220} > I_{311}$ for pure zeolite-Y which reverses upon encapsulation. This observation is empirically correlated with the presence of a large molecule within the zeolite supercage.[13, 14] Such observation is generally absent if the complex is of relatively smaller dimension or formation of the complex taking place on the surface of the host zeolite.[15] The reversal in the intensities is reported as a result of the redistribution of the non-coordinated free cations due to presence of a large complex inside the zeolite.[13] The XRD pattern obtained is well supported by the JCPDS data. All the peaks obtained in XRD correspond perfectly with the JCPDS data except the peak obtained at 32°, which is missing in the simulated data. However, there is strong evidence from the literature indicating the presence of a prominent peak at 32° in the XRD pattern of zeolite-Y, which is exactly in line with our observations.[16, 17]

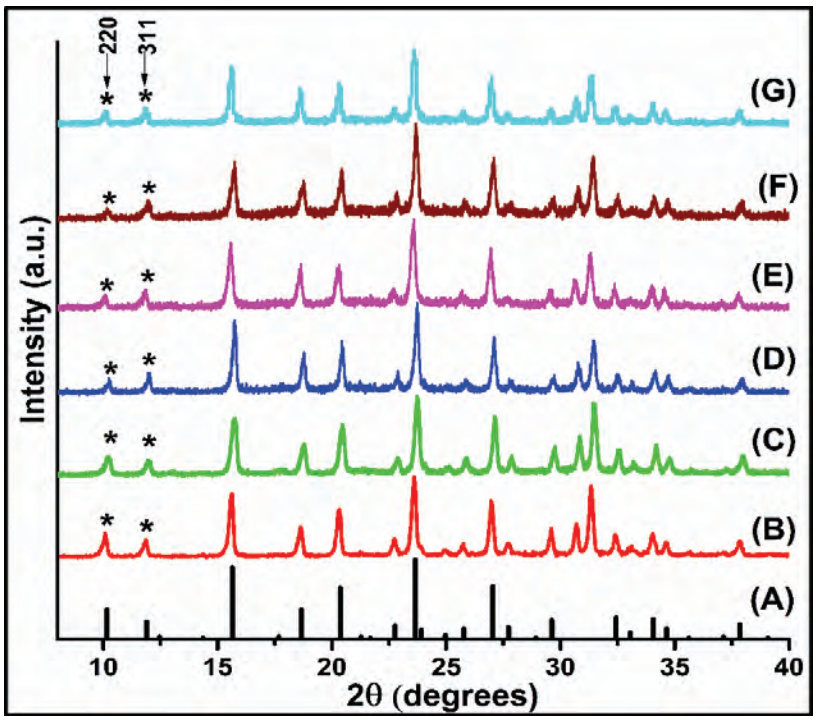

Figure 5.2: Powder XRD patterns of **(A)** JCPDS reference pattern of zeolite-Y (JCPDS card number 00-043-0168, **(B)** Zeolite Na-Y, **(C)** Zinc(II) exchanged-Y, **(D)** ZnL1-Y, **(E)** ZnL2-Y, **(F)** ZnL3-Y, **(G)** ZnL4-Y.

5.2.3 Field Emission Scanning Electron Microscopy (FESEM) analysis

The morphology of the surface of the prepared encapsulated complexes was studied using field emission scanning electron microscopy (FESEM). During the solid-state reaction for the preparation of the encapsulated complex, it is obvious that some of the ligand will remain free and

endure on the surface as an impurity. It is imperative to remove these surface impurities from the complex which is done using Soxhlet extraction. The FESEM images in Figures 5.3 and 5.4 show the encapsulated complex before (i) and after (ii) washing with various solvents. The presence of impurities is clearly visible in the sample before extraction while after Soxhlet extraction, the clear boundaries of the host particles indicate that the surface impurities are removed.[18]

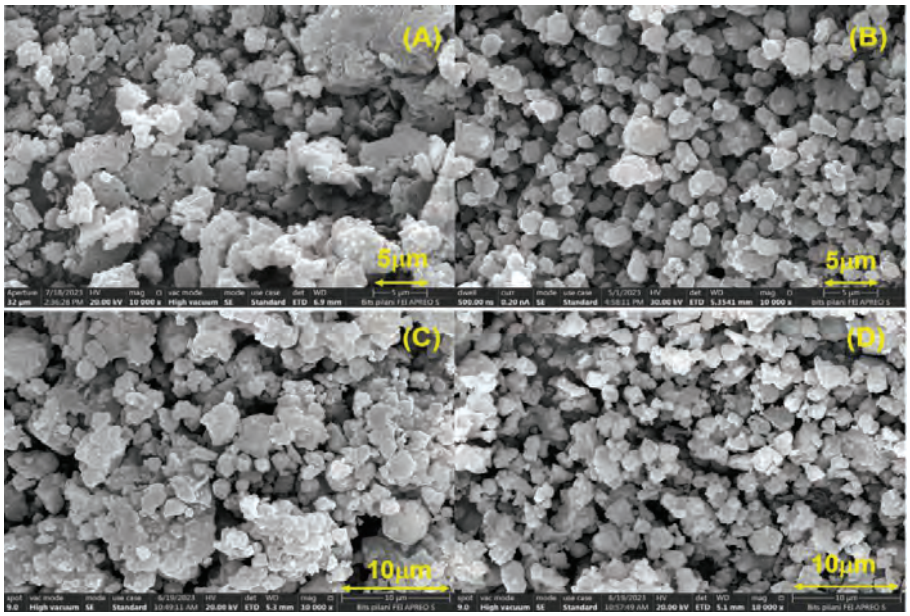

Figure 5.3: FESEM images of **(A)** ZnL1-Y before Soxhlet extraction, **(B)** ZnL1-Y after Soxhlet extraction, **(C)** ZnL2-Y before Soxhlet extraction, **(D)** ZnL2-Y after Soxhlet extraction.

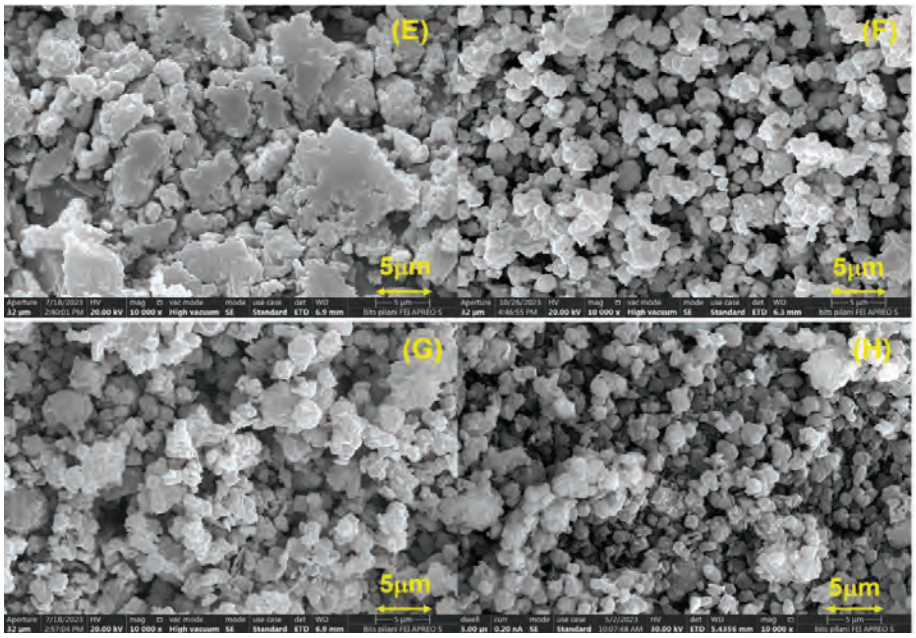

Figure 5.4: FESEM images of **(E)** ZnL3-Y before Soxhlet extraction, **(F)** ZnL3-Y after Soxhlet extraction **(G)** ZnL4-Y before Soxhlet extraction, **(H)** ZnL4-Y after Soxhlet extraction.

5.2.4 Fourier Transform Infrared (FT-IR) spectroscopy Study

The FT-IR spectroscopy was performed to assert the encapsulation of the zinc complex inside the zeolite supercage. The FT-IR spectral data of pure zeolite-Y and encapsulated zinc(II) Schiff base complexes are presented in Figure 5.5 and the values tabulated in Table 5.3. From the FT-IR spectra, we can clearly see the dominance of the characteristic IR bands of zeolite-Y below 1200 cm^{-1}. The prominent peaks arising due to the surface hydroxylic groups and lattice water molecules inherently present in the zeolite appear at 3510 cm^{-1} and 1640 cm^{-1} respectively. The strong peak in the region 1013 cm^{-1} is attributed to the asymmetric stretching vibrations of $(Si/Al)O_4$ units of zeolite framework. Other characteristics bands at 575 cm^{-1}, 718 cm^{-1}, and 788 cm^{-1} are attributed to T−O bending mode, double ring, and symmetric stretching vibrations respectively.[19] The nature and peak positions of the IR bands remain unaltered during the encapsulation process. The characteristic FT-IR bands of zeolite framework remaining invariable during metal exchange reaction and encapsulation process implies that the zeolite framework maintains its integrity upon encapsulation of zinc(II) Schiff-base complexes. However, there is a noticeable difference in the spectral range of 1200−1600 cm^{-1} for the encapsulated complexes where zeolite remains silent. Therefore, all the low-intensity peaks observed in this region are the characteristic vibrations of the guest complex and are typically identified as C=N, C=C and C-O vibrations. The IR peaks of encapsulated zinc(II) Schiff base complex are very weak in intensity due to their low loading level in the zeolite supercage.

We have already discussed the IR peaks of the "neat" complexes in Chapter 3. The characteristic bands of C=N and C-O stretching vibrations for the "neat" complexes appear in the range of 1604-1618 cm^{-1} and 1306-1321 cm^{-1} respectively, for the complexes ZnL1-ZnL4. The bands around 1530 cm^{-1} and 1470 cm^{-1} in the "neat" complexes are assigned to C=C stretching mode while the peak at 1376-1397 cm^{-1} is attributed to ν_{C-H} deformation. The low intensities of the peaks are also indicative of the absence of metal complex on the zeolite-Y surface. The presence of similar FT-IR vibrational bands in the "neat" and encapsulated complexes gives indirect evidence for the presence of a zinc(II) Schiff-base complex inside the super cage of zeolite-Y.[20] The slight shifting in the IR peak positions can be attributed to the effect of the topology of the zeolite framework on the geometry of the zinc complexes entrapped in the zeolite cavities.

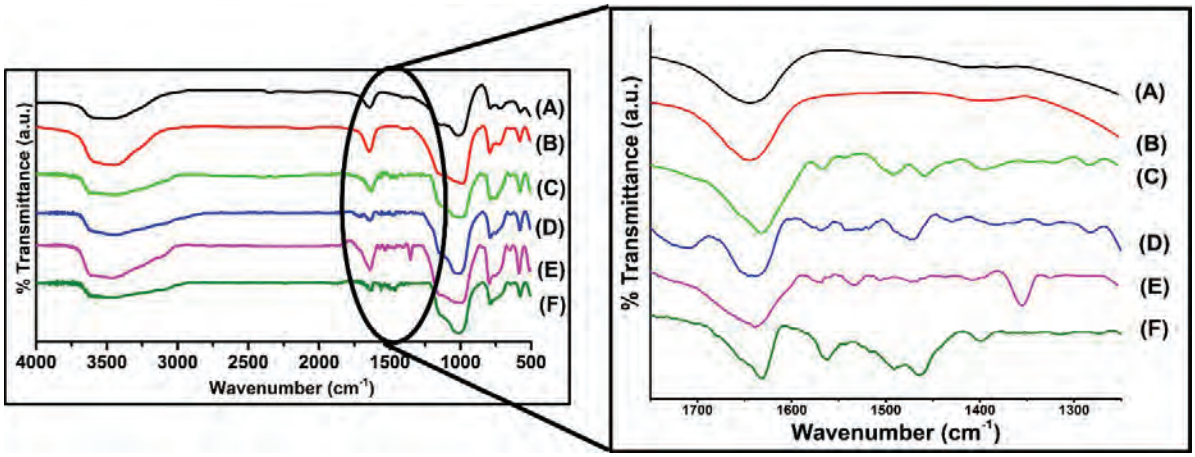

Figure 5.5: FT-IR peaks of **(A)** Zeolite Na-Y, **(B)** Zn(II) exchanged-Y, **(C)** ZnL1-Y, **(D)** ZnL2-Y, **(E)** ZnL3-Y, **(F)** ZnL4-Y (left) and zoomed view of the region 1200-1800 cm^{-1} (right).

Table 5.3: FT-IR data of Zn(II) encapsulated complexes (in cm^{-1})

Complex	T-O bending	T-O stretching (symm)	T-O stretching (asymm)	Lattice water molecules	Surface hydroxyl groups	C=N	C=C	C-H deform	C-O
Na-Y	575	788	1013	1640	3510	-	-	-	-
Zn-Y	579	790	983	1640	3455	-	-	-	-
ZnL1-Y	578	790	1006	1653	3434	1630	1567 1456	1392	1320
ZnL2-Y	578	788	1020	1653	3440	1637	1567 1473	1380	1328
ZnL3-Y	583	794	1003	1657	3461	1637	1568 1472	1402	1352
ZnL4-Y	576	789	1013	1647	3448	1631	1561 1465	1399	1312

5.2.5 Thermal analysis

The thermal stability of the prepared zinc(II) encapsulated complexes was investigated using thermogravimetric analysis (TGA). The TGA thermogram for the complexes is shown in Figure 5.6 and the weight loss percentage tabulated in Table 5.4. The thermogram reveals that ZnL1-Y follows weight loss pattern like zeolite-Y and Zn-Y while the other three complexes show different degradation patterns. The TGA analysis of zeolite entrapped zinc complex reveals that weight loss occurs in two steps. The first weight loss of 9.6 %, 6.6 % and 8.7 % for ZnL2-Y, ZnL3-Y and ZnL4-Y, respectively in the temperature range of 30 °C-150 °C is attributed to the loss of intrazeolite water molecules.[21] The first weight loss occurs at a broader range for ZnL1-Y (30 °C -200 °C), with weight loss of 18.65%. The second weight loss occurs in a wide temperature range for all the complexes, indicating slow decomposition of chelating ligand.[22] The comparatively lesser weight loss of only 7.74 % in the second step for ZnL1-Y suggests towards its higher stability as compared to other complexes.

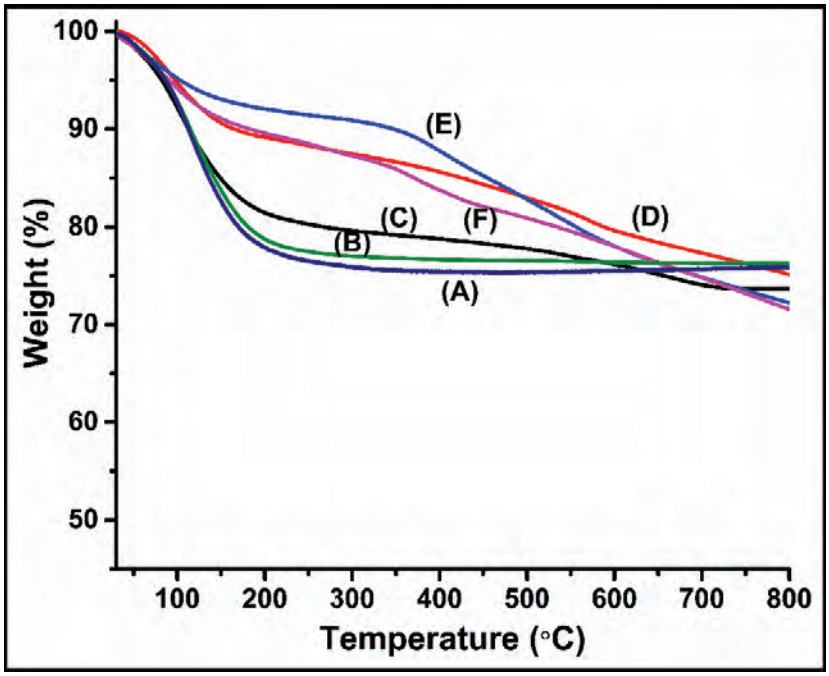

Figure 5.6: TGA thermogram of **(A)** Zeolite Na-Y, **(B)** Zinc(II) exchanged-Y, **(C)** ZnL1-Y, **(D)** ZnL2-Y, **(E)** ZnL3-Y, **(F)** ZnL4-Y.

Table 5.4: TGA weight loss of the encapsulated complexes		
Complex	**Temperature range (°C)**	**Weight loss (%)**
Na-Y	30-200	22.19
Zn-Y	30-200	21.12
ZnL1-Y	30-200 200-725	18.65 7.74
ZnL2-Y	30-155 160-800	9.6 15.04
ZnL3-Y	30-150 330-800	6.68 17.84
ZnL4-Y	30-150 160-800	8.7 19.08

5.2.6 Brunauer-Emmett-Teller (BET) surface area analysis

BET surface area analysis is quite relevant as support of successful encapsulation of zinc(II) Schiff-base complex within the supercage of zeolite-Y. The N_2 adsorption-desorption isotherms and relevant data of pure zeolite-Y and zeolite encapsulated zinc(II) Schiff-base complexes are shown in Figure 5.7 and Table 5.5 respectively. N_2 adsorption-desorption isotherms for pure zeolite-Y and encapsulated zinc complexes indicate medium type I and II isotherms, proving the microporous nature of materials. A distinctive though expected observation emerges from the comparative studies of pore volume and surface area of pure zeolite-Y and the zeolite having zinc complex entrapped. The presence of zinc(II) Schiff-base complexes within the supercage of zeolite-Y is well supported by the decline of the pore volume and surface area of parent zeolite-Y upon encapsulation process. Apart from the micropores, the presence of small amount of mesopores are indicated by the presence of narrow hysteresis loop in the BET plots.[23] The loading level of metal and the size of the complex within the host framework are the decisive factors for the decrease in BET surface area and pore volume upon encapsulation.[18]

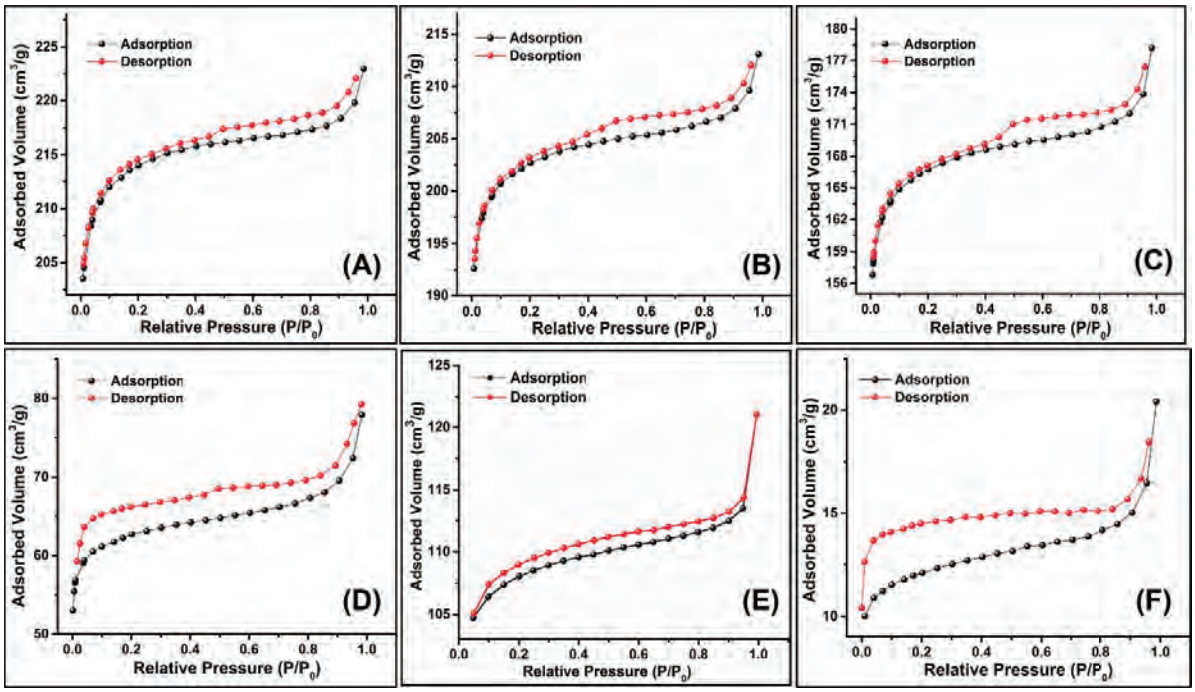

Figure 5.7: BET isotherms for **(A)** Zeolite Na-Y, **(B)** Zinc(II) exchanged-Y, **(C)** ZnL1-Y, **(D)** ZnL2-Y, **(E)** ZnL3-Y, **(F)** ZnL4-Y.

Table 5.5: BET surface area and pore volume of the encapsulated complexes

Complex	BET surface Area (m^2/g)	Total Pore Volume at $P/P_0 = 0.99$ (cm^3/g)
Na-Y	533	0.3448
Zn-Y	505	0.3296
ZnL1-Y	392	0.2757
ZnL2-Y	205	0.1205
ZnL3-Y	351	0.2015
ZnL4-Y	381	0.3152

5.2.7 X-ray photoelectron Spectroscopy (XPS) analysis

XPS analysis is carried out to comprehend the change in the electronic environment of the metal upon encapsulation. XPS results are shown in Figures 5.8 – 5.11 and the data tabulated in Table 5.6. The XPS spectra of the "neat" zinc complexes have already been discussed in Chapter 3. The XPS data of "neat" zinc(II)-salophen complex and the zeolite encapsulated zinc(II) complex suggest the presence of C (1s), N (1s), O (1s), and Zn (2p) elements commonly for both "neat" and encapsulated complexes, whereas, in the case of zeolite encapsulated zinc system, the characteristic peaks of Si (2p), Al (2p) and Na (1s) are also identified. The presence of Zn $2p_{3/2}$ and $2p_{1/2}$ with a binding energy difference of ~23eV suggests the presence of the encapsulated zinc complex in +2 oxidation state.[24] The shifting in the peak position of the zinc (2p) towards higher binding energy upon encapsulation compared to "neat" complexes show that the metal complex has undergone structural modifications, thus experiencing electron deficiency upon encapsulation.[25] A comparison of the XPS signal intensity of Zn (2p) indicates that the encapsulated zinc system has a very low concentration of metal ions compared to that in the "neat" sample, which is again in line with the results obtained from EDX, FT-IR, and UV-vis studies.

The XPS spectra corresponding to C (1s) is deconvoluted into 3 peaks for ZnL1-Y while the other complexes have 4 peaks for the C (1s). These correspond to different environments around carbon, i.e., C-C, C-O and C=N. The N (1s) spectra for all complexes is deconvoluted into two peaks attributing to imine C=N and Zn-N, respectively. The extra peaks for N (1s) in the case of ZnL4-Y shows the presence of the $-NO_2$ substituent. The XPS spectrum of O (1s) is also deconvoluted into three peaks corresponding to C-O, Zn-O and the T-O of zeolite. The presence of only one Zn-O peak in the encapsulated complexes compared to two peaks for Zn-O in respective "neat" form confirms the presence of the monomeric complexes inside the zeolite-Y supercage. XPS spectra of all the zeolite encapsulated zinc(II) complexes also indicate the presence of Si (2p), Al (2p), and Na (1s). XPS observations of zeolite entrapped zinc systems are quite consistent with those for their free-state analogs,[26] proving the successful formation of complex inside the supercage of zeolite-Y.

Table 5.6: XPS data of all the encapsulated complexes (in eV)

Complex	Na (1s)	Si (2p)	Al (2p)	O (1s)	N (1s)	C (1s)	Zn ($2p_{3/2}$)	Zn ($2p_{1/2}$)	ΔBE Zn
ZnL1-Y	1071.94	102.06	74.00	531.07 531.70 532.86	398.13 399.87	284.58 286.26 288.50	1021.60	1044.84	23.24
ZnL2-Y	1072.15	102.52	74.17	531.20 531.73 533.00	398.68 400.40	284.15 284.67 286.04 288.55	1022.00	1045.18	23.18
ZnL3-Y	1071.92	102.14	70.21	531.18 531.80 532.77	398.46 400.35	284.18 284.62 286.04 288.62	1021.90	1044.99	23.09
ZnL4-Y	1071.91	101.96	73.85	531.74 532.33 533.37	398.35 400.04 405.47 406.92	283.83 284.60 286.07 288.61	1021.66	1044.75	23.09

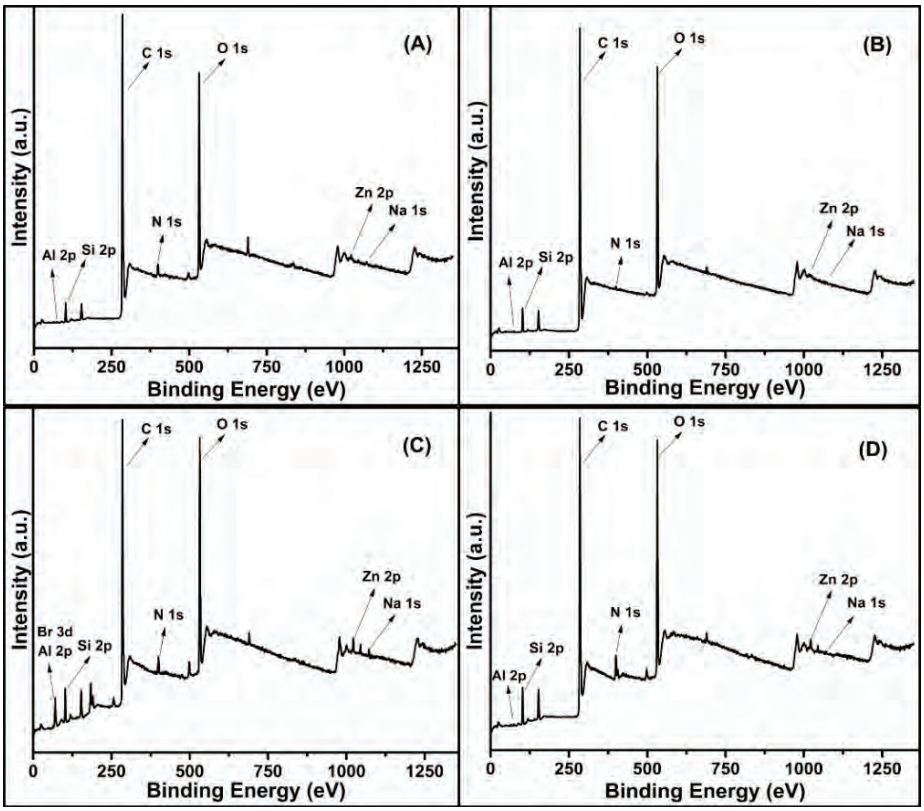

Figure 5.8: XPS survey spectra for **(A)** ZnL1-Y, **(B)** ZnL2-Y, **(C)** ZnL3-Y, **(D)** of ZnL4-Y.

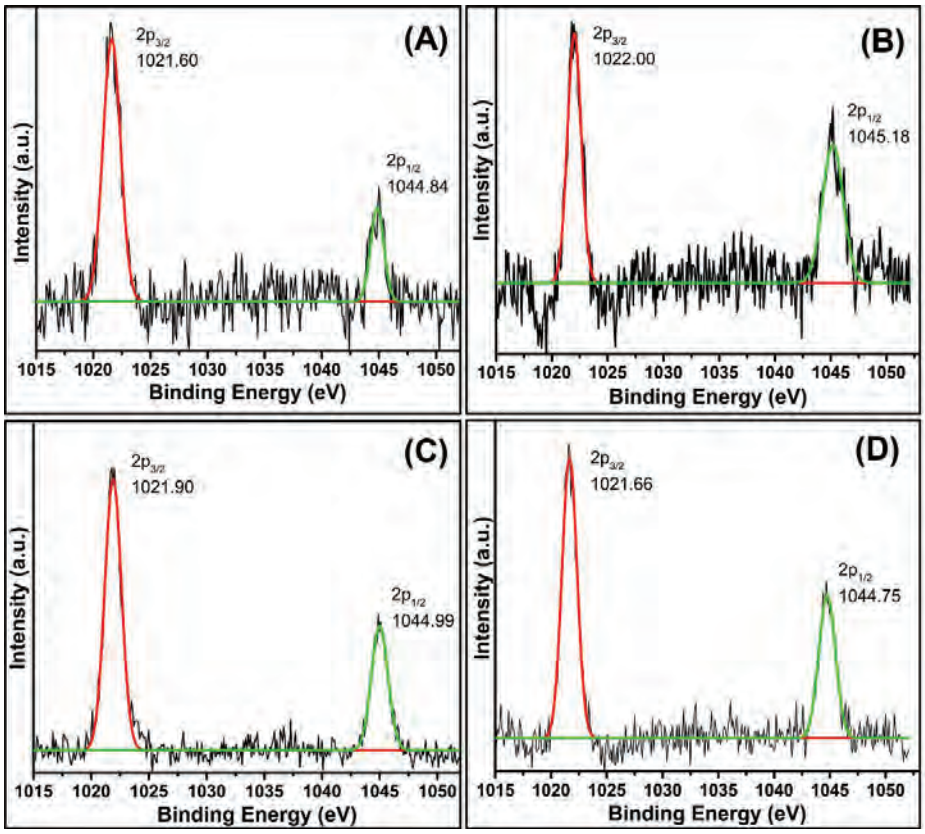

Figure 5.9: XPS profiles for Zn (2p) for **(A)** ZnL1-Y, **(B)** ZnL2-Y, **(C)** ZnL3-Y, **(D)** ZnL4-Y.

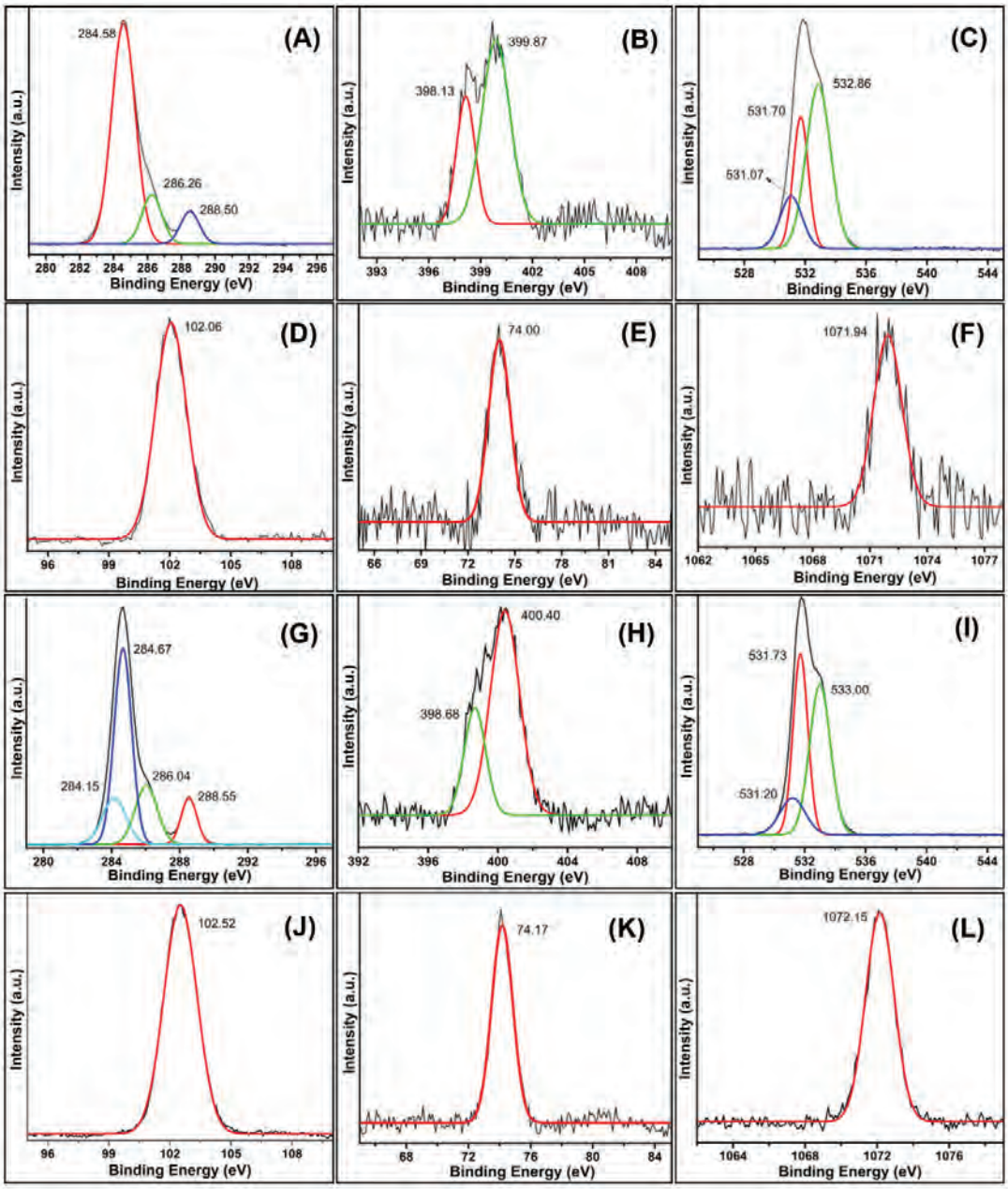

Figure 5.10: XPS profiles for **(A)** C (1s) of ZnL1-Y, **(B)** N (1s) of ZnL1-Y, **(C)** O (1s) of ZnL1-Y, **(D)** Si (2p) of ZnL1-Y, **(E)** Al (2p) of ZnL1-Y, **(F)** Na (1s) of ZnL1-Y, **(G)** C (1s) of ZnL2-Y, **(H)** N (1s) of ZnL2-Y, **(I)** O (1s) of ZnL2-Y, **(J)** Si (2p) of ZnL2-Y, **(K)** Al (2p) of ZnL2-Y, **(L)** Na (1s) of ZnL2-Y.

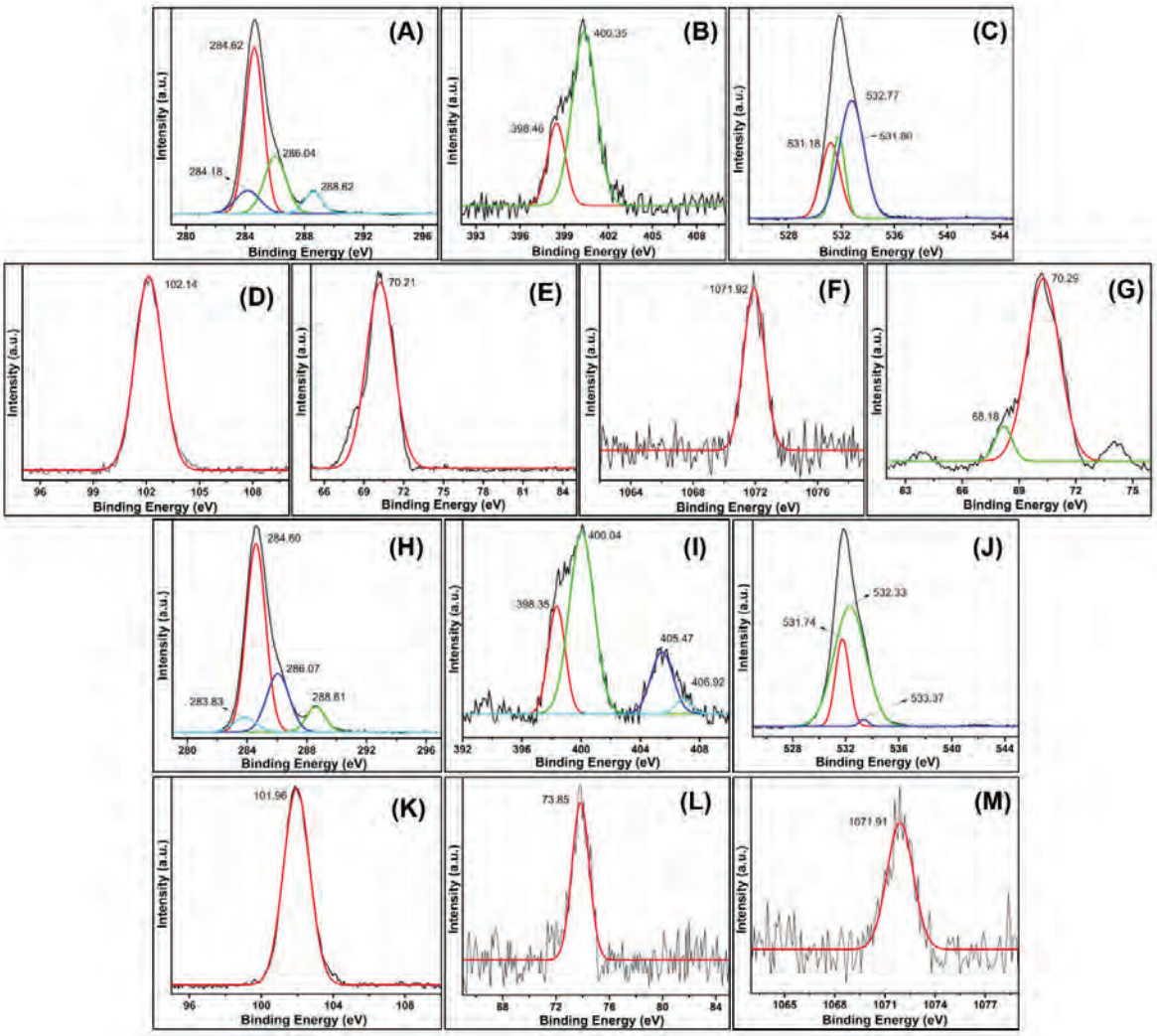

Figure 5.11: XPS profiles for **(A)** C (1s) of ZnL3-Y, **(B)** N (1s) of ZnL3-Y, **(C)** O (1s) of ZnL3-Y, **(D)** Si (2p) of ZnL3-Y, **(E)** Al (2p) of ZnL3-Y, **(F)** Na (1s) of ZnL3-Y, **(G)** Br (3d) of ZnL3-Y, **(H)** C (1s) of ZnL4-Y, **(I)** N (1s) of ZnL4-Y, **(J)** O (1s) of ZnL4-Y, **(K)** Si (2p) of ZnL4-Y, **(L)** Al (2p) of ZnL4-Y, **(M)** Na (1s) of ZnL4-Y.

5.2.8 Ultraviolet-Visible/ Diffuse Reflectance Spectroscopy (UV-vis/DRS)

Electronic spectroscopic studies (UV−Vis/DRS) were carried out to comprehend the coordination environment and geometry around the metal center. The comparative solid-state UV-vis spectra for the zinc(II) Schiff base complexes in both "neat" and encapsulated states are shown in Figure 5.12, along with the data tabulated in Table 5.7. UV-vis bands in the range of 222 nm-

306 nm are characterized as π→π* transitions, while the bands in the range of 303 nm-403 nm are assigned as n→π* transitions in solid-state UV-vis spectra of "neat" and encapsulated systems.[27] Red shift in peak positions of the charge transfer bands and difference in peak-intensities when compared to respective the "neat" complex certainly suggest that the encapsulated complex encounters different electronic environment due its confinement in zeolitic supercage.[27] Parallel observations are also obtained in the XPS studies. Comparative electronic studies of the free-state and encapsulated zinc complexes also show that the charge transfer bands are mainly altered under the encapsulation process, which indicates that the coordination environment surrounding the metal center in the guest complex is largely affected upon encapsulation.

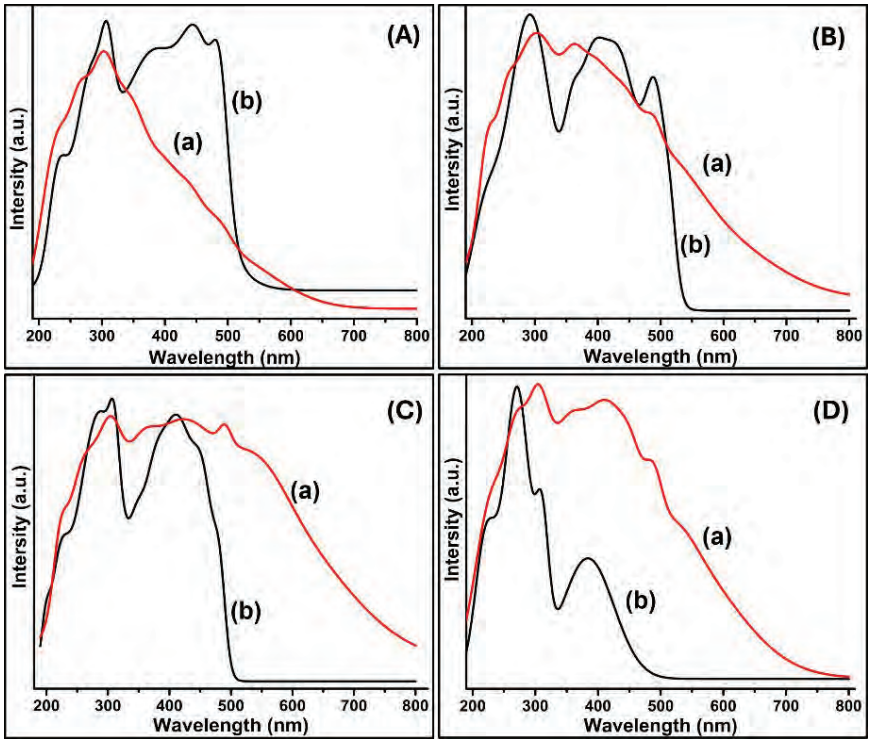

Figure 5.12: Solid state UV of **(A)** (a) ZnL1-Y, (b) ZnL1, **(B)** (a) ZnL2-Y, (b) ZnL2, **(C)** (a) ZnL3-Y, (b) ZnL3, **(D)** (a) ZnL4-Y, (b) ZnL4.

Table 5.7: Solid UV values of all the "neat" and the encapsulated complexes (in nm)				
Complex	**$\pi \rightarrow \pi^*$**	**$n \rightarrow \pi^*$**	**MLCT**	**Difference in MLCT peak from Encapsulated to Neat complex**
ZnL1	234, 281	306, 380	445, 479	488-479 = 9
ZnL1-Y	230, 265	303, 357	440, 488	
ZnL2	222, 292	360, 399	432, 487	547-487 = 60
ZnL2-Y	226, 258, 304	364, 403	444, 490, 547	
ZnL3	227, 285, 306	347, 380	411, 448, 480	552-480 = 72
ZnL3-Y	227, 262, 303	363	423, 491, 552	
ZnL4	224, 270, 306	-	384	486-384 = 102
ZnL4-Y	226, 273, 305	360	413, 443, 486	

5.2.9 Ammonia TPD (NH_3-TPD) studies

NH_3-TPD was used to investigate the distribution of the acidic sites, which were generally divided into three species: weak (50–200 °C), moderate (200–400 °C), and strong (>400 °C) acid sites. The NH_3-TPD profiles of all the complexes are shown in Figure 5.13 and the values tabulated in Table 5.8. Na-Y and Zn-Y show strong peak around 164 °C which is attributed to weak acidic (Lewis acidic) sites. On the other hand, all the complexes show strong peaks in the temperature range greater than 500 °C which is attributed to strong acidic (Brønsted) sites. It is reported that for zeolite ZSM-5, the zinc cations preferentially replace the strong Brønsted acidic sites.[28] Similarly, in our case we see a drastic increase of the strong acidic sites in the complexes compared to Na-Y or Zn-Y. The decrease in the amount of weak acidic sites in the complexes compared to Zn-Y is indicative of paradigm shift in the acidic nature of the zinc present in the encapsulated complex. Thus, zinc in the Zn-Y is majorly located in the weak Lewis acidic sites, while the encapsulated complexes contain the strong Brønsted acidic sites more. Hence, encapsulation is appeared to be a route to improve the acidic property of the guest complex which is fundamental requirement in improving its catalytic property for the studied cycloaddition reaction.

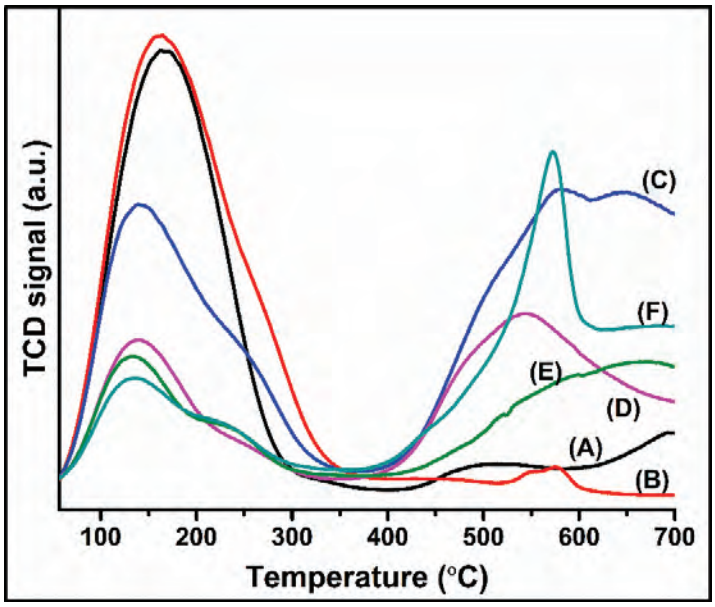

Figure 5.13: NH_3-TPD profiles of **(A)** Zeolite Na-Y, **(B)** Zinc(II) exchanged-Y, **(C)** ZnL1-Y, **(D)** ZnL2-Y, **(E)** ZnL3-Y, **(F)** ZnL4-Y.

Table 5.8: NH_3-TPD data of all the encapsulated complexes (mmol/g)

Complex	Lewis (weak acidic sites)	Brønsted (strong acidic sites)
Na-Y	0.892	0.084
Zn-Y	0.905	0.000
ZnL1-Y	0.551	1.189
ZnL2-Y	0.499	1.216
ZnL3-Y	0.477	0.941
ZnL4-Y	0.509	1.932

5.2.10 Catalytic study for the coupling of styrene oxide to CO_2

The prepared encapsulated complexes were utilized as catalysts for the cycloaddition of CO_2 to styrene oxide. The optimization of the reaction conditions and their activity are shown in Table 5.9 and Table 5.10, respectively. The reaction gave the best results at an ambient pressure of ~1 atm and a comparatively lower temperature of 80 °C for 14 hours using 25 mg of the encapsulated complexes and 0.05 mmol TBAB with styrene oxide. We have already seen the catalytic ability of zeolite alone, as well as the efficiency of the homogeneous metal complex in the previous chapters. The hybrid catalytic system of zeolite encapsulated metal complex is expected to perform better. As anticipated, all the encapsulated complexes performed better than their "neat" counterparts. To compare the activity of the complexes inside the zeolite and in the "neat" form, we have subtracted the activity of the zeolite. ZnL1-Y was the best catalyst, with TOF of 96 h^{-1}, while ZnL1 shows a TOF of only 13.8 h^{-1}. The best performing monomeric homogeneous ZnL4 complex gave a TOF of 16 h^{-1}, while the encapsulated ZnL4-Y showed 3.2 times increase in the TOF with value of 52 h^{-1} (after subtracting the activity of zeolite-Y from the total activity) The catalysts ZnL2-Y and ZnL3-Y also exhibit better TOFs of 60 h^{-1} and 23 h^{-1}, respectively than their "neat" counterparts.

This improved catalytic activity might be the result of the change in the geometry, acidity and the electronic properties of the complex upon encapsulation, which is reflected in the red shift in the UV-vis studies and XPS analysis and TPD studies. The presence of the complex as monomer inside the zeolite supercage, contrary to the dimer in the "neat" form, can also be a major factor for the improved activity. Further, increase in the strong acidity of the complex, and the inherent Lewis acidity of zinc also contribute towards the better activity observed with the encapsulated complexes.

The best performing catalyst, ZnL1-Y was tested for its activity using other epoxides also. The catalyst performed well giving conversions of 91% and 97% and 98% using propylene oxide, epichlorohydrin and cyclohexene oxide respectively It is interesting to note that internal epoxide could not be converted to its corresponding cyclic carbonate. However, the encapsulated complex has shown quite a high conversion. (shown in Table 5.11).

Table 5.9: Optimization of reaction conditions for coupling of styrene oxide to CO_2 using ZnL1-Y			
Temperature (°C)	**Time (h)**	**Catalyst amount (mg)**	**TON of encapsulated system (with zeolite)**
80	10	25	1605
80	10	40	1137
80	10	16	1379
80	10	68.1	380
80	10	136.2	236
80	**14**	**25**	**2095**

The catalyst was also tested for its activity upon recycling. The catalyst performed moderately well with gradual loss of activity over 4 cycles (Shown in Figure 5.14).

Table 5.10: Catalytic activity of the complexes used

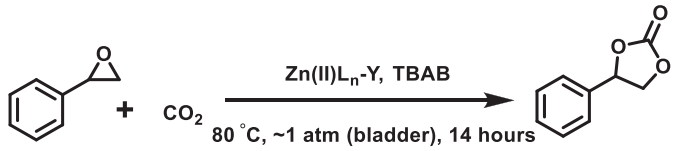

Substituent	**TON of encapsulated system (with zeolite)** [#]	**TOF of the encapsulated system (with zeolite)**[b] **(h^{-1})**	**TON of encapsulated complex (without zeolite)** [#a]	**TOF of the encapsulated complex (without zeolite)**[b] **(h^{-1})**	**TON of "neat" complex**	**TOF of "neat" complex (without zeolite)**[b] **(h^{-1})**
Zn-Y	800	57	425	30	-	-
H	2095	150	1352	96	69	13.8
OMe	1485	106	850	60	71	14.2
Br	875	62.5	326	23	70	14
NO_2	1355	97	731	52	81	16

Reaction conditions - Styrene oxide: 10 mmol, Tetrabutylammonium bromide (TBAB): 0.05 mmol, Complex: 25 mg, 80 °C, 14 hours, ~1 atm CO_2 (bladder) [a] Calculated by GC using bromobenzene as internal standard, [#] (TON = mmol of product formed/mmol of zinc in the catalyst), [a] The TON was calculated by subtracting the mmoles of product obtained only by zeolite-Y (1.36 mmol) from the mmol obtained by the catalyst, [b] TOF = TON/Reaction time

Table 5.11: Activity of the catalyst ZnL1-Y with different epoxides		
Entry	Epoxide	Conversion (%)[a]
1	Styrene oxide	60
2	Propylene oxide[b]	91
3	Epichlorohydrin	97
4	Cyclohexene oxide	98
Reaction conditions - epoxide: 10 mmol, TBAB: 0.05 mmol, Complex: 25 mg, 80 °C, 14 hours, ~1 atm CO_2 (bladder), [a] Conversion calculated by GC using Bromobenzene as internal standard, [b] Reaction carried out at room temperature for 14 h.		

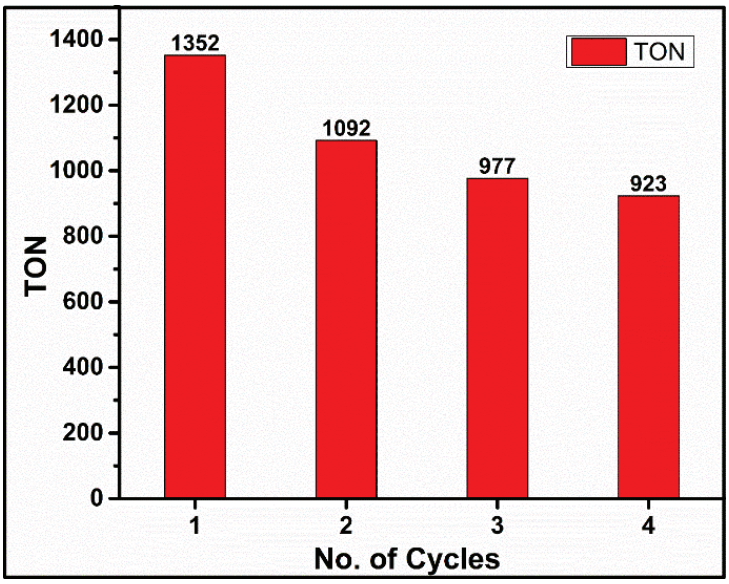

Figure 5.14: Recycle studies of the ZnL1-Y complex.

5.3 Conclusions

Zinc(II) salophen complexes with different substituents (-H, -OCH_3, -Br, -NO_2) were encapsulated inside the supercage of zeolite-Y, characterized thoroughly and utilized as a catalyst for the conversion of CO_2 to cyclic carbonates. The activity of the encapsulated complexes has been compared to their "neat" counterparts and, the results indicate the superior activity of the encapsulated complexes. ZnL1-Y shows the best activity with a TOF of 150 h^{-1} for the overall catalytic system, i.e., the combined activity of the zeolite and the encapsulated complex. Comparing the activity of the "neat" complex and the complex formed inside the zeolite show that ZnL1-Y gives a TOF of 96 h^{-1} while the TOF for ZnL1 is 13.8 h^{-1}. The XPS analysis and the red shift in the UV-visible studies point towards the modification in the geometry of the complex. NH_3-TPD results show an increase in the strong acidic sites of the complex on encapsulation. Encapsulation also renders site isolation, and thus the dimeric neat complexes exist as monomers inside the zeolite supercage. The combined effects of all these factors lead to the superior activity of the encapsulated complexes.

5.4 References

1. Y. Li, J. Zhang, K. Zuo, Z. Li, Y. Wang, H. Hu, C. Zeng, H. Xu, B. Wang and Y. Gao, *Catalysts*, 2021, **11**, 1133.
2. M. Cokoja, M. E. Wilhelm, M. H. Anthofer, W. A. Herrmann and F. E. Kühn, *ChemSusChem*, 2015, **8**, 2436.
3. Q. He, J. W. O'Brien, K. A. Kitselman, L. E. Tompkins, G. C. T. Curtis and F. M. Kerton, *Catalysis Science & Technology*, 2014, **4**, 1513.
4. T. K. Pal, D. De and P. K. Bharadwaj, *Coordination Chemistry Reviews*, 2020, **408**, 213173.
5. L. Hu, L. Chen, X. Peng, J. Zhang, X. Mo, Y. Liu and Z. Yan, *Microporous and Mesoporous Materials*, 2020, **299**, 110123.
6. D. Prasad, K. N. Patil, N. K. Chaudhari, H. Kim, B. M. Nagaraja and A. H. Jadhav, *Catalysis Reviews*, 2022, **64**, 356.
7. F. Zhang, Y. Xie, P. Liu, F. Hao, Z. Yao and H. a. Luo, *Catalysis Letters*, 2014, **144**, 1894.
8. H. He, Q.-Q. Zhu, C. Zhang, Y. Yan, J. Yuan, J. Chen, C.-P. Li and M. Du, *Chemistry – An Asian Journal*, 2019, **14**, 958.
9. R. Srivastava, D. Srinivas and P. Ratnasamy, *Catalysis Letters*, 2003, **89**, 81.
10. S. Kumari, K. Maddipoti, B. Das and S. Ray, *Inorganic Chemistry*, 2019, **58**, 1527.
11. S. Kumari and S. Ray, *New Journal of Chemistry*, 2020, **44**, 14953.
12. K. K. Bania and R. C. Deka, *The Journal of Physical Chemistry C*, 2013, **117**, 11663.
13. W. H. Quayle and J. H. Lunsford, *Inorganic Chemistry*, 1982, **21**, 97.
14. W. H. Quayle, G. Peeters, G. L. De Roy, E. F. Vansant and J. H. Lunsford, *Inorganic Chemistry*, 1982, **21**, 2226.
15. Y. Umemura, Y. Minai and T. Tominaga, *The Journal of Physical Chemistry B*, 1999, **103**, 647.
16. M. S. Hosseini Hashemi, F. Eslami and R. Karimzadeh, *Journal of Environmental Management*, 2019, **233**, 785.
17. A. Oyinade, A. S. Kovo and P. Hill, *Advanced Powder Technology*, 2016, **27**, 750.
18. S. Kumari, A. Choudhary and S. Ray, *Applied Organometallic Chemistry*, 2019, **33**, e4765.
19. K. K. Bania, D. Bharali, B. Viswanathan and R. C. Deka, *Inorganic Chemistry*, 2012, **51**, 1657.

20. A. Choudhary, B. Das and S. Ray, *Dalton Transactions*, 2015, **44**, 3753.
21. S. L. Hailu, B. U. Nair, M. Redi-Abshiro, I. Diaz, R. Aravindhan and M. Tessema, *Chinese Journal of Catalysis*, 2016, **37**, 135.
22. M. Sharma, B. Das, G. V. Karunakar, L. Satyanarayana and K. K. Bania, *The Journal of Physical Chemistry C*, 2016, **120**, 13563.
23. K. Akinlolu, B. Omolara, O. Kehinde, T. Shailendra and M. Kumar, *IOP Conference Series: Materials Science and Engineering*, 2019, **509**, 012061.
24. M. Rakibuddin and R. Ananthakrishnan, *RSC Advances*, 2015, **5**, 68117.
25. S. Sakshi, S. Dey, S. Chowdhury and S. Ray, *ACS Applied Materials & Interfaces*, 2023, **15**, 55518.
26. S. Bhunia, R. A. Molla, V. Kumari, S. M. Islam and A. Bhaumik, *Chemical Communications*, 2015, **51**, 15732.
27. F. Li, D. Hu, Y. Yuan, B. Luo, Y. Song, S. Xiao, G. Chen, Y. Fang and F. Lu, *Molecular Catalysis*, 2018, **452**, 75.
28. L. Yu, S. Huang, S. Zhang, Z. Liu, W. Xin, S. Xie and L. Xu, *ACS Catalysis*, 2012, **2**, 1203.

Chapter 6

Zeolite-Y encapsulated cobalt(II) Schiff-base complexes employed for upcycling CO_2

Abstract: *Planar cobalt(II) Schiff-base complexes show modified structural and functional properties after encapsulation inside zeolite-Y. In the free-state, the reactivity of the cobalt(II) Schiff-base complexes is primarily controlled by the electronic effects of the different substituent groups present in the complexes. However, the encapsulation of these complexes within the supercages of zeolite-Y causes the alteration of the electron density around the metal center and subsequently modifies the reactivity. We have intended to study environment-friendly reactions, i.e., transformation of* CO_2 *with catalysts containing relatively lower metal content like cobalt(II) salophen complexes encapsulated in zeolite-Y. Experimental and theoretical electronic spectroscopic studies clearly revealed successful encapsulation of the guest complex with some alteration of the electronic environment around the metal center. The catalyst with larger end-to-end distance after encapsulation shows better result for the cycloaddition reaction. The TON for* CO_2 *uptake using the heterogeneous catalyst CoL2-Y was found to be 635, while for the same reaction with its homogeneous counterpart, CoL2, the TON was 339.*

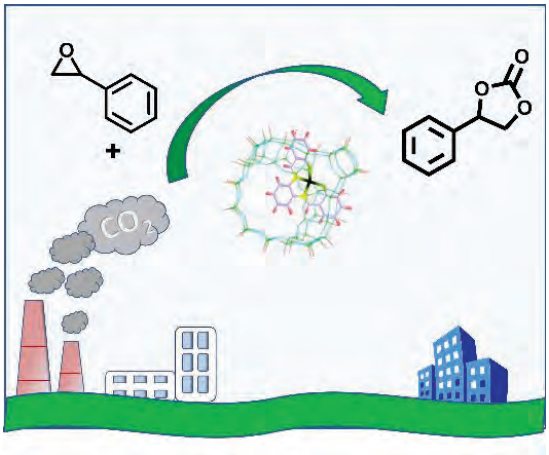

S. Kumari, **A. Ramesh,** B. Das, S. Ray, *Inorg. Chem. Front.*, **2021**, *8*, 1553–1566

6.1 Introduction

In the previous chapter, we have shown the utility of non-toxic zeolite encapsulated zinc(II) salophen complexes as catalysts for the cycloaddition reaction. Cobalt metal complexes containing N_2O_2 coordination sites have also grabbed considerable attention because of their versatile nature.[1, 2] Analogous to zinc, cobalt macrocyclic complexes usually display dimerization which affects the lifetime and stability of the cobalt catalytic systems.[3] This dimerization leads to compromised activity. To tackle this problem, many research groups have used bulky groups like *tert*-butyl (*t*Bu). In fact, for the conversion of epoxide and CO_2 to cyclic carbonates using cobalt salen/salophen type complexes, mostly all the reported complexes use the bulky *t*Bu group (Examples shown in Table 1.2).[4, 5] This brings us to an understanding that the dimerized complex is an inactive catalyst for this reaction. Encapsulation of such complexes within the pores of an appropriate host also prevents multi-molecular deactivation pathways due to site isolation.[6] Hence, encapsulation could be even more beneficial because dimerization of salen, salophen complexes can be prevented *via* this process and the homogeneous catalyst is upgraded to a heterogeneous catalyst. These hybrid systems showcase the properties of their host, like nanocavity size, electrostatic potential, along with the electronic and stereochemical properties of the guest complex.[7, 8] These heterogeneous systems, therefore, can be more advantageous over their homogeneous analogs and can be employed as effective and eco-friendly catalysts for CO_2 conversion. Hence, in this chapter we have chosen catalytically active cobalt metal complex encapsulated in the supercage of zeolite for the cycloaddition reaction.

Herein, we present the application of homogeneous cobalt(II) salophen complexes (shown in Figure 6.1) and their heterogeneous counterparts as catalysts for the cycloaddition of CO_2 to styrene oxide to form styrene carbonate. As discussed in Chapter 1, only a few reports are available in the literature for cycloaddition of CO_2 to epoxide by using zeolite encapsulated metal complexes. Owing to the limited reports, encapsulation of cobalt Schiff base in zeolite becomes a compelling choice. From the previously reported results, a definite correlation between the catalytic activity of the encapsulated complex and its end-to-end distance have been noted.[9, 10] The studies point out that the complex with methoxy group at 5, 5' position undergoes the maximum distortion after encapsulation due to larger size.[11, 12] With this background, in the present chapter, we have prepared a complex with a large end-to-end distance, i.e. with a -OMe group at 5, 5' position and compared its catalytic activity with a complex with comparatively smaller end-to-end distance, i.e.

-H at the 5, 5' position. Kumari *et al.*[13] have reported the synthesis and the detailed characterization of these two complexes and used them as a catalyst for the degradation of rhodamine B dye, hence the detailed characterizations of the complexes will not be discussed here. This chapter builds up on the important results and a correlation between structural modification and their respective catalytic activities for the cyclic carbonate synthesis has been explored.

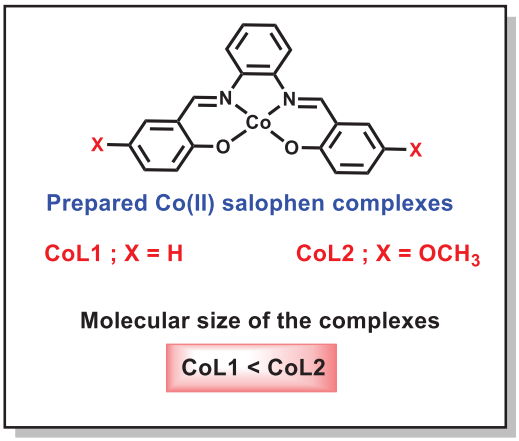

Figure 6.1: Schematic representation of the synthesized cobalt(II) Schiff-base complexes.

6.2 Results and Discussions

Detailed characterization of all the synthesized neat and encapsulated complexes have been carried out previously.[13] The EDX results show that dealumination has not occurred. The SEM images show the successful removal of surface impurities. XRD and FT-IR studies show the retention of the zeolite framework and the successful encapsulation. Thermal analysis points to the improved stability of complexes. Decrease in BET surface area and pore volume confirm the successful encapsulation. Solution UV-vis confirms the formation of complexes. The solid state UV and XPS, along with theoretical studies indicate the alteration in the electronic environment around the metal center in the encapsulated complexes. All the results from the characterizations are presented in Table 6.1 and plots shown in Figure 6.2

Table 6.1: Summary of characterization data for the prepared encapsulated and "neat" complexes

Complex	Cobalt (wt%)	Si/Al Ratio	FT-IR peaks (cm^{-1})	TGA weight loss range	BET Surface area (m^2/g)	Pore volume (cm^3/g)	XPS binding energy (eV)	Solution UV-vis (nm)
Zeolite Na-Y	-	2.79	560 (T-O bending) 717 (double ring) 786 (Symmetric str. vib) 1643 (lattice water) 3500 (surface -OH)	30-180 °C (intrazeolite water molecules)	535	0.3456	-	-
CoL1	-	-	1622 (C=N) 1548, 1464 (C=C) 1368 (C-H) 1307 (C-O)		-	-	780.88 (Co $2p_{3/2}$) 796.17 (Co $2p_{1/2}$)	248, 302 ($\pi \rightarrow \pi^*$) 340, 388 ($n \rightarrow \pi^*$) 440, 583 (CT/d-d transitions)
CoL1-Y	0.51	2.78	1631 (C-N) 1492, 1458 (C=C) 1386 (C-H) 1276 (C-O)	30-180 °C (intrazeolite water molecules) 300-750 °C (decomposition of chelating ligand)	350	0.2015	780.99, 784.46 (Co $2p_{3/2}$) 796.52, 803.15 (Co $2p_{1/2}$)	-

Complex	Cobalt (wt%)	Si/Al Ratio	FT-IR peaks (cm^{-1})	TGA weight loss range	BET Surface area (m^2/g)	Pore volume (cm^3/g)	XPS binding energy (eV)	Solution UV-vis (nm)
CoL2	-	-			-	-	780.52 (Co $2p_{3/2}$) 795.62 (Co $2p_{1/2}$)	239, 260 ($\pi \rightarrow \pi^*$) 302, 375 ($n \rightarrow \pi^*$) 500, 580 (CT/d-d transitions)
CoL2-Y	0.54	2.78		300-750 °C (decomposition of chelating ligand)	325	0.1825	780.60, 784.37 (Co $2p_{3/2}$) 795.92, 804.28 (Co $2p_{1/2}$)	-

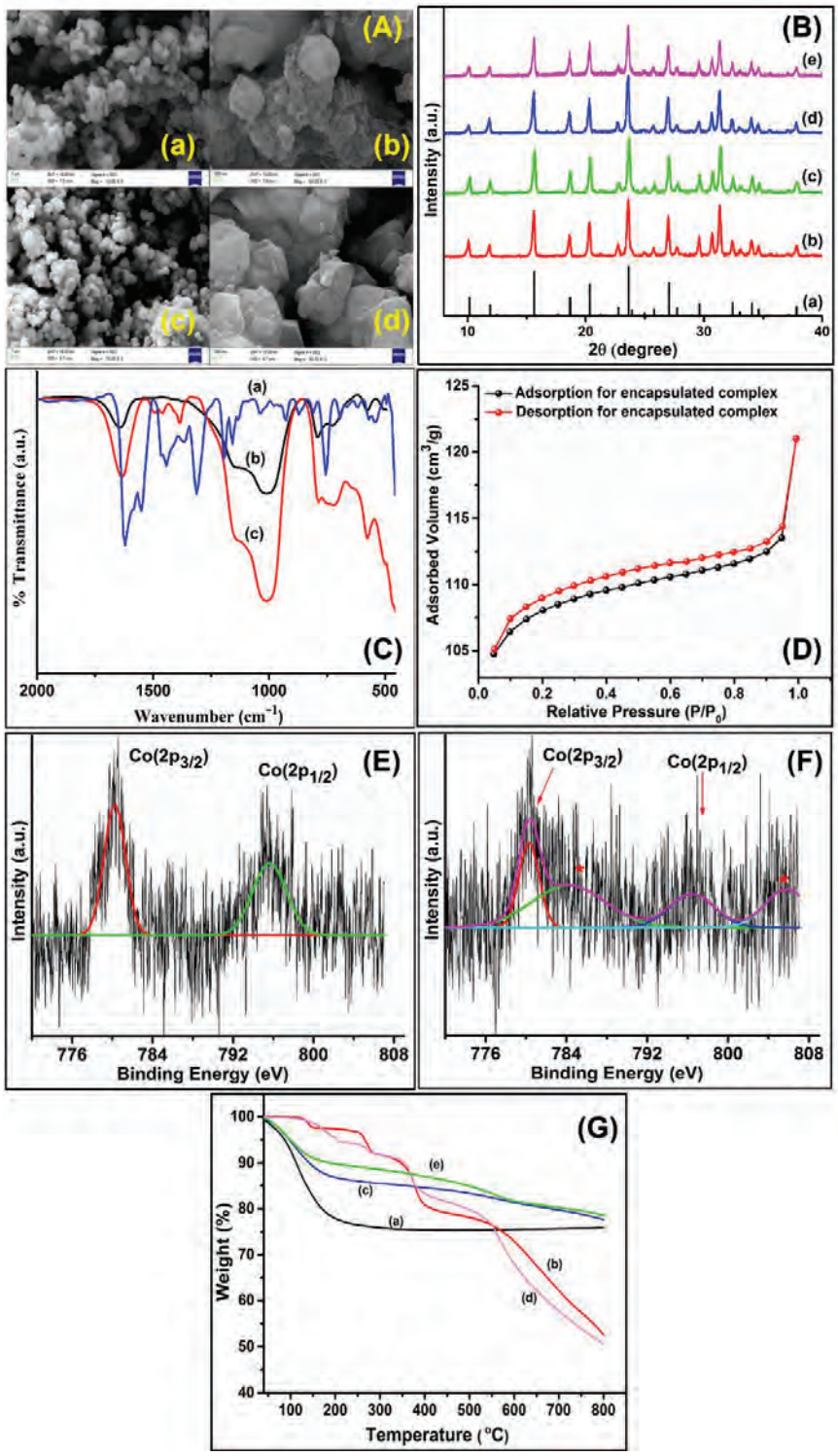

Figure 6.2: SEM images of **(A)** (a) and (b) CoL1-Y before Soxhlet at different resolutions, (c) and (d) CoL1-Y after Soxhlet at different resolutions, **(B)** PXRD patterns of (a) JCPDS reference of zeolite-Y (card number 00-043-0168), (b) Zeolite Na-Y, (c) Cobalt(II) exchanged-Y, (d) CoL1-Y, (e) CoL2-Y, **(C)** FT-IR spectra of (a) CoL1, (b) Zeolite Na-Y, (c) CoL1-Y, **(D)** BET isotherm of CoL2-Y, **(E)** XPS spectra for cobalt of CoL2, **(F)** XPS spectra for cobalt of CoL2-Y, **(G)** TGA curves of (a) Zeolite Na-Y, (b) CoL1, (c) CoL1-Y, (d) CoL2, (e) CoL2-Y.

6.2.1 Theoretical studies and Diffuse Reflectance Spectroscopy (UV−Vis/ DRS)

Previously reported magnetic and crystallographic studies of cobalt(II) salen and salophen complexes reveal the dimeric structure of distorted rectangular based with five coordination having an axial Co-O bond.[3, 14-17] The ground state of dimeric cobalt(II) salen is antiferromagnetically coupled singlet having a relatively small energy difference with the ferromagnetically coupled triplet state. It is also reported that at a higher temperature, spin-crossover from the ground state to the quartet state takes place.[18-20]

The dimerization of the free doublet cobalt(II) salophen complexes was studied. Indeed, the results indicated that the dimerization of CoL1 leads to some energy gain as the binding energy of the dimer formation is 6 kcal. Interestingly, the dimer of cobalt(II) salophen complex may exist as a singlet or triplet, as the two *d*-electrons of two cobalt(II) centers may be aligned anti-parallel or parallel, respectively. Though previous studies of cobalt(II) salen complexes had shown the singlet state dimer is the ground-state,[18, 19] however, the results obtained indicate a triplet ground-state for cobalt(II) salophen complex. The triplet dimeric CoL1 complex is more stable compared to the singlet dimeric CoL1 complex by 41 kcal, indicating the predominance of triplet over singlet state in this case.

Theoretical studies were done to get the structural optimization of CoL1 and CoL2, in the monomeric doublet, dimeric singlet, triplet and CoL1-Y and CoL2-Y in the quartet state. All the results are provided in Table 6.2. In the dimer, the two complexes are facing each other in parallel planes but are not stacked exactly vertical as shown in Figure 6.3 (C) and (D). A significant structural change that accompanies the dimerization process is the destruction of planarity compared to the monomeric, doublet complex. The dimer has an overall curved structure, which are connected in the middle by two Co-O linkages perpendicular to the molecular plane, as shown in Figure 6.3.(C) and (D) The Co-O distances in the dimer is 2.24 Å for the triplet, while for the singlet, it is shorter (2.02 Å).

Upon encapsulation, due to size constraints within the zeolite pore, the encapsulated cobalt(II) salophen complex is monomeric and distorted, making the slightly higher energy quartet state accessible. The distortion of the complex around the cobalt center in the quartet state enables a very strong hybridization between the metal d orbitals with the π framework of the salophen ligand. The distortion around the cobalt(II) results from the cobalt atom moving away from the plane of

the ligand resulting in a disruption of conjugation. Consequently, the dihedral angles ∠Co-N-N-O and ∠N-N-O-O increase to 16.5º and 31.5º, respectively, which indicates the Co, O, and N atoms no longer lie in the same plane. The change in planarity changes the extent of π-conjugation and the ordering of the molecular orbitals, eventually affecting the UV spectra after encapsulation.

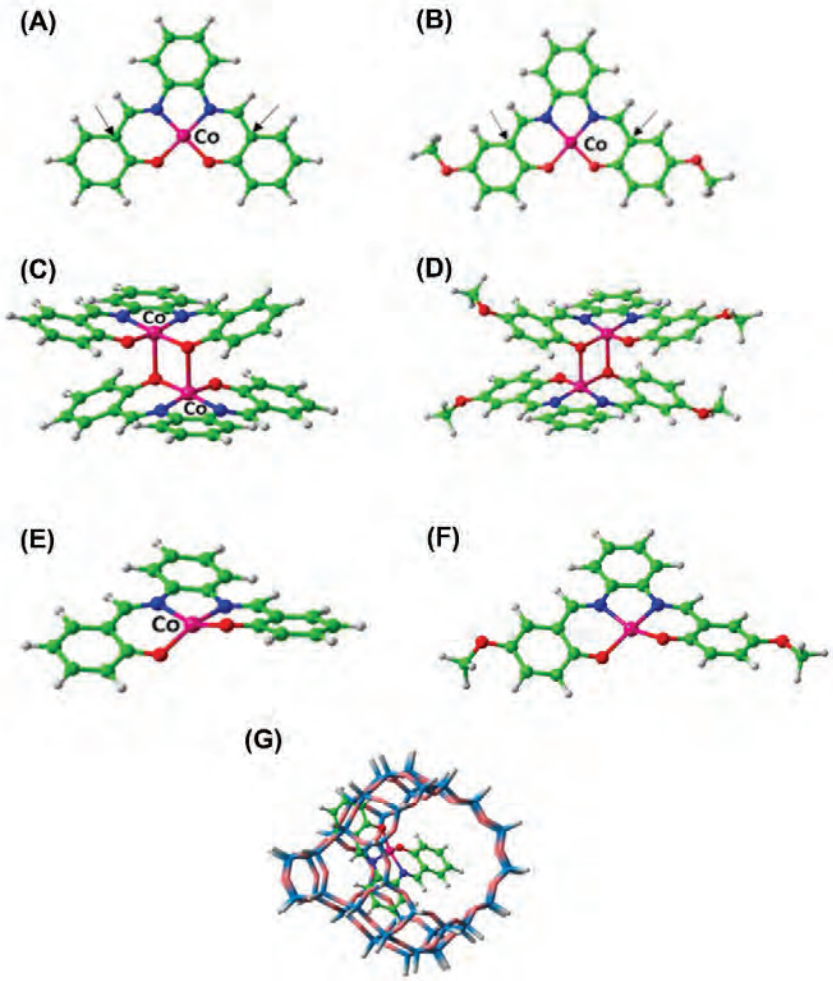

Figure 6.3: Optimized doublet ground-state structures for **(A)** CoL1 and **(B)** CoL2; Optimized triplet ground-state structures for **(C)** CoL1 and **(D)** CoL2; **(E)** The encapsulated and extracted quartet state of CoL1-Y complex **(F)** The encapsulated and extracted quartet state of CoL2-Y complex **(G)** The CoL1 complex is shown encapsulated within model zeolite pore. The C atoms marked by black arrows are considered to measure the angle ∠C-Co-C as reported in Table 6.2.

Table 6.2: Structural parameters and molecular orbital energies of the complexes

Parameters	Monomer CoL1	Monomer CoL2	Dimer CoL1	Dimer CoL2	Dimer CoL1	Dimer CoL2	CoL1-Y	CoL2-Y
	(Doublet)		(singlet)		(triplet)		(Quartet)	
Co-O (Å)	1.82	1.82	2.03 (Vertical) 1.86, 1.88 (Lateral)	2.03 (Vertical) 1.86, 1.89 (Lateral)	2.24 (Vertical) 1.86, 1.90 (Lateral)	2.24 (Vertical) 1.86, 1.90 (Lateral)	1.90	1.90
Co-N (Å)	1.86	1.86	1.88	1.88	1.88	1.88	2.0	2.02
O-C (Å)	1.29	1.29	1.29, 1.32	1.29, 1.33	1.29, 1.31	1.29, 1.31	1.29	1.29
N-C (Å)	1.32	1.32	1.31	1.31	1.31	1.31	1.31	1.31
∠O-Co-N (°)	94.5	94.5	93.2, 94.2	93.2, 94.2	92.8, 94.5	92.8, 94.5	93.2	91.1
∠C-Co-C (°)	178.6	178.7	151.3	152.8	152.5	152.5	176.1	175.1
∠Co-N-N-O (°)	-0.1	-0.3	-4.2, -10.9	-4.9, -11.5	-2.7, -8.7	-2.7, -8.7	-16.5	-12.3
∠N-N-O-O (°)	0.2	0.5	-7.2, -10.9	-8.1, -8.0	6.3	6.3	31.5	23.4

Parameters	Monomer CoL1	Monomer CoL2	Dimer CoL1	Dimer CoL2	Dimer CoL1	Dimer CoL2	CoL1-Y	CoL2-Y
	(Doublet)		(singlet)		(triplet)		(Quartet)	
End to end distance (Å)	12.9	17.1	14.9	19.0	15.0	15.0	13.0	17.3
HOMO (eV)	-5.51 (α) -5.25 (β)	-5.05(α) -5.07(β)	-3.79	-3.65	-4.95 (α) -4.75 (β)	-4.95 (α) -4.75 (β)	-5.08 (α) -5.51 (β)	-4.92(α) -5.08 (β)
LUMO (eV)	-2.18 (α) -2.23 (β)	-2.12 (α) -2.18 (β)	-2.15	-2.00	-1.95 (α) -1.97 (β)	-1.95 (α) -1.97 (β)	-2.18 (α) -2.30 (β)	-2.17(α) -2.21(β)
HOMO-LUMO gap (eV)	3.02	2.87	1.64	1.65	2.78	2.78	2.78	2.71
Spin density on Co (BM)	1.05	1.04	None	none	1.07, 1.07	1.07, 1.07	2.78	2.77

The UV-vis/DRS is an important characterization technique which tells about the change in the electronic environment of the metal in the complex. The spectra are shown in Figure 6.4 and the values tabulated in Table 6.3. Shift in peak positions and difference in peak-intensities of the "neat" and the encapsulated complexes suggest that the encapsulated complex encounters different electronic environment due its confinement in zeolitic supercage. Comparative electronic studies of the free-state and encapsulated cobalt complexes show that the metal transitions (charge transfer and d-d transitions) are mainly altered under the encapsulation process, which indicates that the coordination environment surrounding the metal center in the guest complex is largely affected upon encapsulation. Both the encapsulated systems show a regular blue shift in the metal-related transitions. Such type of observations has been notified in zeolite encapsulated systems.[9] These modified electronic behavior of the metal complex are definitely the outcome of the altered coordination environment, especially around the metal center due to the space constraints imposed by the supercage of the host framework. End-to-end dimensions of both the free-state cobalt(II) Schiff-base complexes are comparable with the dimensions of supercage. Therefore, guest cobalt complex experiences space constraint inside the supercage and is eventually forced to adopt irregular geometries. Theoretical studies are very suggestive and supportive of such types of structural modifications.[21] Amendment in various geometrical variables such as bond lengths, bond angles, and optical gaps of the guest metal complex are observed in the theoretical studies upon encapsulation. (Tabulated in Table 6.2) The optical spectra obtained experimentally was also supported by the theoretical simulations, calculated using time-dependent density functional (TD-DFT) methods. All the important theoretical parameters have already been discussed in Chapter 2, Section 2.4.12. Another fascinating observation is that the guest metal complex with larger molecular dimension experiences more steric hindrance inside the host cavity. Therefore, a higher extent of distortion becomes apparent to reduce the Van der Waal interaction with the wall of zeolite-Y. The larger the molecular dimensions of the guest complexes, the more is the blue shift observed.

Experimentally observed UV-vis spectra (Figure 6.4) of the cobalt(II) salophen complexes are dictated by the electronic transitions occurring between the various molecular orbitals of the complex, so analyzing the nature of the molecular orbitals and their energies can be very insightful.

In case of quartet encapsulated complexes, the optical spectra are calculated without the zeolite supercage, *i.e.* after extracting the encapsulated Cobalt complexes from zeolite and keeping its

geometry fixed. The optical spectra are then analysed in terms of the molecular orbitals of the cobalt complexes in free or encapsulated states. The molecular orbitals are defined with respect to the highest occupied molecular orbital (HOMO) and lowest unoccupied molecular orbital (LUMO) as HOMO-n (H-n) and LUMO+n (L+n).

The HOMO, (-5.51 eV) for CoL1, doublet state for the alpha spin-state has some d_{xz} character which is strongly hybridized with the π orbitals of the ligand, whereas LUMO, (-2.18 eV) is mostly π antibonding type without any metal orbital contribution. In the case of beta spin-states, the HOMO is higher in energy (-5.25 eV), and there is some contribution from Co d_{yz} orbitals along with ligand π orbitals, whereas LUMO (-2.23 eV) is a ligand-based π antibonding orbital. The inspection of the molecular orbitals shows that the HOMO-3 (alpha-spin, -6.33 eV) is primarily localized on Co d_z^2 orbital, but Co d_{xy} orbital is an inner orbital with much lower energy. The HOMO-LUMO gap in the case of CoL1 is 3.02 eV. It is observed that the change in substituents from -H to -OCH_3 does not drastically change the nature of the frontier molecular orbitals, but the HOMO-LUMO gap decreases to 2.87 eV due to a slight increase in HOMO energy. In the case of cobalt(II) salophen dimeric complexes, the degenerate HOMO orbitals of the triplet state have contributions from d_{xz} orbital (alpha), which is formed from the interaction of the HOMOs of two doublet monomers and dimer LUMO is ligand based. The HOMO-LUMO gap for triplet, dimeric CoL1, is 2.78 eV, which is slightly lower than the monomer. When encapsulated within the zeolite pore, the cobalt(II) complex is distorted due to space constraint, which stabilizes the quartet state, with three unpaired electrons. Surprisingly, here the HOMO (alpha) is d_{xy} orbital, which was an inner orbital for the doublet monomer, and the LUMO is mainly a ligand based π* orbital. The HOMO-LUMO gap for the quartet state is 2.78 eV for CoL1, which is lower than doublet monomer but the same as triplet dimer. In the case of CoL2, however, the triplet dimer HOMO-LUMO gap is 2.56 eV, which increases to 2.71 eV when we consider the distorted, quartet complex.

The UV-vis spectra of all the complexes was simulated in the monomeric doublet-state, the dimeric triplet-state and the monomeric quartet -state using TD-DFT. The spectra are presented in Figure 6.4 and the values tabulated in Table 6.3. Since the complexes are dimeric in nature, the simulated triplet-state with the experimental solid-state UV of the neat complex, and the monomeric quartet-state with the experimental solid-state UV of the encapsulated complex have been compared in the UV spectra.

Table 6.3: Assignment of experimental UV-vis peaks and comparison with calculated TD-DFT spectra

Complex	Peaks from experiment (nm)	Peaks from DFT (nm)	Assignment
CoL1	230, 303 389 486, 545, 625	250-300 365, 386 449, 490 (CT), 543 (d-d), 625 (CT), 689	π→π* n→π* CT/d-d transitions
CoL1-Y	249, 299 328, 384 462, 620	606, 645	π→π* n→π* CT/d-d transitions
CoL2	252, 302 405 589, 726	503, 589, 596 , 726	π→π* n→π* CT/d-d transitions
CoL2-Y	228, 302 354 494, 672		π→π* n→π* CT/d-d transitions

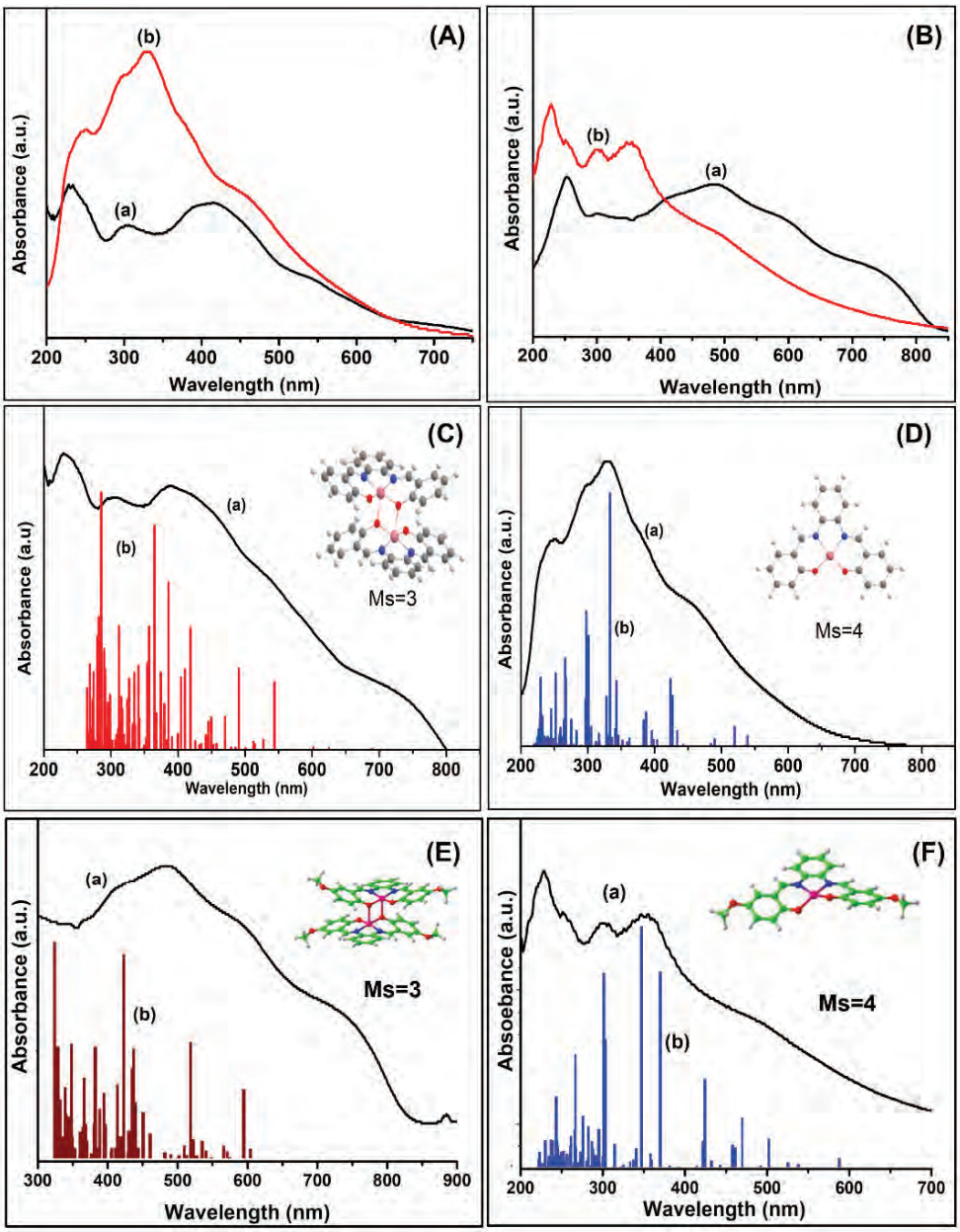

Figure 6.4: Solid state UV-vis spectra of **(A)** (a) CoL1, (b) CoL1-Y, **(B)** (a) CoL2, (b) CoL2-Y, **(C)** (a) Experimental CoL1, (b) DFT simulated triplet of CoL1, **(D)** Experimental CoL1-Y, (b) DFT simulated quartet of CoL1-Y, **(E)** (a) Experimental CoL2, (b) DFT simulated triplet of CoL2, **(F)** Experimental CoL2-Y, (b) DFT simulated quartet of CoL2-Y.

Table 6.4: Comparison of zinc and cobalt for the catalytic reaction		
Catalyst	**TON (including zeolite activity)**	**TON (without zeolite activity)**
CoL1-Y	1206	577.5
ZnL1-Y	2095	1352
Reaction conditions: Temperature: 80 ºC, Time:14 h, CO_2 Pressure: 1 atm, TBAB co- catalyst: 0.05 mmol and 25 mg of encapsulated complex		

6.2.2 Catalytic study for the coupling of styrene oxide and CO_2

All the complexes, i.e. CoL1, CoL1-Y, CoL2 and CoL2-Y have been studied as catalysts for the coupling of styrene oxide and CO_2 to form styrene carbonate, using tetrabutylammonium bromide (TBAB) as a Lewis base co-catalyst. Initially, the reaction was carried out at the reaction conditions used in the previous chapter, i.e., at ~1 atm and 80 °C for 14 hours to compare the activity of metals i.e., zinc and cobalt. Since, ZnL1-Y gave the best results, CoL1-Y was chosen as the probe catalyst and the results were compared. Interestingly, at lower pressure, encapsulated zinc proved to be a better choice for the reaction. (shown in Table 6.4)

To improve the performance of the cobalt catalyst, the reaction was carried out at higher temperature and pressure (data presented in Table 6.5). To get the optimized reaction condition, initially, CoL1 and CoL1-Y were used as the catalyst in the reaction. The reaction was carried out with styrene oxide (10 mmol, 1.2g), TBAB (0.05 mmol, 16.1 mg), encapsulated complex (100 mg) using CO_2 at a pressure of 5 bar at 80 °C for 1.5 hours. We got a conversion of 66% and a TON of 622. By increasing the temperature to 100 °C, the conversion and TON increased to 77% and 720, respectively. Inspired by the improvement in the activity, we further increased the temperature to 130 °C. However, there was no betterment in the activity. We then tried the reaction in the best temperature conditions (5 bar, 130 °C and 1.5 h) but with lesser catalyst loading of 50 mg. To our surprise, there was a significant improvement in TON from 718 to 1595. Encouraged by this result, we further decreased the amount of the catalyst to 25 mg and found that the TON increased even further to 2955 which we considered as the optimized reaction condition. We then tried the same reaction with neat complex at 130 °C with 0.05 mmol of the complex and 0.05 mmol of TBAB.

We got a TON of 173 and upon further decreasing the catalyst and the cobalt-catalyst loading to 0.025 mmol, the TON increased to 330. The increase in activity with decrease in the catalyst loading can be attributed to the optimum number of active catalytic sites provided for the reactants and hence, effectiveness of the catalyst improved .

Table 6.5: Optimization of reaction conditions of coupling of styrene oxide to CO_2

Catalyst	Temperature (°C)	Amount	Time (h)	TON	Conversion (%)
CoL1-Y	80	100 mg	1.5	622	66
CoL1-Y	80	50 mg	1.5	1438	76
CoL1-Y	100	50 mg	1.5	1515	81
CoL1-Y	100	100 mg	1.5	720	77
CoL1-Y	130	100 mg	1.5	718	76
CoL1-Y	130	50 mg	1.5	1595	85
CoL1-Y	**130**	**25 mg**	**1.5**	**2955**	**79**
CoL1	80	0.05 mmol	1.5	160	78
CoL1	80	0.025 mmol	1.5	300	72
CoL1	100	0.05 mmol	1.5	163	80
CoL1	100	0.025 mmol	1.5	306	76
CoL1	130	0.05 mmol	1.5	173	85
CoL1	**130**	**0.025 mmol**	**1.5**	**330**	**82**

With suitable reaction conditions, the activity of CoL2 and CoL2-Y were also tested. Using this complex in neat form, a TON of 339 and yield of 85% was obtained, while the same complex in the encapsulated state gave a TON of 5005 and 83% yield (tabulated in Table 6.6). We observed that though the yield of the product is comparable for these cases, the activity of the encapsulated complex is much higher than that of the neat complex.

Table 6.6: Activity of the catalysts for conversion of styrene oxide and CO_2 to styrene carbonate under optimized conditions

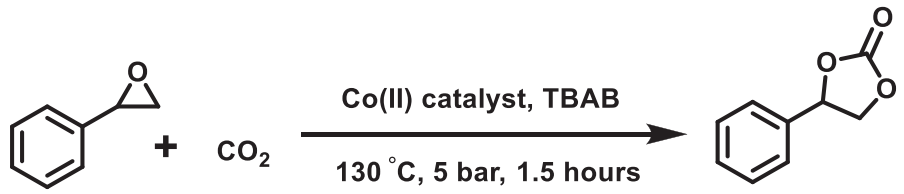

Catalyst	Amount (mmol)	TON (including zeolite activity)	TON (without zeolite activity)	Yield (%)
Zeolite-Y	25 mg	-	-	73
Co-Y	0.0065332	1132	41	74
CoL1	0.025	-	346	79
CoL1-Y	0.0026727	2949	246	82
CoL2	0.025	-	339	85
CoL2-Y	0.0016545	5005	635	83

Reaction conditions: Temperature: 130 °C, Time:1.5 h, CO_2 Pressure: 5 bar, TBAB co-catalyst - 0.05 mmol with encapsulated complex and 0.025 mmol with neat complex

The comparison of the activity of the cobalt complex in its neat and encapsulated forms at ambient pressure of 1 atm and 5 bar was also carried out (shown in Table 6.7). It is obvious that the reaction when carried out at higher temperature and pressure exhibits better results, which is reflected in the TOF. However, while comparing TON, encapsulated CoL1 performs better at milder reaction condition of lower temperature and pressure, which leaves a scope to improve its TOF further.

Table 6.7: Comparison of activity of cobalt complexes at different reaction conditions				
Complex	**At ~1 bar, 80 °C, 14 h**		**At 5 bar, 130 °C, 1.5 h**	
	TON	**TOF**	**TON**	**TOF**
CoL1	80	5.7	346	230
CoL1-Y	577.5 (excluding zeolite activity)	41.25	246 (excluding zeolite activity)	164

As discussed in Chapter 1, the reaction follows epoxide activation mechanism.[22-24] The epoxide is first activated by the Lewis acid metal center, followed by the ring-opening by the halide ion from co-catalyst. Then, finally, the insertion of CO_2 and internal attack of carbonate oxygen takes place to close the ring. The lesser the electron density on the metal atom of the catalyst, the more easily the epoxide can attack on the complex. The neat complex with -OMe substituent, CoL2 is found to be marginally less reactive than CoL1 because the electron-donating group eventually increases the electron density on the metal center, thus making the activation of the epoxide by the metal center difficult. However, upon encapsulation, the order reverses. Due to the loss of the planarity, and the subsequent structural changes upon encapsulation, CoL2-Y has a higher activity.

6.3 Conclusions

Two free-state cobalt(II) salophen complexes and their encapsulated analogs have been synthesized using the flexible ligand method. The catalytic activity of the free-state and zeolite encapsulated cobalt systems have been studied for environmentally sustainable reactions i.e. upcycling CO_2 by its reaction with styrene oxide to produce useful styrene carbonate.

Confinement of the cobalt salophen complexes within the supercage of zeolite framework imposes space constraints on the guest metal complex enforcing the guest to adopt a modified geometry. The DFT study, along with electronic spectroscopic studies, provides an important insight into the variations in structural alterations due to encapsulation. Upon encapsulation, cobalt salophen complexes exist as monomers within zeolite. Such structural modifications lead to change in spin-states of the complexes and subsequently play a vital role in the modified reactivity of the systems. The guest complex with a larger molecular dimension experiences more strain

inside the supercage of zeolite-Y and consequently a more reactive metal center is created. These studies are in line with the observation obtained from catalysis, which showcases CoL2-Y complex most reactive for cycloaddition of CO_2 to styrene oxide. The electronic effect is much protruding in the encapsulated monomeric form and hence encapsulated CoL2-Y complex, with an advantage of lesser metal content in it compared to its traditional analogs, shows fascinating catalytic activity for coupling reaction of CO_2 with epoxides.

The comparative studies between ZnL1-Y and CoL1-Y show that at 1 atm pressure, and 80 °C zinc complex is a better catalyst. Upon increase of the temperature to 130 °C and pressure to 5 bars, the encapsulated CoL1 complex shows better TOF of 164 compared to 41.25 at 1 atm pressure and 80 °C.

6.4 References

1. X. Liu, C. Manzur, N. Novoa, S. Celedón, D. Carrillo and J.-R. Hamon, *Coordination Chemistry Reviews*, 2018, **357**, 144.
2. A. M. Abu-Dief and I. M. A. Mohamed, *Beni-Suef University Journal of Basic and Applied Sciences*, 2015, **4**, 119.
3. Y. Ohashi and M. Nakamura, *Chemistry Letters*, 1993, **22**, 1389.
4. X.-B. Lu and D. J. Darensbourg, *Chemical Society Reviews*, 2012, **41**, 1462.
5. Y. Xie, T.-T. Wang, X.-H. Liu, K. Zou and W.-Q. Deng, *Nature Communications*, 2013, **4**, 1960.
6. T. Sawano, N. C. Thacker, Z. Lin, A. R. McIsaac and W. Lin, *Journal of the American Chemical Society*, 2015, **137**, 12241.
7. C. Modi and P. M. Trivedi, in *Advanced Energy Materials*, ed. S. V. Ashutosh Tiwari, 2014, ch. 15, pp. 555.
8. M. Salavati-Niasari, M. Shakouri-Arani and F. Davar, *Microporous and Mesoporous Materials*, 2008, **116**, 77.
9. S. Kumari, A. Choudhary and S. Ray, *Applied Organometallic Chemistry*, 2019, **33**, e4765.
10. A. Choudhary, S. Kumari and S. Ray, *ACS Omega*, 2017, **2**, 6636.
11. S. Kumari and S. Ray, *New Journal of Chemistry*, 2020, **44**, 14953.
12. A. Choudhary, B. Das and S. Ray, *Dalton Transactions*, 2016, **45**, 18967.
13. S. Kumari, A. Ramesh, B. Das and S. Ray, *Inorganic Chemistry Frontiers*, 2021, **8**, 1553.
14. S. L. Holt, R. DeIasi and B. Post, *Inorganic Chemistry*, 1971, **10**, 1498.
15. M. A. Hitchman, *Inorganic Chemistry*, 1977, **16**, 1985.
16. S. Bruckner, M. Calligaris, G. Nardin and L. Randaccio, *Acta Crystallographica Section B*, 1969, **25**, 1671.
17. W. H. Quayle, G. Peeters, G. L. De Roy, E. F. Vansant and J. H. Lunsford, *Inorganic Chemistry*, 1982, **21**, 2226.
18. K. S. Min, J. Arthur, W. W. Shum, M. Bharathy, H.-C. zur Loye and J. S. Miller, *Inorganic Chemistry*, 2009, **48**, 4593.
19. J. L. Arthur, K. S. Min and J. S. Miller, *Journal of Magnetism and Magnetic Materials*, 2019, **489**, 165375.
20. R. E. Tapscott, *Inorganic Chemistry*, 1975, **14**, 216.
21. S. Kumari, K. Maddipoti, B. Das and S. Ray, *Inorganic Chemistry*, 2019, **58**, 1527.

22. J. A. Castro-Osma, K. J. Lamb and M. North, *ACS Catalysis*, 2016, **6**, 5012.
23. A. Decortes, M. Martínez Belmonte, J. Benet-Buchholz and A. W. Kleij, *Chemical Communications*, 2010, **46**, 4580.
24. Q.-N. Zhao, Q.-W. Song, P. Liu, Q.-X. Zhang, J.-H. Gao and K. Zhang, *Chinese Journal of Chemistry*, 2018, **36**, 187.

Chapter 7

Conclusion and Future Scope

7.1 Scope and nature of the present study

In the present time, the focus of the scientific community has shifted towards sustainable development. Progressive research is being conducted to identify solutions to environmental issues such as pollution, global warming, ocean acidification, depletion of natural resources, and so on. In this context, CO_2 is a major greenhouse gas, and its mitigation is paramount. The synthesis of cyclic carbonates from epoxide and CO_2 is essential because of its industrial relevance. However, a catalyst is required to activate the highly stable CO_2.

The main objective of this thesis is the development of catalysts which are comparatively easy to prepare and have certain advantages over the already existing catalysts for the upcycling of CO_2. The first set of catalysts explored in this thesis is the homogeneous zinc(II) salophen complexes, where the reaction with CO_2 is carried out at an ambient pressure of ~1 atm. Then, towards sustainable catalysis, commercially available aluminosilicates have been used as heterogeneous catalysts. The next set of the catalyst utilized combines the homogeneous complex and the heterogeneous aluminosilicates. The catalyst termed as zeolite encapsulated complex shows fascinating results because of various factors, including modified reactivity due to distortion in geometry, site isolation, change in electronic properties, etc. Catalysis is even more fascinating when the entrapment of transition metal complexes occurs in the cages of microporous zeolites. In the present thesis, two metals having Lewis acidic properties, i.e., zinc and cobalt, are chosen for encapsulation. Finally, the activity of the encapsulated complexes is compared to that of the free state complex, where the encapsulated complexes show superior activity.

In conclusion, the present thesis deals with the synthesis of homogeneous Zn(II) Schiff base complexes and heterogeneous catalysts, including various aluminosilicates and zeolite encapsulated Zn(II) and Co(II) Schiff base complexes and their application towards the upcycling of CO_2 to cyclic carbonates. The thesis is divided into seven chapters, and the conclusion of each chapter is briefly discussed as follows:

Chapter 1

This chapter discusses in detail the need for the conversion of CO_2 and the various types of catalysts required for the conversion of CO_2 to cyclic carbonates. The three major mechanistic pathways to form cyclic carbonates from CO_2 and epoxides are discussed elaborately. This chapter

also highlights the various homogeneous zinc and cobalt-based N_2O_2 Schiff base complexes and aluminosilicate-based heterogeneous catalysts reported for cyclic carbonates synthesis. Furthermore, the chapter emphasizes the significance of encapsulation and the application of zeolite entrapped metal complexes. The gap in the literature for the synthesis of cyclic carbonates with respect to zeolite encapsulated complexes is also addressed.

Chapter 2

This chapter addresses the materials and the methodologies used to synthesize the homogeneous and heterogeneous catalysts used in the thesis. The synthesis of zinc(II) and cobalt(II) metal complexes of Schiff-base ligands with general formula *N, N'*-bis(salicylidene)-1,2-phenylenediamine (L1), *N, N'*-bis(5-methoxysalicylidene)-1,2-phenylenediamine (L2), *N, N'*-bis(5-bromosalicylidene)-1,2-phenylenediamine (L3), *N, N'*-bis(5-nitrosalicylidene)-1,2-phenylenediamine (L4), *N, N'*-bis(5-methylsalicylidene)-1,2-phenylenediamine (L5), *N, N'*-bis(5-chlorosalicylidene)-1,2- phenylenediamine (L6), *N, N'*-bis(5-trifluoromethoxysalicylidene)-1,2-phenylenediamine (L7) is explained. The details of the synthesis of zinc and cobalt Schiff-base complexes in the encapsulated states are also discussed in this chapter. The chapter also describes the protocols of synthesis of cyclic carbonate at various reaction conditions from epoxide and CO_2. Along with this, a brief introduction to the different spectroscopic techniques, including UV-vis (Ultraviolet-visible) spectroscopy, FT-IR (Fourier transform infrared) spectroscopy, BET (Brunauer-Emmett-Teller) surface area analysis, XPS (X-ray photoelectron spectroscopy), NMR (Nuclear magnetic resonance), PXRD (Powder X-ray diffraction), FESEM-EDX (Field emission scanning electron microscopy and energy dispersive X-ray analysis), TGA (Thermogravimetric analysis), AAS (Atomic absorption spectroscopy), NH_3-TPD (Temperature programmed desorption), GC (Gas chromatography) and LC-MS (Liquid chromatography-mass spectroscopy) have been presented. This chapter also includes a brief explanation of the theoretical model of the DFT (Density functional theory) used to study the Zn(II) homogeneous complexes and the zeolite encapsulated cobalt complexes.

Chapter 3

This chapter discusses the synthesis, characterization, and application of a series of homogeneous Zn(II) salophen complexes (ZnL1-ZnL7) as catalysts for the synthesis of cyclic carbonates from epoxide and CO_2. The complexes, prepared by varying the substituents at the 5, 5' positions, have been used to study the effect of the variation in the electronic environment around the metal towards the cycloaddition reaction. The LC-MS and DFT studies point towards the existence of all the complexes except ZnL4 (complex with $-NO_2$ substituent) as dimers. The DFT studies for dimeric and monomeric complexes also capture different rate-determining steps. Although all the dimeric complexes exhibit good to moderate yield for cycloaddition reaction under solvent-free conditions and a relatively low reaction temperature of 80 °C and CO_2 pressure of ~1 atm, the best yield has been achieved by ZnL4, the monomeric complex with the most electron withdrawing $-NO_2$ substituent.

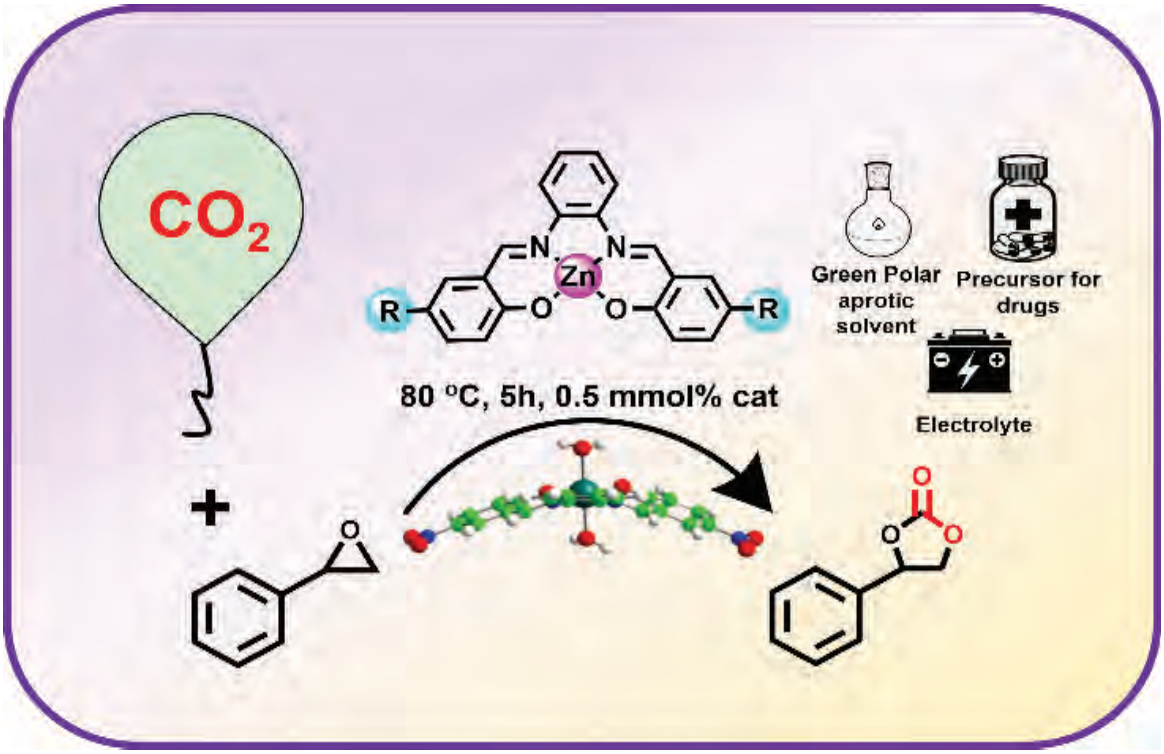

Figure 7.1: Zn(II) salophen complex used for the synthesis of styrene carbonate at 80 °C at ~1 atm pressure.

Chapter 4

This chapter explores the utility of the acidity of commercially available aluminosilicates, namely, zeolite Na-Y, zeolite NH_4^+-ZSM-5, and synthesized Al-MCM-41, without any post-modification as catalysts for capturing CO_2 by styrene oxide. The NH_3-TPD studies indicate the number of weak acidic sites of these materials to be just in accordance with their Si/Al ratios and the yield of the cyclic carbonates obtained. The NH_3-TPD data and the yield of the product carried out with calcined zeolite Na-Y indicate that not only the weak acidic sites but also the role of strong acidic sites might appear crucial for the cycloaddition reaction. The parallels between the acidity and the yield indicate that the acidity of zeolite itself plays a significant role in the cycloaddition reaction.

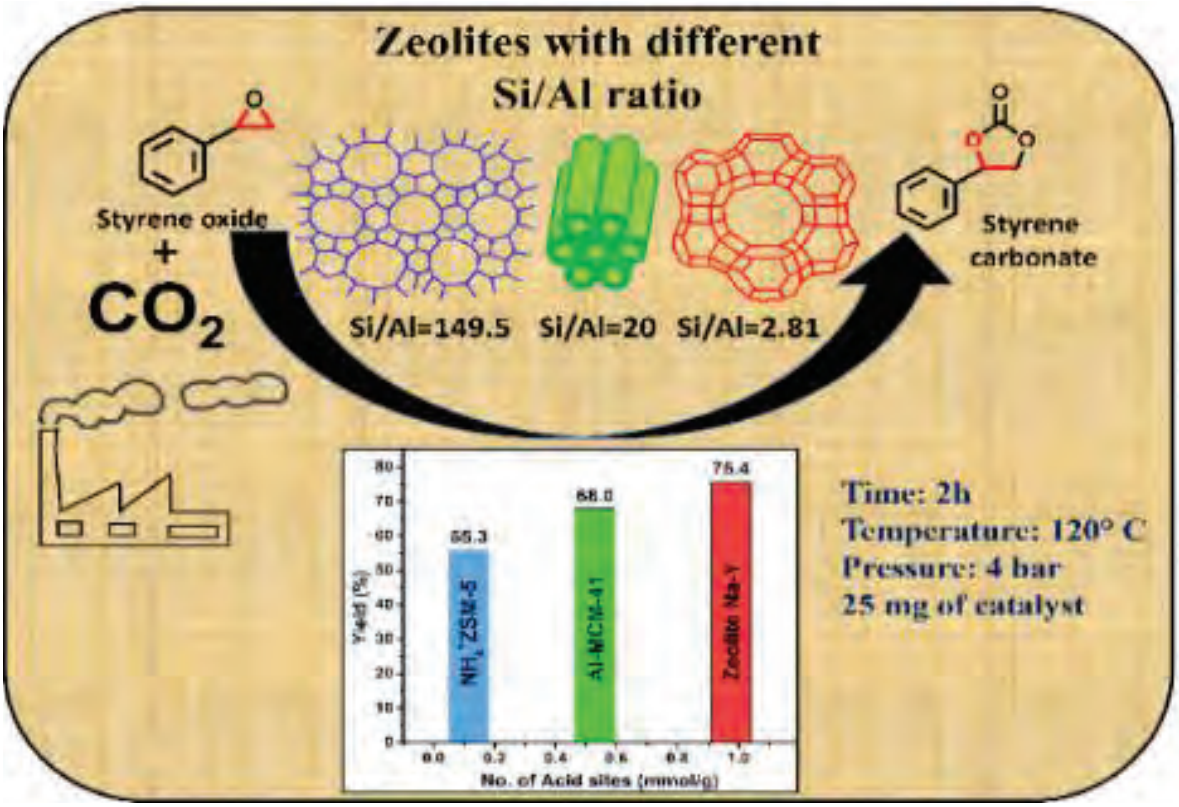

Figure 7.2: Utilization of aluminosilicates as catalysts for the synthesis of styrene carbonate from CO_2 and styrene oxide.

Chapter 5

This chapter is an extension of chapter 3 and depicts the effects of encapsulation of the zinc(II) complexes (ZnL1-Y-ZnL4-Y) inside zeolite-Y on their catalytic performance towards the cycloaddition reaction maintaining the same reaction conditions as for the homogeneous complexes (~1 atm, 80 °C and 14 h). Upon encapsulation, all the complexes undergo a change in geometry due to space constraint imposed by the zeolite supercage, indicated by the significant red shift in the electronic spectra. Encapsulation also leads to the site isolation of the complexes, and hence, all the dimeric "neat" complexes exist as monomers inside the zeolite supercage. The activity of the encapsulated system is anticipated to increase due to the inherent activity of zeolite and the positive results using the homogeneous complexes. As predicted, the encapsulated complexes show superior activity than the "neat" complexes. The encapsulated catalytic system of ZnL1-Y has performed the best, with an overall TOF of 150 h^{-1}. The TOF for neat complex, ZnL1, is only 13.8, while in the case of ZnL1-Y, even after subtracting the zeolite activity, there is seven fold increase in the activity with a TOF of 97 h^{-1}. While the best performing "neat" ZnL4 has a TOF of 16 h^{-1}, the encapsulated complex, ZnL4-Y, upon the subtraction of the activity of zeolite, shows ~3.2 time increase in TOF with a value of 52 h^{-1}. However, if we consider the overall activity of the catalytic system, i.e., the combined activity of the zeolite and the encapsulated complex, the TOF reaches a higher value of 97 h^{-1} for ZnL4-Y. The improved catalytic activity of the complex might be the result of a significant modification of the coordination environment, i.e., from dimeric to the monomeric form on encapsulation and the isolation of the active sites inside the cavities of the zeolite.

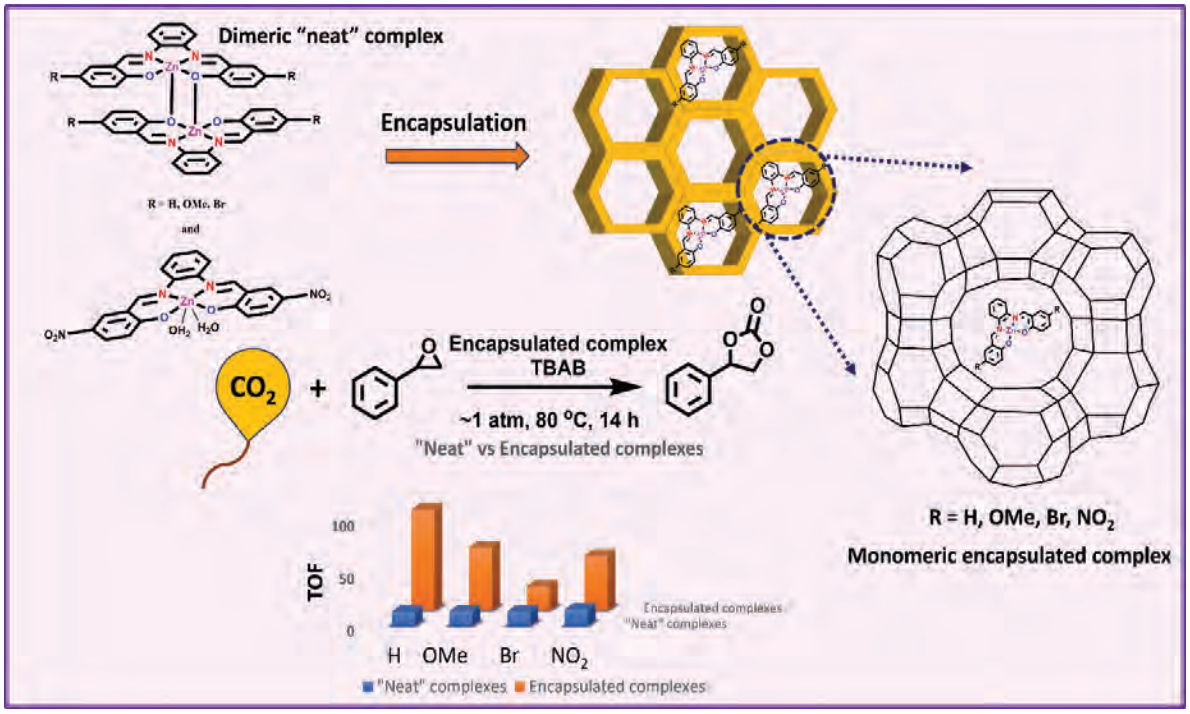

Figure 7.3: Application of "neat" and zeolite-Y encapsulated Zn(II) Schiff base complexes for the synthesis of styrene carbonate.

Chapter 6

Inspired by the remarkable activity shown by the Zn(II) encapsulated complexes, this chapter showcases the application of another active metal, i.e., "neat" and encapsulated cobalt(II) salophen complexes (CoL1, CoL1-Y, CoL2, CoL2-Y) for the synthesis of styrene carbonates. The comparison of the activity of Co(II) and Zn(II) encapsulated complexes maintaining the same reaction condition as used for previously mentioned Zn(II) encapsulated systems shows that zinc is a better choice of catalyst with higher TON of 1352 (for ZnL1-Y) compared to TON of 577.5 using cobalt (for CoL1-Y). Owing to the lower performance of the cobalt catalyst at CO_2 pressure of 1 atm and 80 °C with a reaction time of 14 h, the reaction condition was made a little harsher; however, with lesser reaction time (130 °C, 5 bar, 1.5 h). There is a significant improvement in the TOF from 41.25 h^{-1} to 164 h^{-1}. Moreover, the superiority of the encapsulated complex as a catalyst is reflected in TOF as the encapsulated complexes show better activity (TOF = 41.25 h^{-1}) compared

to their "neat" analogues (TOF = 5.7 h^{-1}) at lower temperature and pressure. The cobalt complexes show some interesting results at a lesser time and higher temperature and pressure (130 °C, 5 bar, 1.5 h). The complex with -H substituent has shown better activity in the "neat" form (TON=346) compared to the encapsulated complex (TON=246). However, the complex with -OMe substituent shows better activity upon encapsulation (TON= 635) compared to its "neat" analogue (TON= 339). Upon encapsulation in zeolite-Y, the square planar "neat" cobalt(II) complexes have shown modified structural and functional properties and interesting catalytic activity. In the free state, the reactivity of the cobalt complexes is primarily controlled by the electronic effects of the substituent groups present in the complexes. However, the encapsulation of these complexes within the supercage of zeolite-Y causes the alteration of the electron density around the metal center, reflected in the electronic spectra of the encaged complexes, and subsequently modifies the reactivity. The catalyst with a larger end-to-end distance shows better results for the cycloaddition reaction after encapsulation.

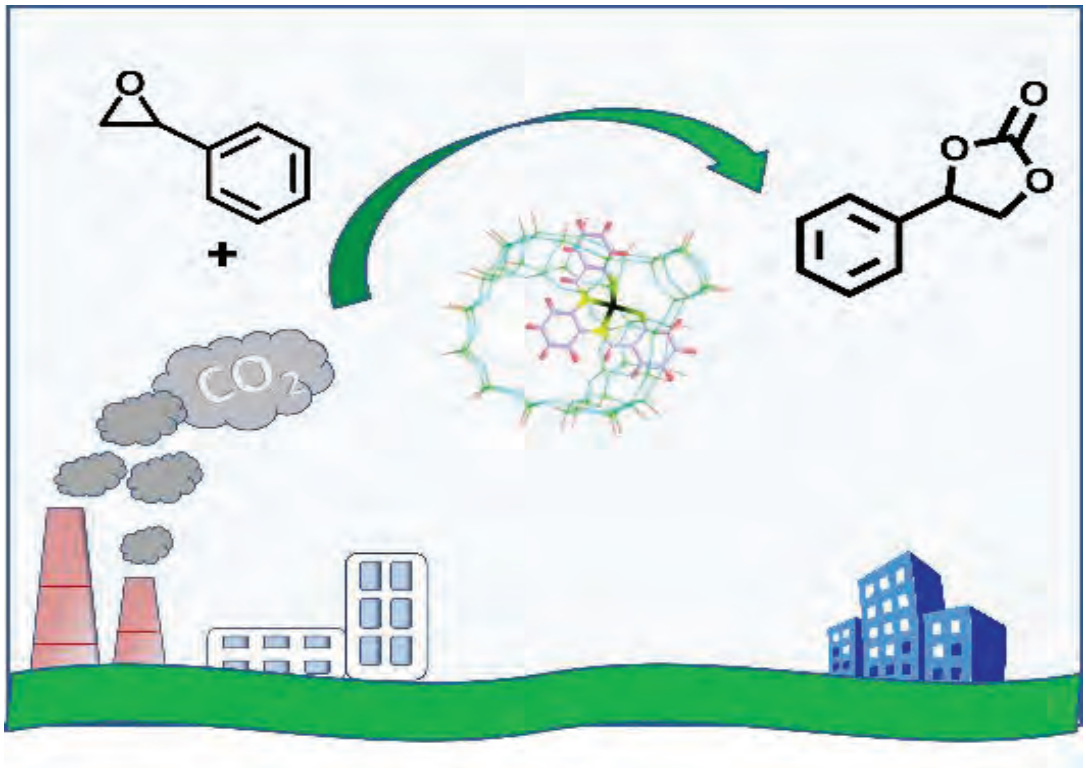

Figure 7.4: Application of "neat" and zeolite-Y encapsulated Co(II) Schiff base complexes for the synthesis of styrene carbonate.

7.2 Overall conclusions of the present work

- The thesis shows the successful synthesis of cobalt and zinc-based salophen complexes in the free and encapsulated state. The encapsulated complexes are synthesized *via* the flexible ligand method.
- The thesis also presents the successful structural analysis and characterization of the synthesized complexes using different analytical techniques.
- All the prepared complexes have been explored for the synthesis of styrene carbonate from CO_2 and styrene oxide. The activity of the "neat" and the encapsulated complexes have been compared, and encapsulated complexes show superior activity in both cases. The results show that in the case of zinc complexes, the site isolation leads to the improvement in the catalytic activity, while in the case of cobalt complexes, the end-to-end distance of the substituents plays a vital role.
- The choice of metal, the inherent acidity of the zeolite, the cooperative effect of the complex and the zeolite for the encapsulated complex and the modified electronic environment upon encapsulation render the encaged complex with improved catalytic performance.

7.3: Future scope

The scientific community is currently at a crucial juncture where a small contribution towards sustainability and green technology can significantly impact the environment. In this context, the upcycling of CO_2 is an essential field of research that scientists have been actively pursuing to achieve a better tomorrow. The high stability of CO_2 limits its usage; hence, the development of various catalysts to activate CO_2 is inevitable. The development of stable and reusable heterogeneous catalysts for the conversion of CO_2 to other valuable chemicals can be beneficial to society. Apart from cyclic carbonates, CO_2 can also be converted to various industrially relevant compounds like urea, dimethyl carbonate, and other fine chemicals like formic acid, methanol, etc. At the same time, the development of heterogeneous catalysts using zeolites leaves a lot of scope to modify the activity of the complex further. The inherent acidity of the zeolites can be further explored for the reactions catalyzed by acids. The additional advantage of site isolation and low metal loading provided by the zeolite encapsulated systems makes it a fascinating choice as a catalyst. The results from the current thesis also indicate that utilization of the complexes of non-

toxic and abundant Zn metal can be an attractive alternative which can promote a benign reaction condition for catalysis. In the future, using zeolite and zeolite based catalysts can be considered enticing for the valorization of CO_2.

Appendices

Additional Information

Calculation of the amount of zinc from AAS:

We have made the calibration curve with zinc standards. Figure A1 shows the calibration curve.

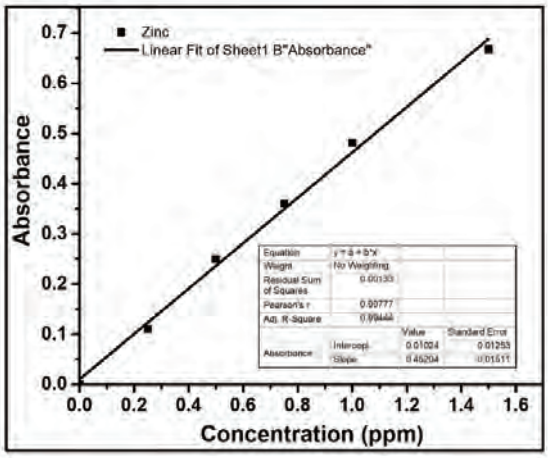

Figure A1: Calibration curve using zinc standards.

To make the solution of our complex, we weighed a particular amount of the complex and digested the complex with nitric acid. Then, we diluted the solution up to 50 mL.

For ZnL1-Y, the amount weighed was 12.3 mg. For ZnL1, the concentration of zinc obtained from AAS was 0.29546 ppm.

0.29546 ppm = 0.29546 mg/L which implies 0.059152 mg/50 mL.

Now, 12.3 mg of the sample contains 0.059152 mg of zinc

100 mg contains 0.48091, which is 0.48%.

The calculation for other complexes is also done in a similar way.

Calculation of yield from GC:

First, we calculate the response factor.

Let the response factor be F for the styrene oxide with respect to internal standard.

Now, area of styrene oxide signal / moles of styrene oxide = F × area of standard signal / moles of standard.

That is, $a_{SO} / m_{SO} = F \times a_{IS} / m_{IS}$

Therefore, $F = a_{SO} \times m_{IS} / a_{IS} \times m_{SO}$……..(1)

where m_{SO} and m_{IS} are the moles of styrene oxide and internal standard respectively.

a_{SO} and a_{IS} are the areas of styrene oxide and of internal standard respectively.

This equation presumes a linear response of the detector to both styrene carbonate and the internal standard.

The consistency of F was checked by taking different concentrations of styrene oxides.

Similarly, a known quantity of styrene carbonate is mixed with the same quantity of the standard as in equation (1), and the response factor is calculated.

Therefore, $F' = a_{SC} \times m_{IS} / a_{IS'} \times m_{SC}$……(2)

where a_{SC} and $a_{IS'}$ are the areas of styrene carbonate and internal standard and m_{SC} and m_{IS} are the moles of styrene carbonate and internal standard, respectively.

F′ = response factor for the carbonate with respect to the standard.

The consistency of F′ was checked by taking different concentrations of styrene carbonate.

In the case of styrene oxide after the reaction is over, $a_{SO'} / m_{SO'} = F \times a_{IS''} / m_{IS'}$

Therefore, $m_{SO'} = a_{SO'} \times m_{IS'} / a_{IS''} \times F$……(3),

where $a_{SO'}$ and $a_{IS''}$ are the area of styrene oxide and internal standard respectively. $m_{SO'}$ is the unknown moles of styrene oxide and $m_{IS'}$ is the moles of the internal standard.

From this equation $m_{SO'}$ can be determined by applying known values of $a_{SO'}$, $a_{IS''}$ and $m_{IS'}$.

In the case of styrene carbonate after the reaction is over, $a_{SC''} / m_{SC''} = F' \times a_{IS'''} / m_{IS''}$

Therefore, $m_{SC''} = a_{SC''} \times m_{IS''} / a_{IS'''} \times F'$…… (4),

where $a_{SC''}$ and $a_{IS'''}$ are the area of styrene carbonate and internal standard respectively.

$m_{IS''}$ is the moles of standard and $m_{SC''}$ is the unknown moles of styrene carbonate. Thus, from equation (4) $m_{SC''}$ was calculated as all other terms are known.

Therefore, % GC yield= [moles of styrene carbonate ($m_{SC''}$) / {moles of styrene oxide ($m_{SO'}$) + moles of styrene carbonate ($m_{SC''}$)}]×100.

List of Publications

1. Susheela Kumari, **Aishwarya Ramesh**, and Saumi Ray, Zeolite-Y encapsulated cobalt(II) Schiff-base complexes employed for photocatalytic dye-degradation and upcycling CO_2, *Inorganic chemistry Frontiers*, **2021**, *8*, 1553-1566.
2. **Aishwarya Ramesh** and Saumi Ray, Importance of the Nature of Acidic Sites of Different Aluminosilicates on Fixation of Carbon Dioxide with Styrene Oxide, *ChemPlusChem*, **2023**, *88*, e202300086.
3. **Aishwarya Ramesh**, Sharmistha De Dalui, Sakshi Bajaj, Bidisa Das and Saumi Ray, CO_2 to Cyclic Carbonate: A Mechanistic Insight of a Benign Route Using Zinc(II) Salophen Complexes (10.1002/ejic.202300610).
4. **Aishwarya Ramesh**, Sakshi Bajaj, and Saumi Ray, Zeolite-Y Encapsulated Zinc(II) Schiff-Base Complexes for Upcycling CO_2 (manuscript under preparation).

Conferences and Workshops Attended

1. 4th workshop on Analytical Instruments for Chemical and Environmental Engineers (WAICEE-2019) organized by IIChE Pilani Regional Centre and Department of Chemical Engineering held at BITS Pilani, March 25-26, 2019.
2. **Aishwarya Ramesh** and Saumi Ray "Insertion of CO_2 to epoxide for the synthesis of industrially useful carbonates by heterogeneous catalysis" National conference on New Frontiers in Chemistry- From Fundamental to Applications (NFCFA2019) organized by BITS Pilani, Goa Campus, December 20-22, 2019.
3. **Aishwarya Ramesh** and Saumi Ray "Importance of the nature of acidic sites of different aluminosilicates on fixation of CO_2 to cyclic carbonates" International Conference On Emerging Materials For Sustainable Development (EMSD-2022) Jointly organized by CSIR-CSIO, Chandigarh and IEEE AcSIR-CSIO student chapter, Chandigarh, October 9-11, 2022.
4. Analytical Advances in Studying Molecules under the aegis of DST-Synergistic Training Program Utilizing the Scientific and Technological Infrastructure (STUTI) Organized by BITS Pilani, Pilani Campus, October 15-21, 2022.

Brief Biography of the Candidate

Ms. Aishwarya Ramesh
Research Scholar
Department of Chemistry
BITS-Pilani, Pilani Campus
Pilani, Rajasthan-333031, India

Ms. Aishwarya Ramesh completed her B.Sc. from Acharya Narendra Dev College, University of Delhi, India (2012-2015) and M.Sc. from the SASTRA University, Thanjavur, India (2015-2017). She joined the Department of Chemistry, BITS Pilani, Pilani Campus, Rajasthan in August 2017 for her doctoral research under the supervision of **Prof. Saumi Ray**. Currently, she has published three research articles in well-renowned international journals and one more publication is in the pipeline. She has presented posters at two conferences. She has also attended workshops on instrument training. Her research interest lies in designing zeolite-based heterogeneous catalysts for upcycling CO_2.

Brief Biography of the Supervisor

Prof. Saumi Ray
Professor
Department of Chemistry
BITS-Pilani, Pilani Campus
Pilani, Rajasthan-333031, India

Prof. Saumi Ray completed her B.Sc. from Bethune College, University of Calcutta (1991) and M.Sc. from the Department of Chemistry, University of Calcutta (1993). She received her Ph.D. degree from the Department of Inorganic and Physical Chemistry, Indian Institute of Science, Bangalore, India (2003) under the supervision of Prof. S. Vasudevan. During her doctoral studies, she worked on zeolites with a detailed understanding of 'Host-guest' Chemistry and Molecular Recognition, ultimately leading to the design and synthesis of advanced materials for different practical purposes like catalysis, separation, and molecular sensing. She has around 18 years of teaching and research experience. Her current research interests are in the field of Material Chemistry and Computational Fluid Dynamics. **Prof. Saumi Ray** joined BITS Pilani in 2005 and has supervised three PhD students (Dr. Priya C Sande, Dr. Archana Choudhary, and Dr. Susheela Kumari) in the field of Computational Fluid Dynamics and Material Chemistry. She is currently guiding five PhD students as supervisor and one PhD student as co-supervisor. As a result of her research accomplishments, she has published research articles in peer-reviewed journals, presented papers at national and international conferences. She has completed one DST-funded research project as PI. Currently she has two ongoing projects, one she is supervising as PI funded by SERB and another as co-investigator funded by BITS-Pilani.

Email Id: *saumi@pilani.bits-pilani.ac.in*